frontiers | Research Topics

Emerging strategies in combatting and managing bacterial biofilms

Edited by
Reham Wasfi, Samira Mohamed Hamed
and Ashraf Zarkan

Published in
Frontiers in Cellular and Infection Microbiology

ISSN 1664-8714
ISBN 978-2-8325-3256-0
DOI 10.3389/978-2-8325-3256-0

About Frontiers

Frontiers is more than just an open access publisher of scholarly articles: it is a pioneering approach to the world of academia, radically improving the way scholarly research is managed. The grand vision of Frontiers is a world where all people have an equal opportunity to seek, share and generate knowledge. Frontiers provides immediate and permanent online open access to all its publications, but this alone is not enough to realize our grand goals.

Frontiers journal series

The Frontiers journal series is a multi-tier and interdisciplinary set of open-access, online journals, promising a paradigm shift from the current review, selection and dissemination processes in academic publishing. All Frontiers journals are driven by researchers for researchers; therefore, they constitute a service to the scholarly community. At the same time, the *Frontiers journal series* operates on a revolutionary invention, the tiered publishing system, initially addressing specific communities of scholars, and gradually climbing up to broader public understanding, thus serving the interests of the lay society, too.

Dedication to quality

Each Frontiers article is a landmark of the highest quality, thanks to genuinely collaborative interactions between authors and review editors, who include some of the world's best academicians. Research must be certified by peers before entering a stream of knowledge that may eventually reach the public - and shape society; therefore, Frontiers only applies the most rigorous and unbiased reviews. Frontiers revolutionizes research publishing by freely delivering the most outstanding research, evaluated with no bias from both the academic and social point of view. By applying the most advanced information technologies, Frontiers is catapulting scholarly publishing into a new generation.

What are Frontiers Research Topics?

Frontiers Research Topics are very popular trademarks of the *Frontiers journals series*: they are collections of at least ten articles, all centered on a particular subject. With their unique mix of varied contributions from Original Research to Review Articles, Frontiers Research Topics unify the most influential researchers, the latest key findings and historical advances in a hot research area.

Find out more on how to host your own Frontiers Research Topic or contribute to one as an author by contacting the Frontiers editorial office: frontiersin.org/about/contact

Emerging strategies in combatting and managing bacterial biofilms

Topic editors

Reham Wasfi — MSA University, Egypt

Samira Mohamed Hamed — October University for Modern Sciences and Arts, Egypt

Ashraf Zarkan — University of Cambridge, United Kingdom

Citation

Wasfi, R., Hamed, S. M., Zarkan, A., eds. (2023). *Emerging strategies in combatting and managing bacterial biofilms*. Lausanne: Frontiers Media SA.

doi: 10.3389/978-2-8325-3256-0

Table of contents

frontiers | Frontiers in Cellular and Infection Microbiology

TYPE Editorial
PUBLISHED 01 August 2023
DOI 10.3389/fcimb.2023.1264346

OPEN ACCESS

EDITED AND REVIEWED BY
Christophe Beloin,
Institut Pasteur, France

*CORRESPONDENCE
Reham Wasfi
rwasfi@msa.edu.eg

RECEIVED 20 July 2023
ACCEPTED 24 July 2023
PUBLISHED 01 August 2023

CITATION
Wasfi R, Zarkan A and Hamed SM (2023) Editorial: Emerging strategies in combatting and managing bacterial biofilms.
Front. Cell. Infect. Microbiol. 13:1264346.
doi: 10.3389/fcimb.2023.1264346

Editorial: Emerging strategies in combatting and managing bacterial biofilms

Reham Wasfi[1]*, Ashraf Zarkan[2] and Samira M. Hamed[1]

[1]Department of Microbiology and Immunology, Faculty of Pharmacy, October University for Modern Sciences and Arts (MSA), Giza, Egypt, [2]Department of Genetics, University of Cambridge, Cambridge, United Kingdom

KEYWORDS

biofilm, microbiome, hospital-acquired infection (HAI), implanted medical devices, multidrug resistance (MDR), biofilm associated infections, catheters

Editorial on the Research Topic
Emerging strategies in combatting and managing bacterial biofilms

Numerous microbes use biofilm formation as a mean of survival. Biofilms are multicellular communities in which microorganisms are encased in a protective matrix that enables them to endure challenging environments and resist traditional therapies. The widespread existence of biofilm-forming bacteria in various settings, including healthcare facilities, is made possible by their capacity to colonize a variety of biotic and abiotic surfaces. They pose a serious threat to human health because they can develop increasing resistance to traditional antibiotics and spread morbidity through both device- and non-device (tissue)-associated infections, as reviewed by Zhao et al. This microbial phenotype consequently became a significant concern in several fields, including public health and medicine.

Biofilms are involved in the pathogenicity of infectious diseases as well as the establishment of healthy microbiomes. Many bacterial species within the gut microbiome grow as biofilms, and disease outcome is greatly impacted by the location of the biofilms within the gastrointestinal tract (Miller et al., 2021). Hammouda et al. reported that hormonal drugs affect biofilm formation by selected gut microbiota such as *Bifidobacterium longum*, *Limosilactobacillus reuteri*, *Bacteroides fragilis*, and *Escherichia coli*, representing the four main phyla in the gut. Despite increasing the adhesion of *L. reuteri* to Caco-2/HT-29 cell line coculture, progesterone inhibited the biofilm development of the Gram-positive bacteria. In contrast, it increased the ability of Gram-negative bacteria to form biofilms and increased the adherence of *B. fragilis* to the cell lines coculture. Both estradiol and thyroxine displayed antibiofilm activity against *L. reuteri*. In the meantime, thyroxine boosted the capacity of *E. coli* to develop a biofilm.

The implication of biofilm-related multi-drug resistance (MDR) in hospital-acquired infections is a significant issue with increased rates of patient mortality and morbidity as well as economic burden, including high healthcare expenses and extended hospital stays (Assefa and Amare, 2022). Hu et al. reported the ability of the emerging opportunistic nosocomial pathogen *Elizabethkingia anophelis* to form biofilms. MDR phenotype was also exhibited by all isolates. The authors concluded that biofilm development and antibiotic

resistance in *E. anophelis* are positively correlated. Such findings will provide the groundwork for future advancements in therapeutic approaches against *E. anophelis* infections. Due to its uncertain mechanism of antibiotic resistance and high mortality rate among nosocomial isolates, *E. anophelis* can be a serious concern to clinicians (Lin et al., 2019).

Another emerging opportunistic pathogen is *Brevundimonas* spp., which is reclassified from *Pseudomonas* spp. (Segers et al., 1994). Gricajeva et al. reported that the biofilm formed by this genus was responsive to treatment by antimicrobial inactivation using natural photosensitizers such as riboflavin (RF) and chlorophyllin (Chl). Importantly, this approach provides a new treatment strategy that does not drive resistance in treated microbial cells (Kashef and Hamblin, 2017).

Another nosocomial pathogen is *Acinetobacter bumannii* which is known for its high resistance and biofilm formation capacity (Abd El-Rahman et al., 2023; Hamed et al., 2023). *A. bumannii* was the subject of a study by Kong et al. who found that the dominance of some sequence types of *A. baumannii* is likely due to resistance to harsh conditions of oxidation, desiccation, and multiple antibiotics rather than their ability to form biofilm, while the non-dominant sequence types were characterized by high biofilm formation.

One approach for reducing the burden of biofilm-associated infections is the search for new and alternative therapies. Between 50-70% of nosocomial infections are caused by biofilm formation on implanted medical devices such as central venous catheters (CVCs) (Asker et al., 2021). Researchers have been looking for novel ways to develop biofilm-free implants via antibiofilm coating and impregnating devices with antibiofilm chemicals (Amer et al., 2022) as well as modifying the implant materials (Gayani et al., 2021). An et al. studied the impact of zinc dimethacrylate (ZDMA) modification of the polymethyl methacrylate (PMMA) denture base resin on its cytotoxic and antifungal activities as well as its surface and physicochemical properties. They confirmed that the ZDMA-modified PMMA showed higher thermal stability, surface hydrophilicity, and surface roughness without enhancing the adhesion of microbes. Additionally, it demonstrated strong antifungal action without causing any negative cellular consequences.

The influence of different surface modifications of implant materials based on cobalt–chromium–molybdenum (CoCrMo) on biofilms was studied by Paulitsch-Fuchs et al., where they compared three smooth surfaces (CoCrMo, CoCrMo polished, and CoCrMo TiN) and three rough surfaces (CoCrMo cpTi, CoCrMo porous coated, and CoCrMo TCP) to the unmodified base alloy. The authors found a relationship between surface roughness and biofilm structure, including proteins, polysaccharides, as wells as expression of biofilm-associated genes. Among all proposed surface modifications, the authors attributed the best performance in reducing biofilms to CoCrMo TiN and polished CoCrMo.

Amer et al. produced a potent biosurfactant from an endophytic *Bacillus amyloliquefaciens* that inhabited the Nile Papyrus. The biosurfactant showed promising antibacterial and antibiofilm activity against MDR global clones of *A. baumannii*. Up to 89.59% reduction in biofilm formation was achieved using sub-MICs of the extract. The potential of the biosurfactant to eradicate *A. baumannii* biofilms at concentrations equivalent to its MIC was also demonstrated by up to 87.3% biomass reduction. Three log10 reductions in the viable adherent bacterial count were achieved in a biosurfactant-impregnated CVC model. The authors linked this biosurfactant activity to several compounds explored by GC-MS analysis of the crude extract. The biosurfactant was hence, proposed as a potential strategy for reducing the burden of catheter-related blood stream infections (CRBSIs).

Early intervention is the key to reducing the clinical burden of biofilm-related infections, which can be facilitated by the early detection of biofilms. As biofilm detection is particularly challenging, innovative sensing, tracking, and diagnostic technologies are needed. The potential application of the BioFilm Ring Test (BRT)® in the diagnosis of biofilm-associated *Pseudomonas* respiratory infections was evaluated by Fernández-Barat et al. For this purpose, mucoid and nonmucoid *Pseudomonas aeruginosa* were recovered from the sputa of patients with bronchiectasis. The biofilm production index (BPI) of the isolates was determined using BRT at 5 and 24 hours. The authors concluded that the capacity of bacteria to form biofilms can be successfully determined using BRT in just five hours, and hence the test may be incorporated into clinical practise for the diagnosis of biofilm-related infections. Another application evaluated by the authors was the determination of the mucoid phenotype of *P. aeruginosa*. A BPI of less than 14.75 successfully predicted the mucoid phenotype at 5 h, but with low sensitivity and specificity (64% and 72%, respectively). A correlation between ciprofloxacin resistance and low BPI was also established by the authors, who recommended further investigation into the use of BRT to predict ciprofloxacin resistance.

To summarise, the contributions of these strategies in combatting and managing bacterial biofilms provide novel insights as well as potential therapeutic and preventive approaches that can be utilised in multiple clinical applications. The Research Topic is certainly of special interest to clinicians, dentists, and implant surgeons.

Author contributions

RW: Writing – original draft. AZ: Writing – review & editing. SH: Writing – review & editing.

Conflict of interest

The authors declare that the research was conducted in the absence of any commercial or financial relationships that could be construed as a potential conflict of interest

Publisher's note

References

Abd El-Rahman, O. A., Rasslan, F., Hassan, S. S., Ashour, H. M., and Wasfi, R. (2023). The RND efflux pump gene expression in the biofilm formation of acinetobacter baumannii. *Antibiotics (Basel)* 12 (2), 1–13. doi: 10.3390/antibiotics12020419

Amer, M. A., Ramadan, M. A., Attia, A. S., and Wasfi, R. (2022). Silicone Foley catheters impregnated with microbial indole derivatives inhibit crystalline biofilm formation by Proteus mirabilis. *Front. Cell. Infect. Microbiol.* 12, 1–12. doi: 10.3389/fcimb.2022.1010625

Asker, D., Awad, T. S., Raju, D., Sanchez, H., Lacdao, I., Gilbert, S., et al. (2021). Preventing pseudomonas aeruginosa biofilms on indwelling catheters by surface-bound enzymes. *ACS Appl. Bio Mater.* 4 (12), 8248–8258. doi: 10.1021/acsabm.1c00794

Assefa, M., and Amare, A. (2022). Biofilm-associated multi-drug resistance in hospital-acquired infections: A review. *Infect. Drug Resist.* 15, 5061–5068. doi: 10.2147/idr.S379502

Gayani, B., Dilhari, A., Kottegoda, N., Ratnaweera, D. R., and Weerasekera, M. M. (2021). Reduced crystalline biofilm formation on superhydrophobic silicone urinary catheter materials. *ACS Omega* 6 (17), 11488–11496. doi: 10.1021/acsomega.1c00560

Hamed, S. M., Elkhatib, W. F., Brangsch, H., Gesraha, A. S., Moustafa, S., Khater, D. F., et al. (2023). Acinetobacter baumannii global clone-specific resistomes explored in clinical isolates recovered from Egypt. *Antibiotics (Basel)* 12 (7), 1–22. doi: 10.3390/antibiotics12071149

Kashef, N., and Hamblin, M. R. (2017). Can microbial cells develop resistance to oxidative stress in antimicrobial photodynamic inactivation? *Drug Resist. Update* 31, 31–42. doi: 10.1016/j.drup.2017.07.003

Lin, J. N., Lai, C. H., Yang, C. H., and Huang, Y. H. (2019). Elizabethkingia infections in humans: from genomics to clinics. *Microorganisms* 7 (9), 1–15. doi: 10.3390/microorganisms7090295

Miller, A. L., Bessho, S., Grando, K., and Tükel, Ç. (2021). Microbiome or infections: amyloid-containing biofilms as a trigger for complex human diseases. *Front. Immunol.* 12. doi: 10.3389/fimmu.2021.638867

Segers, P., Vancanneyt, M., Pot, B., Torck, U., Hoste, B., Dewettinck, D., et al. (1994). Classification of Pseudomonas diminuta Leifson and Hugh 1954 and Pseudomonas vesicularis Büsing, Döll, and Freytag 1953 in Brevundimonas gen. nov. as Brevundimonas diminuta comb. nov. and Brevundimonas vesicularis comb. nov., respectively. *Int. J. Syst. Bacteriol.* 44 (3), 499–510. doi: 10.1099/00207713-44-3-499

frontiers in Cellular and Infection Microbiology

ORIGINAL RESEARCH
published: 01 March 2022
doi: 10.3389/fcimb.2022.837124

Effect of Cobalt–Chromium–Molybdenum Implant Surface Modifications on Biofilm Development of *S. aureus* and *S. epidermidis*

Astrid H. Paulitsch-Fuchs[1,2], *Benjamin Bödendorfer*[1], *Lukas Wolrab*[1], *Nicole Eck*[3], *Nigel P. Dyer*[4] *and Birgit Lohberger*[3]*

[1] Biomedical Sciences, University of Applied Sciences Carinthia, Klagenfurt, Austria, [2] Diagnostic and Research Institute of Hygiene, Microbiology and Environmental Medicine, Medical University of Graz, Graz, Austria, [3] Department of Orthopaedics and Trauma, Medical University of Graz, Graz, Austria, [4] Bioinformatics Research Technology Platform, University of Warwick, Coventry, United Kingdom

OPEN ACCESS

Edited by:
Fany Reffuveille,
Université de Reims Champagne-Ardenne, France

Reviewed by:
Kuntaman Kuntaman,
Airlangga University, Indonesia
Markus Bischoff,
Saarland University Hospital, Germany

***Correspondence:**
Birgit Lohberger
birgit.lohberger@medunigraz.at

Specialty section:
This article was submitted to Biofilms, a section of the journal Frontiers in Cellular and Infection Microbiology

Received: 16 December 2021
Accepted: 04 February 2022
Published: 01 March 2022

Citation:
Paulitsch-Fuchs AH, Bödendorfer B, Wolrab L, Eck N, Dyer NP and Lohberger B (2022) Effect of Cobalt–Chromium–Molybdenum Implant Surface Modifications on Biofilm Development of S. aureus and S. epidermidis. Front. Cell. Infect. Microbiol. 12:837124. doi: 10.3389/fcimb.2022.837124

Periprosthetic infections are an eminent factor in patient care and also having significant economic implications. The number of biofilm-infection related replacement surgeries is increasing and will continue to do so in the following decades. To reduce both the health burden of the patients and the costs to the healthcare sector, new solutions for implant materials resistant to such infections are necessary. This study researches different surface modifications of cobalt–chromium–molybdenum (CoCrMo) based implant materials and their influence on the development of biofilms. Three smooth surfaces (CoCrMo, CoCrMo TiN, and CoCrMo polished) and three rough surfaces (CoCrMo porous coated, CoCrMo cpTi, and CoCrMo TCP) are compared. The most common infectious agents in periprosthetic infections are *Staphylococcus aureus* and Coagulase-negative *staphylococci* (e.g., *Staphylococcus epidermidis*), therefore strains of these two species have been chosen as model organisms. Biofilms were grown on material disks for 48 h and cell number, polysaccharide content, and protein contend of the biofilms were measured. Additionally, regulation of genes involved in early biofilm development (*S. aureus icaA*, *icaC*, *fnbA*, *fnbB*, *clfB*, *atl*; *S. epidermidis atlE*, *aap*) was detected using RT-q-PCR. All results were compared to the base alloy without modifications. The results show a correlation between the surface roughness and the protein and polysaccharide content of biofilm structures and also the gene expression of the biofilms grown on the different surface modifications. This is supported by the significantly different protein and polysaccharide contents of the biofilms associated with rough and smooth surface types. Additionally, early phase biofilm genes (particularly *icaA*, *icaC*, and *aap*) are statistically significantly downregulated compared to the control at 48 h on rough surfaces. CoCrMo TiN and polished CoCrMo were the two smooth surface modifications which performed best on the basis of low biofilm content.

Keywords: *Staphylococcus aureus*, *Staphylococcus epidermidis*, biofilms, CoCrMo, prosthetic infections

INTRODUCTION

Due to a general increase in life expectancy, improved surgical techniques and medical care, the demand for implants (e.g., joint replacement prosthesis) has increased greatly over recent decades. Although new materials or surface modifications for implants are constantly being developed, the struggle with periprosthetic infections is far from coming to an end. As an example, predictions for the US (compared to 2014) and Germany (compared to 2016) show an increase in primary total knee arthroplasty (TKA) by 2030 from 680,000 by 147% (Sloan et al., 2018) and from ~170,000 by between 8 and 49% (Rupp et al., 2020), respectively. Periprosthetic infections have an incidence of approximately 1–4% after primary TKA (Phillips et al., 2006). The incidence rate for a periprosthetic infection following a TKA replacement has been reported to be approximately 0.5% after 1 year, 0.8% after 5 years, and 1.4% after10 years (Tsaras et al., 2012), with cost per patient associated with TKA replacement of up to ~30,000 USD (Palsis et al., 2018).

Those periprosthetic infections can be caused by a number of different organisms, most of which are bacteria. In most cases a bacterial infection forms a biofilm on the surface of the implant which makes it even harder to treat. In a 2020 literature review on the topic of biofilms in periprosthetic infections Shoji and Chen (2020) reported a prevalence of *Staphylococcus aureus* in such infections of 21–43.6% followed by 20–31% Coagulase-negative *Staphylococcus*. Biofilm building *Staphylococcus* species have a large number of attributes allowing them to avoid host defenses and antibiotic treatments. The extracellular polymeric substances (EPS), also called extracellular matrix (ECM), build a physical barrier for transport of chemicals (Singh et al., 2010; Idrees et al., 2021) and immune-cells (Zimmerli et al., 1984) and hold the biofilm structure together. In addition, quorum sensing (Kavanaugh and Horswill, 2016; Kim et al., 2017), higher mutation frequencies (Ryder et al., 2012), and dormant cells (Venter et al., 2017; Lamret et al., 2020; Shoji and Chen, 2020) contribute to the pathogenicity of those strains.

Because treatment of already established biofilms is so difficult, the development of surfaces which are less favorable for the bacteria to attach to in the first place is an ongoing research topic. Cobalt–chromium–molybdenum (CoCrMo) based implants are regularly used not only for total joint replacement but also in dentistry (Chen and Thouas, 2015). The CoCrMo alloy has excellent biocompatibility and mechanical properties, which makes it the preferred material for knee and ankle replacements (Chen and Thouas, 2015). Physical and chemical surface modifications of metallic implant materials aim to improve their surface charge, wettability, topography and chemistry (Munir et al., 2020) in order to improve their osseointegration abilities and in the same time lessen the number of biofilm infections. These modifications can be achieved by mechanical treatment of the surfaces like polishing processes and numerous coating methods like plasma spraying, physical vapor deposition, cathodic arc deposition, and sintering (Munir et al., 2020). For this study five surface modifications have been applied to a casted CoCrMo base alloy: titanium nitride (TiN), mechanical polishing, porous coating, commercially pure titanium coating (cpTi), and a coating with tricalcium phosphate (TCP). Two bacterial species, *S. aureus* and *S. epidermidis*, were used as model organisms to monitor biofilm development after 48 h of incubation on the different alloy surfaces. Total cell count, protein and polysaccharide content of the biofilms were measured and data on biofilm associated gene expression was collected. The aim of the study is to understand the influence of the different CoCrMo surface modifications on the biofilm formation of *S. aureus* and *S. epidermidis*.

MATERIAL AND METHODS

CoCrMo Surface Modifications

All materials tested in this study were manufactured by Implantcast GmbH (Buxtehude, Germany) and were produced in a disc shape with a thickness of 1 mm and a diameter of 14 mm using a precision casting process. Gamma irradiation was used for sterilizing all materials described hereafter. Special coatings were produced and applied by DOT Ltd (Rostock, Germany). The CoCroMo casting alloy is composed of 28.5–29.5% Cr, 5.75–6.25% Mo, less than 1% each of Ni, Fe, C, Si, Mn, W, P, N, Al, Ti; and Co (~61–64%) making up the balance. This lies well within the specifications for this material given by the ISO 5832-3 for CoCrMo casting alloy for surgical implants (ISO 5832-3, 2016). Mechanical properties of the base CoCrMo alloy were tested according to ISO 6892-1 (2019) and are given as: tensile yield point $R_{p0.2}$ ≥450 megapascal (MPa), tensile strength R_m ≥665 MPa and elongation at fracture A ≥8%. Titanium nitride (TiN) modified alloy surfaces show better properties in terms of biocompatibility, wettability, surface roughness, friction coefficient, corrosion resistance, minimized wear and increased temperature resistance; the TiN coating also leads to a reduced release of cobalt and chromium ions (Van Hove et al., 2015; Thomas et al., 2016). The coating of the discs was achieved by cathodic arc deposition. This technique is frequently used to synthesize extremely hard films for protecting the surfaces of materials. For the deposition a TiN target with ~99.4% titanium and less than 0.25% each of Fe, O, C, N and H (all according to ISO 5832-2 (2018)). The coating thickness was 5.5 ± 1.5 μm, the adhesive tensile strength ≥22 MPa and the layer roughness <0.05 μm. On top of the TiN layer an additional layer of ≥0.02 μm gold and cobalt (AuCo; with a maximum percentage of 0.2 ± 0.02% cobalt) was applied using a PVD-DC-Magnetron sputter. The density of the AuCo layer was 19.32 g/cm^3, the specific electrical resistance was 2.35 μΩ • cm and the tensile strength is sufficient to prevent delamination of the coating when using an adhesive film strip-test. Highly polished CoCrMo alloys are commonly used, where the increased surface smoothness is associated with improved corrosion and wear properties (Davis, 2003). The porous coating was applied on the base material using sintering. In this process three layers of 250–355 μm diameter balls were applied on the material discs resulting in a coating thickness of 700–1,060 μm. Porosity of the coating was 30–40%, its tensile strength ≥34.5 MPa and its shear strength ≥20 MPa.

The porous structure allows bone cells to "penetrate" into the implant, leading to a reduced rejection reaction. However, these pores also provide the bacterial cells with an increased surface area for adherence (Shoji and Chen, 2020; Idrees et al., 2021). The commercially pure titanium (cpTi) coating with a layer thickness of 300 ± 50 µm was sprayed onto the disc surfaces using a vacuum plasma spray (VPS). The resulting coating had a porosity of 30 ± 10%, an average roughness of 50 ± 15 µm, a tensile strength of ≥22 MPa and a shear strength of ≥20 MPa. cpTi covered materials show an improved osteogenic differentiation potential (Lohberger et al., 2020a), since the given porous upper layer in combination with the increase in surface energy offers the bone cells an optimal structure for adhesion (Geetha et al., 2009). Tricalcium phosphate coating (TCP, Bonit®) led to a deposited layer of 20 ± 10 µm thickness and to a tensile strength of ≥15 MPa (ISO 13779-2, 2018). TCP consist of 70% brushite ($CaHPO_4 2 \bullet H_2O$) and 30% hydroxyapatite ($Ca_5(PO_4)_3OH$). The calcium phosphate provides an advantage for osteoinduction to its surface as its bioactivity is highly similar to that of bone material and it thus facilitates improved cell growth and cytocompatibility (Dantas et al., 2018).

Scanning Electron Microscopy (SEM)

SEM investigations were performed on a FEI Quanta 250 FEG (Thermo Fisher Scientific, Hillsboro, OR) under high vacuum conditions and 20 kV high tension. The micrographs were recorded in secondary electron (SE) mode with the Everhart–Thornley detector. The disc surfaces of the material were sputter coated with a gold layer (10 nm) to provide adequate electrical conductivity. The energy-dispersive X-ray spectroscopy (EDX) data collection measurements took 60 s each at 20 kV high tension and a Spotsize of 4.5 with a 30 mm^2 Octane Elect Plus Silicon Drift Detector (EDAX Ametek, NJ, USA) and the APEX Standard Software (V1.3.1, 07/2019) was used.

Bacterial Cultures

For each experimental run, one overnight culture was prepared for each *S. aureus* subsp. *aureus* strain Newman D2C (ATCC 25904, Wesel, Germany; also referred to as NCTC 10833 or *S. aureus* subsp. *aureus* Rosenbach) and *S. epidermidis* (ATCC 14990, Wesel, Germany; also referred to as NCTC 11047). Luria–Bertani broth (LB broth) containing 10 g/L tryptone, 5 g/L yeast extract (both Carl Roth), and 5 g/L sodium chloride (Merck, Darmstadt, Germany) was used as growth medium. Per strain one CRYOBANK® pearl (MAST Group, Reinfeld, Germany) was inoculated into 100 ml LB and cultures were incubated at 37°C at 90 rpm.

Biofilm Assay

The material discs (4 discs per material, all 6 materials) were placed in 24-well untreated clear polystyrene plates (Corning®, Wiesbaden, Germany) as shown in **Figure 1**. The bacterial cells from the overnight culture were distributed into 1.5 ml Eppendorf tubes and collected by centrifugation (14,000 rpm, 2 min). The supernatant was discarded and the cells where resuspended and washed in 1.5 ml of phosphate buffered solution (PBS). Cells were centrifuged again (14,000 rpm, 2 min) and then freshly inoculated into LB broth. The cell number was adjusted to 1.5×10^8 CFU/ml in LB broth and 1.5 ml of the adjusted cell solution was added to each well. The plate was then sealed with a Breathe Easy® sealing membrane (Merck, Darmstadt, Germany) and incubated for 48 h at 37°C and 90 rpm. A total of 4 discs per material and species were prepared for each of the 21 experimental runs (biological replicates). Growth controls (bacteria without discs) and sterile controls (sterile LB media on material discs) were run in parallel for every experimental run.

Biofilm Processing

For the collection of the samples the medium was first gently removed without disturbing the biofilm and 1.5 ml PBS was

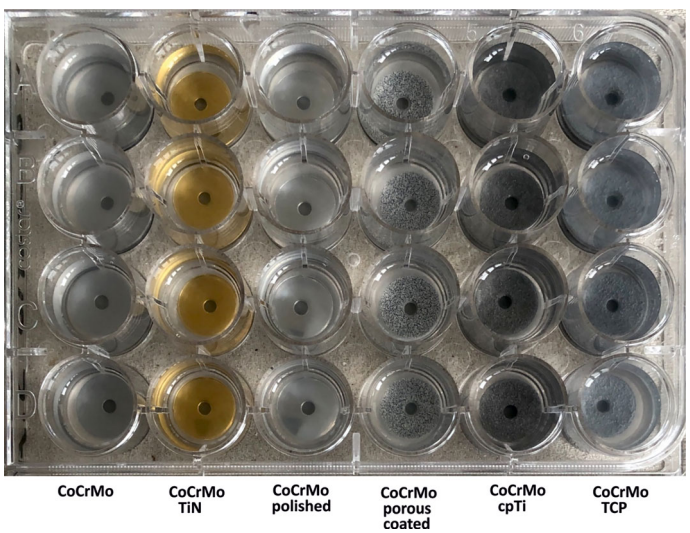

FIGURE 1 | Cell culture plate with the different alloy discs.

added into each well. The discs were picked up using tweezers, shaken within the PBS and the biofilm from all sides of the disk was scraped into a fresh PBS filled well with a mini cell scraper (Biotium, Freemont, CA, USA). At the end of the process the scraper was vigorously rotated in the well to ensure that no biofilm residues remained on the scraper. The content of two wells per material was pooled in a 3.5 ml tube and vortexed until no biofilm parts were visible. This step took up to 30 min on the vortexer in continuous mode and random samples were checked microscopically to ensure that there were no more biofilm parts in the samples before further processing. The growth controls were re-suspended in the medium and then transferred into 3.5 ml tubes; the sterile controls were also pipetted into the individual collection tubes directly. The resulting 3 ml sample volume (per biofilm pool and controls) was divided to provide the volumes needed for the four different measurement protocols (see below). Samples for genetic analysis were frozen at −80°C until further processing, all protein and polysaccharide samples were stored in the fridge at 4°C for no longer than 24 h before analysis, flow cytometry was performed directly after biofilm processing and samples were kept at 4°C until loading onto the instrument.

Polysaccharide Quantification

Polysaccharides of the total biofilm were quantified using an adapted version of an sulfuric acid phenol extraction method (Cuesta et al., 2003). Approximately 250 µl of each sample, 250 µl 99.5% phenol, and 750 µl 95–98% sulfuric acid were added to heat-resistant glass tubes, sealed with aluminum foil (not air tight) and vortexed for at least 20 s. Incubation took place in a water bath at 100°C for 10 min. In an additional water bath samples were cooled to 25°C, vortexed again and 250 µl was transferred into uncoated U-bottom 96-well plates (BRAND®, Sigma-Aldrich, Darmstadt, Germany). Absorbance was read at 490 nm in the Multiskan Sky Microplate Spectrophotometer (Thermo Fisher Scientific). Each sample was measured twice and the statistical mean was compared to a standard glucose curve (Merck; 0–1.5 µg/ml).

Protein Quantification

The 'Pierce ™ BCA Protein Assay Kit' (Thermo Fisher Scientific, Waltham, MA, USA) was used to measure the total protein content of the biofilms. The 562 nm absorbance values of the samples (25 µl sample in 200 µl working reagent from the kit) in uncoated U-bottom 96-well plate were read on a Multiskan Sky Microplate Spectrophotometer. Each sample was measured twice. The standard curve was prepared with bovine serum albumin (BSA, supplied with the BCA kit; 0–2,000 µg/ml, Thermo Fisher Scientific, Waltham, MA, USA) and the arithmetic mean of the duplicate measurement was compared to the curve.

Live Dead Assay

Flow cytometric cell counts were performed applying the 'LIVE/DEAD® BacLightTM Viability Kit (Invitrogen, Carlsbad, CA, USA) for microscopy and quantitative assays'. The Syto9® and propidium iodide dye mixes were freshly prepared for each measurement in a ratio of 1:1. Per sample, 1 ml was stained with 1 µl of the dye mixture and incubated in the dark for 15 min at room temperature and 100 µl per sample were analyzed on a Cyflow® Cube 6 flow cytometer (Sysmex Europe GmbH, Norderstedt, Germany). The flow rate was set at 2 µl/s and a 488 nm laser was used. All samples were measured twice and to avoid signal carryover, cleaning was performed between all measurements.

Statistics

SPSS (IBM, version 25) was used for statistical analyses of protein, polysaccharide, and flow cytometry data. The data was found to be non-Gaussian (Kolmogorov–Smirnov test with Lilliefors correction). Consequently, the Kruskal–Wallis H test was applied. Statistical differences were tested in a pairwise comparison format and the Bonferroni correction for the Kruskal–Wallis test was used.

RNA Isolation

RNA from the samples of three independent experimental runs (3 biological replicates) was extracted with the Monarch® Total RNA Miniprep Kit (New England BioLabs, Ipswich, MA, USA). The enzymatic approach step of the manufacturer's protocol was adapted: additionally, 0.1 mg/ml lysostaphin (Sigma-Aldrich, Darmstadt, Germany) was added to the 3 mg/ml lysozyme which was provided with the kit. Samples were incubated for 25 min at 350 rpm at 37°C before carrying out the rest of the protocol according to the guidelines. Final elution volume was 30 µl per sample.

RT-qPCR

Using the iScript cDNA Synthesis Kit (BioRad Laboratories Inc., Veenendal, The Netherlands) 1 µg RNA was reverse-transcribed with a mixture of oligo (dT) and random hexamer primers. The samples were amplified with the SsoAdvanced Universal SYBR Green Supermix and subsequently measured on a CFX96 Touch (BioRad Laboratories Inc.), as described elsewhere (Lohberger et al., 2020b). A standard 3-step PCR temperature protocol was used with an annealing temperature of 60°C followed by a melting curve protocol to confirm a single gene-specific peak and to detect primer dimerization. The ΔΔCt method was applied for the calculation of the relative quantification of expression levels by means of the geometric mean of the internal control (16s rRNA gene for *S. aureus* and also for *S. epidermidis*; for primer sequences see **Table 1**). The expression levels (Ct) of the target genes were normalized to the reference genes (ΔCt). The ΔΔCt value was calculated using the difference between the ΔCt value of the test sample and the ΔCt of the control sample. The final expression ratio was expressed as 2ΔΔCt (Livak and Schmittgen, 2001). Primers used for RT-qPCR were purchased from Eurofins Genomics (Ebersberg, Germany) and primer sequences are listed in **Table 1**.

RESULTS

Material Surface Characteristics

The surface characteristics of the different modifications to the CoCrMo alloy discs have been studied using both SEM and EDX

TABLE 1 | Primes used in RT-q-PCR.

Strain	Gene	Primer forward	Primer reverse	Reference
S. aureus	*icaA*	5-GAGGTAAAGCCAACGCACTC-3	5-CCTGTAACCGCACCAAGTTT-3	Atshan et al. (2013)
	icaC	5-CTTGGGTATTTGCACGCATT-3	5-GCAATATCATGCCGACACCT-3	Atshan et al. (2013)
	fnbA	5-AAATTGGGAGCAGCATCAGT-3	5-GCAGCTGAATTCCCATTTTC-3	Atshan et al. (2013))
	fnbB	5-ACGCTCAAGGCGACGGCAAAG-3	5-ACCTTCTGCATGACCTTCTGCACCT-3	Atshan et al. (2013)
	clfB	5-AACTCCAGGGCCGCCGGTTG-3	5-CCTGAGTCGCTGTCTGAGCCTGAG-3	Atshan et al. (2013)
	atl	5-TTTGGTTTCCAGAGCCAGAC-3	5-TTGGGTTAAAGAAGGCGATG-3	Yin et al. (2018)
	16S rRNA	5′-GGGACCCGCACAAGCGGTGG-3′	5′-GGGTTGCGCTCGTTGCGGGA-3′	Atshan et al. (2013)
S. epidermidis	*atlE*	5-TGTCCTGCTTTCACGTATGA-3	3-TCTTTGGAATTGGTGCATTT-5	Patel et al. (2012)
	aap	5-TGATCGGATCTCCATCAACT-3	3-AAGGTAGCCAAGAGGACGTT-5	Patel et al. (2012)
	16S rRNA	5′TACACACCGCCCGTCACA	5′CTTCGACGGGCTAGCTCCAAAT	Vandecasteele et al. (2001)

analyses. The topographic characteristics of materials are well known to have a substantial influence on the adhesive properties of bacterial cells and therefore the microscopic investigation is helpful for understanding the data collected in this study. While the base alloy CoCrMo without modifications shows a rather smooth surface at ×100 magnification (**Figure 2A**), a closer look (×10,000, **Figure 2A** inlay) reveals only some cracks and some unevenness and the surface modification with TiN and the polished surface are even smoother. However, the porous coated surface and the cpTi and TCP covered surfaces show very distinct topographic characteristics. While the porous coated surface consists of a thick layer of evenly distributed (**Figure 2D**) and rather smooth balls (surface of the ball in the inlay of **Figure 2D**), the cpTi layer is rougher (**Figure 2E**) and the higher magnification also reveals that this characteristic is also true at the small µm range (inlay **Figure 2E**). Very distinctly different from the rest, the TCP layer forms sharp crystalline structures protruding from the alloy surface (**Figure 2F**). Looking at the surface characteristics, the surfaces can be categorized as either smooth (CoCrMo, CoCrMo TiN, and CoCrMo polished) or rough (CoCrMo porous coated, CoCrMo cpTi, and CoCrMo TCP).

The corresponding EDX data supports the material descriptions given in the material and methods section, showing the elemental composition of the materials as spectrograms and in weight and atom percentages (**Figures 3A–E**; data not available for TCP).

Polysaccharide Content

As all *Staphylococci* can produce polysaccharides in their EPS when forming biofilms (Arciola et al., 2015), an approach that is often applied is to break the polysaccharides down into monosaccharides and measure the content compared to a glucose standard curve (Cuesta et al., 2003). Following this procedure, we found (**Table 2** and **Figure 4**) that the biofilms grown on the smooth surfaces (CoCrMo, CoCrMo TiN, and

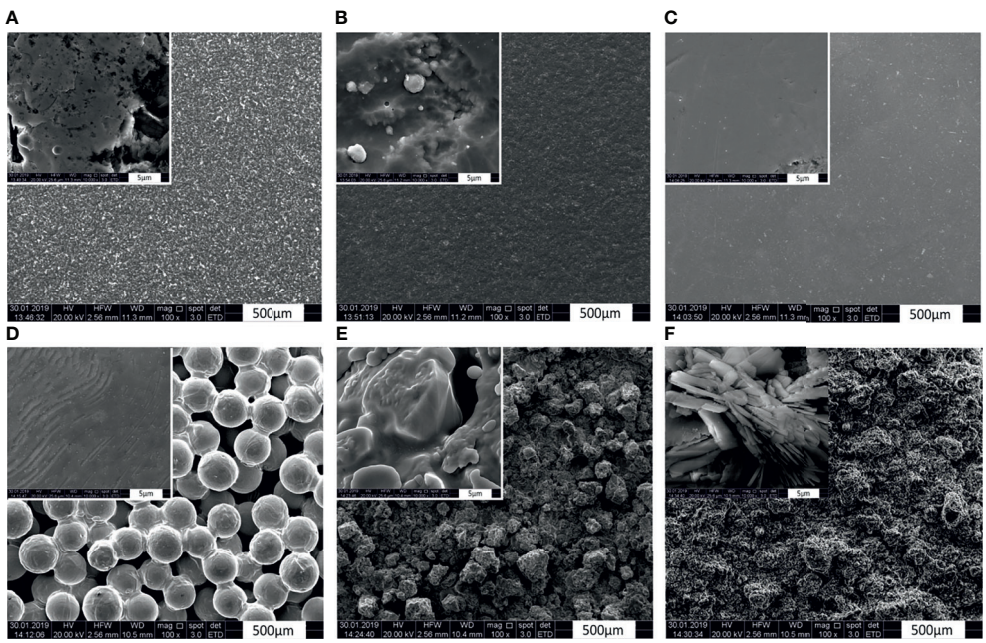

FIGURE 2 | Scanning electron microphotographs of CoCrMo and the different surface modifications. Magnification factor ×100, and inlays ×10,000. **(A)** CoCrMo; **(B)** CoCrMo TiN; **(C)** CoCrMo polished; **(D)** CoCrMo porous coated; **(E)** CoCrMo cpTi, **(F)** CoCrMo TCP.

CoCrMo polished) show a tendency to form less polysaccharide in their EPS compared to those grown on the rough surfaces (CoCrMo porous coated, CoCrMo cpTi, and CoCrMo TCP). The highest polysaccharide levels for *S. aureus* were measured in biofilms grown on CoCrMo cpTi discs with a mean value of 5.69 ± 1.5 µg/ml, the lowest values were measured in biofilms from the CoCrMo TiN and the CoCrMo polished discs with 4.15 ± 0.71 µg/ml and ±0.8 µg/ml respectively (**Table 2**). *S. epidermidis* biofilms showed the highest polysaccharide values on CoCrMo cpTi (6.21 ± 3.06 µg/ml) and the lowest ones on CoCrMo TiN (4.11 ± 0.78 µg/ml) (**Table 2**). In both species the polysaccharide content of the biofilms grown on CoCrMo porous coated, CoCrMo cpTi and CoCrMo TCP shows a highly significant difference ($p < 0.001$) compared to that of the CoCrMo alloy itself (**Figure 4**). **Table 3** summarizes all group comparisons (each alloy compared to each) where a clear statistical difference can be seen whenever a smooth surface is compared to a rough surface. One exception here is the comparison of *S. epidermidis* biofilms on CoCrMo porous coated with biofilms from CoCrMo cpTi surfaces where, in the overall group comparison (adjusted p-value for multiple comparisons), no statistical difference is found (adj. p-value = 0.055). However, if the multiple comparison is disregarded, which is possible in a direct comparison of the two groups in question, the difference becomes significant again ($p = 0.004$). This leads to the conclusion that the CoCrMo porous coated surface is the best performer (smallest biofilm content) in the rough surface group. Additionally, in the

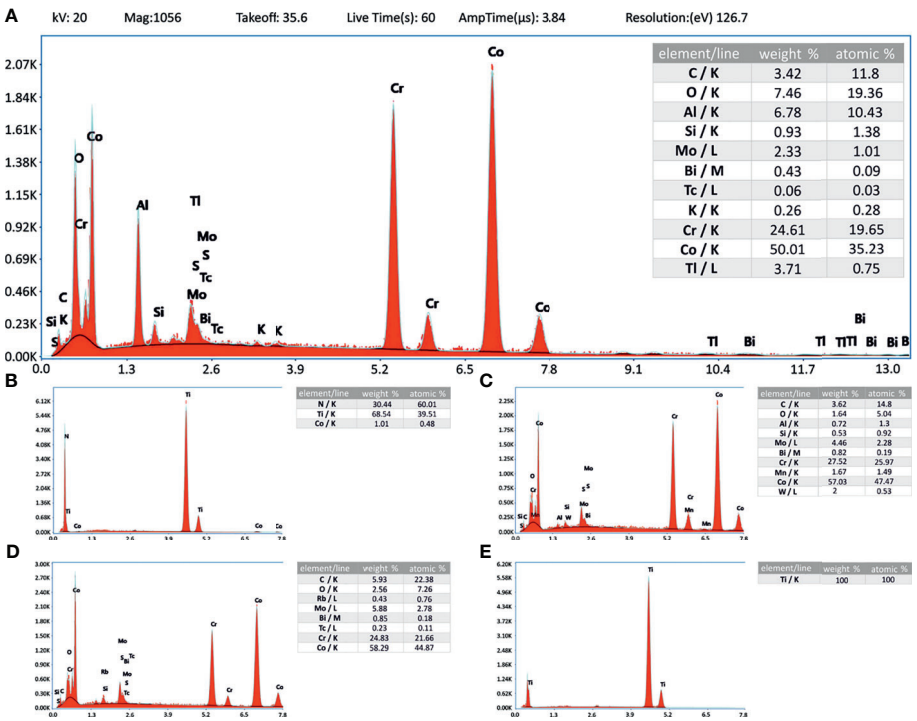

FIGURE 3 | Energy-dispersive X-ray analysis. Inlay tables showing the elemental composition related to the energy level (K-, L- and M-line). Instrument values are given in panel **(A)** and apply also to **(B–E)**. **(A)** CoCrMo; **(B)** CoCrMo TiN; **(C)** CoCrMo polished; **(D)** CoCrMo porous coated; **(E)** CoCrMo cpTi.

TABLE 2 | Mean, minimum and maximum values and standard deviations (SD; 95% confidence interval) of protein and polysaccharide measurements.

Alloy	*S. aureus*				*S. epidermidis*			
	Proteins [µg/ml]		Polysaccharides [µg/ml]		Proteins [µg/ml]		Polysaccharides [µg/ml]	
	mean [min; max] (n = 42)	SD	mean [min; max] (n = 44)	SD	mean [min; max] (n = 42)	SD	mean [min; max] (n = 44)	SD
CoCrMo	124.56 [68.10; 214.10]	34.89	4.46 [3.47; 7.74]	0.91	101.95 [36.5; 203.5]	34.78	4.23 [3.25; 6.47]	0.75
CoCrMo TiN	97.55 [55.40; 148.60]	28.12	4.15 [3.27; 5.82]	0.71	77.65 [26.7; 162.4]	32.12	4.11 [3.15; 7.13]	0.78
CoCrMo polished	96.57 [41.80; 179.40]	30.8	4.15 [3.3; 6.75]	0.8	76.43 [31; 145.6]	30.22	4.12 [3.25; 7;50]	0.87
CoCrMo porous coated	225.33 [64.40; 301.70]	41.88	4.89 [3.77; 6.73]	0.78	207.32 [149; 275.5]	35.68	5.59 [3.77; 29.57]	3.88
CoCrMo cpTi	202.87 [121.20; 269.70]	35.5	5.69 [4.17; 9.01]	1.5	190.23 [115.1; 341.1]	42.79	6.21 [3.76; 22.69]	3.06
CoCrMo TCP	240.08 [153.10; 455.60]	58.6	5.24 [3.95; 8.53]	1.14	215.51 [113.3; 356.6]	56.42	5.27 [3.67; 8.51]	1.19

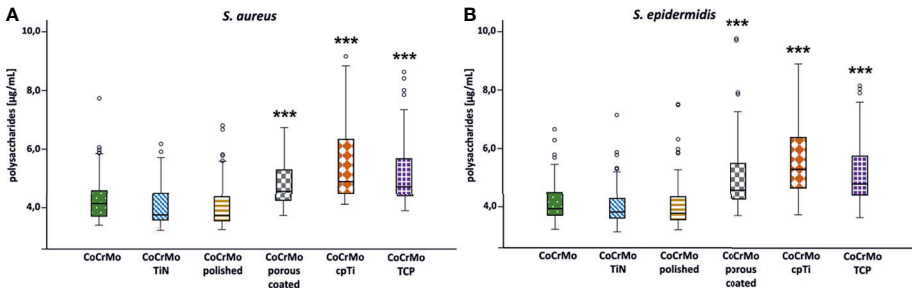

FIGURE 4 | Polysaccharide concentration of *S. aureus* (**A**; n = 42) and *S. epidermidis* (**B**; n = 44) biofilms. Statistically significant differences to CoCrMo are marked *** (adjusted significance < 0.001, Bonferroni correction for the Kruskal–Wallis test).

direct comparison of CoCrMo with CoCrMo polished (p = 0.006), a statistically significant difference is also detected, showing a better performance (less polysaccharides) compared with biofilms grown on the polished CoCrMo surface (again no significant difference in the adj. p-value = 0.086). Overall, CoCrMo polished performs the best with respect to polysaccharide formation of biofilms.

Protein Content

Proteins in the bacterial EPS function as glue which sticks the biofilms to the surface. Measurements of proteins often employ colorimetric methods using the reduction of Cu^{2+} to Cu^{1+} copper ions in alkaline medium and compare the protein content to a bovine serum albumin (BSA) standard. Using a variation of this method (Pierce™ BCA Protein Assay Kit) we found that the highest protein levels in *S. aureus* occurred in biofilms (namely, EPS and cells) grown on CoCrMo TCP discs with a mean value of 240.08 ± 58.6 µg/ml. The lowest values for *S. aureus* were measured in biofilms from the CoCrMo polished discs with 96.57 ± 30.8 µg/ml (**Table 2**). *S. epidermidis* biofilms showed the highest polysaccharide values on CoCrMo TCP as well (215.51 ± 56.42 µg/ml) and the lowest ones on CoCrMo polished (76.43 ± 30.22 µg/ml) (**Table 2**). All *S. aureus* and all *S. epidermidis* biofilms from rough surfaces (CoCrMo porous coated, CoCrMo cpTi, CoCrMo TCP) have statistically significantly higher protein values (p <0.001) when compared to the base alloy (**Figure 5**). Again, all smooth surfaces have a statistically significantly better outcome compared to the rough surfaces (**Table 3**) when comparing them against each other separately. Additionally, in the case of *S. aureus*, CoCrMo polished and CoCrMo TiN perform statistically significantly better than CoCrMo (p = 0.004 and p = 0.005; meaning lower protein content) in the single comparison of groups (this significance however is not applicable for the multiple comparison; p = 0.058), leading overall to the best performance of CoCrMo polished. For the direct group comparison of *S. epidermidis* biofilm on CoCrMo compared to CoCrMo polished (less protein) this also applies (p = 0.006; adj p = 0.086). When considering the cpTi rough surfaces and *S. aureus*, CoCrMo cpTi results in less biofilm protein compared to CoCrMo TCP (p = 0.023; adj p = 0.341).

TABLE 3 | Statistical pairwise comparison of alloys according to the protein and polysaccharide content of the *S. aureus* and *S. epidermidis* biofilms.

Alloy 1	Alloy 2	*S. aureus*				*S. epidermidis*			
		Proteins		Polysaccharides		Proteins		Polysaccharides	
		p-value	adj. p-value	p-value	adj. p-value	p-value	adj. p-value	p-value	adj. p-value
CoCrMo	CoCrMo TiN	0.005	0.074	0.036	0.539	0.011	0.162	0.255	1.000
CoCrMo	CoCrMo polished	0.004	0.058	0.012	0.178	0.006	0.086	0.212	1.000
CoCrMo	CoCrMo porous coated	0.000	0.000	0.000	0.002	0.000	0.000	0.000	0.000
CoCrMo	CoCrMo cpTi	0.000	0.000	0.000	0.000	0.000	0.000	0.000	0.000
CoCrMo	CoCrMo TCP	0.000	0.000	0.000	0.005	0.000	0.000	0.000	0.000
CoCrMo TiN	CoCrMo polished	0.939	1.000	0.675	1.000	0.850	1.000	0.912	1.000
CoCrMo TiN	CoCrMo porous coated	0.000	0.000	0.000	0.001	0.000	0.000	0.000	0.000
CoCrMo TiN	CoCrMo cpTi	0.000	0.000	0.000	0.000	0.000	0.000	0.000	0.000
CoCrMo TiN	CoCrMo TCP	0.000	0.000	0.000	0.000	0.000	0.000	0.000	0.000
CoCrMo polished	CoCrMo porous coated	0.000	0.000	0.000	0.000	0.000	0.000	0.000	0.000
CoCrMo polished	CoCrMo cpTi	0.000	0.000	0.000	0.000	0.000	0.000	0.000	0.000
CoCrMo polished	CoCrMo TCP	0.000	0.000	0.000	0.000	0.000	0.000	0.000	0.000
CoCrMo porous coated	CoCrMo cpTi	0.042	0.632	0.006	0.086	0.076	1.000	0.004	0.055
CoCrMo porous coated	CoCrMo TCP	0.806	1.000	0.199	1.000	0.995	1.000	0.270	1.000
CoCrMo cpTi	CoCrMo TCP	0.023	0.341	0.139	1.000	0.077	1.000	0.072	1.000

P-values (Kruskal–Wallis test); adjusted p-values (Bonferroni correction for the Kruskal–Wallis test of multiple comparisons; $\alpha = 5\%$); smooth surfaces (CoCrMo, CoCrMo TiN, CoCrMo polished) underlaid in light blue; rough surfaces (CoCrMo porous coated, CoCrMo cpTi, CoCrMo TCP) underlaid in gray; p < 0.05 also marked in green.

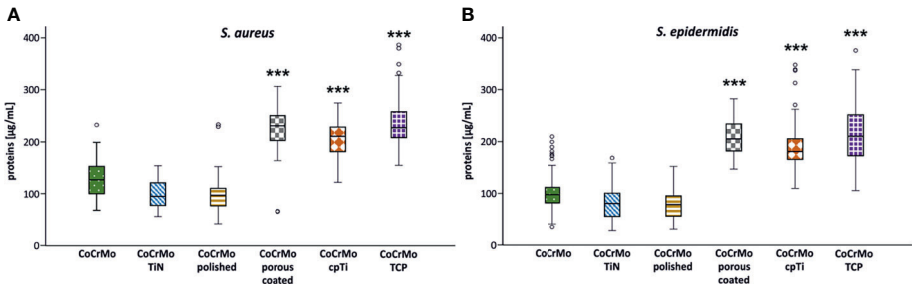

FIGURE 5 | Protein concentration of *S. aureus* (**A**; n = 42) and *S. epidermidis* (**B**; n = 44) biofilms. Statistically significant differences to CoCrMo are marked *** (adjusted significance < 0.001, Bonferroni correction for the Kruskal–Wallis test).

Flow Cytometric Cell Enumeration

Flow cytometric measurements on the samples were meant to show a live-dead count. However, it seems that within 48 h of growth, the dead cell count is negligible which is why the flow cytometry data are only used for cell enumeration. For both species no statistical differences in the number of bacterial cells have been detected (**Figure 6**).

RT-qPCR

Many genes are involved in the biofilm development of *S. aureus* and *S. epidermidis*. A few of them have been chosen to understand the genetic reaction of both species to the different CoCrMo surfaces. Again, the different surface modifications were statistically compared to the base alloy in terms of gene expression levels of the biofilms harvested after 48 h of development (**Figure 7**). For *S. aureus*, *icaA*, and *icaC* were selected from the intercellular adhesion group of genes (*ica*) which is of specific interest for the starting phase in biofilm development. Only CoCrMo TCP showed a significantly decreased level of gene expression for both genes (**Figures 7A, B**). Looking at the fibronectin binding protein *fnb*A gene, our data also shows a significantly increased level for CoCrMo TCP biofilms. However, the closely connected *fnb*B was significantly elevated only in CoCrMo TiN. The *clf*B (bacterial ligand clumping factor) gene of *S. aureus* was, with $p < 0.05$, decreased in CoCrMo TCP, whereas the major autolysine gene (*atl*) showed no significant changes in any of the surface modification biofilms of *S. aureus*. Of the two genes tested for *S. epidermidis*, the major autolysine (*atlE*) also did not show any differences. However, the expression of the *aap* (accumulation association protein) gene was significantly reduced in CoCrMo porous coated and CoCrMo cpTi, but interestingly, not in the third rough surface modification CoCrMo TCP which showed elevated levels (not significant).

DISCUSSION

Biofilm evaluation begins with the organisms chosen for the experiment. *S. aureus* and *S. epidermidis* are the most common causes of periprosthetic infections and have therefor been the model organisms for this study. But also, within the *S. aureus* and *S. epidermidis* isolates, differences in biofilm forming abilities exist, making it difficult to generalize results. *S. aureus* Newman has already been used for many studies on biofilm formation (e.g., Johnson et al., 2008; Abraham and Jefferson, 2012; Forson et al., 2020; Inés Molina et al., 2020; Pinto et al., 2020) although it is not considered a very good biofilm forming strain and the same is true for the *ica* negative *S. epidermidis* strain (e.g., Stepanovic et al., 2000; Lee et al., 2016; Paduszynska et al., 2019; Di Pilato et al., 2020; Paulitsch-Fuchs et al., 2021). However, the variant of the *S. aureus* strain used in this study *S. aureus* Newman D2C is considered to be a relatively good biofilm forming strain (Grundmeier et al., 2004; Tsompanidou et al., 2010; Abraham and Jefferson, 2012; Dauros-Singorenko et al., 2020; Paulitsch-Fuchs et al., 2021). Abraham and Jefferson (2012) showed that the autolysin activity in the Newman D2C variant was low enough to allow the expression of ClfB on the cell surface, which seems to be (at least partly) responsible for the difference in biofilm forming abilities between the two strains. The issue about different *S. aureus* Newman strains deposited to the reference centers with similar names and therefore leading to seemingly controversial results has also already been pointed out, e.g., by Grundmeier et al. (2004). It also has been shown previously (Dauros-Singorenko et al., 2020) that the D2C Newman strain expresses the *agr* (accessory gene regulation) quorum sensing system, which would normally mean that the dispersion in biofilms takes place rather easily (Paulander et al., 2018). However the LB medium we used is iron-rich (Abdul-Tehrani et al., 1999) and high iron contents did show a negative influence on *agr* expression in the hemoglobin study by Dauros-Singorenko et al. (2020), therefore possibly promoting biofilm formation of *S. aureus* Newman D2C in LB medium. This leads to another main influence on biofilm growth which is the medium used for the experiments. Several studies compared different growth media and their influence on the biofilm formation of *S. aureus* and other species (Del mar Cendra et al., 2019; Wijesinghe et al., 2019; Zhou et al., 2019; Liu et al., 2020). For example, in one study LB medium showed the second best performance for biofilm formation in *Pseudomonas aeruginosa* and *S. aureus* (Zhou et al., 2019), in another study (Del mar Cendra et al., 2019) LB medium also promoted the biofilm growth for *S. aureus* Newman (although the wildtype strain was used). A variety of differences exist also for LB

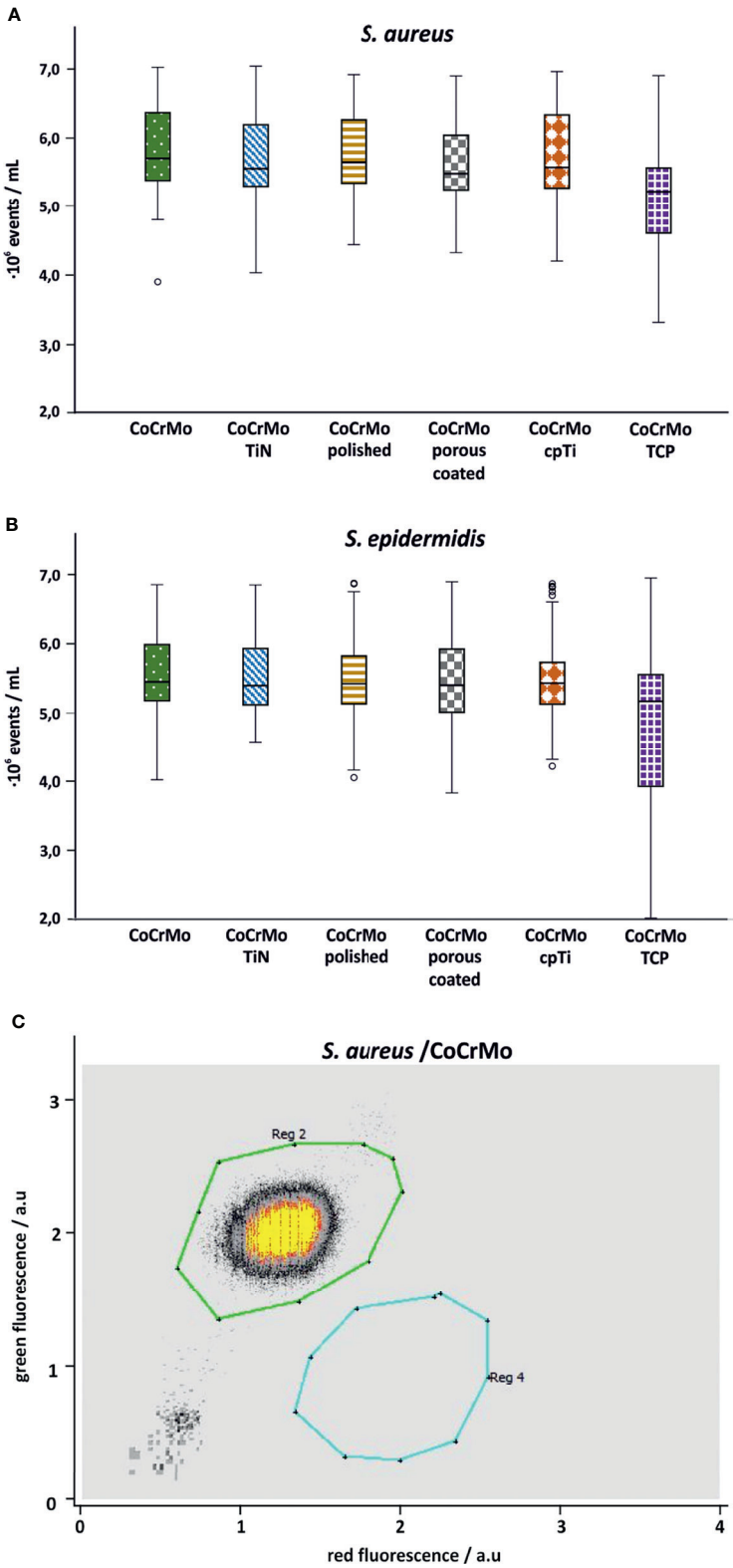

FIGURE 6 | Flow cytometry cell counts for *S. aureus* (**A**; n = 42) and *S. epidermidis* (**B**; n = 44). Subpanel **(C)** shows a representative measurement of *S. aureus* on CoCrMo (Reg 2: living cells; Reg 4: dead cells).

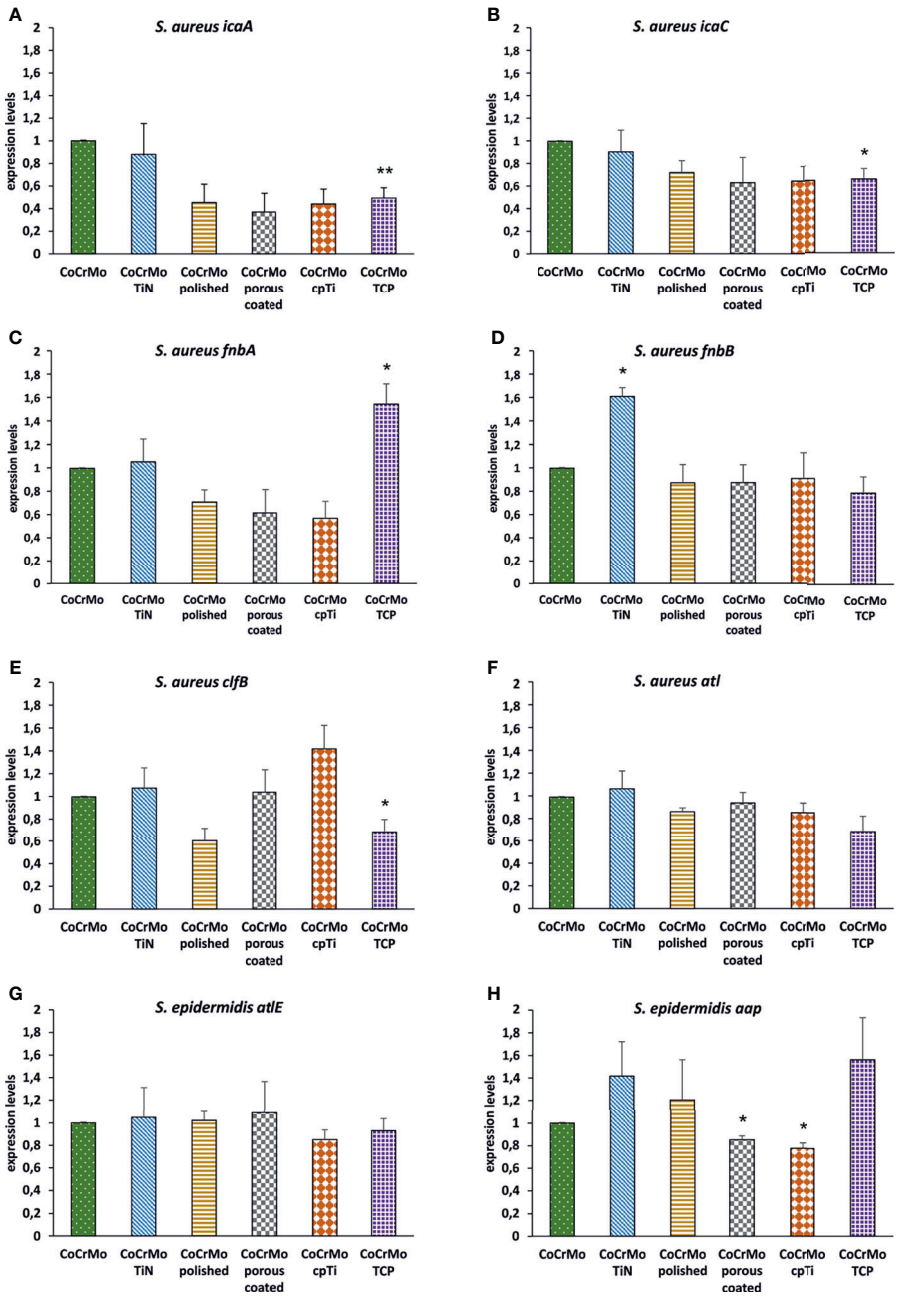

FIGURE 7 | Expression levels of biofilm-associated genes. *S. aureus* (**A**–**F**; n = 3) and *S. epidermidis* (**G**, **H**; n = 3); error bars show the standard error of the mean; statistically significant differences to CoCrMo are marked * (p <0.05).

medium recipes (e.g., supplemented with glucose, higher or lower NaCl content) and most other growth media. Lastly also the number of bacterial cells inoculated for biofilm formation varies greatly in the different studies on this topic. As little as OD_{550} of 0.10 (~0.015×10^7 cells/ml) (Del mar Cendra et al., 2019) and also higher cell numbers of 1×10^7 CFU/ml (Dauros-Singorenko et al., 2020) and inoculum sizes using 0.5 MacFarland cell suspensions (1.5×10^8 cells/ml) (Wijesinghe et al., 2019) are implemented for biofilm studies. Therefore, the choice of the strains, inoculum size and media used in biofilm studies has to be well thought of.

Although the interaction of biofilms with the respected surfaces they grown on is a key factor as well, still understanding is lacking in some areas of this interaction, e.g., the influence of surface roughness on biofilm development and its connection to the regulation of genes connected to biofilm formation. For an

TABLE 4 | Overall comparison of the results of protein, polysaccharide and genetic measurements.

All values compared to CoCrMo	*S. aureus*								*S. epidermidis*			
	Proteins	**Glucose**	***icaA***	***icaC***	***fnbA***	***fnbB***	***clfB***	***atl***	**Proteins**	**Glucose**	***atlE***	***aap***
CoCrMo TiN	–	–	–	–	–	↑	–	–	–	–	–	–
CoCrMo polished	–	–	–	–	–	–	–	–	–	–	–	–
CoCrMo porous coated	↑↑↑	–	–	–	–	–	–	–	↑	↑↑↑	–	↓
CoCrMo cpTi	↑↑↑	↑↑↑	–	–	–	–	–	–	↑↑↑	↑↑↑	–	↓
CoCrMo TCP	↑↑↑	–	↓↓	↓	–	–	–	–	↑↑↑	↑↑↑	–	–

↑, ↑↑ and ↑↑↑ (also underlaid in green; adjusted significance <0.05, <0.01 and 0.001 according to the Bonferroni correction for the Kruskal–Wallis test) and ↓, and ↓↓ (also underlaid in orange; adjusted significance <0.05 and <0.01 according to the Bonferroni correction for the Kruskal–Wallis test).

overview and to facilitate this connection, **Table 4** provides an overall comparison of protein, polysaccharide and gene expression results.

The surfaces studied here vary widely in their surface characteristics and structure (see **Figure 2**), thus providing a good variety of roughness for biofilm formation observations. Both protein and polysaccharide measurements are valuable measurements for the understanding of bacterial adherence and biofilm compactness in later stages of biofilm development. While host-proteins play an important role in the early conditioning of the implant thus strengthening the incorporation of the implant (Wang et al., 2017), proteins of biofilm organisms use the same properties to attach to the material in early biofilm development. Polysaccharides are important surface characteristics of bacterial cells and contribute to EPS development and to the attachment of bacterial cells to surfaces and to each other (Limoli et al., 2015). We show that the surface modifications resulting in rough surfaces (CoCrMo porous coated, CoCrMo cpTi, and CoCrMo TCP) have a higher polysaccharide and protein load in the biofilms than the smooth surfaces (CoCrMo TiN, CoCrMo polished) and the untreated control (CoCrMo). In most cases this is a statistically significant difference and holds for most of the comparisons of the alloys to each other as well (see **Table 3**). Those results are in accordance with earlier studies on the topic (Öztürk et al., 2007; Yoda et al., 2014; Kunrath et al., 2020; Palka et al., 2020; Paulitsch-Fuchs et al., 2021), supporting the conclusion that the higher surface roughness is beneficial for protein and polysaccharide rich biofilms on the surfaces studied here. However, in a review by Zheng et al. (2021), the influence of surface structures has been recently summarized showing that generally, bacteria tend to attach to surfaces more easily when they have a certain roughness, however there are also some rough surfaces achieving the opposite and also different bacterial species can react in different ways to the same surface.

Biofilm gene regulation did not show particularly big differences between the compared groups. As no RNA*later*® or comparable reagent was used to freeze the transcriptome after biofilm removal a shift in the transcriptome might have occurred during the biofilm processing steps. However, as all samples were treated in the same way the relative impact is expected to be the same on the individual samples. For *S. aureus*, Resch et al. (2005) reported the genes *icaA* and *icaC*, which are commonly involved in early biofilm development, not to be upregulated in biofilms compared to planktonic growth after 48 h of growth. Expression of *icaA*, *icaC*, and *aap* gene regulation in *S. epidermidis* biofilms on different materials was reported by Patel et al. (2012) still to be active after 48 h of biofilm development. In an earlier study we found that on different Titanium-alloy surfaces the gene expression of the same set of genes of *S. aureus* Newman D2C followed a similar trend (Paulitsch-Fuchs et al., 2021) in that if there was a statistical difference in the regulation it was a decrease compared to the control (which was the untreated TiAl6V4 alloy, a rather smooth surface). Atshan et al. (2013) reported for four different MRSA isolates peak values of *fnbA*, *fnbB*, and *clfB* after 24 h. Comparing this with our results we conclude that the measurement point at 48 h is late into biofilm development and therefore no upregulation of the genes could be detected (with exception of fnbB on CoCrMo TiN). Together, the results point in the direction that the biofilm at 48 h is already well established and it is possibly not necessary that genes of early attachment are still upregulated. There is no difference in gene regulation between smooth and rough surfaces detectable at this timepoint. The *S. epidermidis* strain used in this study is *icaA* and *icaC* gene negative (this has been confirmed during this study; data not shown). As those genes are involved in the biosynthesis machinery necessary for PIA production in staphylococcal biofilms it is interesting that polysaccharides have been detected in the *S. epidermidis* strain which is *ica* negative. The explanation might be that other polysaccharide species (which are not regulated by the *ica* family of genes) are expressed in the strain used in this study. For example Spiliopoulou et al. (2012), have reported a 20-kDa polysaccharide (composed of glucose and N-acetylglucosamine) in the *S. epidermidis* EPS which is independent from *ica*. The two genes detected in the present study, *atlE* and *aap*, were both reported to be still active after 48 h of biofilm development by Patel et al. (2012). Similarly, the results presented here show an upregulation compared to the CoCrMo control on the smooth surfaces (not significant), the biofilms on the rough surfaces show a downregulation in at least one of the two genes after 48 h, CoCrMo cpTi in both genes (one of them significantly lower than the control). On those rough surfaces, the amount of proteins and polysaccharides was significantly higher in all cases, indicating that single cells in biofilms on rougher surfaces are producing a higher amount of proteins and polysaccharides. Otto (2013) shows a difference between early and late maturation phase in terms of

adhesive and disruptive factors. We speculate that the biofilms on the rough surfaces in our study do not need the *atlE* and *aap* gene products, which are involved mainly in mediation of the early attachment and in accumulation (Patel et al., 2012; Arciola et al., 2015), anymore. To prove this conclusively further studies on biofilm developmental stages are necessary.

In conclusion, the rough CoCrMo surface-modifications are prone to biofilms showing a higher amount of proteins and polysaccharides. The transcription rate of the genes studied here needs to be studied at different time points in order to draw a hard conclusion as to the impact of surfaces on the regulation of those genes. Follow-up studies therefore should include more time points, defined biofilm forming strains and clinical isolates for gene analysis in order to get a better understanding of time-dependent development. In addition, a study of human osteoblast cell cultures and bacterial cells being co-incubated on the surfaces might provide insights in the competition for the place on the surfaces.

DATA AVAILABILITY STATEMENT

The original contributions presented in the study are included in the article/supplementary material. Further inquiries can be directed to the corresponding author.

AUTHOR CONTRIBUTIONS

A.P-F.: Conceptualization, Methodology, Validation, Visualization, Supervision, Writing—Original Draft, Writing—Review & Editing, Project administration. B.B.: Investigation, Formal analysis, Writing Original Draft. L.W.: Investigation, Formal analysis, Visualization. N.D.: Statistical Assessment, Rewriting and Editing. N.E.: Investigation, Formal Analysis. B.L.: Funding acquisition, Project administration, Supervision, Writing—Review & Editing. All authors listed have made a substantial, direct, and intellectual contribution to the work and approved it for publication.

FUNDING

The authors acknowledge financial support from the FFG Bridge program (Grant No. 861608).

ACKNOWLEDGMENTS

We would like to thank our co-workers at the respective laboratories for their support concerning laboratory organization and the fruitful discussions.

REFERENCES

Abdul-Tehrani, H., Hudson, A. J., Chang, Y. S., Timms, A. R., Hawkins, C., Williams, J. M., et al. (1999). Ferritin Mutants of Escherichia Coli Are Iron Deficient and Growth Impaired, and Fur Mutants are Iron Deficient. *J. Bacteriol.* 181, 1415. doi: 10.1128/jb.181.5.1415-1428.1999

Abraham, N. M., and Jefferson, K. K. (2012). Staphylococcus Aureus Clumping Factor B Mediates Biofilm Formation in the Absence of Calcium. *Microbiology* 158, 1504. doi: 10.1099/MIC.0.057018-0

Arciola, C. R., Campoccia, D., Ravaioli, S., and Montanaro, L. (2015). Polysaccharide Intercellular Adhesin in Biofilm: Structural and Regulatory Aspects. *Front. Cell. Infect. Microbiol.* 5. doi: 10.3389/fcimb.2015.00007

Atshan, S. S., Shamsudin, M. N., Karunanidhi, A., van Belkum, A., Lung, L. T. T., Sekawi, Z., et al. (2013). Quantitative PCR Analysis of Genes Expressed During Biofilm Development of Methicillin Resistant Staphylococcus Aureus (MRSA). *Infect. Genet. Evol.* 18, 106–112. doi: 10.1016/j.meegid.2013.05.002

Chen, Q., and Thouas, G. A. (2015). Metallic Implant Biomaterials. *Mater. Sci. Eng. R Rep.* 87, 1–57. doi: 10.1016/j.mser.2014.10.001

Cuesta, G., Suarez, N., Bessio, M. I., Ferreira, F., and Massaldi, H. (2003). Quantitative Determination of Pneumococcal Capsular Polysaccharide Serotype 14 Using a Modification of Phenol-Sulfuric Acid Method. *J. Microbiol. Methods* 52, 69–73. doi: 10.1016/S0167-7012(02)00151-3

Dantas, T. A., Costa, M. M., Miranda, G., Silva, F. S., Abreu, C. S., and Gomes, J. R. (2018). Effect of HAp and β-TCP Incorporation on the Tribological Response of Ti6Al4V Biocomposites for Implant Parts. *J. Biomed. Mater. Res. - Part B Appl. Biomater.* 106, 1010–1016. doi: 10.1002/jbm.b.33908

Dauros-Singorenko, P., Wiles, S., and Swift, S. (2020). Staphylococcus Aureus Biofilms and Their Response to a Relevant *In Vivo* Iron Source. *Front. Microbiol.* 11. doi: 10.3389/FMICB.2020.509525/FULL

Davis, J. R. (2003). "Overview of Biomaterials and Their Use in Medical Devices," in *Handbook of Materials for Medical Devices* Russell Township (in Ohio, USA): ASM International. Ed. J. R. Davis. Russell Township (in Ohio, USA): ASM International. 1–11. doi: 10.1361/hmmd2003p001

Del mar Cendra, M., Blanco-Cabra, N., Pedraz, L., and Torrents, E. (2019). Optimal Environmental and Culture Conditions Allow the *In Vitro* Coexistence of Pseudomonas Aeruginosa and Staphylococcus Aureus in Stable Biofilms. *Sci. Rep.* 9, 1–17. doi: 10.1038/s41598-019-52726-0

Di Pilato, V., Ceccherini, F., Sennati, S., D'Agostino, F., Arena, F., D'Atanasio, N., et al. (2020). *In Vitro* Time-Kill Kinetics of Dalbavancin Against Staphylococcus Spp. Biofilms Over Prolonged Exposure Times. *Diagn. Microbiol. Infect. Dis.* 96, 114901. doi: 10.1016/J.DIAGMICROBIO.2019.114901

Forson, A. M., van der Mei, H. C., and Sjollema, J. (2020). Impact of Solid Surface Hydrophobicity and Micrococcal Nuclease Production on Staphylococcus Aureus Newman Biofilms. *Sci. Rep.* 10, 1–10. doi: 10.1038/S41598-020-69084-X

Geetha, M., Singh, A. K., Asokamani, R., and Gogia, A. K. (2009). Ti Based Biomaterials, the Ultimate Choice for Orthopaedic Implants - A Review. *Prog. Mater. Sci.* 54, 397–425. doi: 10.1016/j.pmatsci.2008.06.004

Grundmeier, M., Hussain, M., Becker, P., Heilmann, C., Peters, G., and Sinha, B. (2004). Truncation of Fibronectin-Binding Proteins in Staphylococcus Aureus Strain Newman Leads to Deficient Adherence and Host Cell Invasion Due to Loss of the Cell Wall Anchor Function. *Infect. Immun.* 72, 7155–7163. doi: 10.1128/IAI.72.12.7155-7163.2004

Idrees, M., Sawant, S., Karodia, N., and Rahman, A. (2021). Staphylococcus Aureus Biofilm: Morphology, Genetics, Pathogenesis and Treatment Strategies. *Int. J. Environ. Res. Public Heal.* 18, 7602 18, 7602. doi: 10.3390/IJERPH18147602

Inés Molina, R. D., Campos-Silva, R., Díaz, M. A., Macedo, A. J., Blázquez, M. A., Alberto, M. R., et al. (2020). Laurel Extracts Inhibit Quorum Sensing, Virulence Factors and Biofilm of Foodborne Pathogens. *LWT* 134, 109899. doi: 10.1016/J.LWT.2020.109899

ISO *ISO 13779-2:2018 - Implants for Surgery — Hydroxyapatite — Part 2: Thermally Sprayed Coatings of Hydroxyapatite*. Available at: https://www.iso.org/standard/64617.html (Accessed September 7, 2021).

ISO *ISO 5832-2:2018 - Implants for Surgery — Metallic Materials — Part 2: Unalloyed Titanium*. Available at: https://www.iso.org/standard/69907.html (Accessed September 3, 2021).

ISO *ISO 5832-3:2016 - Implants for Surgery — Metallic Materials — Part 3: Wrought Titanium 6-Aluminium 4-Vanadium Alloy*. Available at: https://www.iso.org/standard/66637.html (Accessed May 16, 2021).

ISO *ISO 6892-1:2019(En), Metallic Materials — Tensile Testing — Part 1: Method of Test at Room Temperature*. Available at: https://www.iso.org/obp/ui/#iso:std:iso:6892:-1:ed-3:v1:en (Accessed May 16, 2021).

Johnson, M., Cockayne, A., and Morrissey, J. A. (2008). Iron-Regulated Biofilm Formation in Staphylococcus Aureus Newman Requires Ica and the Secreted Protein Emp. *Infect. Immun.* 76, 1756. doi: 10.1128/IAI.01635-07

Kavanaugh, J. S., and Horswill, a. R. (2016). Impact of Environmental Cues on Staphylococcal Quorum Sensing and Biofilm Development. *J. Biol. Chem.* 291, 12556–12564. doi: 10.1074/jbc.R116.722710

Kim, M. K., Zhao, A., Wang, A., Brown, Z. Z., Muir, T. W., Stone, H. A., et al. (2017). Surface-Attached Molecules Control Staphylococcus Aureus Quorum Sensing and Biofilm Development. *Nat. Microbiol.* 2, 17080. doi: 10.1038/NMICROBIOL.2017.80

Kunrath, M. F., Monteiro, M. S. G., Gupta, S., Hubler, R., and de Oliveira, S. D. (2020). Influence of Titanium and Zirconia Modified Surfaces for Rapid Healing on Adhesion and Biofilm Formation of Staphylococcus Epidermidis. *Arch. Oral. Biol.* 117, 104824. doi: 10.1016/J.ARCHORALBIO.2020.104824

Lamret, F., Colin, M., Mongaret, C., Gangloff, S. C., and Reffuveille, F. (2020). Antibiotic Tolerance of Staphylococcus Aureus Biofilm in Periprosthetic Joint Infections and Antibiofilm Strategies. *Antibiot* 9, 547 9, 547. doi: 10.3390/ANTIBIOTICS9090547

Lee, J. H., Kim, Y. G., Yong Ryu, S., and Lee, J. (2016). Calcium-Chelating Alizarin and Other Anthraquinones Inhibit Biofilm Formation and the Hemolytic Activity of Staphylococcus Aureus. *Sci. Rep. 2016 61* 6, 1–11. doi: 10.1038/srep19267

Limoli, D. H., Jones, C. J., and Wozniak, D. J. (2015). Bacterial Extracellular Polysaccharides in Biofilm Formation and Function. *Microbiol. Spectr.* 3, 1–19. doi: 10.1128/MICROBIOLSPEC.MB-0011-2014

Liu, Y., Zhang, J., and Ji, Y. (2020). Environmental Factors Modulate Biofilm Formation by Staphylococcus Aureus. *Sci. Prog.* 103, 36850419898659. doi: 10.1177/0036850419898659

Livak, K. J., and Schmittgen, T. D. (2001). Analysis of Relative Gene Expression Data Using Real-Time Quantitative PCR and the 2-ΔΔCT Method. *Methods* 25, 402–408. doi: 10.1006/meth.2001.1262

Lohberger, B., Eck, N., Glaenzer, D., Lichtenegger, H., Ploszczanski, L., and Leithner, A. (2020a). Cobalt Chromium Molybdenum Surface Modifications Alter the Osteogenic Differentiation Potential of Human Mesenchymal Stem Cells. *Materials (Basel)* 13, 1–14. doi: 10.3390/ma13194292

Lohberger, B., Stuendl, N., Glaenzer, D., Rinner, B., Donohue, N., Lichtenegger, H. C., et al. (2020b). CoCrMo Surface Modifications Affect Biocompatibility, Adhesion, and Inflammation in Human Osteoblasts. *Sci. Rep.* 10, 1–8. doi: 10.1038/s41598-020-58742-9

Munir, K., Biesiekierski, A., Wen, C., and Li, Y. (2020). "Surface Modifications of Metallic Biomaterials,". In: *Metallic Biomaterials Processing and Medical Device Manufacturing*, ed. C. Wen (Cambridge, MA: Elsevier), 387–424. doi: 10.1016/b978-0-08-102965-7.00012-6

Otto, M. (2013). Staphylococcal Infections: Mechanisms of Biofilm Maturation and Detachment as Critical Determinants of Pathogenicity. *Annu. Rev. Med.* 64, 175–188. doi: 10.1146/annurev-med-042711-140023

Öztürk, O., Sudagidan, M., and Türkan, U. (2007). Biofilm Formation by Staphylococcus Epidermidis on Nitrogen Ion Implanted CoCrMo Alloy Material. *J. Biomed. Mater. Res. A* 81, 663–668. doi: 10.1002/JBM.A.31037

Paduszynska, M. A., Maciejewska, M., Neubauer, D., Golacki, K., Szymukowicz, M., Bauer, M., et al. (2019). Influence of Short Cationic Lipopeptides With Fatty Acids of Different Chain Lengths on Bacterial Biofilms Formed on Polystyrene and Hydrogel Surfaces. *Pharm* 11, 506 11, 506. doi: 10.3390/PHARMACEUTICS11100506

Palka, L., Mazurek-Popczyk, J., Arkusz, K., and Baldy-Chudzik, K. (2020). Susceptibility to Biofilm Formation on 3D-Printed Titanium Fixation Plates Used in the Mandible: A Preliminary Study. *J. Oral. Microbiol.* 12, 1–12. doi: 10.1080/20002297.2020.1838164

Palsis, J. A., Brehmer, T. S., Pellegrini, V. D., Drew, J. M., and Sachs, B. L. (2018). The Cost of Joint Replacement Comparing Two Approaches to Evaluating Costs of Total Hip and Knee Arthroplasty. *J. Bone Jt. Surg. - Am.* 100, 326–333. doi: 10.2106/JBJS.17.00161

Patel, J. D., Colton, E., Ebert, M., and Anderson, J. M. (2012). Gene Expression During S. Epidermidis Biofilm Formation on Biomaterials. *J. Biomed. Mater. Res. - Part A* 100 A, 2863–2869. doi: 10.1002/jbm.a.34221

Paulander, W., Varming, A. N., Bojer, M. S., Friberg, C., Bæk, K., and Ingmer, H. (2018). The Agr Quorum Sensing System in Staphylococcus Aureus Cells Mediates Death of Sub-Population. *BMC Res. Notes* 11, 503. doi: 10.1186/S13104-018-3600-6

Paulitsch-Fuchs, A. H., Wolrab, L., Eck, N., Dyer, N. P., Bödendorfer, B., and Lohberger, B. (2021). TiAl6V4 Alloy Surface Modifications and Their Impact on Biofilm Development of S. Aureus and S. Epidermidis. *J. Funct. Biomater.* 12, 36. doi: 10.3390/jfb12020036

Phillips, J. E., Crane, T. P., Noy, M., Elliott, T. S. J., and Grimer, R. J. (2006). The Incidence of Deep Prosthetic Infections in a Specialist Orthopaedic Hospital A 15-YEAR PROSPECTIVE SURVEY. *J. Bone Jt. Surg. [Br]* 88, 943–951. doi: 10.1302/0301-620X.88B7

Pinto, H. B., Brust, F. R., Macedo, A. J., and Trentin, D. S. (2020). The Antivirulence Compound Myricetin Possesses Remarkable Synergistic Effect With Antibacterials Upon Multidrug Resistant Staphylococcus Aureus. *Microb. Pathog.* 149, 104571. doi: 10.1016/j.micpath.2020.104571

Resch, A., Rosenstein, R., Nerz, C., and Go, F. (2005). Differential Gene Expression Profiling of Staphylococcus aureus Cultivated under Biofilm and Planktonic Conditions. *Appl. Environ. Microbiol.* 71, 2663–2676. doi: 10.1128/AEM.71.5.2663

Rupp, M., Lau, E., Kurtz, S. M., and Alt, V. (2020). Projections of Primary TKA and THA in Germany From 2016 Through 2040. *Clin. Orthop. Relat. Res.* 478, 1622. doi: 10.1097/CORR.0000000000001214

Ryder, V. J., Chopra, I., and O'Neill, A. J. (2012). Increased Mutability of Staphylococci in Biofilms as a Consequence of Oxidative Stress. *PloS One* 7, e47695. doi: 10.1371/JOURNAL.PONE.0047695

Shoji, M. M., and Chen, A. F. (2020). Biofilms in Periprosthetic Joint Infections: A Review of Diagnostic Modalities, Current Treatments, and Future Directions. *J. Knee Surg.* 33, 119–131. doi: 10.1055/s-0040-1701214

Singh, R., Ray, P., Das, A., and Sharma, M. (2010). Penetration of Antibiotics Through Staphylococcus Aureus and Staphylococcus Epidermidis Biofilms. *J. Antimicrob. Chemother.* 65, 1955–1958. doi: 10.1093/jac/dkq257

Sloan, M., Premkumar, A., and Sheth, N. P. (2018). Projected Volume of Primary Total Joint Arthroplasty in the U.s. 2014 to 2030. *J. Bone Jt. Surg. - Am. Vol.* 100, 1455–1460. doi: 10.2106/JBJS.17.01617

Spiliopoulou, A. I., Krevvata, M. I., Kolonitsiou, F., Harris, L. G., Wilkinson, T. S., Davies, A. P., et al. (2012). An Extracellular Staphylococcus Epidermidis Polysaccharide: Relation to Polysaccharide Intercellular Adhesin and its Implication in Phagocytosis. *BMC Microbiol.* 12, 1–15. doi: 10.1186/1471-2180-12-76/TABLES/3

Stepanovic, S., Vukovic, D., Dakic, I., Savic, B., and Svabic-Vlahovic, M. (2000). A Modified Microtiter-Plate Test for Quantification of Staphylococcal Biofilm Formation. *J. Methods Microbiol. J. Microbiol. Methods* 40, 175–179. doi: 10.1016/S0167-7012(00)00122-6

Thomas, P., Weik, T., Roider, G., Summer, B., and Thomsen, M. (2016). Influence of Surface Coating on Metal Ion Release: Evaluation in Patients With Metal Allergy. *Orthopedics* 39, S24–S30. doi: 10.3928/01477447-20160509-08

Tsaras, G., Osmon, D. R., Mabry, T., Lahr, B., Sauveur, J., Yawn, B., et al. (2012). Incidence, Secular Trends, and Outcomes of Prosthetic Joint Infection: A Population-Based Study, Olmsted County, Minnesota 1969–2007. *Infect. Control Hosp. Epidemiol.* 33, 1207–1212. doi: 10.1086/668421

Tsompanidou, E., Sibbald, M. J. J. B., Chlebowicz, M. A., Dreisbach, A., Back, J. W., Van Dijl, J. M., et al. (2010). Requirement of the Agr Locus for Colony Spreading of Staphylococcus Aureus. *J. Bacteriol.* 193, 1267–1272. doi: 10.1128/JB.01276-10

Vandecasteele, S. J., Peetermans, W. E., Merckx, R., and Van Eldere, J. (2001). Quantification of Expression of Staphylococcus Epidermidis Housekeeping Genes With Taqman Quantitative PCR During *In Vitro* Growth and Under Different Conditions. *J. Bacteriol.* 183, 7094. doi: 10.1128/JB.183.24.7094-7101.2001

Van Hove, R. P., Sierevelt, I. N., Van Royen, B. J., and Nolte, P. A. (2015). Titanium-Nitride Coating of Orthopaedic Implants: A Review of the Literature. *BioMed. Res. Int.* 2015, 1–9. doi: 10.1155/2015/485975

Venter, H., Bui, L. M. G., Conlon, B. P., and Kidd, S. P. (2017). Antibiotic Tolerance and the Alternative Lifestyles of Staphylococcus Aureus. *Essays Biochem.* 61, 71–79. doi: 10.1042/EBC20160061

Wang, Z., Yan, Y., and Qiao, L. (2017). Protein Adsorption on Implant Metals With Various Deformed Surfaces. *Colloids Surfaces B Biointerfaces* 156, 62–70. doi: 10.1016/j.colsurfb.2017.05.015

Wijesinghe, G., Dilhari, A., Gayani, B., Kottegoda, N., Samaranayake, L., and Weerasekera, M. (2019). Influence of Laboratory Culture Media on *In Vitro* Growth, Adhesion, and Biofilm Formation of Pseudomonas Aeruginosa and Staphylococcus Aureus. *Med. Princ. Pract.* 28, 28. doi: 10.1159/000494757

Yin, S., Jiang, B., Huang, G., Zhang, Y., You, B., Chen, Y., et al. (2018). The Interaction of N-Acetylcysteine and Serum Transferrin Promotes Bacterial Biofilm Formation. *Cell. Physiol. Biochem.* 45, 1399–1409. doi: 10.1159/000487566

Yoda, I., Koseki, H., Tomita, M., Shida, T., Horiuchi, H., Sakoda, H., et al. (2014). Effect of Surface Roughness of Biomaterials on Staphylococcus Epidermidis Adhesion. *BMC Microbiol.* 14, 1–7. doi: 10.1186/s12866-014-0234-2

Zheng, S., Bawazir, M., Dhall, A., Kim, H. E., He, L., Heo, J., et al. (2021). Implication of Surface Properties, Bacterial Motility, and Hydrodynamic Conditions on Bacterial Surface Sensing and Their Initial Adhesion. *Front. Bioeng. Biotechnol.* 9. doi: 10.3389/FBIOE.2021.643722

Zhou, G., Peng, H., Wang, Y. S., Huang, X. M., Xie, X. B., and Shi, Q. S. (2019). Enhanced Synergistic Effects of Xylitol and Isothiazolones for Inhibition of Initial Biofilm Formation by Pseudomonas Aeruginosa ATCC 9027 and Staphylococcus Aureus ATCC 6538. *J. Oral. Sci.* 61, 255–263. doi: 10.2334/JOSNUSD.18-0102

Zimmerli, W., Lew, P. D., and Waldvogel, F. A. (1984). Pathogenesis of Foreign Body Infection. Evidence for a Local Granulocyte Defect. *J. Clin. Invest.* 73, 1191–1200. doi: 10.1172/JCI111305

Conflict of Interest: The authors declare that the research was conducted in the absence of any commercial or financial relationships that could be construed as a potential conflict of interest.

Publisher's Note: All claims expressed in this article are solely those of the authors and do not necessarily represent those of their affiliated organizations, or those of the publisher, the editors and the reviewers. Any product that may be evaluated in this article, or claim that may be made by its manufacturer, is not guaranteed or endorsed by the publisher.

frontiers | Frontiers in Cellular and Infection Microbiology

TYPE Original Research
PUBLISHED 28 July 2022
DOI 10.3389/fcimb.2022.953780

OPEN ACCESS

EDITED BY
Fang Bai,
Nankai University, China

REVIEWED BY
Morteza Saki,
Ahvaz Jundishapur University of Medical Sciences, Iran
Edward D. Walker,
Michigan State University, United States

*CORRESPONDENCE
Beiwen Zheng
zhengbw@zju.edu.cn
Yonghong Xiao
xiaoyonghong@zju.edu.cn

SPECIALTY SECTION
This article was submitted to Biofilms, a section of the journal Frontiers in Cellular and Infection Microbiology

RECEIVED 26 May 2022
ACCEPTED 01 July 2022
PUBLISHED 28 July 2022

CITATION
Hu S, Lv Y, Xu H, Zheng B and Xiao Y (2022) Biofilm formation and antibiotic sensitivity in *Elizabethkingia anophelis*. *Front. Cell. Infect. Microbiol.* 12:953780. doi: 10.3389/fcimb.2022.953780

Biofilm formation and antibiotic sensitivity in *Elizabethkingia anophelis*

Shaohua Hu[1], Yan Lv[2], Hao Xu[1], Beiwen Zheng[1,3]* and Yonghong Xiao[1,3]*

[1]State Key Laboratory for Diagnosis and Treatment of Infectious Diseases, National Clinical Research Center for Infectious Diseases, Collaborative Innovation Center for Diagnosis and Treatment of Infectious Diseases, The First Affiliated Hospital, Zhejiang University School of Medicine, Hangzhou, China, [2]Department of Blood Transfusion, The First Affiliated Hospital, Zhejiang University School of Medicine, Hangzhou, China, [3]Department of Structure and Morphology, Jinan Microecological Biomedicine Shandong Laboratory, Jinan, China

Elizabethkingia anophelis has recently gained global attention and is emerging as a cause of life-threatening nosocomial infections. The present study aimed to investigate the association between antimicrobial resistance and the ability to form biofilm among *E. anophelis* isolated from hospitalized patients in China. Over 10 years, a total of 197 non-duplicate *E. anophelis* strains were collected. Antibiotic susceptibility was determined by the standard agar dilution method as a reference assay according to the Clinical and Laboratory Standards Institute. The biofilm formation ability was assessed using a culture microtiter plate method, which was determined using a crystal violet assay. Culture plate results were cross-checked by scanning electron microscopy imaging analysis. Among the 197 isolates, all were multidrug-resistant, and 20 were extensively drug-resistant. Clinical *E. anophelis* showed high resistance to current antibiotics, and 99% of the isolates were resistant to at least seven antibiotics. The resistance rate for aztreonam, ceftazidime, imipenem, meropenem, trimethoprim-sulfamethoxazole, cefepime, and tetracycline was high as 100%, 99%, 99%, 99%, 99%, 95%, and 90%, respectively. However, the isolates exhibited the highest susceptibility to minocycline (100%), doxycycline (96%), and rifampin (94%). The biofilm formation results revealed that all strains could form biofilm. Among them, the proportions of strong, medium, and weak biofilm-forming strains were 41%, 42%, and 17%, respectively. Furthermore, the strains forming strong or moderate biofilm presented a statistically significant higher resistance than the weak formers ($p < 0.05$), especially for piperacillin, piperacillin-tazobactam, cefepime, amikacin,

and ciprofloxacin. Although *E. anophelis* was notoriously resistant to large antibiotics, minocycline, doxycycline, and rifampin showed potent activity against this pathogen. The data in the present report revealed a positive association between biofilm formation and antibiotic resistance, which will provide a foundation for improved therapeutic strategies against *E. anophelis* infections in the future.

KEYWORDS

***Elizabethkingia anophelis*, nosocomial infections, multidrug-resistant, biofilm formation, biofilm-specific resistance**

Introduction

E. anophelis is an emerging pathogen that can pose a significant threat to patients due to its unclear mechanism of antibiotic resistance and high mortality rate among nosocomial isolates (Janda and Lopez, 2017; Lin et al., 2019). *E. anophelis* is a class of Gram-negative, non-fermenting bacillus that is ubiquitously recovered from hospital environments (Kyritsi et al., 2018; Nicholson et al., 2018; Choi et al., 2019; Lee et al., 2021). Unexpectedly, it has been reported that the bacterium can be isolated from contaminated corona virus disease 2019 (COVID-19) swab kits (Xu et al., 2022). Moreover, it is related to mainly immunocompromised patients and has been clinically identified as one of the most important opportunistic pathogens responsible for nosocomial infections or healthcare-associated infections (Janda and Lopez, 2017; Lin et al., 2019). Since the first *E. anophelis* meningitis case was reported in 2012 (Frank et al., 2013), an increasing number of infections have been reported recently, including bacteremia, pneumonia, meningitis, catheter-related bloodstream infections, skin and soft-tissue infections, urinary tract infections, and eye infections (Lau et al., 2016; Hu et al., 2017; Bulagonda et al., 2018; Chew et al., 2018; Nielsen et al., 2018; Lin et al., 2018a; Auffret et al., 2021). In addition, several life-threatening outbreaks of infections caused by *E. anophelis* have successively been described in many regions worldwide, including Singapore, the United States, Hong Kong, Taiwan, and South Korea (Teo et al., 2013; Navon et al., 2016; Perrin et al., 2017; Lin et al., 2018a; Choi et al., 2019). In addition, in previous studies, it has been revealed that the incidence of *E. anophelis* infection was highly underestimated due to its frequent misidentification as *Elizabethkingia meningoseptica* by conventional laboratory identification methods (Lau et al., 2016; Lin et al., 2017; Kelly et al., 2019). Undoubtedly, such a high underestimation and mortality rate of *E. anophelis* infections cause a tremendous burden on a country's health system.

It has been documented that *E. anophelis* is notorious for its high resistance to many antibacterial drugs, including penicillins, cephalosporins, carbapenems, aminoglycosides, tetracyclines, and β-lactamase inhibitors (Lin et al., 2018a; Lin et al., 2018b; Wang et al., 2019; Chiu et al., 2021; Larkin et al., 2021; Tang et al., 2021). Several investigations have revealed that *E. anophelis* isolates usually express resistance to multiple current commonly used antibiotics. In contrast, results from other studies have indicated susceptibility to several antibacterial agents, such as certain β-lactams, carbapenems, aminoglycosides, fluoroquinolones, or sulfa antibiotics (Teo et al., 2013; Navon et al., 2016; Han et al., 2017; Perrin et al., 2017; Lin et al., 2018a; Choi et al., 2019; Wang et al., 2020; Chiu et al., 2021). These inconsistent antimicrobial susceptibility testing (AST) patterns may be attributed to an insufficient sample size and the various origins of the strains in different countries and regions. Limited drug susceptibility test data are available for this bacterium, especially in mainland China. Therefore, further thorough exploration of drug resistance in *E. anophelis* from diverse sources is of utmost importance.

Biofilm is defined as the microbial population consisting of groups of bacterial cells, which are adherent to a surface and are comprised within a self-produced extracellular matrix, including proteins, extracellular DNA, and polysaccharides (Harika et al., 2020; Hashemzadeh et al., 2021). Bacterial cells within the biofilm are highly coordinated and undergo phenotypic switches to generate communities that are resistant to an adverse external environment (Shenkutie et al., 2020). Such a phenotype switch can also contribute to the emergence of antibiotic resistance by encoding antibiotic resistance genes, genetic mutation, restricting antibiotics, or counteracting host immunity (Shenkutie et al., 2020). Nearly all multidrug-resistant (MDR) Gram-negative bacteria and their virulence factors are persistent problematic responses in hospitalized patients during biofilm production (Husain et al., 2021). Among them, the indwelling device is the most important in biofilm formation and colonization (Karami et al., 2020). Biofilms protect bacteria from the host immune system and antimicrobial agents. For example, the formation of biofilms by *P. mirabilis* strengthens the complexity of bacterial resistance, prolongs treatment time,

and further intensifies the infection ability (Ranjbar-Omid et al., 2015). The bacteria became very robust against all available bacteriostatic agents, and the underlying mechanisms involved were developed. Hence, it is important to create connections between biofilm production and drug resistance in clinical isolates of *E. anophelis*.

In recent years, the formation of biofilm by *Elizabethkingia* species has been discussed in a few studies (Jacobs and Chenia, 2011; Tang et al., 2021). However, too little research data are available, and no study has reported a correlation between biofilm formation and antibiotic resistance in *Elizabethkingia* species from humans. Therefore, the association between the biofilm formation capability and antibiotic resistance in clinical *E. anophelis* isolates is unknown. Here, we used the Clinical and Laboratory Standards Institute (CLSI)–recommended standard agar dilution method as a reference assay and examined the antimicrobial susceptibility results for 197 clinical *E. anophelis* isolates to fill those research gaps. The present study aimed to study biofilm formation and different antibiotic sensitivity in *E. anophelis* strains that cause nosocomial infections in China and present any possible link between the ability to form biofilm and MDR. To the best of our knowledge, this is the first study that investigated biofilm formation and a correlation between antibiotic resistance in *E. anophelis* isolates. Data on the phenotypic characterization of the biofilm-forming capacity and the correlation between antibiotic susceptibility may offer valuable insights into the development of medication and preventive strategies for *E. anophelis* nosocomial infections.

Materials and methods

Sampling and bacterial isolation

The database of the Clinical Strain Library of the First Affiliated Hospital of Zhejiang University School of Medicine was searched from January 2010 to April 2019 for microbial cultures that yielded *E. anophelis*. The collected isolates were kept in brain-heart infusion broth (Oxoid, UK) containing 20% glycerol at −80°C until use. All 197 isolates used in this study were routinely collected from patients according to their clinical requirements. All used strains of *E. anophelis* species that were previously collected from blood, sputum, abdominal fluid, cerebrospinal fluid (CSF), bronchoalveolar fluid (BAL), urine, other soft tissue, etc. Samples were mainly collected from patients in the intensive care unit, hematology department, infectious disease department, and surgical ward. Of these patients, 76.4% (149 of 195) were men and 23.6% (46 of 195) were women. Detailed data for two isolates were unavailable. The mean age of the patients was 61 ± 18 years. Among them, except for two babies, none of the patients were under 18 years of age, and 76 patients were over 50 years of age. Isolates were incubated at 37°C for 24 h from the −80°C stock in Mueller–Hinton Agar (MHA) (Oxoid, UK) without antibiotics in aerophilic conditions. Microbial isolates derived from patients were initially identified using conventional tests by a matrix-assisted laser desorption ionization time-of-flight mass spectrometry (Bruker Daltonics, USA) and were verified by genomic average nucleotide identity analysis.

Antimicrobial susceptibility testing

Agar dilution techniques determined antimicrobial sensitivity testing according to the procedures described in the CLSI guidelines (2020). The antimicrobial resistance of the isolates to 19 antibiotics (Meilunbio, China), including piperacillin, piperacillin-tazobactam, ceftazidime, cefepime, imipenem, meropenem, aztreonam, gentamicin, amikacin, minocycline, doxycycline, tetracycline, tigecycline, ciprofloxacin, levofloxacin, trimethoprim-sulfamethoxazole, rifampin, vancomycin, and chloramphenicol, was investigated. Susceptible, intermediate, and resistant interpretation was based on the CLSI guidelines for "other non-Enterobacteriaceae". The susceptibility criteria for tigecycline were interpreted according to "Enterobacteriaceae breakpoints" (susceptible, ≤ 2 mg/L; intermediate, = 4 mg/L; resistant, ≥ 8 mg/L), provided by the US Food and Drug Administration (Chiu et al., 2021). Moreover, for rifampin and vancomycin, the susceptibility testing results and minimum inhibitory concentration (MICs) were interpreted according to the "*Enterococcus* species" of the CLSI standards for rifampin and vancomycin. Bacteria *E. coli* ATCC 25922, *Pseudomonas aeruginosa* ATCC 27853, and *Staphylococcus aureus* ATCC 29213 were used as quality control strains. The standardized definition of MDR, extensively drug-resistant (XDR), and pan-drug-resistant (PDR) bacteria has been well studied. MDR strains were defined as strains that acquired non-susceptibility to at least one agent per three or more antimicrobial categories, XDR strains were defined as non-susceptible to at least one agent in all but two or fewer antimicrobial classes, and PDR strains were defined as non-susceptible to all agents in all antimicrobial categories (Magiorakos et al., 2012).

Biofilm formation and quantification assay

Biofilm-forming capacities of the isolates were evaluated in triplicate using the crystal violet method for *Elizabethkingia* species as previously described with modifications (Jacobs and Chenia, 2011; Tang et al., 2021). Briefly, overnight grown *E. anophelis* [cultured at 37°C in 2 ml of Mueller–Hinton Broth (MHB) (Oxoid, UK)] was harvested. Then, the cultures were diluted in MHB medium adjusted approximately to 0.5 McFarland. A 20-µl aliquot of each suspension was then diluted 1:10 in 180 µl of MHB in a 96-well cell culture-treated

polystyrene plate (Corning Incorporated, USA). Following 24 h of growth at 37°C overnight, plates were washed three times with 200 µl of phosphate-buffered saline (PBS; 0.01mol/L) to remove unattached bacteria. After air drying, adherent cells were fixed with 200 µl of methanol for 15 min and stained with 200 µl of 1% crystal violet (Beyotime, China) for 15 min at room temperature. The staining solution was removed, and the plate was washed three times with 200 µl of PBS (0.01mol/L). After removing the washing solution, 150 µl of 33% acetic acid was added to each well to dissolve the biofilm-bound crystal violet and incubated for 5 min on a shaking table. The optical density (OD) of each well was measured at 595 nm using a microtiter plate reader Epoch2 (BioTek, USA). The OD at 595 nm was obtained as an index of adherent bacteria and biofilm formation. The OD value of sterile medium with fixative and dye was recorded and subtracted from the results to determine the background OD. All strains were classified into the following four categories: the first category comprised those not considered biofilm producers when OD595 ≤ ODc (the mean OD of the negative control). The other three were weak biofilm formation, OD595 >ODc-2XODc; moderate biofilm formation, OD595 >2XODc–4XODc; and strong biofilm formation, OD595 >4XODc.

Scanning electron microscopy analysis

Scanning electron microscopy imaging (SEM) analysis was performed in the State Key Laboratory of Rice Biology of Zhejiang University, using a Scanning Electron Microscope (TM 4000 PLUS, HITACHI, Tokyo, Japan). Bacteria were incubated for 24 h at 37°C with 15 ml of MHB under shaking conditions. After centrifugation, the precipitated bacteria were immediately fixed in 2.5% fresh glutaraldehyde and fixed for 2 h. Next, bacteria were rinsed three times with distilled water (centrifugal discard supernatant at each step, distilled water was added, and clots were blown with a straw). Then, dehydration was performed with increasing concentration of ethanol: 20 min at 50%, 20 min at 75%, 20 min at 85%, 20 min at 95%, and two times for 20 min in 100% ethanol prior to crucial point drying. Subsequently, critical point drying, ion sputtering, and microscope observation were carried out successively.

Statistical analysis

Statistical analyses were performed using SPSS version 23.0 software (IBM, Armonk, NY, USA). To examine the effect of biofilm production on the susceptibility of the strains, data normality of continuous variables was initially verified using the Shapiro–Wilk test. The t-test and Mann–Whitney U test were used to compare the differences between the two groups. The Kruskal–Wallis test was employed for multiple comparisons. The statistical significance was set at $P < 0.05$.

Results

Antimicrobial susceptibility patterns

The susceptibility to 19 antimicrobials of human clinical significance was investigated in all 197 clinical *E. anophelis* isolates. According to the CLSI-recommended agar dilution method, drug susceptibilities of the *E. anophelis* isolates and MIC ranges for all 19 tested antimicrobials are presented in Table 1 and Table S1. MDR was observed in all 197 *E. anophelis* isolates (Table 1). Ten percent of pan-resistant strains (XDR) was detected among them. All strains presented intermediate susceptibility to six antibiotics and presented no susceptibility to at least four antibiotics. Of the tested antibiotics, *E. anophelis* isolates showed low varying degrees of MDR. However, none of the strains of *E. anophelis* investigated was pan-susceptible (susceptible to all antimicrobials tested), whereas two isolates (1% of the isolates; one strain from sputum and one from fluid) were resistant to only four antibiotics.

Furthermore, on the basis of the acquired antibiotic resistance pattern, 177 (89.9%) isolates were resistant to at least nine antibiotics, and 195 (99%) isolates were resistant to at least seven antibiotics. All isolates were resistant to β-lactams, including piperacillin, piperacillin-tazobactam, ceftazidime, cefepime, meropenem, and imipenem. High resistance rates were observed for piperacillin (98; 49.8%) in contrast to the decreased resistance when in combination β-lactamase inhibitors, namely, piperacillin-tazobactam (57; 28.9%). Only one and two strains were susceptible to ceftazidime and cefepime, respectively. Moreover, 196 (99.5%) isolates were resistant to imipenem, and 195 (99.5%) isolates were resistant to meropenem, which may be tricky for clinical treatment. *Elizabethkingia* isolates were extremely highly resistant to aztreonam; it was observed that none favored *in vitro* activity. They also exhibited high resistance rates to trimethoprim-sulfamethoxazole (195; 99%), tetracycline (178; 90.4%), gentamicin (174; 88.3%), amikacin (154; 78.7%), and chloramphenicol (113; 57.3%), respectively.

Interestingly, consistently with previous studies, doxycycline, minocycline, and rifampin inhibited >90% of all *E. anophelis* isolates. In particular, minocycline was more active compared with doxycycline and tigecycline [susceptible rates, 197 (100%) versus 189 (95.9%) and 70 (35.5%), respectively]. In this study, favored *in vitro* activity of fluoroquinolones was also observed, and the susceptibility rate for levofloxacin was higher than that of ciprofloxacin. In contrast, a significant difference was noted between the susceptibility rates of *E. anophelis* against levofloxacin (150; 76.1%) and ciprofloxacin (95; 48.2%),

TABLE 1 Antimicrobial MICs (mg/L) and susceptible rates of 197 *E. anophelis* isolates determined using the agar dilution.

Antimicrobial agent	Susceptibility testing assay				
	Agar dilution (mg/L)	MIC range	S no. (%)	I no. (%)	R no. (%)
Piperacillin	0.5–256	8–>256	49 (24.87)	50 (25.38)	98 (49.75)
Piperacillin-tazobactam	0.5–256+4	4/4–>256/4	67 (34.01)	73 (37.06)	57 (28.93)
Ceftazidime	0.25–64	4–>64	1 (0.51)	0 (0)	196 (99.49)
Cefepime	0.06–64	2–>64	2 (1.02)	7 (3.55)	188 (95.43)
Imipenem	0.03–32	0.25–>32	1 (0.51)	0 (0)	196 (99.49)
Meropenem	0.008–32	0.06–>32	2 (1.02)	0 (0)	195 (98.98)
Aztreonam	0.03–64	32–>64	0 (0)	0 (0)	197 (100)
Gentamicin	0.125–32	4–>32	7 (3.55)	16 (8.13)	174 (88.32)
Amikacin	0.25–128	4–>128	12 (6.09)	31 (15.74)	154 (78.17)
Minocycline	0.125–32	0.25–2	197 (100)	0 (0)	0 (0)
Doxycycline	0.25–32	0.5–16	189 (95.94)	7 (3.56)	1 (0.5)
Tetracycline	0.25–32	1–>32	5 (2.54)	14 (7.1)	178 (90.36)
Tigecycline	0.015–32	0.5–16	70 (35.53)	97 (49.24)	30 (15.23)
Ciprofloxacin	0.004–8	0.125–>8	95 (48.22)	49 (24.88)	53 (26.9)
Levofloxacin	0.008–16	0.125–>16	150 (76.14)	8 (4.06)	39 (19.8)
Trimethoprim-sulfamethoxazole	0.25–8+4.75–152	4/38–>8/152	2 (1.02)	0 (0)	195 (98.98)
Rifampin	0.25–32	0.25–32	185 (93.91)	3 (1.52)	9 (4.57)
Vancomycin	0.25–64	4–>64	1 (0.51)	146 (74.11)	50 (25.38)
Chloramphenicol	1–64	8–>64	11 (5.58)	73 (37.06)	113 (57.36)

respectively. Taken together, these results evidently suggested that the bacteria were dangerous and highly resistant to the antibiotics. Although *E. anophelis* was resistant to a series of antibiotics, minocycline, doxycycline, and rifampin showed potent *in vitro* activity against this pathogen. Our findings provide potential alternative treatment options for *E. anophelis* infections.

Biofilm formation of multidrug-resistant bacteria

Among the MDR behavior, each *E. anophelis* strain was screened for the ability to form biofilm. A simple culture plate assay was performed for the positive biofilm effect in tested *E. anophelis*. Compared with any other method, this assay is the most reliable and most straightforward method for identifying biofilm formation. In previous studies, this assay was found highly suitable for current research on the detection of biofilm formation in Gram-negative bacteria. *E. anophelis* strains collected in this study were highly susceptible to crystal violet observation. On the basis of the results of the culture plate, biofilm-positive *E. anophelis* were divided into three groups, namely, weak, moderate, and strong biofilm formers, and results are presented in Figure S1. In this study, our data revealed that all clinical *E. anophelis* isolates 197(100%) were biofilm-positive, with OD values >ODc at 595 nm. Moreover, 80 (40.6%) isolates tested positive for strong biofilm formation, with OD >4ODc at 595 nm, and four (Ea109, Ea124, Ea131, and Ea143) had the highest OD values, with values >1.5 (Figure S1). Of the 197 tested isolates, only 35 (17.8%) were weak biofilm formers, and 82 (41.6%) isolates were moderate biofilm formers. *E. anophelis* was strongly adherently after culture at 37°C in MHB.

Although the ability of *Elizabethkingia* to form biofilm was previously demonstrated, it must be pointed out that the percentage of biofilm-forming strains of *E. anophelis* was observed in the present investigation. We next compared the biofilm formation level (OD595) among the strains from different sources (Figure S2). There were significant differences among the other groups. Figure S2 shows the percentage of strong, moderate, and weak biofilm formation levels in isolates from sputum, blood, abdominal fluid, CSF, and clinical/other strains. In contrast, sputum samples showed the highest ($p < 0.05$) percentage of strong biofilm-forming strains, whereas weak biofilms were formed mainly in bloodstream infection strains ($p < 0.05$). In addition, all strains isolated from abdominal and fluid CSF formed moderate biofilms. The different biofilm-forming ability for different origin isolates is still unclear, and further studies are needed to explain these findings.

Furthermore, results of the tissue culture plate were cross-checked by the SEM analysis method. Eight *E. anophelis* sample clones were selected randomly for investigation by light microscopy, starting from the surface of the glass slide and scanning several planes interspersed by short distances to visualize biofilm architecture and microbial behavior

throughout the depth of the individual flow chambers. Figure 1 displays the *in vitro* biofilm formation results by four selected strains studied by SEM. Microcolonies merged to form a thick, complex biofilm structure across the entire surface of the coverslips. Each of these four strains showed thick biofilms, as densely stacked and layered bacteria were observed. In addition, differences in biofilm structure and cover channel surface were observed between stronger and weaker biofilm-forming strains. Compared with weaker biofilm-forming strains, the others contained thicker biofilms, and their bacteria were more densely stacked and layered (Figure 1).

Correlation between resistance and biofilm formation capability

One noteworthy point is that strong or moderate biofilm formers presented a statistically significantly higher ($p = 0.0006$) average number of resistances (11.01 ± 0.1643) compared with the weak formers (9.657 ± 0.3477) (Figure 2A). Figure 2B shows that the average number of resistances per strain between strong (11.10 ± 0.2247) and moderate (10.93 ± 0.2403) biofilm formers was not statistically significant ($p > 0.05$). Furthermore, both were statistically significant ($p < 0.05$) higher than that in weak biofilm formation classes (Figure 2B). This is the first time that a direct relationship has been reported between antibiotic resistance and biofilm formation in *E. anophelis*. Further studies are needed to support these findings.

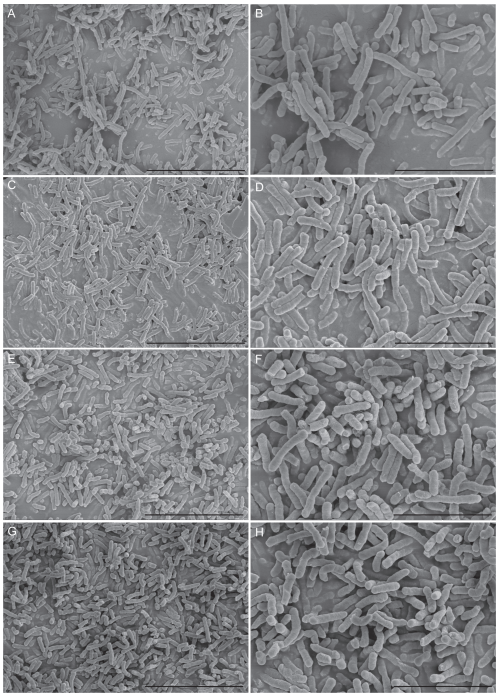

FIGURE 1
Scanning electron microscopy imaging analysis of four *E. anophelis* biofilm formations. The four strains were as follows: weak biofilm-forming strain SKL 051060 **(A, B)**; moderate biofilm-forming strain SKL014219 **(C, D)**; strong biofilm-forming strain SKL067015 **(E, F)**; and SKL068512 **(G, H)**. Among them, the left part of the figure **(A, C, E, G)** is the imaging result at 5,000-fold magnification (5.00k SE), bar = 10.0 μm; the right part of the figure **(B, D, F, H)** is the image result of 10,000-fold magnification (10.00k SE), bar = 5.00μm. The data show that the cell morphology is intact and densely stacked, and layered bacteria can be observed.

The antimicrobial resistance pattern of *E. anophelis* isolates among strong, moderate, and weak biofilm formers is shown in Table 2. In general, the antimicrobial resistance rates among strong and moderate biofilm-forming *E. anophelis* strains were significantly higher than that of weak biofilm-forming isolates (Table 2 and Figure 3). In particular, for ceftazidime, cefepime, imipenem, and meropenem, susceptible strains were only detected in bacteria that showed weak biofilm formation. Similarly, the isolates resistant to doxycycline or rifampin were merely found in strong and moderate biofilm-forming *E. anophelis*. A discrepancy was observed in the correlation between the degree of biofilm formation and antimicrobial resistance rates in most antibiotics from different classes, including piperacillin, piperacillin-tazobactam, ceftazidime, cefepime, meropenem, gentamicin, amikacin, doxycycline, tetracycline, tigecycline, ciprofloxacin, levofloxacin, rifampin, and vancomycin. However, the correlation could not be distinguished in case of aztreonam, minocycline, and trimethoprim-sulfamethoxazole (Table 2 and Figure 3). Furthermore, after analyzing 12 antibiotics by the Kruskal–Wallis test, the difference between biofilm formation (among strong, moderate, and weak) and the proportion of antimicrobial-resistance was confirmed statistically significant ($p < 0.05$) in case of piperacillin, piperacillin-tazobactam, cefepime, amikacin, and ciprofloxacin, respectively (Figure 4).

Discussion

E. anophelis is an emerging pathogen that will cause life-threatening nosocomial infections in humans with compromised immune systems. Recently, *E. anophelis* infections in humans are increasing in many countries and showed high mortality, which consolidated the importance of early identification and treatment (Janda and Lopez, 2017; Lin et al., 2019). Furthermore, many global *E. anophelis* outbreak infections have been uncovered in recent years (Teo et al., 2013; Navon et al., 2016; Perrin et al., 2017; Lin et al., 2018a; Choi et al., 2019). Therefore, further exploration of antimicrobial resistance and virulence mechanisms in *E. anophelis* are of utmost importance. In the present study, the antimicrobial susceptibility characteristics and biofilm formation of nosocomial *E. anophelis* isolates were investigated, which were confirmed and obtained in China.

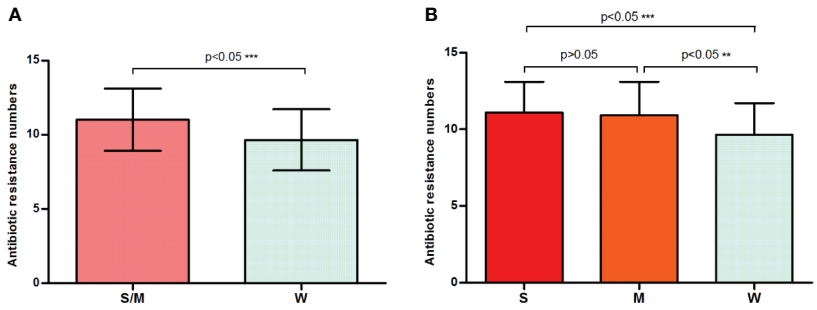

FIGURE 2
A bar graph displays the relationship between biofilm formation intensity and antimicrobial resistance. **(A)** Strong or moderate biofilm-forming strains presented a significantly higher average number of resistances than the weak producers. **(B)** The discrepancy in antimicrobial resistance among weak, moderate, and strong biofilm-producing isolates. W, weak biofilm formation; M, moderate biofilm formation; S, strong biofilm formation; S/W, strong or moderate biofilm formation. ** means significant at 0.01 level, *** means significant at 0.001 level.

First, we found that *E. anophelis* isolates exhibited high MDR. The strains used in this study showed stabilized degrees of MDR to the tested antibiotics. Corresponding to previous reports, they were resistant to many commonly used antibacterial drugs, including penicillin, cephalosporin, carbapenem, aminoglycoside, fluoroquinolone, tetracyclines, sulfonamide, and carbapenem (Chen et al., 2015; Han et al., 2017; Chew et al., 2018; Lin et al., 2018a; Lin et al., 2018b; Choi et al., 2019). In this study, the antimicrobial resistance rates observed were as follows: piperacillin (49.8%), piperacillin-tazobactam (93%), ceftazidime (99.5%), imipenem (99.5%), meropenem (99%), aztreonam (100%), gentamicin (88.3%), amikacin (78.2%), tetracycline (90.4%), tigecycline (15.2%), ciprofloxacin (26.9%), levofloxacin (19.8%), trimethoprim-sulfamethoxazole (98.9%), vancomycin (25.4%), and chloramphenicol (57.4%), respectively. As presented in

TABLE 2 The relationship among biofilm-forming ability of *E. anophelis* with antibiotic resistance pattern.

Biofilm formation ability	Strong (n = 80)			Moderate (n = 82)			Weak (n = 35)		
Antibiotics	**R No. (%)**	**I No. (%)**	**S No. (%)**	**R No. (%)**	**I No. (%)**	**S No. (%)**	**R No. (%)**	**I No. (%)**	**S No. (%)**
Piperacillin	56 (70)	17 (21.25)	7 (8.75)	36 (43.9)	18 (21.95)	28 (34.15)	6 (17.14)	15 (42.86)	14 (40)
Piperacillin-tazobactam	29 (36.25)	38 (47.5)	13 (16.25)	24 (29.27)	21(25.61)	37(45.12)	4 (11.43)	14 (40)	17(48.57)
Ceftazidime	80 (100)	—	—	82 (100)	—	—	34 (97.14)	—	1 (2.86)
Cefepime	80 (100)	—	—	78 (95.12)	4 (4.88)	—	30 (85.71)	3 (8.57)	2 (5.72)
Imipenem	80 (100)	—	—	82 (100)	—	—	34 (97.14)	—	1(2.86)
Meropenem	80 (100)	—	—	82 (100)	—	—	33 (94.29)	—	2 (5.71)
Aztreonam	80 (100)	—	—	82 (100)	—	—	35 (100)	—	—
Gentamicin	74 (92.5)	5 (6.25)	1 (1.25)	70 (85.37)	8 (9.75)	4 (4.88)	30 (85.72)	3 (8.57)	2 (5.71)
Amikacin	67 (83.75)	10 (12.5)	3 (3.75)	64 (78.05)	13 (15.85)	5 (6.1)	23 (65.71)	8 (22.86)	4 (11.43)
Minocycline	—	—	80(100)	—	—	82(100)	—	—	35(100)
Doxycycline	—	2 (2.5)	78 (97.5)	1 (1.22)	4 (4.88)	77 (93.9)	—	1 (2.86)	34 (97.14)
Tetracycline	69 (86.25)	8 (10)	3 (3.75)	79 (96.34)	3 (3.66)	—	30 (85.71)	3 (8.57)	2 (5.72)
Tigecycline	10 (12.5)	44 (55)	26 (32.5)	17 (20.73)	37 (45.12)	28 (34.15)	3 (8.58)	16 (45.71)	16 (45.71)
Ciprofloxacin	18 (22.5)	25 (31.25)	37 (46.25)	28 (34.15)	19 (23.17)	35 (42.68)	7 (20)	5 (14.29)	23 (65.71)
Levofloxacin	14 (17.5)	—	66 (82.5)	21(25.61)	6 (7.32)	55 (67.07)	4 (11.43)	2 (5.71)	29 (82.86)
Trimethoprim-sulfamethoxazole	80 (100)	—	—	80(97.56)	—	2 (2.44)	35(100)	—	—
Rifampin	3 (3.75)	1 (1.25)	76 (95)	6 (7.32)	1(1.22)	75 (91.46)	—	1(2.86)	34 (97.14)
Vancomycin	31 (38.75)	48 (60)	1 (1.25)	12 (14.63)	70 (85.37)	—	7 (20)	28 (80)	—
Chloramphenicol	37 (46.25)	37 (46.25)	6 (7.5)	53 (64.63)	27 (32.93)	2 (2.44)	23 (65.71)	9 (25.72)	3 (8.57)

R, resistant; S, susceptible; I, intermediate resistant.

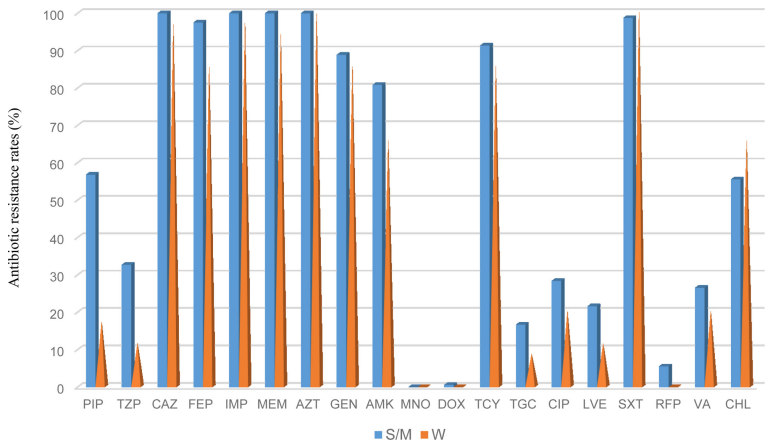

FIGURE 3
The frequency of antibacterial resistance in strong/moderate biofilm formation and weak biofilm producer *E. anophelis* isolates. S/W, strong or moderate biofilm formation; W, weak biofilm formation. PIP, piperacillin; TZP, piperacillin-tazobactam; CAZ, ceftazidime; FEP, cefepime; IPM, imipenem; MEM, meropenem; AZT, aztreonam; GEN, gentamicin; AMK, amikacin; MNO, minocycline; DOX, doxycycline; TCY, tetracycline: TGC, tigecycline; CIP, ciprofloxacin; LVX, levofloxacin; SXT, trimethoprim-sulfamethoxazole; RFP, rifampin; VA, vancomycin; and CHL, chloramphenicol.

previous reports, minocycline, doxycycline, rifampin, and levofloxacin were active against *E. anophelis in vitro* in our study (Wang et al., 2020; Chiu et al., 2021; Kuo et al., 2021), which may be the first choice of empirical medication for the clinical treatment of this bacterial infection. Interestingly, as reported in Taiwan and by others, tigecycline, the derivative of minocycline, showed inferior antimicrobial activity in the present study (Jian et al., 2019; Chang et al., 2021; Kuo et al., 2021).

However, inconsistent AST results were reported for some antibiotics, especially for piperacillin-tazobactam, levofloxacin, rifampin, and vancomycin. For an *Elizabethkingia* infection, successful treatment has been described using piperacillin-tazobactam. An infant's unusual presentation of *E. anophelis*

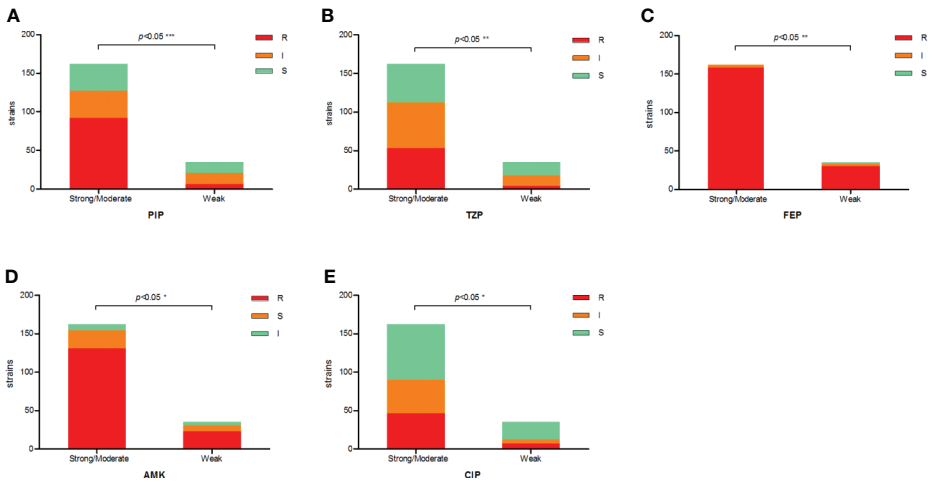

FIGURE 4
The correlation between antibiotic resistance and biofilm-forming capacity of clinical *E. anophelis* isolates to five antibiotics. **(A–E)** For piperacillin (PIP), piperacillin-tazobactam (TZP), cefepime (FEP), amikacin (AMK), and ciprofloxacin (CIP). Susceptible isolates tended to form weaker biofilms than non-susceptible isolates. Significant differences were detected between groups. The p-values obtained by Mann–Whitney analysis were as follows: piperacillin ($p < 0.0001$), piperacillin-tazobactam ($p = 0.0088$), cefepime ($p = 0.0022$), amikacin ($p = 0.0442$), and ciprofloxacin ($p = 0.0461$). * means significant at 0.05 alpha level, ** means significant at 0.01 level, *** means significant at 0.001 level.

infection indicated the pathogen was sensitive only to piperacillin-tazobactam (Mantoo et al., 2021). After antibiotic treatment was changed to piperacillin-tazobactam, the patient soon recovered and was discharged (Mantoo et al., 2021). According to a report by Wang et al., the antimicrobial susceptibilities of piperacillin-tazobactam were high at 86.5% (Wang et al., 2020). Moreover, in another report, it was also demonstrated that the combinations showed reasonable *in vitro* activity with a 71.8% susceptibility rate (Chang et al., 2021). In contrast, a significant difference was observed in our study. Only 34.01% of agent was active against *E. anophelis* isolates *in vitro*.

In line with the data in the present study, Chiu et al. revealed that piperacillin-tazobactam was notoriously active against 84 *E. anophelis* isolates *in vitro*. No susceptibility strain was found (Chiu et al., 2021). The variability in fluoroquinolone susceptibility has also been detected in the majority literature. Against levofloxacin and ciprofloxacin, different previous reports showed a different susceptibility of the *E. anophelis* pathogen. Although favored high *in vitro* activity of levofloxacin was observed in our study, the susceptibility rate of ciprofloxacin was much lower than that. In agreement with our results, in previous studies, it was concluded that, compared with levofloxacin, ciprofloxacin exhibited inferior activity against *E. anophelis* (Burnard et al., 2020; Tang et al., 2021). In other reports, when comparing our results, a significant difference was observed between the susceptibility rates of *E. anophelis* against ciprofloxacin (92% and 100%, respectively) (Lau et al., 2016; Perrin et al., 2017). In contrast, both ciprofloxacin and levofloxacin exhibited poor activity against *E. anophelis* isolates in hospitals in South Korea and Taiwan (Han et al., 2017; Lin et al., 2018a). These two AST results indicated that all the susceptibility rates were less than 30%, which is contradictory to our and previous findings (Han et al., 2017; Lin et al., 2018a).

It has been reported that the rifampin agent is less active against Gram-negative bacilli due to its weaker ability to readily penetrate the outer membrane of these pathogens (Goldstein, 2014). Chang et al. found that rifampin is unproductive to against *E. anophelis*, and the susceptibility rate was only 20.5% (Chang et al., 2021). Nevertheless, in most other studies, it was reported that rifampin is potent in fighting *E. anophelis* bacteria; even more than 95% of strains remained sensitive (Han et al., 2017; Seong et al., 2020; Wang et al., 2020; Chiu et al., 2021). Corresponding to these reports, rifampin also showed high *in vitro* activity inhibiting *E. anophelis* in our study. For rifampin, the underlying mechanism of high effectiveness to confront *E. anophelis* is yet known and warrants further investigation. Vancomycin has been suggested as a potential therapy for *Elizabethkingia* infections, particular in meningitis (Han et al., 2017; Jean et al., 2017; Lin et al., 2019; Seong et al., 2020). Therefore, in our study, *E. anophelis* strains were screened against vancomycin, but only 0.51% of susceptible isolates were detected. In line with our results, vancomycin is ineffective in the treatment of *Elizabethkingia* infection and has also been observed in previous reports (Han et al., 2017; Wang et al., 2020; Chang et al., 2021; Chiu et al., 2021; Kuo et al., 2021). Unfortunately, these results suggest that the choice of the abovementioned empirical antimicrobial therapy for *E. anophelis* remains controversial, and further investigations are urgently needed to determine the optimal antibiotics for treating this bacterium infection.

In the present study, all detected *E. anophelis* isolates were capable of forming biofilms. As mentioned, 40.6%, 41.6%, and 31% of clinical isolates formed strong, moderate or weak biofilms, respectively. These findings were comparable with the results reported by Tang et al., who noted that biofilm formation was high at 96.7%, as only one *E. anophelis* isolate tested negative for biofilm formation (Tang et al., 2021). Moreover, it was indicated that more than a quarter of the isolates tested positive for strong biofilm formation, with the highest OD values reaching 2.0 (Tang et al., 2021). In contrast, the biofilm-forming ability of the strain that we isolated was superior. Next, our data showed that the biofilm formation was higher in sputum samples, whereas weak biofilms were mainly formed in bloodstream infection *E. anophelis* strains. However, there may be a limitation because no comparable study can be obtained of *E. anophelis*. Thus, future investigations among *E. anophelis* strains from different sources are warranted.

In previous studies, it was documented that biofilm-forming bacteria could reduce antibiotic susceptibilities and be more resistant to the antibacterial agent than non–biofilm-forming strains (Yang et al., 2019; Shenkutie et al., 2020; Hashemzadeh et al., 2021). By comparing the results in this study, a similar outcome was found for the *E. anophelis* pathogen. The strains that obtained strong or moderate biofilm formation presented statistically significant higher resistances compared with the weak producers ($p < 0.05$), especially for piperacillin, piperacillin-tazobactam cefepime, amikacin, and ciprofloxacin. In a previous study, it was demonstrated that biofilm formation in MDR *Staphylococcus saprophyticus* isolates was significantly higher than that of non MDR *Staphylococcus saprophyticus* isolates. At the same time, no significant relationship was detected between MDR and biofilm formation intensity (strong, moderate, and weak) (Hashemzadeh et al., 2021). The result was similar to our findings, and in the present study, no significant relationship was observed between MDR, XDR, and biofilm-forming intensity. Compared with previous investigations, our results indicated that the correlation between the antibacterial agent and biofilm strength was different among the different antibiotics (Fauzia et al., 2020; Shadkam et al., 2021). For gentamicin, tetracycline, vancomycin, and chloramphenicol, no significant difference in biofilm formation between sensitive and resistant isolates was observed. We presume that this was partially due to the difference sample size, which may affect the statistical analysis. For example, 174 isolates were non-susceptible to gentamicin, and only seven were susceptible. For tetracycline, 178 isolates were non-susceptible, and only five were susceptible. It is important to understand and clarify the biofilm formation and antibiotic resistance mechanism of *E. anophelis* and identify effective method of blocking-up biofilm for the prevention and treatment of this species. However, previous studies in other

bacteria have documented that biofilm-acquired drug resistance is complicated and likely involves the expression of virulence genes and efflux pumps, growth and metabolic adaptations, horizontal gene transfer, gene mutation, stress response, and others factors (Bonifait et al., 2008; Soto, 2013; Dutkiewicz et al., 2018; Yi et al., 2020). Thus, outcomes from our investigation should be interpreted with caution, because the methods utilized in this investigation cannot be used to adequately assess biofilm-mediated MDR mechanisms.

To overcome this limitation, more thorough investigations to study the relationship between biofilm formation and antibacterial resistance, including faster conjugative plasmid transfer or multiplication of specific regulatory horizontal gene transfer genes, should be conducted in future studies to clarify these underlying mechanisms of action. In conclusion, studies on *E. anophelis* biofilms are still in its infancy. The result obtained in this study may be an essential stepping-stone for considering biofilm formation in drug susceptibility testing to improve the antimicrobial therapy effect with *E. anophelis* infections.

Data availability statement

The original contributions presented in the study are included in the article/**Supplementary Material**. Further inquiries can be directed to the corresponding authors.

Ethics Statement

No potentially identifiable human images or data was presented in this study and the surveillance was part of the hospital infection control.

Author contributions

Conceptualization: SH and BZ; data curation: SH, YL, and HX; formal analysis: SH and HX; funding acquisition: BZ and YX; methodology: BZ and YX; project administration: SH and YL; resources: BZ and YX; software: HX; supervision: BZ; writing—original draft preparation: SH; writing—review and editing: BZ and YX. All authors have read and agreed to the published version of the manuscript.

Funding

This work was supported by the Zhejiang Provincial Natural Science Foundation of China (Grant No. LQ21H190002), the Zhejiang Provincial Natural Science Foundation of China (Grant No. LQ20H080002), and the National Natural Science Foundation of China (No. 82072314). The Research Project of Jinan Microecological Biomedicine Shandong Laboratory (JNL-2022006B and JNL-2022011B), the Fundamental Research Funds for the Central Universities (2022ZFJH003), and CAMS Innovation Fund for Medical Sciences (2019-I2M-5-045).

Acknowledgments

SEM imaging was performed in the State Key Laboratory of Rice Biology of Zhejiang University, with the support of Dr. Fang Wang.

Conflict of interest

The authors declare that the research was conducted in the absence of any commercial or financial relationships that could be construed as a potential conflict of interest.

Publisher's note

Supplementary material

The Supplementary Material for this article can be found online at: https://www.frontiersin.org/articles/10.3389/fcimb.2022.953780/full#supplementary-material

References

Auffret, N., Anghel, R., Brisse, S., Rey, B., Schenesse, D., and Moquet, O. (2021). *Elizabethkingia anophelis* meningitis in a traveler returning from the americas. *Infect. Dis. Now* 51, 503–505. doi: 10.1016/j.medmal.2020.10.023

Bonifait, L., Grignon, L., and Grenier, D. (2008). Fibrinogen induces biofilm formation by *Streptococcus suis* and enhances its antibiotic resistance. *Appl. Environ. Microbiol.* 74, 4969–4972. doi: 10.1128/AEM.00558-08

Bulagonda, E. P., Manivannan, B., Mahalingam, N., Lama, M., Chanakya, P. P., Khamari, B., et al. (2018). Comparative genomic analysis of a naturally competent *Elizabethkingia anophelis* isolated from an eye infection. *Sci. Rep.* 8, 8447. doi: 10.1038/s41598-018-26874-8

Burnard, D., Gore, L., Henderson, A., Ranasinghe, A., Bergh, H., Cottrell, K., et al. (2020). Comparative genomics and antimicrobial resistance profiling of *Elizabethkingi*a isolates reveal nosocomial transmission and *In vitro* susceptibility

to fluoroquinolones, tetracyclines, and trimethoprim-sulfamethoxazole. *J. Clin. Microbiol.* 58, e00730–20. doi: 10.1128/JCM.00730-20

Chang, Y., Zhang, D., Niu, S., Chen, Q., Lin, Q., and Zhang, X. (2021). MBLs, rather than efflux pumps, led to carbapenem resistance in fosfomycin and Aztreonam/Avibactam resistant *Elizabethkingia anophelis*. *Infect. Drug Resistance* 14, 315–327. doi: 10.2147/IDR.S294149

Chen, S., Bagdasarian, M., and Walker, E. D. (2015). *Elizabethkingia anophelis*: molecular manipulation and interactions with mosquito hosts. *Appl. Environ. Microbiol.* 81, 2233–2243. doi: 10.1128/AEM.03733-14

Chew, K. L., Cheng, B., Lin, R. T. P., and Teo, J. W. P. (2018). *Elizabethkingia anophelis* is the dominant *Elizabethkingia* species found in blood cultures in Singapore. *J Clin Microbiol* 56, e01445–17. doi: 10.1128/JCM.01445-17

Chiu, C. T., Lai, C. H., Huang, Y. H., Yang, C. H., and Lin, J. N. (2021). Comparative analysis of gradient diffusion and disk diffusion with agar dilution for susceptibility testing of *Elizabethkingia anophelis*. *Antibiotics (Basel)* 10, 450. doi: 10.3390/antibiotics10040450

Choi, M. H., Kim, M., Jeong, S. J., Choi, J. Y., Lee, I. Y., Yong, T. S., et al. (2019). Risk factors for *Elizabethkingia* acquisition and clinical characteristics of patients, south Korea. *Emerg. Infect. Dis.* 25, 42–51. doi: 10.3201/eid2501.171985

Clinical and Laboratory Standards Institute (2020). *Performance standards for antimicrobial susceptibility testing, M100. 30th ed* (Wayne, PA, USA: CLSI).

Dutkiewicz, J., Zając, V., Sroka, J., Wasiński, B., Cisak, E., Sawczyn, A., et al. (2018). *Streptococcus suis*: a re-emerging pathogen associated with occupational exposure to pigs or pork products. part II - pathogenesis. *Ann. Agric. Environ. Med.* 25, 186–203. doi: 10.26444/aaem/85651

Fauzia, K. A., Miftahussurur, M., Syam, A. F., Waskito, L. A., Doohan, D., Rezkitha, Y. A. A., et al. (2020). Biofilm formation and antibiotic resistance phenotype of *Helicobacter pylori* clinical isolates. *Toxins (Basel)* 12, 473. doi: 10.3390/toxins12080473

Frank, T., Gody, J. C., Nguyen, L. B., Berthet, N., Le Fleche-Mateos, A., Bata, P., et al. (2013). First case of *Elizabethkingia anophelis* meningitis in the central African republic. *Lancet* 381, 1876. doi: 10.1016/S0140-6736(13)60318-9

Goldstein, B. P. (2014). Resistance to rifampicin: a review. *J. Antibiot (Tokyo)* 67, 625–630. doi: 10.1038/ja.2014.107

Han, M. S., Kim, H., Lee, Y., Kim, M., Ku, N. S., and Choi, J. Y. (2017). Relative prevalence and antimicrobial susceptibility of clinical isolates of *Elizabethkingia* species based on 16S rRNA gene sequencing. *J. Clin. Microbiol.* 55, 274–280. doi: 10.1128/JCM.01637-16

Harika, K., Shenoy, V. P., Narasimhaswamy, N., and Chawla, K. (2020). Detection of biofilm production and its impact on antibiotic resistance profile of bacterial isolates from chronic wound infections. *J. Glob. Infect. Dis.* 12, 129–134. doi: 10.4103/jgid.jgid_150_19

Hashemzadeh, M., Dezfuli, A. A. Z., Nashibi, R., Jahangirimehr, F., and Akbarian, Z. A. (2021). Study of biofilm formation, structure and antibiotic resistance in *Staphylococcus saprophyticus* strains causing urinary tract infection in women in ahvaz, Iran. *New Microbes New Infect.* 39, 100831. doi: 10.1016/j.nmni.2020.100831

Hu, S., Jiang, T., Zhang, X., Zhou, Y., Yi, Z., Wang, Y., et al. (2017). *Elizabethkingia anophelis* isolated from patients with multiple organ dysfunction syndrome and lower respiratory tract infection: Report of two cases and literature review. *Front. Microbiol.* 8, 382. doi: 10.3389/fmicb.2017.00382

Husain, F. M., Perveen, K., Qais, F. A., Ahmad, I., Alfarhan, A. H., and El-Sheikh, M. A. (2021). Naringin inhibits the biofilms of metallo-β-lactamases (MβLs) producing *Pseudomonas* species isolated from camel meat. *Saudi J. Biol. Sci.* 28, 333–341. doi: 10.1016/j.sjbs.2020.10.009

Jacobs, A., and Chenia, H. Y. (2011). Biofilm formation and adherence characteristics of an *Elizabethkingia meningoseptica* isolate from *Oreochromis mossambicus*. *Ann. Clin. Microbiol. Antimicrob.* 10, 16. doi: 10.1186/1476-0711-10-16

Janda, J. M., and Lopez, D. L. (2017). Mini review: New pathogen profiles: *Elizabethkingia anophelis*. *Diagn. Microbiol. Infect. Dis.* 88, 201–205. doi: 10.1016/j.diagmicrobio.2017.03.007

Jean, S. S., Hsieh, T. C., Ning, Y. Z., and Hsueh, P. R. (2017). Role of vancomycin in the treatment of bacteraemia and meningitis caused by *Elizabethkingia meningoseptica*. *Int. J. Antimicrob. Agents* 50, 507–511. doi: 10.1016/j.ijantimicag.2017.06.021

Jian, M. J., Cheng, Y. H., Chung, H. Y., Cheng, Y. H., Yang, H. Y., Hsu, C. S., et al. (2019). Fluoroquinolone resistance in carbapenem-resistant *Elizabethkingia anophelis*: phenotypic and genotypic characteristics of clinical isolates with topoisomerase mutations and comparative genomic analysis. *J. Antimicrob. Chemother.* 74, 1503–1510. doi: 10.1093/jac/dkz045

Karami, N., Lindblom, A., Yazdanshenas, S., Lind, N. ,. V., and Åhr, N. ,. C. (2020). Recurrence of urinary tract infections with extended-spectrum β-lactamase-producing escherichia coli caused by homologous strains among which clone ST131-O25b is dominant. *J. Glob. Antimicrob. Resist.* 22, 126–132. doi: 10.1016/j.jgar.2020.01.024

Kelly, A. J., Karpathy, S. E., Gulvik, C. A., Ivey, M. L., Whitney, A. M., Bell, M. E., et al. (2019). A real-time multiplex PCR assay for detection of *Elizabethkingia* species and differentiation between *Elizabethkingia anophelis* and *E. meningoseptica*. *J. Clin. Microbiol.* 57, e01619–18. doi: 10.1128/JCM.01619-18

Kuo, S. C., Tan, M. C., Huang, W. C., Wu, H. C., Chen, F. J., Liao, Y. C., et al. (2021). Susceptibility of elizabethkingia spp. to commonly tested and novel antibiotics and concordance between broth microdilution and automated testing methods. *J. Antimicrob. Chemother.* 76, 653–658. doi: 10.1093/jac/dkaa499

Kyritsi, M. A., Mouchtouri, V. A., Pournaras, S., and Hadjichristodoulou, C. (2018). First reported isolation of an emerging opportunistic pathogen (*Elizabethkingia anophelis*) from hospital water systems in Greece. *J. Water Health* 16, 164–170. doi: 10.2166/wh.2017.184

Larkin, P. M. K., Mortimer, L., Malenfant, J. H., Gaynor, P., Contreras, D. A., Garner, O. B., et al. (2021). Investigation of phylogeny and drug resistance mechanisms of *Elizabethkingia anophelis* isolated from blood and lower respiratory tract. *Microb. Drug Resist.* 27, 1259–1264. doi: 10.1089/mdr.2020.0263

Lau, S. K., Chow, W. N., Foo, C. H., Curreem, S. O., Lo, G. C., Teng, J. L., et al. (2016). *Elizabethkingia anophelis* bacteremia is associated with clinically significant infections and high mortality. *Sci. Rep.* 6, 26045. doi: 10.1038/srep26045

Lee, Y. L., Liu, K. M., Chang, H. L., Lin, J. S., Kung, F. Y., Ho, C. M., et al. (2021). A dominant strain of *Elizabethkingia anophelis* emerged from a hospital water system to cause a three-year outbreak in a respiratory care center. *J. Hosp Infect.* 108, 43–51. doi: 10.1016/j.jhin.2020.10.025

Lin, J. N., Lai, C. H., Yang, C. H., and Huang, Y. H. (2018a). Comparison of clinical manifestations, antimicrobial susceptibility patterns, and mutations of fluoroquinolone target genes between *Elizabethkingia meningoseptica* and *Elizabethkingia anophelis* isolated in Taiwan. *J. Clin. Med.* 7, e538. doi: 10.3390/jcm7120538

Lin, J. N., Lai, C. H., Yang, C. H., and Huang, Y. H. (2019). *Elizabethkingia* infections in humans: from genomics to clinics. *Microorganisms* 7, e295. doi: 10.3390/microorganisms7090295

Lin, J. N., Lai, C. H., Yang, C. H., Huang, Y. H., and Lin, H. H. (2018b). Clinical manifestations, molecular characteristics, antimicrobial susceptibility patterns and contributions of target gene mutation to fluoroquinolone resistance in *Elizabethkingia anophelis*. *J. Antimicrob. Chemother.* 73, 2497–2502. doi: 10.1093/jac/dky197

Lin, J. N., Lai, C. H., Yang, C. H., Huang, Y. H., Lin, H. F., and Lin, H. H. (2017). Comparison of four automated microbiology systems with 16S rRNA gene sequencing for identification of *Chryseobacterium* and *Elizabethkingia* species. *Sci. Rep.* 7, 13824. doi: 10.1038/s41598-017-14244-9

Magiorakos, A. P., Srinivasan, A., Carey, R. B., Carmeli, Y., Falagas, M. E., Giske, C. G., et al. (2012). Multidrug-resistant, extensively drug-resistant and pandrug-resistant bacteria: an international expert proposal for interim standard definitions for acquired resistance. *Clin. Microbiol. Infect.* 18, 268–281. doi: 10.1111/j.1469-0691.2011.03570.x

Mantoo, M. R., Ghimire, J. J., Mahopatra, S., and Sankar, J. (2021). *Elizabethkingia anophelis* infection in an infant: an unusual presentation. *BMJ Case Rep.* 14, e243078. doi: 10.1136/bcr-2021-243078

Navon, L., Clegg, W. J., Morgan, J., Austin, C., Mcquiston, J. R., Blaney, D. D., et al. (2016). Notes from the field: Investigation of *Elizabethkingia anophelis* cluster - Illinois 2014-2016. *MMWR Morb Mortal Wkly Rep.* 65, 1380–1381. doi: 10.15585/mmwr.mm6548a6

Nicholson, A. C., Gulvik, C. A., Whitney, A. M., Humrighouse, B. W., Graziano, J., Emery, B., et al. (2018). Revisiting the taxonomy of the genus *Elizabethkingia* using whole-genome sequencing, optical mapping, and MALDI-TOF, along with proposal of three novel *Elizabethkingia* species: Elizabethkingia bruuniana sp. nov., *Elizabethkingia ursingii* sp. nov., and *Elizabethkingia occulta* sp. nov. *Antonie Van Leeuwenhoek* 111, 55–72. doi: 10.1007/s10482-017-0926-3

Nielsen, H. L., Tarpgaard, I. H., Fuglsang-Damgaard, D., Thomsen, P. K., Brisse, S., and Dalager-Pedersen, M. (2018). Rare *Elizabethkingia anophelis meningitis* case in a Danish male. *JMM Case Rep.* 5, e005163. doi: 10.1099/jmmcr.0.005163

Perrin, A., Larsonneur, E., Nicholson, A. C., Edwards, D. J., Gundlach, K. M., Whitney, A. M., et al. (2017). Evolutionary dynamics and genomic features of the elizabethkingia anophelis 2015 to 2016 Wisconsin outbreak strain. *Nat. Commun.* 8, 15483. doi: 10.1038/ncomms15483

Ranjbar-Omid, M., Arzanlou, M., Amani, M., Shokri Al-Hashem, S. K., Amir Mozafari, N., and Peeri Doghaheh, H. (2015). Allicin from garlic inhibits the biofilm formation and urease activity of *Proteus mirabilis in vitro*. *FEMS Microbiol. Lett.* 362, fnv049. doi: 10.1093/femsle/fnv049

Seong, H., Kim, J. H., Kim, J. H., Lee, W. J., Ahn, J. Y., M D, N., et al. (2020). Risk factors for mortality in patients with *Elizabethkingia* infection and the clinical impact of the antimicrobial susceptibility patterns of *Elizabethkingia* species. *J. Clin. Med.* 9, 1431. doi: 10.3390/jcm9051431

Shadkam, S., Goli, H. R., Mirzaei, B., Gholami, M., and Ahanjan, M. (2021). Correlation between antimicrobial resistance and biofilm formation capability among *Klebsiella pneumoniae* strains isolated from hospitalized patients in Iran. *Ann. Clin. Microbiol. Antimicrob.* 20, 13. doi: 10.1186/s12941-021-00418-x

Shenkutie, A. M., Yao, M. Z., Siu, G. K., Wong, B. K. C., and Leung, P. H. (2020). Biofilm-induced antibiotic resistance in clinical *Acinetobacter baumannii* isolates. *Antibiotics (Basel)* 9, 817. doi: 10.3390/antibiotics9110817

Soto, S. M. (2013). Role of efflux pumps in the antibiotic resistance of bacteria embedded in a biofilm. *Virulence* 4, 223–229. doi: 10.4161/viru.23724

Tang, H. J., Lin, Y. T., Chen, C. C., Chen, C. W., Lu, Y. C., Ko, W. C., et al. (2021). Molecular characteristics and *in vitro* effects of antimicrobial combinations on planktonic and biofilm forms of *Elizabethkingia anophelis*. *J. Antimicrob. Chemother* 76, 1205–1214. doi: 10.1093/jac/dkab018

Teo, J., Tan, S. Y., Tay, M., Ding, W., Kjelleberg, S., Givskov, M., et al. (2013). First case of *E anophelis* outbreak in an intensive-care unit. *Lancet* 382, 855–856. doi: 10.1016/S0140-6736(13)61858-9

Wang, M., Gao, H., Lin, N., Zhang, Y., Huang, N., Walker, E. D., et al. (2019). The antibiotic resistance and pathogenicity of a multidrug-resistant *Elizabethkingia anophelis* isolate. *Microbiologyopen* 8, e804. doi: 10.1002/mbo3.804

Wang, L., Zhang, X., Li, D., Hu, F., Wang, M., Guo, Q., et al. (2020). Molecular characteristics and antimicrobial susceptibility profiles of *Elizabethkingia* clinical isolates in shanghai, China. *Infect. Drug Resist.* 13, 247–256. doi: 10.2147/IDR.S240963

Xu, L., Peng, B., He, Y., Cui, Y., Hu, Q., Wu, Y., et al. (2022). Isolation of *Elizabethkingia anophelis* from COVID-19 swab kits. *Front. Microbiol.* 12, 799150. doi: 10.3389/fmicb.2021.799150

Yang, C. H., Su, P. W., Moi, S. H., and Chuang, L. Y. (2019). Biofilm formation in *Acinetobacter baumannii*: Genotype-phenotype correlation. *Molecules* 24, 1849. doi: 10.3390/molecules24101849

Yi, L., Jin, M., Li, J., Grenier, D., and Wang, Y. (2020). Antibiotic resistance related to biofilm formation in. *Streptococcus Suis* 104, 8649–8660. doi: 10.1007/s00253-020-10873-9

frontiers | Frontiers in Cellular and Infection Microbiology

TYPE Original Research
PUBLISHED 21 September 2022
DOI 10.3389/fcimb.2022.1006723

OPEN ACCESS

EDITED BY
Rodnei Dennis Rossoni,
Independent researcher, São José dos Campos, Brazil

REVIEWED BY
Daniel Heredia,
Universidad Nacional de Río Cuarto, Argentina
Svetlana A. Ermolaeva,
N.F. Gamaleya Scientific Research Institute of Epidemiology and Microbiology (RAMS), Russia

*CORRESPONDENCE
Alisa Gricajeva
alisa.gricajeva@gmc.vu.lt

SPECIALTY SECTION
This article was submitted to Biofilms, a section of the journal Frontiers in Cellular and Infection Microbiology

RECEIVED 01 August 2022
ACCEPTED 01 September 2022
PUBLISHED 21 September 2022

CITATION
Gricajeva A, Buchovec I, Kalėdienė L, Badokas K and Vitta P (2022) Riboflavin- and chlorophyllin-based antimicrobial photoinactivation of *Brevundimonas* sp. ESA1 biofilms. *Front. Cell. Infect. Microbiol.* 12:1006723. doi: 10.3389/fcimb.2022.1006723

Riboflavin- and chlorophyllin-based antimicrobial photoinactivation of *Brevundimonas* sp. ESA1 biofilms

Alisa Gricajeva[1]*, Irina Buchovec[2], Lilija Kalėdienė[1], Kazimieras Badokas[2] and Pranciškus Vitta[2]

[1]Department of Microbiology and Biotechnology, Life Sciences Center, Institute of Biosciences, Vilnius University, Vilnius, Lithuania, [2]Institute of Photonics and Nanotechnology, Faculty of Physics, Vilnius University, Vilnius, Lithuania

Some *Brevundimonas* spp. are globally emerging opportunistic pathogens that can be dangerous to individuals with underlying medical conditions and for those who are immunocompromised. Gram-negative *Brevundimonas* spp. can form resilient sessile biofilms and are found not only in different confined terrestrial settings (e.g., hospitals) but are also frequently detected in spacecraft which is inhabited by astronauts that can have altered immunity. Therefore, *Brevundimonas* spp. pose a serious health hazard in different environments, especially in its biofilm form. Conventional antimicrobials applied to disrupt, inactivate, or prevent biofilm formation have limited efficiency and applicability in different closed-loop systems. Therefore, new, effective, and safe biofilm control technologies are in high demand. The present work aimed to investigate antimicrobial photoinactivation (API) of *Brevundimonas* sp. ESA1 monocultural biofilms mediated by non-toxic, natural photosensitizers such as riboflavin (RF) and chlorophyllin (Chl) with an emphasis of this technology as an example to be safely used in closed-loop systems such as spacecraft. The present study showed that Chl-based API had a bactericidal effect on *Brevundimonas* sp. ESA1 biofilms at twice the lower irradiation doses than was needed when applying RF-based API. Long-term API based on RF and Chl using 450 nm low irradiance plate has also been studied in this work as a more practically applicable API method. The ability of *Brevundimonas* sp. ESA1 biofilms to reduce alamarBlue™ and regrowth analysis have revealed that after the applied photoinactivation, bacteria can enter a viable but non-culturable state with no ability to resuscitate in some cases.

KEYWORDS

bacterial biofilms, antimicrobial photoinactivation, riboflavin, chlorophyllin, *Brevundimonas*

1 Introduction

Naturally most of the bacteria are found living in a multicellular coordinated functional communities known as biofilms. Bacterial biofilms consist of bacterial cells encased in a self-produced extracellular polymeric substance (EPS) made of polysaccharides, proteins, and extracellular DNA (eDNA) (Flemming et al., 2016; Penesyan et al., 2021). EPS is the underlying physical factor determining the ability of bacterial cells to be more resistant to adverse external impacts than free-living cells (Hall-Stoodley et al., 2004; Reichhardt et al., 2014). Bacterial biofilms are common in different industrial settings, food facilities, water systems, bathrooms, laboratories, hospitals, and even spacecraft (Buchovec et al., 2020). Once established, biofilms become less susceptible to common antimicrobials such as antibiotics, chemical disinfectants, physical stress, and the human immune system (Mora et al., 2019; Muhammad et al., 2020; Ciofu et al., 2022). Therefore, biofilms are of special concern not only in confined areas such as hospitals, industrial food-associated premises on Earth, but also closed-loop spacecraft systems. Human-manned spacecraft is a unique environment encountering dangerous microbial contamination even though the spacecraft is assembled in a cleanroom (Checinska et al., 2015; Mora et al., 2016; Bashir et al., 2016; Nakajima et al., 2017). Spacecraft conditions such as space radiation, microgravity, and elevated carbon dioxide levels adversely affect health and the immune system of the astronauts. Therefore, microbial contamination, especially in the form of biofilms, can be very dangerous for the immunocompromised spacecraft crew members and the overall material integrity (Decelle and Taylor, 1976; Sobisch et al., 2019). The most abundant airborne and surface bacteria in spacecraft belong to *Staphylococcus* spp., *Bacillus* spp., *Enterococcus* spp., *Corynebacterium* spp. and *Propionibacterium* spp. (Borisov et al., 2003; La Duc et al., 2004a; Novikova et al., 2006; Venkateswaran et al., 2014; Checinska et al., 2015; Koskinen et al., 2017; Regberg et al., 2020). *Methylobacterium* spp., *Sphingomonas paucimobilis*, *Cupriavidus* spp., *Chryseobacterium* spp., and *Ralstonia* spp. are most frequently found in potable water systems (La Duc et al., 2004b; Wong et al., 2010; Mijnendonckx et al., 2013; Nakajima et al., 2017; Thompson et al., 2020). Most spacecraft bacteria are human-associated and play the main role in the formation and the diversity of spacecraft microbiota (Mora et al., 2016; Be et al., 2017; Zea et al., 2018).

However, according to recent findings, one of the emerging bacterial genera that is not so abundant but is also frequently detected in different spacecraft samples is *Brevundimonas* spp. (Kawamura et al., 2001; La Duc et al., 2004b; Li et al., 2004; Ghosh et al., 2010; Stieglmeier et al., 2012; Vornhagen et al., 2013) *Brevundimonas* spp. are non-fermenting Gram-negative bacteria that can form sessile biofilms, with some of the species being a cause of serious infections in individuals with underlying medical conditions (Vornhagen et al., 2013). The genus was established by Segers et al. (1994) when authors presented the re-classification of *Pseudomonas diminuta* and *Pseudomonas vesicularis* to *Brevundimonas diminuta* and *Brevundimonas vesicularis*, respectively (Segers et al., 1994). *B. diminuta* and *B. vesicularis* are concerned to be emerging global opportunistic pathogens due to recent findings of multiple infections caused by these species indicating that the genus may be a more widespread pathogen than it was hitherto thought. And apparently, infections caused by *Brevundimonas* spp. can be invasive and dangerous for people having chronic diseases or those who are immunocompromised (Han and Andrade, 2005; Ryan and Pembroke, 2018). Therefore, it is a matter of concern that the species of the genus are being constantly detected not only in different terrestrial facilities but also in spacecraft. In a varying abundance, *Brevundimonas* spp. was recovered from ISS-associated potable water samples at various stages of their purification, storage, and transport. Detection of *Brevundimonas* spp. in the water system of spacecraft means that it can survive in spacecraft essential systems, forming more resistant biofilm forms (La Duc et al., 2004b; Vornhagen et al., 2013). A study of the abundance and diversity of microbial bioburden in European spacecraft-associated clean rooms by molecular analysis revealed that *Brevundimonas* was among the most common (Stieglmeier et al., 2012).

Recently, *Brevundimonas* sp., among some other species, was determined to form biofilms that developed higher concentration of antibiotic resistant bacteria (ARB) under the disinfection pressure of chlorination and chloramination. This study indicated that biofilm detachment might become a cause of the movement of biofilm clusters with higher ARB concentration into water, thereby increasing the antibiotic resistance of bacteria in tap water (Zhang et al., 2019a). In a study of Low et al. (2016), as a genus of *Proteobacteria*, *Brevundimonas* was found to be resistant to eight antibiotics and was reported to contain tetracycline resistance genes (Miranda et al., 2003; Adelowo and Fagade, 2009). *Brevundimonas* spp. can exhibit resistance to heavy metals as well (Zhang et al., 2019b).

The most interesting finding about *Brevundimonas* is that it is found to be one of a few bacteria exhibiting high survival rates under simulated Martian conditions. Dartnell et al. (2010) have studied the survival responses of some novel psychrotolerant bacterial strains (isolated from the Antarctic Dry Valleys) to ionizing radiation while frozen at -79 °C, the temperature that is typical to Martian near-subsurface environment. Interestingly, one of the novel isolates of the Antarctic Dry Valleys was identified as *Brevundimonas* sp. MV.7 and was determined to be the most resistant to radiation. Experimental irradiation combined with previous radiation modelling indicated that *Brevundimonas* sp. MV.7 in 30 cm deep Martian dust could survive the space radiation for up to 100,000 years before having a 10^6 population reduction (Dartnell et al., 2010).

Therefore, some of the *Brevundimonas* species, due to its multiple resilience should pose serious concern in some terrestrial and especially spacecraft environments. Since conventional antimicrobials applied to disrupt, inactivate, or prevent biofilm formation have limited efficiency and applicability in closed-loop systems like spacecraft, new, effective, environmentally friendly, and safe biofilm control technologies are in a high demand.

One of the potential alternatives that provide many significant advantages is antimicrobial photoinactivation (API) (also known as antimicrobial photodynamic therapy - aPDT) - a technology based on interaction between non-toxic photosensitizer (PS), molecular oxygen, and appropriate doses of visible light of a certain wavelength that excites the PS (St. Denis et al., 2011; Hamblin, 2016). Usually, after light excitation, the triplet-state of PS interacts with molecular oxygen, electron donors or acceptors and can produce reactive oxygen species (ROS), thereby triggering photo-oxidative reactions that initiate various cellular damages and destruction of microorganisms (Hu et al., 2018). Different investigators have confirmed that microorganisms, including bacteria, viruses, molds, and protozoa, whether *in vitro* or *in vivo*, can be killed by API treatment (Wainwright, 2004; Jori and Brown, 2004; Luksiene, 2005; Buchovec et al., 2016; Temba et al., 2016). One of the major advantages of API is that the resistance of bacteria to API is unlikely to occur and it can be safely used in closed-loop systems (Liu et al., 2015; Maisch, 2015; Kashef and Hamblin, 2017). For the inactivation of both planktonic and sessile biofilm forms of bacteria in spacecraft and other sensitive confined systems - a non-toxic, chemically pure and stable, non-bleaching, easy-to-produce, and water-soluble PSs should be used. Most of the natural PSs meet the above-listed criteria and are one of the safest options of PSs for spacecraft use that have been proposed to date. Currently, four main natural products have been applied for API: curcumin, riboflavin, perylenequinones (hypericin, hypocrellin), psoralens (Yin et al., 2014). Recently, chlorophyll derivatives, such as sodium chlorophyllin were shown to be effective as natural PSs as well (Luksiene et al., 2010; Buchovec et al., 2010; Buchovec et al., 2017; Krüger et al., 2019; Luksiene and Buchovec, 2019; Buchovec et al., 2022). This study focuses on natural promising PSs - riboflavin (RF) or vitamin B2 and chlorophyllin (Chl) that could be potentially used in closed-loop systems as non-toxic and harmless to humans and plants. Both PSs – RF and Chl - are known photoactive compounds used as food colorants having "Generally Recognized As Safe" (GRAS) status. Also, it is essential to note that both PSs, RF and Chl, are photoactive in the visible-light range and have absorption maximums at 440 and 402 nm, respectively (Buchovec et al., 2020). RF is a naturally occurring water-soluble compound and an essential human nutrient and is used as a food colorant E 101. It plays an important role in the metabolism of the cells and can be considered safe when administered to humans (Astanov et al., 2014; Sheraz et al., 2014). Chl is also water-soluble food colorant - sodium magnesium chlorophyllin (E 140 (ii)), which is extracted from different plants such as spinach, grass, dandelion, green cabbage, water hyacinth, and algae. Chl is a semi-synthetic porphyrin obtained from chlorophyll which generates ROS with antimicrobial activity after exposure to visible light (Buchovec et al., 2017). Nevertheless, studies and applications of the RF-based (RF-API) and Chl-based (Chl-API) API to control Gram-negative bacteria pathogens, especially their biofilms, remain scarce. Furthermore, no API, neither with natural nor with other PSs has been performed on *Brevundimonas* spp. that are a matter of concern in both terrestrial and spacecraft settings. The present study aims to investigate whether RF-based and Chl-based API can efficiently inactivate biofilms of *Brevundimonas* sp. ESA1.

2 Materials and methods

2.1 Photosensitizers

Non-copperized chlorophyllin sodium salt (Chl) (M_W = 684.9 g/mol) was obtained from Carl Roth (Germany). The aqueous stock solution of 0.15 mM Chl (pH = 6.8) was prepared by dissolving Chl in distilled water. Riboflavin (RF) (M_W = 376.36 g/mol)) was obtained from Sigma-Aldrich (USA). Aqueous stock solution of 0.11 mM RF (pH 6.2) was prepared according to the method of Mazzotta et al. (2014): RF was dissolved in distilled water using a magnetic stirrer at 25°C in the dark. Both PSs were filter-sterilized before use for the photoinactivation experiments. All working solutions were freshly prepared by diluting them with 0.01 M PBS buffer (pH 7.4) (Carl Roth, Germany) on the day of use.

2.2 Light source

The LED-based light source (an irradiation box) (Figure 1A) for RF-API and Chl-API was developed at the Institute of Photonics and Nanotechnology of Vilnius University (VU). Two types of LEDs (402 nm and 440 nm) with emission peaks near the maximum absorption of RF and Chl (Buchovec et al., 2022) were used (Figure 1B).

The light irradiance at the surface of the samples reached 5, 20 and 25 mW/cm^2. The irradiation dose was calculated as irradiance multiplied by irradiation time. The sample exposure time was adjusted according to the equation:

$$E = P \times t$$

where E is the energy density (dose) in J/cm^2, P is the irradiance (light flux density) in mW/cm^2, and t is the time in seconds. The exemplary irradiation dose calculations are shown in Table 1.

10.3389/fcimb.2022.1006723

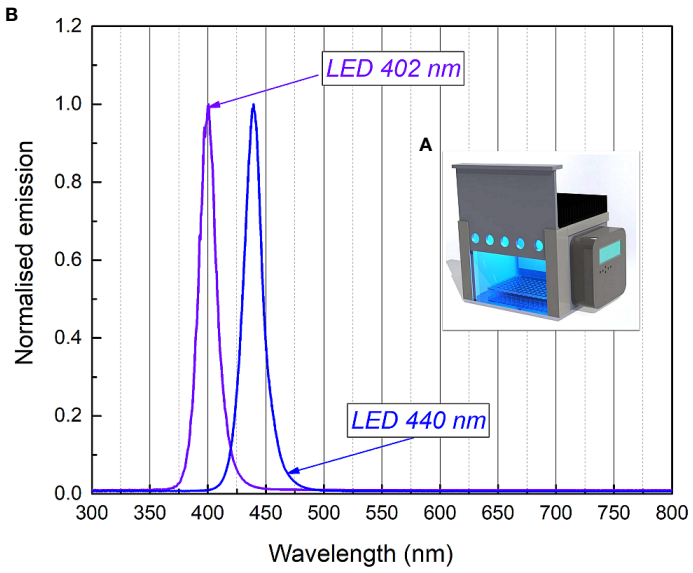

FIGURE 1
3D render picture **(A)** of the developed illumination system (the irradiation box) and normalized emission spectra of the 402 nm (Kingbright KTDS-3534UV405B), 440 nm (Osram GD QSSPA1.14) LEDs installed into the illumination system **(B)**.

The light source used for long-term irradiation of biofilms was developed and constructed as a Constant Irradiation Plate (CIP; developed in the Institute of Photonics and Nanotechnology, VU) with 1.4 mW/cm^2 uniform irradiance by LEDs peaked at 450 nm (Figure 2). The CIP is a multicolor micro-controller controlled LED source for upward irradiation. The device has an internal temperature feed-back circuit to maintain irradiation stability under long-term experiments. CIP was calibrated before the experiments with a spectro-radiometer (Avantes AvaSpec-ULS2048LTEC with AvaSphere-50-LS-HAL-CAL).

TABLE 1 Irradiation doses used in experiments.

Time (min)	Irradiation dose (J/cm^2)		
	402 nm/440 nmIrradiance 5 mW/cm^2	402 nmIrradiance 20 mW/cm^2	440 nmIrradiance 25 mW/cm^2
2	0.6	n	n
5	1.5	n	n
10	3	n	n
15	4.5	n	n
20	6	n	n
25	7.5	n	n
30	9	36	45
35	10.5	n	n
45	13.5	n	n
55	16.5	n	n
60	n	72	90
65	19.5	n	n
75	22.5	n	n
90	27	108	135
120	36	144	180
150	n	180	n
180	n	216	n

n-was not used.

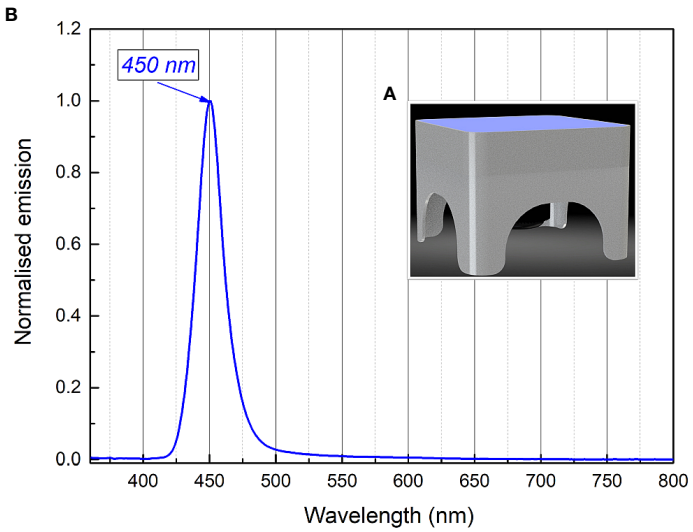

FIGURE 2
Constant irradiance plate 3D model **(A)**, relative irradiance spectrum **(B)**.

2.3 Spectrophotometric measurements of RF and Chl

Aqueous solutions of 0.011 mM RF (pH 7.4) and 0.015 mM Chl (pH 7.4) were illuminated with a LED-based light source (irradiation box) for analysis of the photostability of the PSs. The changes in the absorption spectra of RF and Chl were investigated after LED illumination at 440 nm and 402 nm, respectively. For this purpose, 200 µL of the PSs were transferred to sterile flat-bottom 96-well microtiter plates (MtP) and exposed to 5 mW/cm^2 irradiance. After each irradiation dose applied separately, the samples (3 mL) were collected into cuvettes and used for spectrophotometric measurements.

The absorption spectra of both PSs solutions were recorded by means of a LAMBDA 950 UV-VIS-NIR spectrophotometer (PerkinElmer, USA) in spectral range of 300-600 nm. Polymethyl methacrylate cuvettes of 1 cm optical thickness were used for the measurements. All measurements were performed at 20 ± 2°C.

2.4 Bacterial genus confirmation by 16S rDNA analysis

Bacterial strain that was used as a model organism for RF-API and Chl-API studies was obtained from the collection of microorganisms of the Department of Microbiology and Biotechnology, Institute of Biosciences, Life Sciences Center, VU. For the confirmation of the genus of the strain, DNA sequence of the bacteria coding for 16S rRNA was amplified as described previously (Gricajeva et al., 2016) using 27F (5′-GAG AGT TTG ATC CTG GCT CAG-3′) and 1495R (5′-CTA CGG CTA CCT TGT TAC GA-3′) universal primers (METABION, Germany). Purified amplicon was sequenced at VU Life Sciences Center, Institute of Biotechnology (Lithuania). NCBI Basic Local Alignment Search Tool (BLASTn) (Altschul et al., 1990) was used for database similarity searches.

2.5 Culture conditions of planktonic bacterial cells

Bacteria were grown in Luria Bertani (LB) (Carl Roth, Germany) broth at 37°C under constant 180 rpm shaking (IKA, Germany) overnight. The overnight culture was inoculated to a fresh LB media and grown under the same conditions until optical density (OD) of 0.22 at 600 nm (OD_{600}) corresponding to the concentration of 10^9 CFU/mL was reached. Bacterial cells were harvested by centrifugation (5 min, 5000 × *g*), resuspended in 0.01 M PBS (pH 7.4) and immediately used for the RF-API and Chl-API experiments.

2.6 Photoinactivation of planktonic bacteria

For the assay of antimicrobial inactivation of free-floating (planktonic) *Brevundimonas* sp. ESA1, bacterial cells of the strain were resuspended to a final concentration of 10^7 CFU/mL in 0.011 mM RF (pH 7.4) or 0.015 mM Chl (pH 7.4) in the dark. Solution consisting of bacterial suspension in 0.01 M PBS (pH 7.4) was used as a control. Aliquots of 200 µL of prepared

mixtures of bacterial suspensions with appropriate PSs (RF or Chl, pH 7.4) or 0.01 M PBS (pH 7.4) were pipetted into sterile flat-bottom 96-well polystyrene MtP and exposed to different irradiation doses (Table 1). The light source (Figure 1A) used for the photoinactivation experiments consisted of a LED array (λ = 440 nm for RF and λ = 405 nm for Chl) with an intensity of 5 mW/cm^2 at a distance of approximately 7 cm. Following irradiation, at each sampling step, withdrawn bacterial suspensions were appropriately diluted, spread on LB agar plates and incubated at 37°C for 16-36 h. Residual bacterial cell viability was determined by counting CFU. The numbers of surviving bacteria (CFU/mL) were transformed to $\log_{10}$ scale. CFU counts of the bacterial cells that were incubated with RF, Chl or PBS in the dark (dark controls) were also determined.

2.7 Monocultural bacterial biofilm formation in microtiter plates

For the monocultural biofilm formation bacterial strain was grown as it was described in Section 2.5 until OD_{600} corresponding to the concentration of 10^8 CFU/mL. Then 100 µL of the suspension was pipetted into sterile flat-bottom 96-well polystyrene MtP wells. MtPs with the required number of wells filled with bacterial suspension were statically incubated 20 h at 37°C. Biofilms that formed in the wells of MtP were washed three times with 0.01 M PBS (pH 7.4) in order to remove residual planktonic cells. Biofilms were further used for the API (Section 2.8). Formation of *Brevundimonas* sp. ESA1 biofilms in the MtP wells was verified by staining with 0.1% solution of crystal violet (Merritt et al., 2005; Trotonda et al., 2008).

2.8 Photoinactivation of biofilm

Brevundimonas sp. ESA1 biofilms were formed in MtPs as it was described in Section 2.7. For the API, the wells of the 96-well MtPs containing the biofilm were filled with 0.011 mM RF (pH 7.4), 0.015 mM Chl (pH 7.4) or 0.01 M PBS (pH 7.4) by adding 200 µL of the appropriate solution. Then biofilms were immediately placed into irradiation boxes and irradiated with 440 nm at 25 mW/cm^2 or 402 nm at 20 mW/cm^2 for the photoactivation of RF and Chl, respectively. The control samples were also illuminated with the same wavelength of light. Biofilms were exposed to different illumination doses (Table 1). At each step of sampling, bacterial biofilms were mechanically detached from the MtP well walls, vigorously vortexed and diluted for the further viability determination by counting CFU on LB agar plates which after the spreading of samples were incubated at 37°C for 16-36 h. The numbers of surviving bacteria (CFU/mL) were transformed to $\log_{10}$ scale. CFU counts of *Brevundimonas* sp. ESA1 biofilm-forming cells that were incubated with RF/Chl or without RF/Chl in the dark were also determined.

2.9 Viability assay of photoinactivated biofilms using alamarBlue™ by fluorescence

Following photoinactivation, additionally to residual CFU count determination after RF-API and Chl-API, viability, and metabolic function of *Brevundimonas* sp. ESA1 biofilms was quantitatively analyzed by evaluating their ability to reduce resazurin-based compound alamarBlue™ (Invitrogen, USA). Non-toxic reagent alamarBlue™ is used as an indicator of cellular reducing environment or cell viability and death. The reagent is modified in reducing conditions that are characteristic to viable cells and becomes detectable due to its subsequently occurring color change or/and high fluorescence. Dead or non-viable cells are not able to change the color of alamarBlue™ (Rampersad, 2012).

In the current experiment *Brevundimonas* sp. ESA1 biofilms after RF-API and Chl-API that caused ≥3 $\log_{10}$ reduction (and corresponding dark controls) were mechanically detached, vortexed and added to alamarBlue™. The volume ratio of alamarBlue™ and disrupted biofilms was 1:10. Samples were incubated 3 h at 37°C (according to the manufacturer's recommendations) and then fluorescence changes were measured every hour (in total for 11 h) using a plate reader (Thermo Fisher Scientific Verioscan Flash, USA). Fluorescence changes were read using excitation at 560 nm and emission at 590 nm.

Percentage reduction of alamarBlue™ by fluorescence indicating cell viability or death of all RF-API and Chl-API tested groups was determined by using the equation:

$$\textbf{\% reduction of alamarBlue}^{\textbf{TM}} = \frac{\textbf{FI 590 of test agent} - \textbf{FI 590 of untreated control}}{\textbf{FI 590 of 100 \% reduced alamarBlue} - \textbf{FI of untreated control}} \times 100\,\%,$$

where FI 590 is fluorescence intensity at 590 nm emission (excitation at 560 nm).

2.10 Long-term RF- and Chl-API of *Brevundimonas* sp. ESA1 biofilms

Long-term RF-based and Chl-based API experiments were performed to test the photoinactivation efficacy of *Brevundimonas* sp. ESA1 biofilm by using CIP that emits 450 nm blue light. For the long-term RF-API and Chl-API experiments, *Brevundimonas* sp. ESA1 biofilms were formed as described previously (Section 2.7). Wells with biofilms filled with 200 µL of 0.015 mM Chl, 0.011 mM RF and 0.01 M PBS solutions were illuminated with 450 nm light on the CIP (Figure 2A) at 1.4 mW/cm^2 irradiance for 28 h (to achieve irradiation dose of 141.1 J/cm^2) for RF-API and 20 h (to achieve irradiation dose of 100.8 J/cm^2) for Chl-API. Irradiation doses

using CIP were chosen to correspond to those that caused ≥3 log_{10} reduction of CFU of biofilms using irradiation boxes. The irradiation dose of long-term Chl-API was higher than using the irradiation box due to suboptimal Chl photoactivation wavelength emitted by CIP. Results of long-term irradiation were evaluated by determining CFU counts on LB plates and the ability of the photoinactivated biofilm cells to reduce alamarBlue™, as described previously (Sections 2.8 and 2.9).

2.11 *Brevundimonas* sp. ESA1 re-growth after photoinactivation

For the evaluation of *Brevundimonas* sp. ESA1 biofilm-forming cell's capability to resuscitate and re-grow after API, mechanically detached and vortexed biofilms were inoculated into liquid LB media and incubated for 72 h at 37°C under constant 180 rpm shaking. During the incubation, OD_{600} of the bacteria was measured once in 24 h. Re-growth capability of the dark controls (bacterial biofilms incubated with and without RF/Chl in the dark) of *Brevundimonas* sp. ESA1 were evaluated in the same way as for the irradiated bacteria.

2.12 Scanning electron microscopy of biofilms

The effect of RF-API and Chl-API on the morphology of *Brevundimonas* sp. ESA1 biofilm were investigated by scanning electron microscopy (SEM) (CamScan Apollo 300, Cambridge, UK). For the SEM analysis biofilms were grown in MtPs as it is described in Section 2.7. After the RF-API and Chl-API treatment (as described in Section 2.8) at 25 mW/cm^2 for 95 min and 20 mW/cm^2 for 60 min (irradiation conditions under which 3 log_{10} reduction was achieved), respectively, irradiated biofilms and dark controls were mechanically detached by scraping them of the MtP well walls by pipette tip, then 10 µl of each sample was transferred on a SEM specimen stub covered with copper foil tape, air-dried at room temperature and coated with 50 nm gold layer using Q150T ES sputter coater (Quorum Technologies, Lewes, England). The scanning was performed using an electron beam with an accelerating voltage of 20 kV.

2.13 Statistical analysis

All experiments were performed at least three times (independently) and the results were reported providing mean ± SD. Students t-test and one-way ANOVA statistical tests were applied. Statistically significant differences among groups were considered when $p \leq 0.05$. Graph construction was performed with Origin Pro 8.1 (OriginLab Corporation, USA) and GraphPad Prism V. 6 (GraphPad Software, USA) software. Statistical analysis was performed with GraphPad Prism V. 6 software.

3 Results

3.1 RF and Chl photostability study

Before the API of *Brevundimonas* sp. ESA1, the photostability of the aqueous solutions of 0.011 mM RF (pH 6.4) and 0.015 mM Chl (pH 6.8) was tested. It is known that RF absorbance spectra have four maximums: 223, 267, 373, 444 nm (Astanov et al., 2014). Therefore, the LEDs of 440 nm (irradiation box, Section 2.2) were used in experiments for the optimal excitation of RF. Chl is widely known as a water-soluble photoactive compound with the main absorption maximum at about 405 nm (Buchovec et al., 2017). Therefore, 402 nm LEDs of the irradiation box were used in experiments for the optimal excitation of Chl.

Both PSs are known to exhibit optical absorbance reduction after the activation by light. These changes show the activation dependence on excitation dose and can be used to compare the irradiation efficiency by different spectral components. We primarily studied the absorption characteristics of RF and Chl after illumination with an optimal excitation wavelength of 440 nm and 402 nm, respectively (Figure 3).

The aqueous solutions of RF are sensitive to light and degraded to various photoproducts: formylmethylflavin, lumichrome, lumiflavin, carboxymethylflavin, 2,3-butanedione, a β-keto acid and a diketo compound. The type of the photoproduct depends on the solvent, pH, buffer type, concentration, oxygen content, light intensity, and wavelengths used (Sheraz et al., 2014). Figure 3A illustrates the spectra of 0.011 mM RF (pH 6.4) after blue light irradiation at 5 mW/cm^2 for several durations (0 - 30 min, corresponding to 0-9 J/cm^2 irradiance doses). As shown in Figure 3A, the absorbance of 0.011 mM RF at 373 and 444 nm was dramatically decreased after 440 nm irradiation (9 J/cm^2). The photodegradation experiments helped assess the level of RF stability and revealed its photodegradation products after certain illumination exposures. Studies have shown that 0.011 mM RF (pH 6.4) photodegraded and probable formation of lumichrome photoproduct is observed at 9 J/cm^2 (440 nm) exposure, according to the previous studies (Buchovec et al., 2022).

Figure 3B shows the spectra recorded after illumination of 0.015 mM Chl solution (pH 6.8) in distilled water at 5 mW/cm^2 for different time periods (0-30 min, which corresponds to 0-9 J/cm^2 irradiance doses). The illumination at 402 nm significantly diminished the peak magnitude after 30 min (9 J/cm^2).

Although PSs were photobleached after 30 min of irradiation, antimicrobial effect can still be effectively implemented. In the case of RF, photoproducts, which can

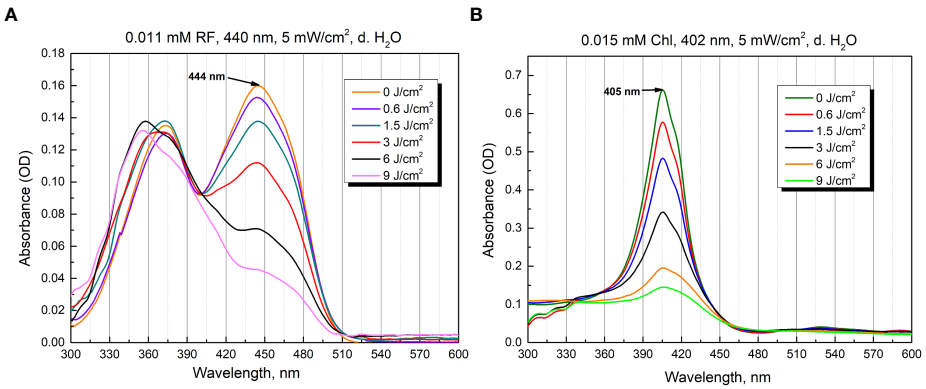

FIGURE 3
Photostability as optical absorbance spectra of 0.011 mM RF **(A)** and 0.015 mM Chl **(B)** after treatment of different irradiation doses (5 mW/cm^2 irradiance).

serve as PSs, are produced. Additionally, 440 nm light itself can have antibacterial effect as well. In the case of Chl, after its photoexcitation ROS that can cause significant damage are produced, and further, when Chl photodegrades, the ROS produced by 402 nm itself can have an antibacterial effect (Gwynne and Gallagher, 2018; Buchovec et al., 2022; Hadi et al., 2020).

3.2 RF- and Chl-API of planktonic bacteria and biofilms

The main objective of the study was to determine the bactericidal effect of RF-based and Chl-based API on *Brevundimonas* sp. ESA1 monocultural biofilm, although planktonic cells were also studied. RF and Chl were used to inactivate planktonic cells and biofilm in combination with 440 nm and 402 nm lights, respectively. Moreover, *Brevundimonas* sp. ESA1 biofilms were subjected to RF-API and Chl-API using a lower irradiance plate emitting 450 nm light. Partial sequence of 16S rRNA gene of the microorganisms used as a model in this study was deposited in GeneBank under the accession number ON237360.

3.2.1 Photoinactivation using 402 and 440 nm LED irradiance box

Bactericidal effect of API was defined as ≥3 $\log_{10}$ (99.9%) reduction in count of CFU according to the National Committee for Clinical Laboratory (NCCLS), M26-A standard (Thornsberry, 1983; CLSI, 1999). The minimal required dose of irradiation for the achievement of reduction of ≥3 $\log_{10}$ in CFU counts of planktonic cells after RF-API was determined to be 22 J/cm^2. Inactivation causing ≥3 $\log_{10}$ reduction in CFU counts after Chl-API required almost twice lower irradiation dose - only 11.5 J/cm^2 (Figures 4A, B).

During RF-API and Chl-API, respective samples of dark controls (samples that were incubated in the dark during/in parallel to API illuminations) were collected and analyzed by determining CFU counts as well. Respective dark controls with and without PSs (RF or Chl) during the time of its incubation parallel to the illumination experiments did not change significantly and fluctuated within appropriate limits (Table 2).

The minimal required doses of irradiation to achieve ≥3 $\log_{10}$ CFU reduction of *Brevundimonas* sp. biofilm ESA1 by RF-API and Chl-API were determined to be 138 J/cm^2 and 67,5 J/cm^2, respectively (Figures 5A, B). Overall, API studies revealed that *Brevundimonas* sp. ESA1 in its sessile and planktonic growth modes is more sensitive to 402 nm light in combination with Chl.

During RF-API and Chl-API, respective samples of dark controls were collected and analyzed by determining CFU. Respective dark controls with and without PSs (RF or Chl) during the time of its incubation parallel to the illumination experiments did not change significantly and fluctuated within appropriate limits, as well (Table 3).

It was also determined that effective inactivation of *Brevundimonas* sp. ESA1 biofilms using 402 nm light irradiation without Chl can also be achieved. Although, to reach the minimal 3 $\log_{10}$ reduction, a higher dose of ~95 J/cm^2 was required compared to Chl-based photoinactivation (Figure 5B).

For a better understanding of the intrinsic sensitivity of the *Brevundimonas* sp. ESA1 biofilms to the 402 nm light, high irradiation doses were also applied on the planktonic state cells. Results showed that planktonic cells of *Brevundimonas* sp. ESA1 are also sensitive to 402 nm light irradiation without using appropriate PS. Compared to biofilm, ~60 J/cm^2 dose of 402 nm light was needed to achieve ≥3 $\log_{10}$ reduction of CFU counts. Either way, the photoinactivation of *Brevundimonas* sp. ESA1 biofilms solely by 402 nm light need to be studied in more detail to make unquestionable conclusions about the reasons and internal mechanisms of such sensitivity. Nevertheless, both planktonic and

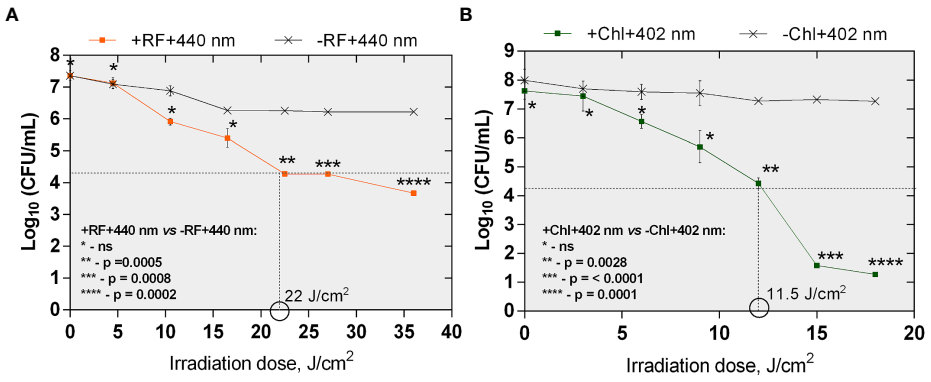

FIGURE 4
The effect of RF-API **(A)** and Chl-API **(B)** on *Brevundimonas* sp. ESA1 free-floating (planktonic) cells. Horizontal and vertical dashed lines shown in the graphs indicate the minimal irradiation doses thet were required to achieve a 3 $\log_{10}$ reduction of CFU counts of the planktonic cells. +RF +440 nm: irradiated using RF, -RF +440 nm: irradiated not using RF, +Chl +402 nm: irradiated using Chl, -Chl +402 nm: irradiated not using Chl; ns – non-significant. Error bars of some points are too small to be visible.

biofilm states *Brevundimonas* sp. ESA1 were generally determined to be more effectively killed by light (both 402 and 440 nm) in combination with the corresponding Chl and RF PSs used in this work. In addition, compared to the use of light only, using light in combination with PSs ensures that bacteria will not develop resistance to this antibacterial technology.

3.2.2 Photoinactivation using constant 450 nm irradiation plate

One of the possibilities to practically apply 402 or 440 nm illumination (in hospitals, food settings or spacecraft) to ensure API is to increase the blue part of the general illumination light sources. However, general illumination light sources (even if re-worked to have API function) cannot provide such high irradiance on a wide surface, e.g., 5 mW/cm^2 and higher values that were used in this work to have a bactericidal effect on planktonic and sessile bacterial cells. Therefore, irradiation for more than 24 h to achieve the desired illumination doses should be considered. To test the long-term illumination, an experiment using constant lower irradiance (1.4 mW/cm^2) plate emitting only 450 nm blue light was used (Figure 2A). Such a "Royal blue" color illumination spectra was chosen since it is widely used in LED-based illuminations systems from plant or aquarium illumination, color lighting to general lighting (part of white light). Furthermore, modern LEDs are achieving extraordinarily high efficiency compared to other light sources. In the current study, only *Brevundimonas* sp. ESA1 biofilm was subjected to a long-term API using a CIP.

Results of API of *Brevundimonas* sp. ESA1 biofilm using CIP at 1.4 mW/cm^2 showed that long illumination using lower irradiance in combination with either RF or Chl or even without any PSs could be highly effective. For RF-API, irradiation time of 28 h using CIP was equal to a dose of 141.1 J/cm^2, and for Chl-API, irradiation time for 20 h ensured a dose of 100.8 J/cm^2 (Figure 6). Such long-term irradiation time were used for testing since it was determined that RF-API and Chl-

TABLE 2 CFU counts of dark controls (reported in $\log_{10}$ scale) of the planktonic cells.

	Planktonic bacteria growth mode											
	-RF-440 nm ** (CFU/mL)						+RF-440 nm*** (CFU/mL)					
Incubation time, min	15	35	55	75	90	120	15	35	55	75	90	120
	6.8± 0.08*	6.9± 0.07*	6.6± 0.1*	6.5± 0.1*	6.5± 0.1*	6.5± 0.05*	6.9± 0.1*	6.8± 0.1*	6.7± 0.03*	6.5± 0.07*	6.5± 0.1*	6.4± 0.07*
	-Chl-402 nm* (CFU/mL)						+Chl -402 nm** (CFU/mL)					
Incubation time, min	10	20	30	40	50	60	10	20	30	40	50	60
	7.67± 0.1*	7.63± 0.3*	7.7± 0.08*	7.7± 0.2*	7.43± 0.1*	7.42± 0.02*	7.58± 0.3*	7.5 ± 0.2*	7.52± 0.1*	7.23± 0.2*	7.42± 0.01*	7.48± 0.07*

* - +RF+440 nm vs -RF-440 and +RF-440 nm or +Chl+402 nm vs –Chl-402 nm and +Chl-402 nm ANOVA test p value <0.05,
** - dark control without RF or Chl, respectively; *** - dark control with RF or Chl, respectively; n – was not evaluated.

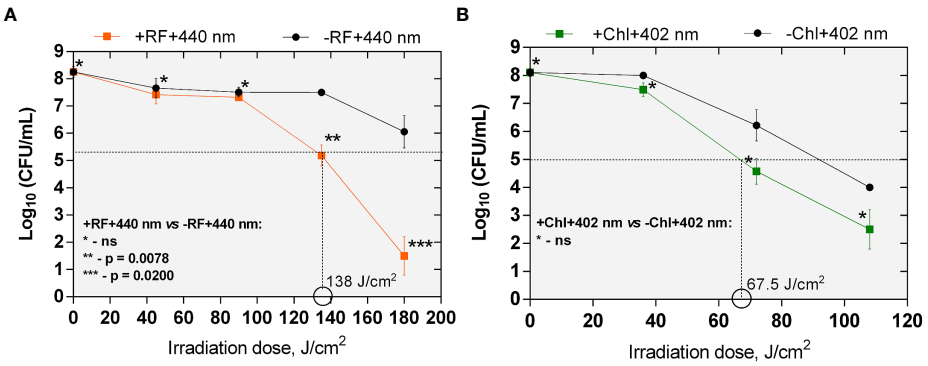

FIGURE 5
The effect of RF- **(A)** and Chl-API **(B)** on *Brevundimonas* sp. ESA1 biofilm. Horizontal and vertical dashed lines shown in the graphs indicate the minimal irradiation doses that were required to achieve 3 $\log_{10}$ reduction of CFU counts of the tested bacterial biofilm. +RF +440 nm: irradiated using RF, -RF +440 nm: irradiated not using RF, +Chl +402 nm: irradiated using Chl, -Chl +402 nm: irradiated not using Chl; ns – non-significant. Error bars of some points are too small to be visible.

API doses of 138 J/cm^2 and 67.5 J/cm^2, respectively, ensure ≥3 $\log_{10}$ reduction of CFU when using LED irradiation boxes (Figures 5A, B). Long-term Chl-API resulted in >4.3 $\log_{10}$ CFU count reduction of the biofilm (Figure 6), although 450 nm irradiance is not optimal for the photoexcitation of Chl. In the previous experiment using the irradiation box emitting 402 nm at 20 mW/cm^2 in combination with Chl, a dose of 67,5 J/cm^2 was needed to achieve a minimal 3 $\log_{10}$ reduction of CFU count of *Brevundimonas* sp. ESA1 biofilm (Figure 5B). Long-term Chl-API irradiation time for the achievement of minimal 3 $\log_{10}$ reduction can be probably reduced.

Long-term RF-API resulted in ≥3.3 $\log_{10}$ reductions of CFU counts of the biofilm (Figure 6). The latter result corresponds to the one obtained using the irradiation box (440 nm at 25 mW/cm^2 dose 138 J/cm^2) (Figure 5A). Long-term illumination of the biofilm without PSs resulted in a bactericidal effect (>3 $\log_{10}$ CFU reduction) as well. Therefore, long-term irradiation is efficient not only with RF but also Chl, even though 450 nm is not optimal for the photoexcitation of Chl. Interestingly, long-term blue light (450 nm) irradiation used without PSs is also highly effective in killing *Brevundimonas* sp. ESA1 biofilm caused ≥3.4 $\log_{10}$ CFU count reduction of the biofilm.

3.3 Biofilm viability study using alamarBlue™

Brevundimonas sp. ESA1 biofilm viability after the RF-API and Chl-API (using the irradiation box and irradiation plate) was also investigated by analyzing biofilm-forming cells' ability to reduce resazurin-based dye alamarBlue™. The latter helps monitor the living cell's reducing environment and quantitatively measure its

TABLE 3 CFU counts of dark controls (reported in $\log_{10}$ scale) of the biofilm.

	Sessile (biofilm) growth mode							
	-RF-440 nm** (CFU/mL)				+RF-440 nm*** (CFU/mL)			
Incubation time, min	30	60	90	120	30	60	90	120
	8.2 ± 0.1*	8.2 ± 0.1*	8.0 ± 0.3*	8.0 ± 0.3*	8.3 ± 0.14*	8.0 ± 0.4*	8.0 ± 0.3*	8.0 ± 0.3*
	-Chl-402 nm* (CFU/mL)				-*hV* +Chl nm** (CFU/mL)			
Incubation time, min	30	60	90	120	30	60	90	120
	8.1 ± 0.1*	7.3 ± 0.3*	7.2 ± 0.2*	n	7.8 ± 0.2*	7.7 ± 0.3*	7.8 ± 0.2*	n

* - +RF+440 nm vs -RF-440 and +RF-440 nm or +Chl+402 nm vs –Chl-402 nm and +Chl-402 nm ANOVA test p value <0.05,
** - dark control without RF or Chl, respectively; *** - dark control with RF or Chl, respectively; n – was not evaluated.

viability changes. The dye is water-soluble, non-toxic and permeates cell membranes easily; it is stable (even in culture media) and, therefore, long monitoring is possible. The main active component of alamarBlue™ – resazurin is a redox indicator and has an oxidation-reduction potential (E_0) of +380 mV at 25°C, pH 7. In a living cell, resazurin (oxidized form) that is blue and non-fluorescent can be reduced in multiple metabolic reactions (by NADPH (E_0 = 320 mV), FADH (E_0 = 220 mV), dihydrolipoamine dehydrogenases, NAD(P)H: quinoneoxidoreductases, etc.) to resofurin (reduced state) which has pink color and is highly fluorescent. The change from oxidized to reduced state allows quantitative colorimetric and fluorometric measurements, which in turn allow to determine cell health and viability (Rampersad, 2012; Bonnier et al., 2015). In this study alamarBlue™ changes from reduced to the oxidized state were measured by determining changes in fluorescence.

Viability determination *via* testing of photoinactivated *Brevundimonas* sp. ESA1 biofilm's ability to reduce alamarBlue™ showed that 3 $\log_{10}$ CFU count reduction causing RF-API (irradiation dose ~138 J/cm^2) and Chl-API (irradiation dose ~67.5 J/cm^2) induced cellular changes that lead to the inability to reduce alamarBlue™. Such findings approve previously achieved results that *Brevundimonas* sp. ESA1 biofilm after the RF- and Chl-API suffers significant viability loss.

Calculated percentage reduction of alamarBlue™ during the recorded time of incubation of appropriately photoinactivated biofilm, and the dye did not reach more than 15% (Figure 7A) and 10% (Figure 7B) after RF-API (+RF+440 nm) and Chl-API (+Chl+402 nm), respectively. The biofilm irradiated with 440 nm light without RF (-RF+440 nm) could reduce alamarBlue™, and the ability grew during the incubation time until 8-9 h. At the later time point, percentage reduction reached ~68%; however, subsequent decline was further determined. Dark control biofilm that was incubated with RF (+RF-440 nm) showed an upward dye percentage reduction ability trend with a maximum of ~70% reached at 10-11 h. The biofilm that was incubated in the dark without RF (PBS buffer was used instead) showed increasing alamarBlue™ percent reduction ability during the time of incubation and reached maximum ~85% at 11 h of incubation. Test groups that were irradiated without RF (-RF+440 nm) and incubated (dark control) with RF (+RF-440 nm) had a rather strong ability to reduce the alamarBlue™, which means that the mentioned conditions of treatment of

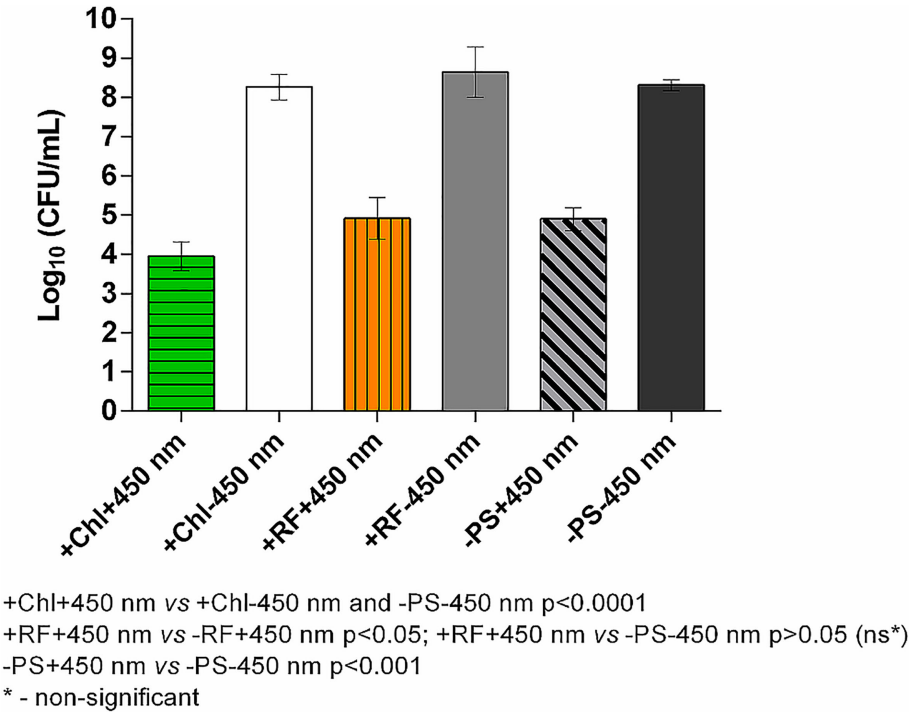

FIGURE 6
Effect of long-term Chl- and RF-API using CIP at 1.4 mW/cm^2 (450 nm). +Chl+450 nm/-Chl+450 nm – irradiated 20 h with and without Chl, respectively; +RF+450 nm/-RF+450 nm – irradiated 28 h with and without RF, respectively; -PS+450 nm/-PS-450 nm – irradiated and not irradiated 20-28 h without PSs (Chl or RF), respectively.

biofilms did not significantly affect the viability (Figure 7A). Test groups of biofilms that were irradiated without Chl (-Chl+402 nm) or incubated in the dark with (+Chl-402 nm) or without Chl (-Chl-402 nm), exhibited similar alamarBlue™ percentage reduction values (Figure 7B) as it was determined after RF-API (Figure 7A).

In general, viability testing with alamarBlue™ after RF-API and Chl-API (using the irradiation box) confirmed the results obtained by determining CFU counts of surviving cells.

After the photoinactivation using 450 nm CIP at 1.4 mW/cm^2 in combination with RF and Chl, the biofilm of *Brevundimonas* sp. ESA1 exhibited, respectively, only less than 10% or no alamarBlue™ reduction activity. Such results indicate that irradiation using a low irradiance intensity plate for a long period of time caused a significant or total viability loss when using RF or Chl, respectively, compared to AFI using the irradiation box. The control biofilm group that was irradiated with 450 nm without RF or Chl (PBS buffer was used instead of PSs) showed the ability to reduce no more than 20% of alamarBlue™ during all the incubation period (Figures 7C, D). Dark control groups, where biofilm was incubated with RF or Chl (groups +RF-450 nm and +Chl-450 nm, respectively) in the dark for an amount of time corresponding to the irradiation time that was used to cause ≥3 $\log_{10}$ CFU reduction, showed a low percentage ability of alamarBlue™ reduction. The percentage reduction of the latter tended to grow; however, in the last 4 h of incubation of biofilms with the alamarBlue™ it reached maximal values that were ~60% (Figures 7C, D). In comparison to +RF-440 nm, +Chl-402 nm and -RF-440 nm, -Chl-402 nm groups that were incubated for a shorter time using the irradiation box, +RF-450 nm, +Chl-450 nm and -RF/-Chl-450 nm after the long dark incubation showed ~20% lower ability to reduce alamarBlue™. The prolonged incubation that was carried out in the study with CIP could itself have a negative effect on reduction capability that reflects the viability of the biofilm. A negative effect on cell viability could have occurred due to the lack of nutrients during the long incubation time.

3.4 Regrowth of RF-API and Chl-API treated biofilm-forming cells

The ability of the *Brevundimonas* sp. ESA1 biofilm to resuscitate and grow in the planktonic state in nutrient-rich liquid LB media (in which planktonic cells for biofilm formation were routinely grown) was lost following irradiation with 450 nm at 1.4 mW/cm^2 for 20 (Chl-API) and 28 h (RF-API). No changes in OD_{600} of the +RF+450 nm and +Chl+450 nm groups were detected for 72 h (Table 4).

Regrowth analysis of the biofilm test group, which was illuminated with 450 nm without PSs (-PS+450 nm) showed that for the first 48 h the growth did not occur; however, on the third day (in 72 h) OD_{600} reached 1.96 ± 0.02. Irradiation with 450 nm without PSs delayed regrowth for 2 days. All the tested dark controls (+RF-450 nm, +Chl-450 nm, -PSs(+PBS)-450 nm) demonstrated the ability to regrow (Table 4).

Regrowth of *Brevundimonas* sp. ESA1 biofilm following 3 $\log_{10}$ CFU reduction causing RF- and Chl-API using the irradiation box did not occur for 48 h (OD_{600} = 0) but bacteria visibly resuscitated on the third day of cultivation in LB with OD_{600} values reaching 3.55 ± 0.07. Biofilms that were illuminated either with 402 or 440 nm regrew up to OD_{600} values equal to 3.5 ± 0.70 and 3.65 ± 0.91, respectively, on the second day of growth measurement. Illumination in combination with PSs and sole illumination delayed the regrowth of *Brevundimonas* sp. ESA1 for 2 and 1 day, respectively. Biofilms that formed dark control groups did not have such lag phases. OD_{600} changes of all tested biofilm groups after the photoinactivation using the irradiation box are shown in Table 5.

The studies of the ability of the biofilm cells to regrow in suspension and previous viability testing experiments *via* evaluation of alamarBlue™ reduction after the RF- and Chl-API have revealed that, apparently, some cells after the RF-, Chl-API or irradiation without PSs enter viable but non-culturable state (VNBC). Such a conclusion was made since some photoinactivated biofilm test groups were metabolically active (reduced alamarBlue™) but at the same time did not grow in the liquid nutritionally rich LB medium. The biofilm that was exposed to 450 nm light (test group +450 nm -RF/-Chl (+PBS)) was metabolically active and reduced alamarBlue™ for more than 11 h up to ~20% (Figure 7C). However, its OD_{600} values over 48 h were equal to 0 with subsequent growth detection at 72 h (Table 4). Such results indicate that only a part of the cells entered a VBNC state which was a cause of bacterial resuscitation, while most biofilm cells did not survive after exposure. VBNC state was also induced in *Brevundimonas* sp. ESA1 biofilm cells were exposed to RF-API (+RF+440 nm test group) and Chl-API (+Chl+402 nm test group) using the irradiation box. Biofilms of these test groups after appropriate PS-based photoinactivations could reduce alamarBlue™ up to ~60-70% at 12-14 h incubation points (Figures 7A, B), but at the same time cell growth in LB media was not detected for 48 h. Subsequently, bacteria resuscitated only on the third day of growth, reaching OD_{600} corresponding to those measured for the dark controls (Table 5), meaning that most of the bacterial cell population transitioned to VBNC state. Biofilm cells that were exposed to 402 or 440 nm irradiation without PS, recovered

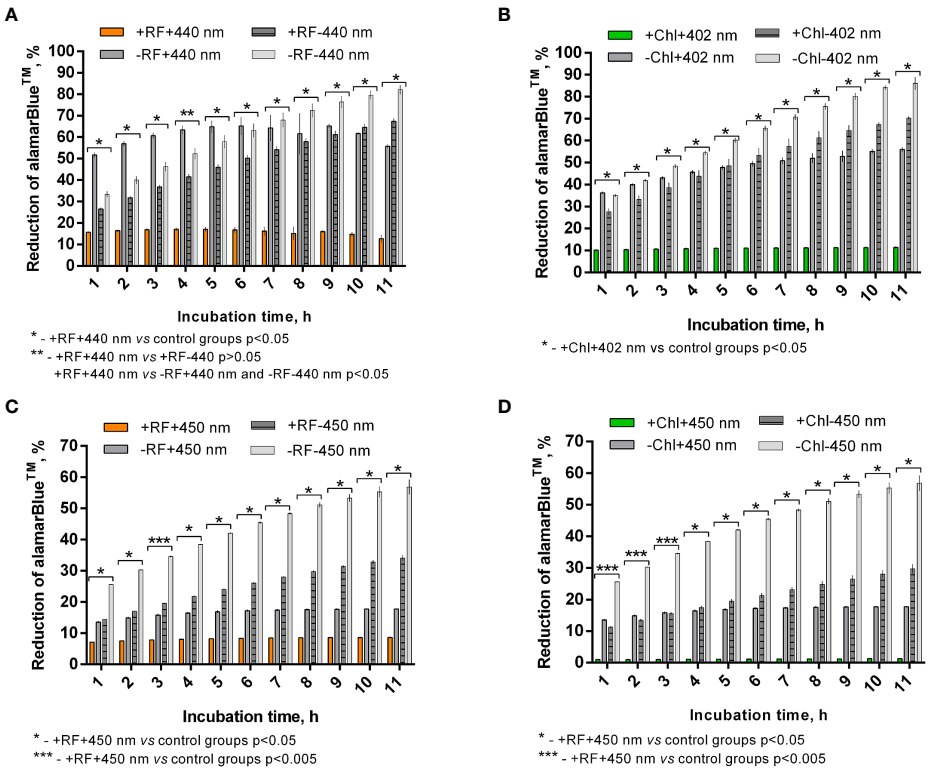

FIGURE 7
Brevundimonas sp. ESA1 biofilm ability to reduce alamarBlue™ after API: **(A)** - RF-API (440 nm at 25 mW/cm^2 until dose of 138 J/cm^2 was reached) and **(B)** – after Chl-API (402 nm at 20 mW/cm^2 until dose 67.5 J/cm^2 was reached) using the irradiation box; **(C)** - after RF-API (450 nm at 1.4 mW/cm^2 until dose of 141.1 J/cm^2 was reached) and **(D)** - Chl-API (450 nm at 1.4 mW/cm^2 until the dose of 100.8 J/cm^2 was reached) using irradiation plate. Described irradiation doses ensured the reduction of ≥3 $\log_{10}$ in CFU counts. Designations: A, B - +RF+440 nm/-RF+440 nm, +Chl+402 nm/-Chl+402 nm: biofilms irradiated by 440 nm or 402 nm with/without 0.011 mM RF or 0.015 mM Chl, respectively; +RF-440 nm/-RF-440 nm, +Chl-402 nm/-Chl-402 nm: dark controls where biofilms were and were not, respectively, incubated with 0.011 mM RF or 0.015 mM Chl; C, D - +RF-450 nm/-RF-450 nm, +Chl-450 nm/-Chl-450 nm: dark controls of long-term irradiation experiment where biofilms were and were not, respectively, incubated with 0.011 mM RF or 0.015 mM Chl. In cases where irradiation or incubation without PSs was performed, 0.01 M PBS (pH 7.4) was used.

faster than those that were subjected to photoinactivation in combination with PSs (Table 5).

3.5 Scanning electron microscopy

Scanning electron microscopy revealed that RF-API and Chl-API using the irradiation box at doses of 138 J/cm^2 and ~70 J/cm^2, respectively, have induced changes in biofilm cell morphology of investigated bacteria compared to untreated cells (Figure 8).

After both RF-API and Chl-API, mechanically detached biofilm cells appeared to have disrupted and perforated cell walls, and some appeared lysed. Significant morphological changes were also seen after irradiation with 402 nm without using Chl. That is a logical outcome since CFU count analysis after irradiation has shown that 402 nm light without PS can have a reducing effect on viability as well (Figure 5B). Cells of the dark controls did not have any noticeable damage to the cell walls, but the surface of those incubated in the dark with RF did not look as smooth as after incubation with Chl.

4 Discussion

4.1 Photoinactivation of *Brevundimonas* sp. ESA1

This study was the first to demonstrate the efficiency of the RF- and Chl-mediated photoinactivation of *Brevundimonas* sp. ESA1 biofilms. In particular, it was shown that Chl-based API required half the irradiation dose

TABLE 4 Ability of the biofilm-forming *Brevundimonas* sp. ESA1 cells to regrow in LB media after long-term RF-API and Chl-API (+RF+450 nm and +Chl+450 nm, respectively) using CIP, irradiation without PSs (-PSs(+PBS)+450 nm).

Test group name	OD_{600} change in time		
	24 h	48 h	72 h
+RF+450 nm	0	0	0
+Chl+450 nm	0.05 ± 0.01	0	0
-PS(+PBS)+450 nm	0	0.01 ± 0.01	1.96 ± 0.02
+RF-450 nm	0.71 ± 0.4	1.91 ± 0.04	3.08 ± 0.34
+Chl-450 nm	1.09 ± 0.09	1.82 ± 0.11	2.72 ± 0.51
-PSs(+PBS)-450 nm	0.78 ± 0.57	1.78 ± 0.1	2.87 ± 0.29

Respective dark controls incubated with or without RF or Chl (+RF-450 nm, +Chl-450 nm and -PSs(+PBS)-450 nm are also indicated in the table.

compared to RF-API. Therefore, Chl-API can be considered a more effective method for the inactivation of studied biofilms and planktonic cells. Moreover, it was determined that effective inactivation of *Brevundimonas* sp. ESA1 biofilms using 402 nm light irradiation without Chl can also be achieved. Although to reach the minimal 3 $\log_{10}$ reductions, a higher dose was required compared to Chl-based photoinactivation (95 J/cm^2 instead of 67.5 J/cm^2). Such phenomenon has not been observed after RF-API and Chl-API of *Brevundimonas* sp. ESA1 planktonic cells in the used dosage range of the photoinactivation. The use of PS, in the case of Chl-API of *Brevundimonas* sp. ESA1 biofilm can be considered redundant/unnecessary to achieve inactivation (bactericidal or bacteriostatic effect). The fact that biofilms can be sensitive to light without PSs can have practical significance in facilitating the application of the technology in systems where spreading PSs can be complicated, e.g., in a spacecraft environment, where microgravity conditions prevail. However, the cause of *Brevundimonas* sp. ESA1 to be sensitive, particularly in its biofilm form to 402 nm only (without Chl) is currently unknown. In general, the sensitivity of biofilms to blue light can be explained by the fact that bacteria can have endogenous porphyrins that can be sensitized by 402 nm and can generate ROS, resulting in cellular photo-oxidative reactions that initiate various cellular damages and death; the light can also activate prophages that cause bacterial cell lysis (Ferrer-Espada et al., 2019). A few studies have shown that biofilms of different Gram-negative (*Salmonella*, *Escherichia coli* O157:H7, etc.) bacteria can be equally sensitive or even more sensitive to irradiation compared to planktonic cells (Niemira and Solomon, 2005; Niemira, 2007; Niemira, 2010). The sensitivity to API of the biofilm and the planktonic cells of bacteria can be different and depend on the metabolic states and the growth phase as well (Blee et al., 2020). It can also be assumed that the cause of the higher sensitivity of the *Brevundimonas* sp. ESA1 biofilm to the 402 nm light is somehow associated with its extracellular polymeric matrix (Flemming and Wingender, 2010). Although, EPS is usually the cause of the higher doses needed to inactivate bacteria in sessile form compared to planktonic cells. For example, this study's experimental results have shown that about 6 times higher irradiation

TABLE 5 Ability of the biofilm-forming *Brevundimonas* sp. ESA1 cells to regrow in LB media after short-term RF- and Chl-API (+RF+440 nm and +Chl+402 nm, respectively) using the irradiation box, irradiation without PSs (-RF+440 nm and -Chl+402 nm).

Test group name	OD_{600} change in time		
	24 h	48 h	72 h
+RF+440 nm	0.005 ± 0.01	0.015 ± 0.021	3.55 ± 0.07
-RF+440 nm	0.005 ± 0.01	3.65 ± 0.91	4.25 ± 0.55
-RF-440 nm	2.25 ± 0.55	3.75 ± 0.9	3.75 ± 0.52
-RF-440 nm	2.14 ± 0.65	3.5 ± 0.70	3.84 ± 0.62
+Chl+402 nm	0.01	0.01 ± 0.014	3.52 ± 0.11
-Chl+402 nm	0.015 ± 0.01	3.5 ± 0.70	4.07 ± 0.86
+Chl-402 nm	2.16 ± 0.62	3.9 ± 0.69	3.61 ± 0.6
-Chl-402 nm	2.95 ± 0.0.64	4.15 ± 0.91	3.8 ± 0.57

Respective dark controls incubated with or without RF or Chl (+RF-440 nm, -RF-440 nm and +Chl-402 nm, -Chl-402 nm) are also indicated in the table.

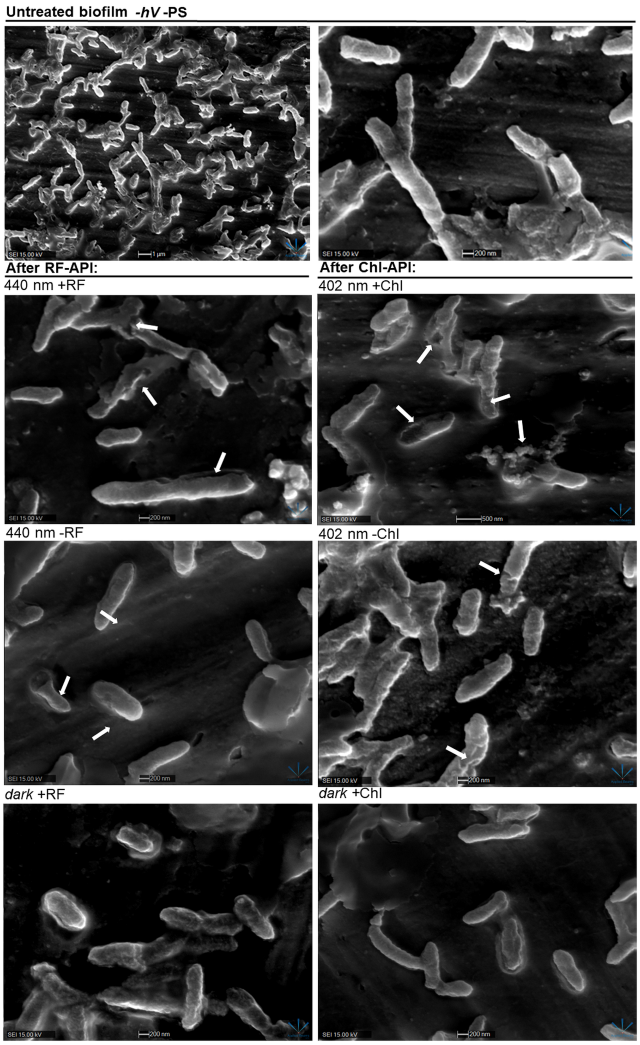

FIGURE 8
SEM images of *Brevundimonas* sp. ESA1 biofilm cells: *untreated (-hV* –PS: no PSs (RF nor Chl) in dark conditions); after *RF-API*: 440 nm +RF (treated with 0.011 mM RF and irradiated by 440 nm up to 140 J/cm^2), 440 nm -RF (not treated with 0.011 mM RF prior to irradiation, cells were covered with 0.1 M phosphate buffer (pH 7.4) and irradiated by 440 nm up to 140 J/cm^2), *dark* +RF (biofilms treated with 0.011 mM RF and incubated in the dark for an amount of time corresponding to time needed to achieve 140 J/cm^2); after *Chl-API*: 402 nm +Chl (treated with 0,015 mM Chl and irradiated by 402 nm up to 70 J/cm^2), 402 nm -Chl (not treated with 0,015 mM Chl prior to irradiation, cells were covered with 0.1 M phosphate buffer (pH 7.4) and irradiated by 402 nm up to 70 J/cm^2), *dark* +Chl (biofilms treated with 0,015 mM M Chl and incubated in the dark for an amount of time corresponding to time needed to achieve 70 J/cm^2).

doses are needed to achieve the bactericidal effect on biofilms compared to planktonic cells. Therefore, the improvement of API technology for the more effective killing of bacterial biofilms should be certainly considered. The efficiency of API can be improved by testing higher concentrations of PSs, a step of preincubation with PSs before irradiation and synergy studies. Additionally, using antimicrobials can be done as well.

API is a two-stage technology consisting of the natural PS, which must be applied on a surface, and an illumination system providing a sufficient dose of light to inactivate bacteria. This makes it complicated, especially for the application in microgravity conditions, and requires a well-developed application plan as well as proper engineering solutions. Reworking of currently installed lighting fixtures (e.g. SSLAs on ISS), increasing the blue part of the general lightning, and long irradiation time could be one of the options. Based on this assumption, to test the long-term illumination, an experiment using constant lower irradiance (1.4 mW/cm^2) plate emitting only 450 nm blue light was used (Figure 2A). Such color illumination spectrum was chosen since it is widely used in LED-based systems such as general lighting (part of white light).

Results of API of *Brevundimonas* sp. ESA1 biofilm using CIP at 1.4 mW/cm^2 showed that long illumination using lower irradiance in combination with either RF or Chl or even without any PSs could be highly effective. However, some additional long-term irradiation experiments using CIP can be performed to evaluate the 450 nm effect in combination with RF, Chl or without the use of PSs, and if the internal porphyrins might have had a significance for the API of the *Brevundimonas* sp. ESA1. The latter phenomenon has already attracted increasing attention and several studies have shown that blue light, particularly in the wavelength range of 405–470 nm has intrinsic antimicrobial effect on different microbes including Gram-positive and Gram-negative bacteria without the addition of exogenous PSs (Dai et al., 2012; Hoenes et al., 2018; Gwynne and Gallagher, 2018: Hadi et al., 2020). Nevertheless, long-term irradiation indeed showed to be effective and promising for practical implementation of API customization. However, reworking installed lighting fixtures or sending additional API-dedicated illumination to spacecraft definitely results in extra expenses that must be evaluated and weighted in detail. On the other hand, when developing new modules for ISS or other space missions, the API could be considered an antimicrobial technique. Therefore, if performed on earth, the integration of API illumination systems would have a neglectable effect on the total costs and weight of the project.

4.2 Transition of *Brevundimonas* sp. ESA1 to VBNC state

Viability testing with alamarBlue™ after RF-API and Chl-API (using the irradiation box and CIP) confirmed the results obtained by determining CFU counts of surviving cells. However, alamarBlue™ reduction studies in addition to bacterial regrowth studies, had shown that *Brevundimonas* sp. ESA1 biofilm cells, after the application of RF-API and Chl-API, enter VBNC state.

Only a few published studies announce the transition of certain bacterial species to the VBNC state after exposure to blue light or violet-blue lights (Abana et al., 2017; Hoenes et al., 2018).

In general, VBNC state is characteristic to non-spore-forming, usually Gram-negative bacteria and appears under various stressful conditions. VBNC cells may be resuscitated back to cultivable cells under suitable stimuli. The conditions that trigger the induction of the VBNC state and resuscitation can be different for different bacteria species, e.g., pathogens usually resuscitate only *in vivo* (Li et al., 2014; Zhang et al., 2021). This study was the first to demonstrate that bacteria belonging to the genus *Brevundimonas* sp. ESA1 can enter the VBNC state after its photoinactivation and in some cases resuscitate in nutrient-rich conditions. Moreover, undesired growth after the long-term RF- and Chl-API is unlikely to occur even in nutrient-rich environments.

4.3 Guidelines for further research and development of API in space conditions

Despite the efficiency of Chl- and RF-based API against *Brevundimonas* sp. ESA1 and other bacteria (that was demonstrated elsewhere), use of the PSs have a huge potential for improvement. For example, the mixes of PSs and the combinations of PSs with polymers and other materials can be investigated. Moreover, an in-depth investigation of the long-term, low-irradiance API technologies could help find photoinactivation solutions under general or natural lighting conditions.

Design and development of the API PS solution already integrated into the newly developed space premises and/or modules should be considered in order to apply the technology conveniently in conditions of low gravity. If the integration of the PSs is not possible, investigation and design of API application techniques (e.g. sprinklers) in microgravity conditions must be considered as well.

5 Conclusions

API based on natural PSs RF or Chl and illumination by blue light (402-450 nm) has the potential to be applied as an antimicrobial technique against planktonic and, most importantly, more recalcitrant biofilm form of *Brevundimonas* sp. ESA1. Recently, some species of the latter bacterial genus have been revealed as a global opportunistic pathogen that can be dangerous for individuals with chronic underlying diseases and immunocompromised people. *Brevundimonas* spp. are abundant in terrestrial and even confined spacecraft environments.

The main advantage of the RF- and Chl-mediated API compared to other antimicrobial methods is that this technology is non-toxic and could be safely used in closed-loop, food, drinking water, and other systems as an antimicrobial technology posing no risk to humans or other living creatures. Moreover, there has been only a neglectable or no resistance development towards API observed since the beginning of its use. Implementing the API technology in the confined systems as spacecraft, its application could consist of three steps, in particular, preparation of the aqueous solutions of the PSs, application of the PSs on the target surface, and irradiation of that surface by the required light spectrum and sufficient light amount (dose).

In this work, by comparing the optical absorption spectra of the PSs and irradiance spectra of LEDs, it was determined that 402 nm and 440 nm are optimal to excite Chl and RF, respectively. Photostability experiments showed the photomodifications of both PSs under the conditions subsequently used to inactivate *Brevundimonas* sp. ESA1. Besides the demonstration of the RF-based and Chl-based API conditions needed to inactivate *Brevundimonas* biofilms using two different illumination systems, a study of the API treated

bacteria to reduce alamarBlue™ and regrowth studies revealed that *Brevundimonas* sp. ESA1 enters VNBC state without resuscitation after long-term irradiation in conditions tested in this work.

Nevertheless, further investigation of the API applicability should be carried out, focusing on certain application areas such as HVAC, water supply, sanitary systems, plant growth facilities, etc.

Data availability statement

The data presented in the study are deposited in the NCBI GenBank repository, accession number ON237360; https://www.ncbi.nlm.nih.gov/nuccore/ON237360.1/.

Author contributions

AG and IB, conceptualization, methodology, and data processing. AG, IB, and KB, experiment implementation. AG, formal analysis, writing – original draft, writing – review and editing, visualization. IB, LK, and PV, writing – original draft, writing – review and editing. All authors contributed to the article and approved the submitted version.

Funding

Part of the research was funded by the European Space Agency (LT5_1 ESA Contract No. 40000129495/19/NL/SSC).

Acknowledgments

Authors would like to acknowledge the European Space Agency (ESA).

Conflict of interest

The authors declare that the research was conducted in the absence of any commercial or financial relationships that could be construed as a potential conflict of interest.

Publisher's note

References

Abana, C. M., Brannon, J. R., Ebbott, R. A., Dunigan, T. L., Guckes, K. R., Fuseini, H., et al. (2017). Characterization of blue light irradiation effects on pathogenic and nonpathogenic *Escherichia coli*. *Microbiologyopen.* 6 (4), e00466. doi: 10.1002/mbo3.466

Adelowo, O. O., and Fagade, O. E. (2009). The tetracycline resistance gene tet39 is present in both gram-negative and gram-positive bacteria from a polluted river, southwestern Nigeria. *Lett. Appl. Microbiol.* 48, 167–172. doi: 10.1111/j.1472-765x.2008.02523.x

Altschul, S. F., Gish, W., Miller, W., Myers, E. W., and Lipman, D. J. (1990). Basic local alignment search tool. *J. Mol. Biol.* 215 (3), 403–410. doi: 10.1016/S0022-2836(05)80360-2

Astanov, S., Sharipov, M. Z., Fayzullaev, A. R., Kurtaliev, E. N., and Nizomov, N. (2014). Spectroscopic study of photo and thermal destruction of riboflavin. *J. Mol. Struct.* 1071, 133–138. doi: 10.1016/j.molstruc.2014.04.077

Bashir, M., Ahmed, M., Weinmaier, T., Ciobanu, D., Ivanova, N., Pieber, T. R., et al. (2016). Functional metagenomics of spacecraft assembly cleanrooms: presence of virulence factors associated with human pathogens. *Front. Microbiol.* 9 (7). doi: 10.3389/fmicb.2016.01321

Be, N. A., Avila Herrera, A., Allen, J. E., Singh, N., Sielaff, A., Jaing, C., et al. (2017). Whole metagenome profiles of particulates collected from the international space station. *Microbiome.* 5 (1), 81. doi: 10.1186/s40168-017-0292-4

Blee, J. A., Roberts, I. S., and Waigh, T. A. (2020). Membrane potentials, oxidative stress and the dispersal response of bacterial biofilms to 405 nm light. *Phys. Biol.* 17 (3), 036001. doi: 10.1088/1478-3975/ab759a

Bonnier, F., Keating, M. E., Wróbel, T. P., Majzner, K., Baranska, M., Garcia-Munoz, A., et al. (2015). Cell viability assessment using the alamar blue assay: A comparison of 2D and 3D cell culture models. *Toxicol. Vitro.* 29 (1), 124–131. doi: 10.1016/j.tiv.2014.09.014

Borisov, V., Deshevaya, E., Grachov, E., Grigoryan, O., Tchurilo, I., and Tsetlin, V. (2003). The "SCORPION" experiment onboard the international space station. *Preliminary results. Adv. Space Res.* 32 (11), 2373–2378. doi: 10.1016/SO273-1177(03)00726-9

Buchovec, I., Gricajeva, A., Kalėdienė, L., and Vitta, P. (2020). Antimicrobial photoinactivation approach based on natural agents for control of bacteria biofilms in spacecraft. *IJMS.* 21 (18), 6932. doi: 10.3390/ijms21186932

Buchovec, I., Klimkaitė, L., Sužiedėlienė, E., and Bagdonas, S. (2022). Inactivation of opportunistic pathogens *Acinetobacter baumannii* and *Stenotrophomonas maltophilia* by antimicrobial photodynamic therapy. *Microorganisms.* 10 (3), 506. doi: 10.3390/microorganisms10030506

Buchovec, I., Lukseviciūtė, V., Kokstaite, R., Labeikyte, D., Kaziukonyte, L., and Luksiene, Z. (2017). Inactivation of gram (–) bacteria *Salmonella enterica* by chlorophyllin-based photosensitization: Mechanism of action and new strategies to enhance the inactivation efficiency. *J. Photochem. Photobiol. B Biol.* 172, 1–10. doi: 10.1016/j.jphotobiol.2017.05.008

Buchovec, I., Lukseviciute, V., Marsalka, A., Reklaitis, I., and Luksiene, Z. (2016). Effective photosensitization-based inactivation of gram (–) food pathogens and molds using the chlorophyllin–chitosan complex: Towards photoactive edible coatings to preserve strawberries. *Photochem. Photobiol. Sci.* 15, 506–516. doi: 10.1039/c5pp00376h

Buchovec, I., Paskeviciute, E., and Luksiene, Z. (2010). Photodynamic inactivation of food pathogen listeria monocytogenes. *Food Technol. Biotechnol.* 48 (2), 207–213.

Checinska, A., Probst, A. J., Vaishampayan, P., White, J. R., Kumar, D., Stepanov, V. G., et al. (2015). Microbiomes of the dust particles collected from the international space station and spacecraft assembly facilities. *Microbiome.* 3, 50. doi: 10.1186/s40168-015-0116-3

Ciofu, O., Moser, C., Jensen, P.Ø., and Høiby, N. (2022). Tolerance and resistance of microbial biofilms. *Nat. Rev. Microbiol.* 20, 621–635. doi: 10.1038/s41579-022-00682-4

Clinical and Laboratory Standards Institute (CLSI) (1999). Methods for determining bactericidal activity of antimicrobial agents; approved guideline. *CLSI document M26-A* 19 (18), 1–29.

Dai, T., Gupta, A., Murray, C. K., Vrahas, M. S., Tegos, G. P., and Hamblin, M. R. (2012). Blue light for infectious diseases: Propionibacterium acnes, helicobacter

pylori, and beyond? *Drug Resist. Update* 4 (15), 223–236. doi: 10.1016/j.drup.2012.07.001

Dartnell, L. R., Hunter, S. J., Lovell, K. V., Coates, A. J., and Ward, J. M. (2010). Low-temperature ionizing radiation resistance of *Deinococcus radiodurans* and Antarctic dry valley bacteria. *Astrobiology.* 10 (7), 717–732. doi: 10.1089/ast.2009.0439

Decelle, J. G., and Taylor, G. R. (1976). Auto flora in the upper respiratory tract of Apollo astronauts. *Appl. Environ. Microbiol.* 32, 659–665. doi: 10.1128/aem.32.5.659-665.1976

Ferrer-Espada, R., Liu, X., Goh, X. S., and Dai, T. (2019). Antimicrobial blue light inactivation of polymicrobial biofilms. *Front. Microbiol.* 10. doi: 10.3389/fmicb.2019.00721

Flemming, H.-C., and Wingender, J. (2010). The biofilm matrix. *Nat. Rev. Microbiol.* 8, 623–633. doi: 10.1038/nrmicro2415

Flemming, H.-C., Wingender, J., Szewzyk, U., Steinberg, P., Rice, S. A., and Kjelleberg, S. (2016). Biofilms: an emergent form of bacterial life. *Nat. Rev. Microbiol.* 14, 563–575. doi: 10.1038/nrmicro.2016.94

Ghosh, S., Osman, S., Vaishampayan, P., and Venkateswaran, K. (2010). Recurrent isolation of extremotolerant bacteria from the clean room where phoenix spacecraft components were assembled. *Astrobiology.* 10 (3), 325–335. doi: 10.1089/ast.2009.0396

Gricajeva, A., Bendikienė, V., and Kalėdienė, L. (2016). Lipase of *Bacillus stratosphericus* L1: cloning, expression and characterization. *Int. J. Biol. Macromol.* 92, 96–104. doi: 10.1016/j.ijbiomac.2016.07.015

Gwynne, P. J., and Gallagher, M. P. (2018). *Light as broad-spectrum antimicrobial. Front. Microbiol.* 9:119. doi: 10.3389/fmicb.2018.00119

Hadi, J., Wu, S., and Brightwell, G. (2020). Antimicrobial blue light versus pathogenic bacteria: mechanism, application in the food industry, hurdle technologies and potential resistance. *Foods.* 9 (12), 1895. doi: 10.3390/foods9121895

Hall-Stoodley, L., Costerton, J. W., and Stoodley, P. (2004). Bacterial biofilms: from the natural environment to infectious disease. *Nat. Rev. Microbiol.* 2, 95–108. doi: 10.1038/nrmicro821

Hamblin, M. R. (2016). Antimicrobial photodynamic inactivation: a bright new technique to kill resistant microbes. *Curr. Opin. Microbiol.* 33, 67–73. doi: 10.1016/j.mib.2016.06.008

Han, X. Y., and Andrade, R. A. (2005). *Brevundimonas diminuta* infections and its resistance to fluoroquinolones. *J. Antimicrob. Chemother.* 55 (6), 853–859. doi: 10.1093/jac/dki139

Hoenes, K., Hess, M., Vatter, P., Spellerberg, B., and Hessling, M. (2018). 405 nm and 450 nm photoinactivation of *Saccharomyces cerevisiae*. *Eur. J. Microbiol. Immunol.* 8 (4), 142–148. doi: 10.1556/1886.2018.00023

Hu, X., Huang, Y. Y., Wang, Y., Wang, X., and Hamblin, M. R. (2018). Antimicrobial photodynamic therapy to control clinically relevant biofilm infections. *Front. Microbiol.* 9 (1299). doi: 10.3389/fmicb.2018.01299

Jori, G., and Brown, S. B. (2004). Photosensitized inactivation of microorganisms. *Photochem. Photobiol. Sci.* 3 (5), 403–405. doi: 10.1039/b311904c

Kashef, N., and Hamblin, M. R. (2017). Can microbial cells develop resistance to oxidative stress in antimicrobial photodynamic inactivation? *Drug Resist. Updat.* 31, 31–42. doi: 10.1016/j.drup.2017.07.003

Kawamura, Y., Li, Y., Liu, H., Huang, X., Li, Z., and Ezaki, T. (2001). Bacterial population in Russian space station "Mir". *Microbiol. Immunol.* 45, 819–828. doi: 10.1111/j.1348-0421.2001.tb01321.x

Koskinen, K., Rettberg, P., Pukall, R., Auerbach, A., Wink, L., Barczyk, S., et al. (2017). Microbial biodiversity assessment of the European space agency's ExoMars 2016 mission. *Microbiome.* 5 (1), 143. doi: 10.1186/s40168-017-0358-3

Krüger, M., Richter, P. R., Strauch, S. M., Nasir, A., Burkovski, A., Antunes, C. A., et al. (2019). What an *Escherichia coli* mutant can teach us about the antibacterial effect of chlorophyllin. *Microorganisms.* 7, 59. doi: 10.3390/microorganisms7020059

La Duc, M. T., Kern, R., and Venkateswaran, K. (2004a). Microbial monitoring of spacecraft and associated environments. *Microb. Ecol.* 47 (2), 150–158. doi: 10.1007/s00248-003-1012-0

La Duc, M. T., Sumner, R., Pierson, D., Venkat, P., and Venkateswaran, K. (2004b). Evidence of pathogenic microbes in the international space station drinking water: reason for concern? *Habitation (Elmsford).* 10 (1), 39–48. doi: 10.3727/154296604774808883

Li, Y., Kawamura, Y., Fujiwara, N., Naka, T., Liu, H., Huang, X., et al. (2004). *Sphingomonas yabuuchiae* sp. nov. and *Brevundimonas nasdae* sp. nov., isolated from the Russian space laboratory mir. *Int. J. Syst. Evol.* 54 (3), 819–825. doi: 10.1099/ijs.0.02829-0

Li, L., Mendis, N., Trigui, H., Oliver, J. D., and Faucher, S. P. (2014). The importance of the viable but non-culturable state in human bacterial pathogens. *Front. Microbiol.* 5. doi: 10.3389/fmicb.2014.00258

Liu, Y., Qin, R., Zaat, S. A. J., Breukink, E., and Heger, M. (2015). Antibacterial photodynamic therapy: Overview of a promising approach to fight antibiotic-resistant bacterial infections. *J. Clin. Transl. Res.* 1 (3), 140–167. doi: 10.18053/jctres.201503.002

Low, A., Ng, C., and He, J. (2016). Identification of antibiotic resistant bacteria community and a GeoChip based study of resistome in urban watersheds. *Water Res.* 106, 330–338. doi: 10.1016/j.watres.2016.09.032

Luksiene, Z. (2005). New approach to inactivation of harmful and pathogenic microorganisms by photosensitization. *Food Technol. Biotechnol.* 43 (4), 411–418.

Luksiene, Z., and Buchovec, I. (2019). Impact of chlorophyllin-chitosan coating and visible light on the microbial contamination, shelf life, nutritional and visual quality of strawberries. *Innov. Food Sci. Emerg. Technol.* 52, 463–472. doi: 10.1016/j.ifset.2019.02.003

Luksiene, Z., Buchovec, I., and Paskeviciute, E. (2010). Inactivation of *Bacillus cereus* by Na-chlorophyllin-based photosensitization on the surface of packaging. *J. Appl. Microbiol.* 109, 1540–1548. doi: 10.1111/j.1365-2672.2010.04780.x

Maisch, T. (2015). Resistance in antimicrobial photodynamic inactivation of bacteria. *Photochem. Photobiol. Sci.* 14, 1518–1526. doi: 10.1038/s41598-018-35594-y

Mazzotta, C., Caragiuli, S., and Caporossi, A. (2014). ""Riboflavin and the cornea and implications for cataracts"," in *Handbook of nutrition, diet and the eye.* Ed. V. R. Preedy (London, UK: Academic Press), 123–130. doi: 10.1016/B978-0-12-401717-7.00013-7

Merritt, J. H., Kadouri, D. E., and O'Toole, G. A. (2005). Growing and analyzing static biofilms. *Curr. Protoc. Microbiol.* 1, 1B.1. doi: 10.1002/9780471729259.mc01b01s00

Mijnendonckx, K., Provoost, A., Ott, C. M., Venkateswaran, K., Mahillon, J., Leys, N., et al. (2013). Characterization of the survival ability of *Cupriavidus metallidurans* and *Ralstonia pickettii* from space-related environments. *Microb. Ecol.* 65 (2), 347–360. doi: 10.1007/s00248-012-0139-2

Miranda, C. D., Kehrenberg, C., Ulep, C., Schwarz, S., and Roberts, M. C. (2003). Diversity of tetracycline resistance genes in bacteria from chilean salmon farms. *Antimicrob. Agents Chemother.* 47, 883–888. doi: 10.1128/AAC.47.3.883-888.2003

Mora, M., Mahnert, A., Koskinen, K., Pausan, M. R., Oberauner-Wappis, L., Krause, R., et al. (2016). Microorganisms in confined habitats: microbial monitoring and control of intensive care units, operating rooms, cleanrooms, and the international space station. *Front. Microbiol.* 7. doi: 10.3389/fmicb.2016.01573

Mora, M., Wink, L., Kogler, I., Mahnert, A., Rettberg, P., Schwendner, P., et al. (2019). Space station conditions are selective but do not alter microbial characteristics relevant to human health. *Nat. Commun.* 10 (1), 3990. doi: 10.1038/s41467-019-11682-z

Muhammad, M. H., Idris, A. L., Fan, X., Guo, Y., Yu, Y., Jin, X., et al. (2020). Beyond risk: bacterial biofilms and their regulating approaches. *Front. Microbiol.* 11. doi: 10.3389/fmicb.2020.00928

Nakajima, Y., Yoshizawa, S., Nakamura, K., Ogura, Y., Hayashi, T., and Kogure, K. (2017). Draft genome sequences of *Tersicoccus phoenicis* DSM 30849$_T$, isolated from a cleanroom for spacecraft sssembly, and tersicoccus sp. strain bi-70, isolated from a freshwater lake. *Genome Announc.* 5 (13), e00079–e00017. doi: 10.1128/genomeA.00079-17

Niemira, B. A. (2007). Irradiation sensitivity of planktonic and biofilm-associated *Escherichia coli* O157:H7 isolates is influenced by culture conditions. *Appl. Environ. Microbiol.* 73, 3239–3244. doi: 10.1128/aem.02764-06

Niemira, B. A. (2010). Irradiation sensitivity of planktonic and biofilm-associated *Listeria monocytogenes* and l. innocua as influenced by temperature of biofilm formation. *Food Bioprocess Technol.* 3, 257–264. doi: 10.1007/s11947-008-0079-5

Niemira, B. A., and Solomon, E. B. (2005). Sensitivity of planktonic and biofilm-associated *Salmonella* spp. to ionizing radiation. *Appl. Environ. Microbiol.* 71 (5), 2732–2736. doi: 10.1128/AEM.71.5.2732-2736.2005

Novikova, N., De Boever, P., Poddubko, S., Deshevaya, F., Polikarpov, N., and Rakova, N. (2006). Survey of environmental biocontamination on board the international space station. *Res. Microbiol.* 157 (1), 5–12. doi: 10.1016/j.resmic.2005.07.010

Penesyan, A., Paulsen, I. T., Kjelleberg, S., and Gillings, M. R. (2021). Three faces of biofilms: a microbial lifestyle, a nascent multicellular organism, and an incubator for diversity. *NPJ Biofilms Microbiomes.* 7, 80. doi: 10.1038/s41522-021-00251-2

Rampersad, S. N. (2012). Multiple applications of alamar blue as an indicator of metabolic function and cellular health in cell viability bioassays. *Sensors (Basel Switzerland).* 12, 12347–12360. doi: 10.3390/s120912347

Regberg, A. B., Castro, C. L., Connolly, H. C.Jr., Davis, R. E., Dworkin, J. P., Lauretta, D. S., et al. (2020). Prokaryotic and fungal characterization of the facilities used to assemble, test, and launch the OSIRIS-REx spacecraft. *Front. Microbiol.* 11. doi: 10.3389/fmicb.2020.530661

Reichhardt, C., Lim, J. Y., Rice, D., Fong, J. N., and Cegelski, L. (2014). Structure and function of bacterial biofilms by solid-state NMR. *Biophys. J.* 106 (2), 192A. doi: 10.1016/j.bpj.2013.11.1139

Ryan, M. P., and Pembroke, J. T. (2018). *Brevundimonas* spp: Emerging global opportunistic pathogens. *Virulence.* 9 (1), 480–493. doi: 10.1080/21505594.2017.1419116

Segers, P., Vancanneyt, M., Pot, B., Torck, U., Hoste, B., Dewettinck, D., et al. (1994). Classification of *Pseudomonas diminuta* leifson and Hugh 1954 and *Pseudomonas vesicularis* büsing, döll, and freytag 1953 in *Brevundimonas* gen. nov. as *Brevundimonas diminuta* comb. nov. and *Brevundimonas vesicularis* comb. nov., respectively. *Int. J. Syst. Bacteriol.* 44, 499–510. doi: 10.1099/00207713-44-3-499

Sheraz, M. A., Kazi, S. H., Ahmed, S., Anwar, Z., and Ahmad, I. (2014). Photo, thermal and chemical degradation of riboflavin. *Beilstein J. Org. Chem.* 10, 1999–2012. doi: 10.3762/bjoc.10.208

Sobisch, L.-Y., Rogowski, K.-M., Fuchs, J., Schmieder, W., Vaishampayan, A., Oles, P., et al. (2019). Biofilm forming antibiotic resistant gram-positive pathogens isolated from surfaces on the international space station. *Front. Microbiol.* 10. doi: 10.3389/fmicb.2019.00543

St Denis, T. G., Dai, T., Izikson, L., Astrakas, C., Anderson, R. R., Hamblin, M. R., et al. (2011). All you need is light: antimicrobial photoinactivation as an evolving and emerging discovery strategy against infectious disease. *Virulence.* 2 (6), 509–520. doi: 10.4161/viru.2.6.17889

Stieglmeier, M., Rettberg, P., Barczyk, S., Bohmeier, M., Pukall, R., Wirth, R., et al. (2012). Abundance and diversity of microbial inhabitants in European spacecraft-associated clean rooms. *Astrobiology.* 12 (6), 572–585. doi: 10.1089/ast.2011.0735

Temba, B. A., Fletcher, M. T., Fox, G. P., Harvey, J. J. W., and Sultanbawa, Y. (2016). Inactivation of *Aspergillus flavus* spores by curcumin-mediated photosensitization. *Food Control.* 59, 708–713. doi: 10.1016/j.foodcont.2015.06.045

Thompson, A. F., English, E. L., Nock, A. M., Willsey, G. G., Eckstrom, K., Cairns, B., et al. (2020). Characterizing species interactions that contribute to biofilm formation in a multispecies model of a potable water bacterial community. *Microbiol. (Reading Engl.).* 166 (1), 34–43. doi: 10.1099/mic.0.000849

Thornsberry, C. (1983). NCCLS standards for antimicrobial susceptibility tests. *Lab. Med.* 14 (9), 549–553. doi: 10.1093/labmed/14.9.549

Trotonda, M. P., Tamber, S., Memmi, G., and Cheung, A. L. (2008). MgrA represses biofilm formation in *Staphylococcus aureus.* infect. *Immun.* 76 (12), 5645–5654. doi: 10.1128/iai.00735-08

Venkateswaran, K., Vaishampayan, P., Cisneros, J., Pierson, D., Rogers, S. O., and Perry, J. (2014). International space station environmental microbiome — microbial inventories of ISS filter debris. *Appl. Microbiol. Biotechnol.* 98 (14), 6453–6466. doi: 10.1007/s00253-014-5650-6

Vornhagen, J., Stevens, M., McCormick, D. W., Dowd, S. E., Eisenberg, J. N., Boles, B. R., et al. (2013). Coaggregation occurs amongst bacteria within and between biofilms in domestic showerheads. *Biofouling.* 29 (1), 53–68. doi: 10.1080/08927014.2012.744395

Wainwright, M. (2004). Photoinactivation of viruses. *Photochem. Photobiol. Sci.* 3, 406–411. doi: 10.1039/b311903n

Wong, W. C., Dudinsky, L. A., Garcia, V. M., Ott, C. M., and Castro, V. A. (2010). Efficacy of various chemical disinfectants on biofilms formed in spacecraft potable water system components. *Biofouling.* 26 (5), 583–586. doi: 10.1080/08927014.2010.495772

Yin, R., Wang, M., Huang, Y.-Y., Landi, G., Vecchio, D., Chiang, L. Y., et al. (2014). Antimicrobial photodynamic inactivation with decacationic functionalized fullerenes: Oxygen-independent photokilling in presence of azide and new mechanistic insights. *Free Radic. Biol. Med.* 79, 14–27. doi: 10.1016/j.freeradbiomed.2014.10.514

Zea, L., Nisar, Z., Rubin, P., Cortesao, M., Luo, J., McBride, A., et al. (2018). Design of a spaceflight biofilm experiment. *Acta Astronaut.* 148, 294–300. doi: 10.1016/j.actaastro.2018.04.039

Zhang, X. H., Ahmad, W., Zhu, X. Y., Chen, J., and Austin, B. (2021). Viable but nonculturable bacteria and their resuscitation: implications for cultivating uncultured marine microorganisms. *Mar. Life Sci. Technol.* 3, 189–203. doi: 10.1007/s42995-020-00041-3

Zhang, J., Li, W., Chen, J., Wang, F., Qi, W., and Li, Y. (2019a). Impact of disinfectant on bacterial antibiotic resistance transfer between biofilm and tap water in a simulated distribution network. *Environ. pollut.* 246, 131–140. doi: 10.1016/j.envpol.2018.11.077

Zhang, X., Zhao, S., Gao, J., Lei, Y., Yuan, Y., Jiang, Y., et al. (2019b). Microbial action and mechanisms for cr (VI) removal performance by layered double hydroxide modified zeolite and quartz sand in constructed wetlands. *J. Environ. Manage.* 246, 636–646. doi: 10.1016/j.jenvman.2019.06.017

frontiers | Frontiers in Cellular and Infection Microbiology

TYPE Original Research
PUBLISHED 20 February 2023
DOI 10.3389/fcimb.2023.1118285

OPEN ACCESS

EDITED BY
Chuan Chiang-Ni,
Chang Gung University, Taiwan

REVIEWED BY
Gisela Di Venanzio,
Washington University in St. Louis, United States
Cheng-Yen Kao,
National Yang Ming Chiao Tung University, Taiwan

*CORRESPONDENCE
Yonghong Xiao
xiaoyonghong@zju.edu.cn

SPECIALTY SECTION
This article was submitted to Molecular Bacterial Pathogenesis, a section of the journal Frontiers in Cellular and Infection Microbiology

RECEIVED 07 December 2022
ACCEPTED 31 January 2023
PUBLISHED 20 February 2023

CITATION
Kong X, Chen T, Guo L, Zhou Y, Lu P and Xiao Y (2023) Phenotypic and genomic comparison of dominant and nondominant sequence-type of *Acinetobacter baumannii* isolated in China.
Front. Cell. Infect. Microbiol. 13:1118285.
doi: 10.3389/fcimb.2023.1118285

Phenotypic and genomic comparison of dominant and nondominant sequence-type of *Acinetobacter baumannii* isolated in China

Xiaoyang Kong[1], Tao Chen[1], Lihua Guo[1], Yanzi Zhou[2], Ping Lu[1] and Yonghong Xiao[1,3]*

[1]State Key Laboratory for Diagnosis and Treatment of Infectious Diseases, National Clinical Research Center for Infectious Diseases, Collaborative Innovation Center for Diagnosis and Treatment of Infectious Diseases, The First Affiliated Hospital, Zhejiang University School of Medicine, Hangzhou, China, [2]Department of Rheumatology, Affiliated Hangzhou First People's Hospital, School of Medicine, Zhejiang University, Hangzhou, China, [3]Jinan Microecological Biomedicine Shandong Laboratory, Jinan, China

A. baumannii is a common clinical pathogen that often causes pneumonia and bloodstream infections in ICU patients. Sequence types (ST) are used to investigate the distribution and spread of *A. baumannii*. Biological characteristics such as virulence and resistance may play a role in *A. baumannii* becoming a specific dominant ST(DST,ST191, ST195 and ST208) strain. To characterize the biological, genetic, and transcriptomic differences between the DST and non-dominant ST (NST,ST462 and ST547,etc.) strains in *A. baumannii*, we performed several biological experiments and genetic, and transcriptomic analyses. The DST group displayed more resistance ability to desiccation, oxidation, multiple antibiotics, and complement killing than the NST group. However, the latter had higher biofilm formation ability than the former. The genomic analysis showed the DST group exhibited more capsule-related and aminoglycoside-resistant genes. Besides, GO analysis indicated that functions involved in lipid biosynthetic, transport, and the metabolic process were up-regulated in the DST group, while KEGG analysis manifested that the two-component system related to potassium ion transport and pili were down-regulated. In short, resistance to desiccation, oxidation, multiple antibiotics, and serum complement killing are important reasons for the formation of DST. Genes related to capsule synthesis and lipid biosynthesis and metabolism play an important role at the molecular level in the formation of DST.

KEYWORDS

***Acinetobacter baumannii*, sequence type, resistance, virulence, transcriptome**

1 Introduction

A. baumannii is a Gram-negative bacterium that causes a number of clinically important, life-threatening infections including ventilator-associated pneumonia, bloodstream infections, and intracranial infections (Joly-Guillou, 2005; Maragakis and Perl, 2008; Freire et al., 2016). Furthermore, because of its inherent antibiotic resistance and the ease with

which it acquires resistance elements from elsewhere to develop multidrug resistance, carbapenem-resistant *A. baumannii* has become a common clinical pathogen and is listed by WHO as a pathogenic bacterium requiring priority development of new antibacterial drugs (World Health Organization; Lee et al., 2017).

ST is often used to investigate the prevalence, transmission, and outbreaks of *A. baumannii* clones in different regions or hospitals, and thus to assist in formulating appropriate hospital infection control measures (Schultz et al., 2016). Several studies, in different regions of China, have shown that ST191, ST195, and ST208 (Oxford scheme) are the most prevalent *A. baumannii* ST types isolated (Deng et al., 2014; Xiao et al., 2016; Ning et al., 2017; Zhou et al., 2018). ST208 and ST191 accounted for 58.7% and 10.9%, respectively, of strains isolated in Shanghai, whereas 41.7% and 13.1% of the strains isolated in the south of China were ST195 and ST208, respectively. ST191 was also shown to be the most prevalent strain in Korea (Son et al., 2020). Consequently,we define ST191 ST195 and ST208 these top three dominant ST types as the DST, and the other ST types including ST462, ST547 and STn(new types of numbers not yet assigned) as non-dominant sequence type(NST).

Studies have shown that the outer membrane protein OmpA, phospholipase, capsule capsular polysaccharide(CPS), iron acquisition system, efflux pump, Csu chaperone usher-type pilus, and secretion system are all important virulence factors of *A. baumannii* (Harding et al., 2018). Moreover, the ability to survive in unfavorable environments has been suggested as an important virulence strategy. Indeed, it has been reported that specific ST strains are highly virulent and correlate with poor clinical prognosis in infected patients (Yoon et al., 2019).

Although desiccation resistance has been reported to contribute to the spread and persistence of type-specific *A. baumannii* in the hospital setting (Giannouli et al., 2013). The factors that facilitate the generation of DST, and the phenotypic and genotypic differences between DST and NST strains of *A. baumannii*, have not been fully elucidated. We combined biological experiments with genomic and transcriptomic analysis, therefore, to comprehensively elucidate the biological properties, especially those relating to virulence and resistance, that differentiate DST and NST strains.

2 Materials and methods

2.1 Isolates, culture conditions, and susceptibility tests

All *A. baumannii* strains were isolated from a tertiary, first-class teaching hospital in East China, and the strain number, ST type, etc. are shown in Table S1. 10 strains of ST191, 12 strains of ST195, 11 strains of ST208, 10 strains of ST462, and 9 strains of ST547, total 52 strains were used for each biological experiments. Two strains from each ST type above, plus two STn strains, a total of 12 strains were selected for subsequent genomic and transcriptomic analysis based on their ability to resist complement killing. The antimicrobial susceptibility of all *A. baumannii* isolates was determined using agar dilution according to the Clinical and Laboratory Standards Institute (CLSI) guidelines from 2020. Resistance breakpoints determined by the European Committee on Antimicrobial Susceptibility Testing (EUCAST) were used for polymyxin B.

2.2 Growth curves

Growth curves were performed as described previously with slight modifications (Hall et al., 2014) Briefly, A. baumannii in the log-phase of growth were adjusted to 0.5 absorbance units (OD600) and diluted 50-fold with LB medium. Aliquots (200 µl) were added to a 96-well plate, placed in a microplate reader at 37°C, and shaken for 5 s every 30 min, and the OD600 was measured for 24 h.

2.3 Desiccation resistance assays

Desiccation resistance assays were completed as previously described (Boll et al., 2015) Log-phase A. baumannii were harvested and washed twice with an equal volume of LB medium. Each sample was adjusted to 1×108 CFU/ml and then serially diluted and plated to determine the input CFU. Bacterial suspension (10 µl) was spotted onto 96-well polystyrene plates and desiccated at 30°C at a humidity of 40%. PBS (200 µl) was added to each well to resuspend the bacteria after 48 h and 96 h, respectively, and the resuspended bacteria were serially diluted and plated to calculate the output CFU. The percent of survival was defined as the ratio of output to input CFUs.

2.4 Oxidative killing assay

A. baumannii in the log-phase of growth were adjusted to OD_{600} = 0.5 and spread evenly on an MH agar plate. A sterile filter paper disk with a diameter of 6 mm was placed in the middle of the inoculated agar, and 10 µl 20% (v/v) hydrogen peroxide was pipetted onto the filter paper. The plates were incubated at 37°C for 18 h, after which the growth inhibition zone around the disk was measured using Vernier calipers.

2.5 Antiserum complement killing

Blood collected from healthy volunteers was centrifuged and filtered with a 0.22 µm pore size syringe filter to obtain sterilized serum. Half of the serum was inactivated by heating in a 56°C water bath for 30 min. *A. baumannii* in the log-phase of growth were adjusted to 2×10^6 CFU/ml and mixed with normal or inactivated serum at a ratio of 1:9, respectively. After incubation for 1 h at 37°C, samples were serially diluted and spread on MH agar plates. After overnight incubation at 37°C, bacteria colonies were counted, and the bacterial survival rate was calculated by the following formula: Bacterial survival rate = (number of colonies in normal serum/ number of colonies in inactivated serum) × 100%.

2.6 Biofilm formation

A. baumannii in the log-phase of growth were adjusted to 0.5 absorbance units (OD_{600}), before 200 µl aliquots were pipetted into the wells of a 96-well plate. Bacteria were cultivated in an incubator for 24 h at 37°C and 5% CO_2, to allow biofilm formation, before nonattached bacteria were removed from the wells by aspiration. Biofilms were gently washed with ddH_2O, after which the 96-well plate was inverted on absorbent paper for 15 min at room temperature. Biofilm cells were fixed by adding 4% (v/v) paraformaldehyde to each well for 20 min and were then stained with 1% (w/v) crystal violet for 15 min. Biofilms were washed thoroughly with ddH_2O, before the bound crystal violet was eluted with 200 µl 95% ethanol, and were then incubated at 37°C for 30 min. The crystal violet eluted from each biofilm was measured colorimetrically at OD_{570}.

2.7 G. mellonella larvae infection

A. baumannii in the log-phase were adjusted to 1×10^7 CFU/ml. *G. mellonella* larvae weighing ~300 mg was divided randomly into groups, with each group containing 15 larvae. Each larva was infected with 10 µl of the adjusted bacterial suspension, incubated at 37°C, and observed once every 12 h for 3 days. Larval survival status was assessed using the acupuncture method, and no response was considered as death.

2.8 Whole genome sequencing and genome analysis

A. baumannii genomes were extracted using QIAamp DNA Mini Kit (QIAGEN, Valencia, CA), whole genome sequencing was performed by Illumina HiSeq 2500 (Illumina, San Diego, CA), and the raw sequencing results were quality-controlled using FastQC v.0.11.5. Trimmomatic v.0.40 was used to trim splice regions. The trimmed reads were assembled and annotated by SPAdes(http://cab.spbu.ru/software/spades/) v.3.6 and RAST(https://rast.nmpdr.org/), respectively. Antibiotic resistance genes and virulence genes were identified using the ResFinder (Bortolaia et al., 2020) and VFDB databases (Chen et al., 2016), respectively, with 80% identity and 80% query coverage as the cutoff values.

2.9 RNA sequencing and quality control

A. baumannii RNA library preparation, construction, sequencing, and processing of reads were performed at the Novogene Co., Ltd. (Beijing, China). The raw data were first processed by a Perl script to remove reads with adapters, those containing poly-N and low-quality reads. The sequencing error rate for a single base position should be less than 1% and no more than 6% (Table S2). All the analyses below were based on high-quality clean data.

2.10 Quantification of gene expression levels and analysis of differentially expressed genes (DEGs)

Clean reads were mapped to *A. baumannii* MDR-ZJ06 (accession No. CP001937.2) using Bowtie2-2.2.3. Counting the reads numbers mapped to each gene was achieved using HTSeq v0.6.1. Differential expression analysis for the DST and NST groups was performed using the DESeq R package (1.18.0), and *p*-values were corrected using the Benjamini–Hochberg method to control for false discovery rate (Glickman et al., 2014). Genes for which corrected *p*-values <0.05 were obtained, after DESeq processing, were defined as differentially expressed.

2.11 GO, COG, and KEGG enrichment analysis

Gene ontology (GO) enrichment analysis of DEGs was performed using the GOseq R package. GO terms with *p*-values less than 0.05 were considered significantly enriched for DEGs. Subsequently, the COG database was used to identify the functions of the proteins encoded by the DEGs. KOBAS software was used to test the statistical enrichment of DEGs in the KEGG pathway.

2.12 Quantitative real-time PCR

For analysis of expression of specific genes, *A. baumannii* RNA was first stabilized with RNA protection solution (Qiagen, 74124) and then extracted and purified according to the instructions of the RNeasy Mini Kit (Qiagen, 74104). One microliter RNA was added to nine microliter reaction buffer from the PrimeScript™ RT reagent Kit (Takara, RR037A) in the appropriate ratio, and then reverse transcribed to generate cDNA as follows: 37°C for 15 min, 85°C for 5 sec, and 4°C. cDNA was added to the reaction system of the TB Green® Premix Ex Taq™ (Takara, 420A), and PCR was carried out as follows: 95°C, 30 s for one cycle (stage 1); 95°C, 5 s, 60°C, 34 s for 40 cycles (stage 2); and 95°C, 15 s, 60°C,1 min, 95°C 15 s (stage 3). The genes and primers used are shown in Table S3, and *recA* was selected as the internal reference. The relative expression of different genes was calculated by the $2^{-\Delta\Delta Ct}$ method.

2.13 Statistics

Statistics were performed using prism9. Two groups were compared using the Mann-Whitney t-test, and the five groups were compared using a one-way ANOVA, with horizontal lines representing means ± standard error of means; $^*p < 0.05$, $^{**}p < 0.01$, $^{***}p < 0.001$, $^{****}p < 0.0001$.The biological experiments were repeated at least three times, except for the growth curve experiment and anti-desiccation assay, where two biological replicates were done, and the biofilm experiment, where four biological replicates were done.

3 Results

3.1 Comparison of the biological functions of DST and NST groups

We first compared their growth and there was no difference in the growth rates of strains in the two groups (Figure S1, $p = 0.42$).

As resistance to desiccation and oxidative stress are essential for the persistence of *A. baumannii* in the medical environment, we compared their abilities in these two aspects. After 96 h of desiccation, strains in the DST group had a mean survival rate of 10.38%, while strains in the NST group had a mean survival rate of 5.13% ($p < 0.0001$; Figure 1A). Moreover, the oxidative stress analysis showed that the hydrogen-peroxide-induced growth inhibition zone for the DST group was lower than that for the NST group (zone diameter 36.29 mm vs. 37.16 mm; $p = 0.027$), indicating that the DST strains were more resistant to oxidative stress than the NST strains (Figures 1B, C).

The DST group had higher resistance to complement-mediated killing (mean survival 11.00% vs. 5.31%; $p < 0.0001$; Figure 1D), but lower biofilm formation ability (OD_{570} 0.31 vs. 0.42; $p < 0.0001$), than the NST group (Figure 1E).

When *G. mellonella* was used as an *in vivo* bacterial infection model, larvae infected with the DST group had a higher mean survival rate than those infected with the NST group in the early (12 h), middle (36 h), and late (72 h) stages of infection, however, all this difference was not statistically significant (Figures 1F, S2).

3.2 Antimicrobial susceptibility

All strains belonging to the DST group were resistant to all three cephalosporins, while the strains of the NST group displayed resistance rates of 33.34%, 66.66%, and 33.34% to ceftazidime, cefepime, and

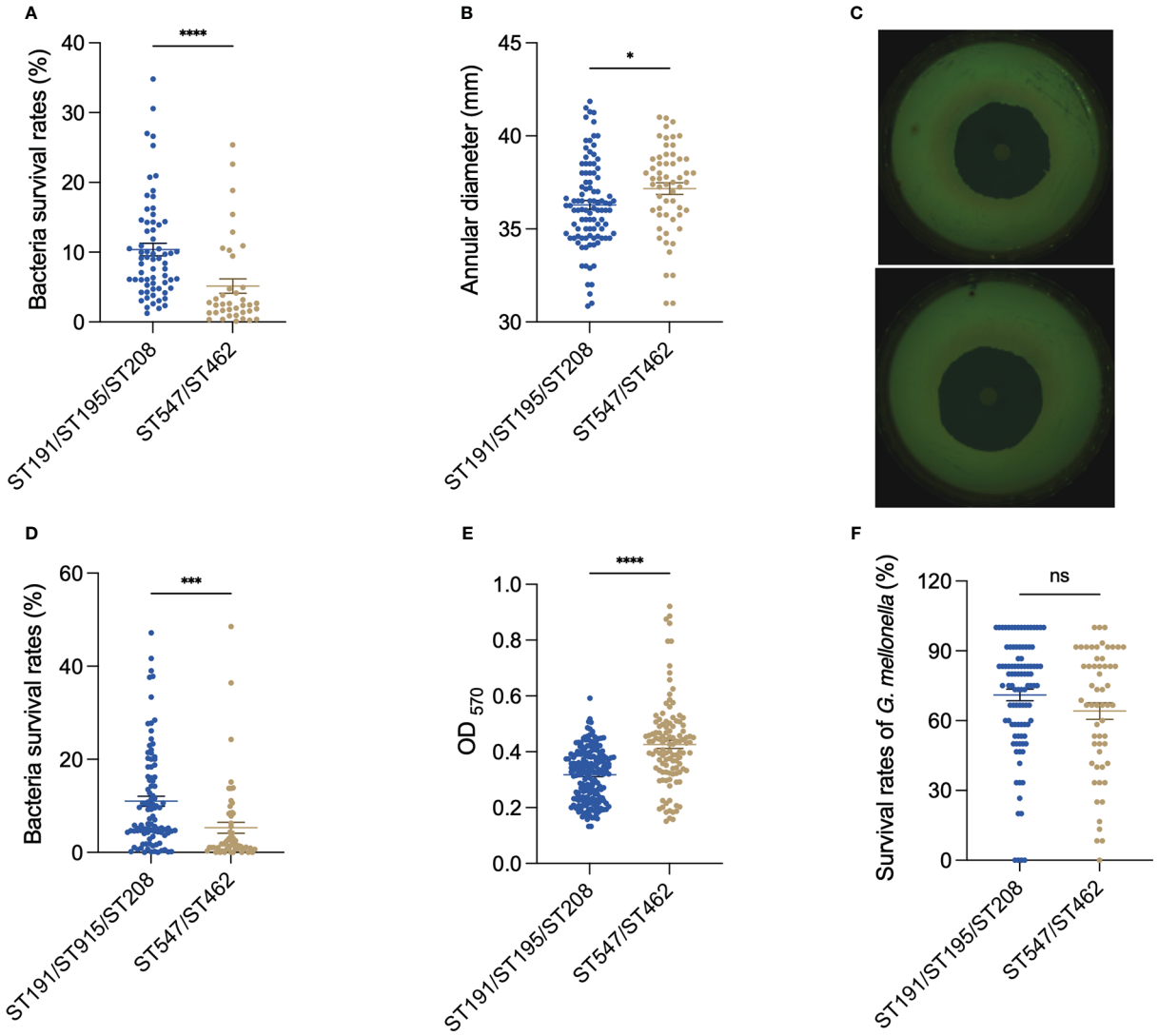

FIGURE 1
Comparison of (*A*) *baumannii* DST and NST group phenotypes. **(A)** Antidesiccation *in vitro*. **(B)** Antioxidation *in vitro*. **(C)** Representative pictures of the antioxidation *in vitro*. The upper figure is the inhibition circle of hydrogen peroxide in the DST group, while the lower is the inhibition circle in the NST group. **(D)** Antiserum killing *in vitro*. **(E)** Biofilm formation ability of bacteria *in vitro*. **(F)** The survival rate of G. mellonella after being infected with A. baumannii at 72 h. Each point represents data from one biological experiment for one bacterium. Each experiment included 10 strains of ST191, 12 strains of ST195, 11 strains of ST208, 10 strains of ST462, and 9 strains of ST547, and bar plots illustrate means ± SEM. Meaning of symbols "*, ***, **** and ns" indicate p<0.05, p<0.001, p<0.0001 and no statistical difference (p>0.05), respectively.

ceftriaxone, respectively. Similarly, the DST strains were all resistant to carbapenems, whereas 66.66% of the NST group strains showed resistance. However, for aminoglycosides, the resistance rate was 66.66% for the DST group and 16.66–33.34% for the NST group. All the DST group strains were resistant to quinolones, while the NST group strains had a resistance rate of 66.66%. The overall MICs of the DST group were also higher than those of the ST group for minocycline and combined antibiotics (Table 1).

3.3 Virulence and resistance genes analysis based on genomes of DST group and NST group

The general features of the twelve genomes were shown in Table S4. The phylogenetic tree built using roary software (default parameters) indicates that strains of the same ST type were closely related, but ST208 of the DST group was evolutionarily distant from ST191 and ST195. ST547 of the NST group was also distant from ST462 and the STn type strains (Figure S3).

The results appeared that the two groups shared significant virulence genes. The encoded products of which included adhesion-related outer membrane protein OmpA, serum resistance-associated penicillin-binding protein PbpG, cleavage cell membrane related phospholipase Plc and PlcD, iron acquisition protein BarAB, BauABCDE, AbaI and AbaR related to quorum sensing, PgaABCD involved in biofilm formation, the CPS synthesis component, Wza, Wzb and Wzc related to immune escape, etc (Figure 2). This is consistent with the similar virulence seen for strains in the two groups in the *G. mellonella* infection model.

Twenty-four virulence genes associated with CPS were found only in strains of the DST group. These include glycosyltransferase-related genes *itrB2*, *gtr3/4/5/8/20/21/22*, *kpsS*, CMP-glycan pathway-related *pseB/C/F/H/I*, UDP-glycan pathway-related *fnlA/fnlB*, dehydrogenase *pgt1*, and isomerase *wecB*. However, 17 virulence-associated genes were found exclusively in strains from the NST group. These include 15 genes related to the CPS (CMP-glycan pathway-related *legC*, *lgaA/F/G* gene, glycosyltransferase *gtr14/15/52*, *M3Q_295/296*, and *weeH*) and two genes related to iron acquisition.

Overall, strains of the DST group harbored a greater number of CPS synthesis-related genes than those of the NST group, consistent with the increased resistance to complement killing and desiccation previously reported for DST group strains (Russo et al., 2010; Tipton et al., 2018). Many different genes related to the K locus, which is associated with CPS synthesis in *A. baumannii*, were unique to members of each of the two groups, consistent with the high variability previously reported for the middle region at the K locus (Kenyon and Hall, 2013).

To explore why the DST group strains had higher antibiotic resistance rates than those of the NST group, the profile of resistance genes in each strain was analyzed using the ResFinder database. Although strains in the two groups had several resistance genes in common, including genes encoding aminoglycoside, β-lactam, and sulfonamide resistance, many other resistance genes were found only in the DST group, correlating with the differences in drug susceptibility observed for the two groups. These unique genes included *ant(3")-Ia_1* and *armA_1* (aminoglycoside resistance),

TABLE 1 Antibiotic susceptibility of *A. baumannii* DST and NST strains.

Class	ST	Strains	SCP	CZA	SAM	TZP	SXT	CAZ	FEP	CRO	IMP	MEM	GEN	AMK	CIP	LVX	MIN	POL
DST	191	15923	128/64	>32/4	64/32	>128/4	>8/152	128	32	>128	>64	>64	>128	>128	>32	16	8	0.5
	191	26128	128/64	>32/4	>128/64	>128/4	>8/152	128	>128	>128	>64	>64	8	4	>32	16	2	0.5
	195	16149	128/64	>32/4	128/64	>128/4	0.5/9.5	>128	64	>128	>64	>64	>128	>128	>32	8	4	0.5
	195	16354	>128/64	>32/4	>128/64	>128/4	>8/152	>128	128	>128	>64	>64	>128	>128	>32	8	4	0.25
	208	19701	128/64	>32/4	32/16	>128/4	>8/152	128	32	>128	>64	>64	>128	>128	>32	8	8	1
	208	17493	>128/64	>32/4	>128/64	>128/4	>8/152	128	128	>128	>64	>64	8	8	>32	16	8	1
NST	462	24443	128/64	>32/4	64/32	>128/4	<0.25/4.75	4	64	16	>64	>64	8	16	>32	8	<0.25	0.5
	462	19595	128/64	>32/4	32/16	>128/4	<0.25/4.75	4	32	16	64	>64	16	16	>32	8	<0.25	0.5
	547	18190	>128/64	>32/4	>128/64	>128/4	>8/152	>128	>128	>128	>64	>64	>128	>128	>32	8	4	0.25
	547	12134	128/64	>32/4	>128/64	>128/4	>8/152	>128	128	>128	>64	>64	8	8	>32	8	4	0.5
	New	6070	128/64	>32/4	16/8	16/4	<0.25/4.75	4	2	16	0.5	0.5	1	4	0.5	0.125	<0.25	1
	New	24484	128/64	4/4	8/4	16/4	<0.25/4.75	4	2	16	0.25	0.25	1	2	1	0.25	<0. 25	0.5

SCP, cefoperazone/sulbactam; CZA, ceftazidime/avibactam; SAM, ampicillin/sulbactam; TZP, piperacillin/tazobactam; SXT, cotrimoxazole; CAZ, ceftazidime; FEP, cefepime; CRO, ceftriaxone; IPM, imipenem; MEM, meropenem; GEN, gentamicin; AMK, amikacin. CIP, ciprofloxacin; LVX, levofloxacin; MIN, minocycline; POL, polymyxin B.

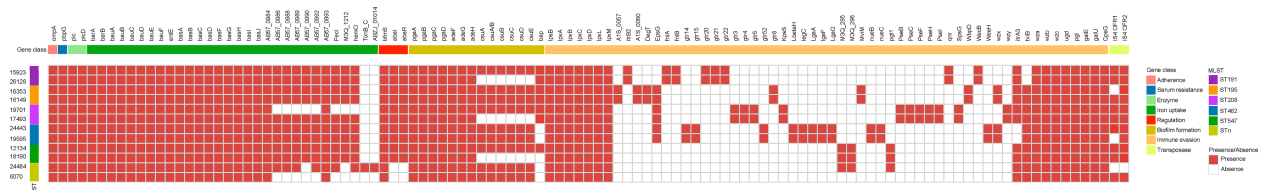

FIGURE 2
Comparison of virulence genes present in *A. baumannii* DST and NST strains. The first row represents the virulence gene name, and the second row represents gene functional classification. The columns from left to right represent the name and ST type. Both identity and coverage are greater than 80% as the threshold for the presence of genes.

*bla*TEM-1D_1 (β-lactam resistance), *mph(E)_1* (macrolide resistance), and *sul1_5* (sulfonamide resistance; Figure 3). Interestingly, the only resistance genes unique to the NST group were β-lactam-related genes, such as *bla*OXA-120_1, *bla*OXA-51_1, and *bla*OXA-531_1 (Figure 3).

3.4 Transcriptome analysis

Transcriptome analysis showed that a total of 620 protein-coding genes were differentially expressed between the two groups (padj < 0.05), with 492 genes upregulated and 128 genes downregulated, in DST compared with NST, accounting for approximately 15% of all protein-coding genes (Figure 4). After screening by $\log_2$ FoldChange (DST/NST) ≥ 2, 128 genes were identified as being significantly upregulated in the DST group, including nine CPS synthesis-related genes, one efflux pump gene, and three T6SS secretion system-related genes. Loci corresponding to gene_ids for all these genes were identified in the genomes of the DST strains being analyzed (Table S5). After screening by $\log_2$ FoldChange (DST/NST) ≤-2, 53 genes were identified as being significantly downregulated in the DST group, including three genes related to CPS biosynthesis and six genes related to iron uptake (Table S6). Meanwhile, we randomly selected two genes for Q-PCR validation, respectively. The results showed that the relative trend in the expression of these genes, in strains from the different groups, was consistent with the transcriptomic data (Figures 4B, C).

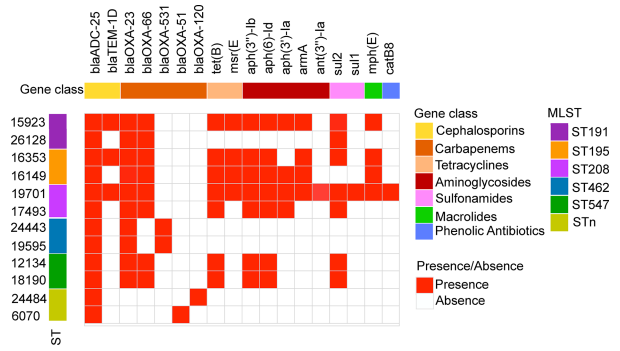

FIGURE 3
Antibiotic resistance gene profiles of *A. baumannii* DST and NST strains. The first row represents the resistance gene designation, and the second row represents the gene functional classification. The columns from left to right represent the strain name and ST type. Both identity and coverage are greater than 80% as the threshold for the presence of genes.

GO analysis showed that the most dramatically enriched gene set related to "lipid biosynthesis process," which contains the *wecB*, *capD*, and *galE* genes involved in CPS synthesis, as well as the *fabB*, *fabF*, and *psd* genes involved in lipid syntheses. Other functional groups enriched in the DST upregulated genes group included "lipid metabolism process" and "carbohydrate transmembrane transport activity" (Figure 5A). The most significantly enriched, downregulated genes in the DST group were "potassium-transporting ATPase activity" and "ATPase activity, coupled to transmembrane movement of ions, phosphorylative mechanism," with both of these functional sets containing the potassium ion transport genes *kdpA* and *kdpC*. Other functional sets with higher levels of enrichment in the DST downregulated genes group included "chemotaxis" and "taxis," both of which include the *chpA* and *pilI* genes (Figure 5B).

Similar to the GO analysis, the COG analysis revealed that the "lipid transport and metabolism" category was enriched in the upregulated genes in the DST group (Figure 6). Additionally, the functional categories with the next largest differences in the number of genes expressed between the two groups were "Transcription" and "Replication,". Although upregulated genes outnumbered downregulated genes in many functional categories, the "intracellular trafficking, secretion, and vesicular transport" category only contained downregulated genes. This suggests that strong secretion and vesicular transport abilities may be less important to DST strains.

The KEGG pathway enrichment analysis indicated that the most significant pathway enriched for upregulated genes was "starch and sucrose metabolism" (p = 0.0054), which contains three genes, *galU*, *ugd*, and *pgi*, related to the CPS biosynthesis. This is in agreement with the fact that the most significant terms in the GO analysis also contain three CPS synthesis-related genes. Other enriched pathways were "Pentose phosphate pathway," "Biotin metabolism," and "Fatty acid biosynthesis" (Figure 7). The most significant of the downregulated gene-enriched pathways were the "two-component systems" (p=1.20E-07), which include proteins associated with potassium uptake (kdpA, kdpB, and kdpC) and motility (pilJ, pilH, pilI, pilG, PilR).

3.5 Virulence and resistance genes in DEGs based on transcriptomic analysis

Differences in DEGs associated with virulence and antibiotic resistance were next investigated since these two phenotypes are closely linked to the clinical significance of bacteria and to their survival in the environment.

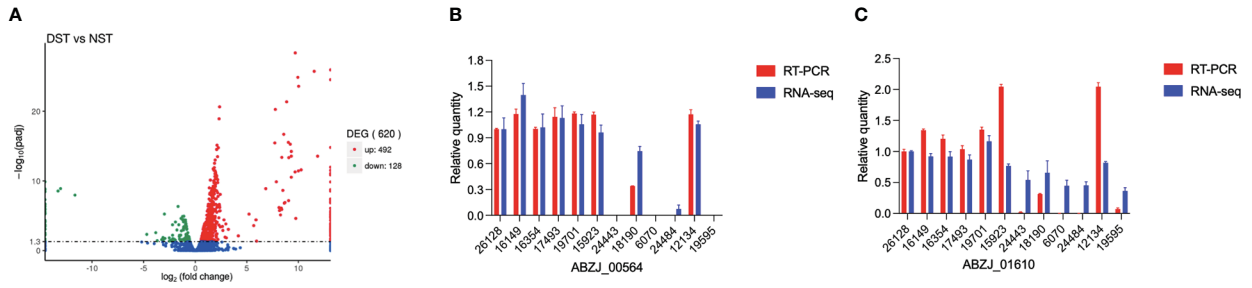

FIGURE 4
Relative expression of genes in DST and NST strains. **(A)** The y-axis shows -$\log_{10}$padj values for each gene, while the x-axis shows $\log_2$ fold change of DST vs NST. Red represents upregulation genes, and green represents downregulation genes; FDR ≤ 0.05 was the criterion for significant differences. **(B)**, **(C)** RNA-seq data of several highly expressed genes were validated using Q-PCR.

The VFDB database and the one-way blast approach for SwissProt annotation were combined to identify 42 virulence-related genes among the upregulated genes in strains of the DST group. The genes identified were similar to those identified by genomic analysis, the functions of which related mainly to CPS synthesis and transport (*wza*/*wzb*/*wzc*, etc.), iron uptake (Heme utilization genes, TonB-dependent iron carrier receptors, and iron regulatory proteins), type VI secretion systems (*vgrg*, *vgrgA*, contractile small subunits, and PAAR domain-containing proteins), and biofilm formation (*pilin*/*pgaB*, *ompW*, *oprM*, *abaR*). In addition, the toxin-antitoxin *cdiA*/*cdiB*, RNA chaperone *hfq*, sensor protein *pilS*, and the redox-sensitive transcriptional activator *soxR* were also highly expressed in strains of the DST group (Table S7). The functions of 36 virulence genes identified as downregulated in the DST groups mainly involved type IV pilus synthesis, and included genes encoding pilus assembly proteins (*pilC, pilB, pilJ, pilG, pilH, pilI, pilT*) and the pilus regulatory protein gene (*PilR*). In addition, genes downregulated in the DST group contained genes related to iron uptake, CPS synthesis, potassium transport, chemotactic and competition functions, type II secretion system, and phospholipase synthesis (Table S8).

Alignment of DEGs with the antibiotic resistance database ResFinder identified that genes encoding resistance to several antibiotic classes, including aminoglycosides, tetracyclines, β-lactam, chloramphenicol, and cationic antimicrobial peptide, were upregulated in the DST group (Table S9), while chlorhexidine, chloramphenicol, and aminoglycoside resistance genes were downregulated in the DST group (Table S10).

4 Discussion

A. baumannii is a significant cause of pneumonia and bloodstream infection in critically ill patients, and its high rate of multidrug resistance poses a great challenge to clinical treatment. Consequently, research on *A. baumannii* has focused mainly on revealing its antibiotic resistance mechanism. However, as the understanding of this pathogen deepens, it has become clear that virulence mechanisms of *A. baumannii* also play a very important role in human infections and disease prognosis. Sequence typing has attracted the attention of public health clinicians because it helps to study the transmission, outbreak, and prevalence of *A. baumannii*

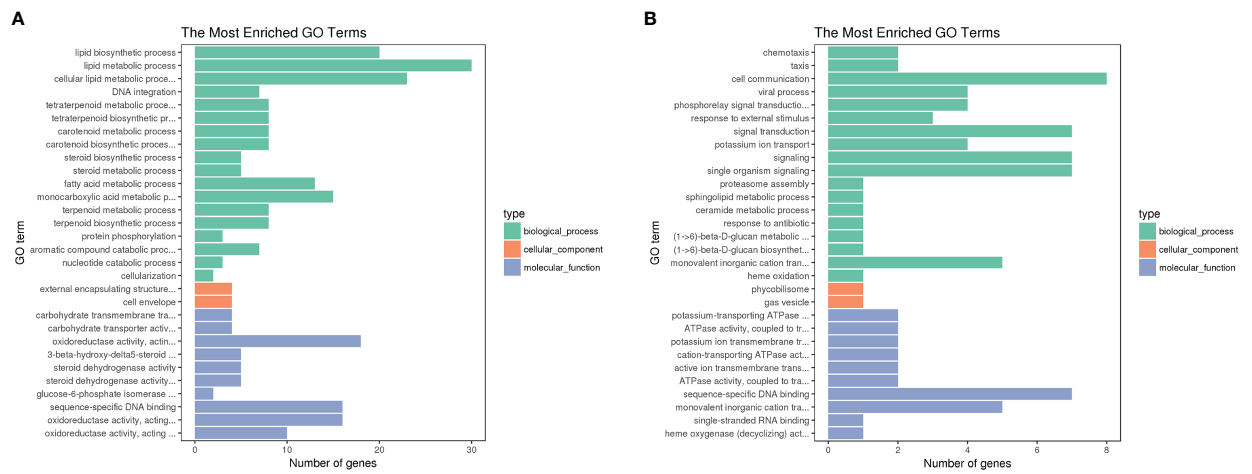

FIGURE 5
GO term functional analysis. Vertical coordinates are GO term functional modules; horizontal coordinates represent the number of enriched genes, where green represents biological processes, red represents cellular components, and gray represents molecular functions. We selected the 30 most significantly enriched GO terms to be shown in the figure, or all of them if there are less than 30. **(A)** GO enrichment of up-regulated DEGs in DST strains; **(B)** GO enrichment of down-regulated DEGs in DST strains. **(B)** Enrichment of genes downregulated in DST strains.

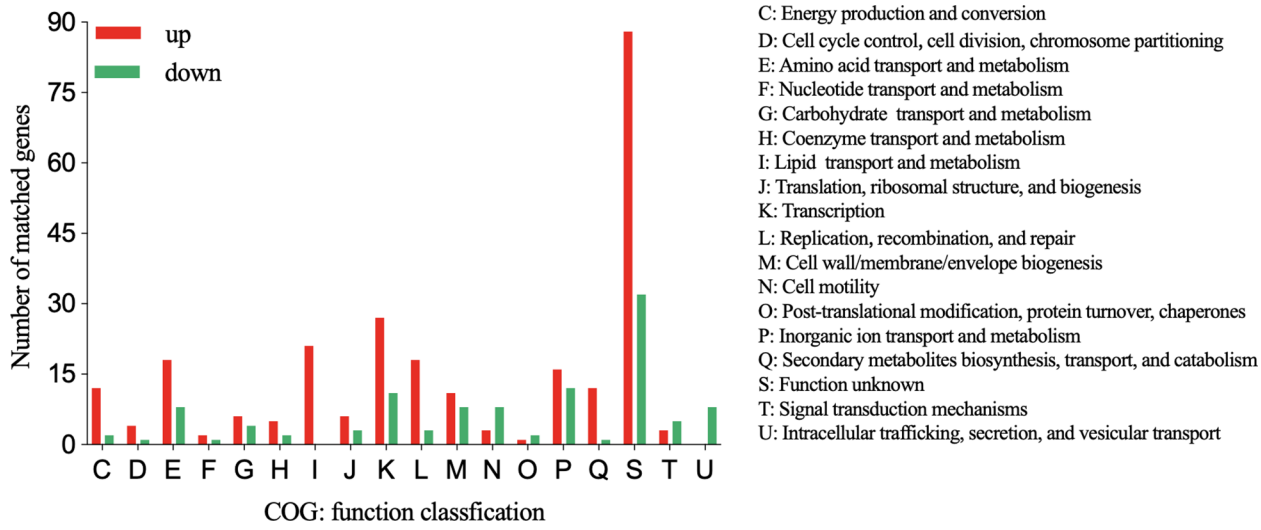

FIGURE 6
COG functional classification of up- and downregulated genes in the DST group relative to the NST group. Y-axis represents the number of up- or downregulated genes, and X-axis represents the COG functional classification.

strains. Although sporadic studies have investigated the *A. baumannii* characteristics that contribute to specific STs becoming DSTs (Ali et al., 2017; Zahra et al., 2018; de Azevedo et al., 2019), research in this area is still in its infancy. Thus, a more integrated approach, which explores the relationship between the virulence, antibiotic resistance, and ST of specific dominant strains, is required.

Based on previously published studies, we identified ST191, ST195, and ST208 as the DSTs and ST 547 and ST462 as the NSTs of *A. baumannii*, and selected around ten strains of each ST for experimental research in this study. As serum complement killing assay is an important indicator of virulence of A. baumannii, we selected two strains from each of the three DST with high complement killing resistance, and two strains from each of the ST462, ST547 plus two STn that were sensitive to complement killing, for subsequent genomic and transcriptomic analyses.

As we expected, the DST group was more tolerant to various adverse environments, including oxidation, desiccation, and complement-mediated killing. This also correlated with the demonstration that the DST group possessed more genes related to CPS biosynthesis, and that the expression of these genes was higher than related genes in the NST strains. This is in agreement with previous studies, in which CPS was shown to play a vital role in desiccation resistance and anticomplement killing in *Acinetobacter* (Ophir and Gutnick, 1994; Tipton et al., 2018). Norton et al. (2013)

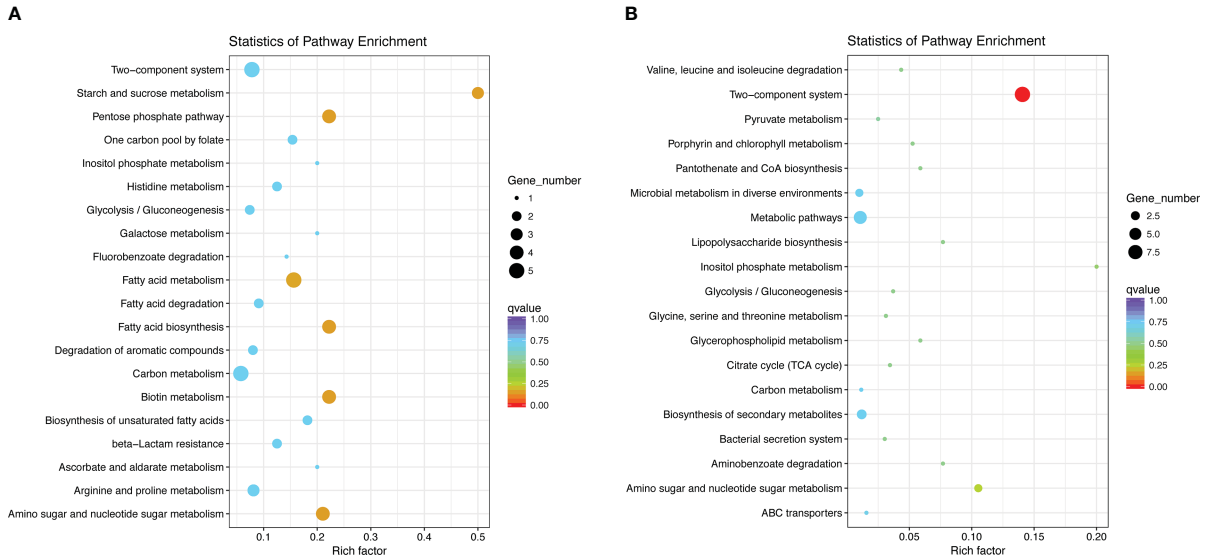

FIGURE 7
Statistics of pathway enrichment. We selected the 20 most significantly enriched pathway entries and displayed them in the graph. If the enriched pathway entries were less than 20, we displayed all of them. The ordinate represents the name of the pathway, the abscissa represents the Rich factor, the size of the point represents the number of DEGs in this pathway, and the color of the point corresponds to a different Q value. **(A)** KEGG enrichment of upregulated DEGs in DST strains; **(B)** KEGG enrichment of downregulated DEGs in DST strains.

revealed that desiccation stress can induce resistance to antibiotics, corresponding to higher resistance rates in the *A. baumannii* DST group (Norton et al., 2013).

Previous studies have shown that *A. baumannii* can form robust biofilms on wounds and medical devices such as endotracheal tubes (Thompson et al., 2014; Greene et al., 2016), as well as increase the tolerance to various extracellular stress (Espinal et al., 2012; Greene et al., 2016). To our surprise, the biofilm-forming ability of the DST group was not as strong as that of the NST group. Moreover, the biofilm formation-related genes *adeFGH*, *bap*, *csu* fimbriae, *pga/b/c/d*, *abaR*, and *abaI* all existed in the genomes of both groups, and there was no significant difference in the transcription of these genes by either group. The evolution of ST dominant strains may partly be driven by their sustained exposure to nutrient-deficient environments, and as such, 24 h biofilm formation experiments in a nutrient-rich environment do not accurately mimic these conditions. Alternatively, other, as yet unidentified, genes of *A. baumannii* may be important in the ability bacteria of this organism to form biofilms.

The evolutionary process of bacteria, on the one hand, desires to be resistant to as many antibiotics as possible, and on the other hand to retain their ability to survive in unfavorable environments and infect hosts, however, no bacteria can be highly pathogenic, pan-resistant, permanently prevalent and existence in all (Imperi et al., 2011; Da Silva and Domingues, 2017). This may explain why the DST group, which has a higher drug resistance rate and is more resistant to complement killing, has a weaker biofilm formation ability than the NST group.

Among the highly expressed virulence factors genes in the DST group (log_2Foldchange(DST/NST) ≥2) were CPS biosynthesis and T6SS component-associated genes, whereas the downregulated virulence factors genes (log_2Foldchange(DST/NST) ≤-2) were iron uptake related. This may be due to the fact that the capsule promotes the survival of *A. baumannii* both in the hospital setting and in patients. T6SS also contributes to the dominance of *A. baumannii* owing to its competition with other bacteria (Repizo et al., 2015; Weber et al., 2016). However, although the iron acquisition system helps bacteria to acquire iron in hosts with iron-deficient environments, it does not necessarily play an important role in promoting dominant clone formation (Penwell et al., 2015; Runci et al., 2019).

Interestingly, many type 4 pili genes related to adherence and motility, including *pilR*, *pilB*, *pilC*, *pilJ*, *pilG*, *pilH*, *pilI*, and *pilT*, were downregulated in the DST group, which showed higher resistance to serum complement. By contrast, a previous study showed that type IV pili of *A. baumannii* were upregulated while growing in serum (Jacobs et al., 2012). There are several conceivable explanations for this apparent anomaly. First, the media used for the growth of *A. baumannii* differed between the two studies. In our study, transcriptome analysis was carried out following growth of the bacterium in LB broth, whereas in the other study, the organism was grown in the presence of serum. Second, the *A. baumannii* strains used were different. Third, since glycosylation of pili has been shown to contribute to the survival of *P. aeruginosa* in the pulmonary environment (Smedley et al., 2005), post-transcriptional modifications may also play important roles in *A. baumannii* phenotypes; such modifications were not investigated in this study.

The transposon-sequence (Tn-seq) technique was used to identify 50 genes required for survival, in human serum, of a strain of *A. baumannii* isolated from a case of osteomyelitis (Sanchez-Larrayoz et al., 2017). Several of the genes identified in that study, such as CPS-related genes *wza*, and *wzb*, correlate with those we found to be upregulated in the DST group.

Lipid biosynthesis plays an important role in the synthesis of phospholipids in bacteria, and asymmetric bacterial cell membranes are an important permeability barrier that contributes to bacterial resistance to many antibiotics (Zhang and Rock, 2008; Simpson and Trent, 2019). This is consistent with one of our most important findings, namely, that genes associated with lipid biosynthesis and transport pathways are enriched in those genes upregulated in the DST group. Moreover, the upregulated *fabB* and *fabF* involved in this pathway exhibit a prolonged effect on fatty acid synthesis, and the knockdown of *fabB* in *E. coli* leads to unsaturated fatty acid nutrient deficiency and failure to grow properly (Wang and Cronan, 2004). The knockdown of *fabF* also reduces motility in *P. aeruginosa* (Overhage et al., 2007). To date, however, there is little information on the roles in the virulence and adaptation of *Acinetobacter baumannii* of many of the genes in this pathway.

Naturally, our study has some shortcomings; for example, the number of the strains used in the genome and transcriptome analysis is small and may not be particularly representative. What's more, it would be impossible to collect and analyze all possible environmental conditions (e.g., temperature, humidity, rainfall, and other climatic factors) that may influence the evolution of the strains.

In conclusion, tolerance to desiccation, oxidation, and complement killing all play an important role in the evolution of DST *A. baumannii* strains, while CPS biosynthesis, T6SS, and especially lipid synthesis pathway-related genes also play an indispensable role in this process. Our study further revealed the relationship between antibiotic resistance, virulence, and specific dominant ST of *A. baumannii*, laying a foundation for better prevention, control, and treatment of infections by this organism in the future.

Data availability statement

The datasets presented in this study can be found in online repositories. The names of the repository/repositories and accession number(s) can be found below: https://www.ncbi.nlm.nih.gov/, PRJNA906176.

Author contributions

XK completed most of the experiments and wrote the first draft of the manuscript. TC and PL contributed in toxicity testing of bacteria analysis. LG and YZ performed the bioinformatics analysis. YX

contributed to conception and design of the study and revised the manuscript. All authors contributed to the article and approved the submitted version.

Funding

This study was supported by the National Key Research and Development Program of China (2021YFC2300300), the Key research and development program of Zhejiang province (No. 2021C03068), the Research Project of Jinan Microecological Biomedicine Shandong Laboratory (JNL-2022006B), and the Fundamental Research Funds for the Central Universities (2022ZFJH003).

Acknowledgments

We thank Jinru Ji, Chaoqun Ying, and Zhiying Liu for their help with sample collection in the laboratory, Wangxiao Zhou for providing assistance with Genome Analysis. Qixia Luo, and Beiwen Zheng for providing assistance with manuscript revision.

Conflict of interest

The authors declare that the research was conducted in the absence of any commercial or financial relationships that could be construed as a potential conflict of interest.

Publisher's note

Supplementary material

The Supplementary Material for this article can be found online at: https://www.frontiersin.org/articles/10.3389/fcimb.2023.1118285/full#supplementary-material

References

Ali, H. M., Salem, M. Z. M., El-Shikh, M. S., Megeed, A. A., Alogaibi, Y. A., and Talea, I. A. (2017). Investigation of the virulence factors and molecular characterization of the clonal relations of multidrug-resistant acinetobacter baumannii isolates. *J. AOAC Int.* 100, 152–158. doi: 10.5740/jaoacint.16-0139

Boll, J. M., Tucker, A. T., Klein, D. R., Beltran, A. M., Brodbelt, J. S., Davies, B. W., et al. (2015). Reinforcing lipid a acylation on the cell surface of acinetobacter baumannii promotes cationic antimicrobial peptide resistance and desiccation survival. *mBio* 6, e00478–e00415. doi: 10.1128/mBio.00478-15

Bortolaia, V., Kaas, R. S., Ruppe, E., Roberts, M. C., Schwarz, S., Cattoir, V., et al. (2020). ResFinder 4.0 for predictions of phenotypes from genotypes. *J. Antimicrob. Chemother.* 75, 3491–3500. doi: 10.1093/jac/dkaa345

Chen, L., Zheng, D., Liu, B., Yang, J., and Jin, Q. (2016). VFDB 2016: hierarchical and refined dataset for big data analysis–10 years on. *Nucleic Acids Res.* 44, D694–D697. doi: 10.1093/nar/gkv1239

Da Silva, G. J., and Domingues, S. (2017). Interplay between colistin resistance, virulence and fitness in acinetobacter baumannii. *Antibiotics (Basel)* 6(4), 28–38. doi: 10.3390/antibiotics6040028

de Azevedo, F., Dutra, V., Nakazato, L., Mello, C. M., Pepato, M. A., de Sousa, A., et al. (2019). Molecular epidemiology of multidrug-resistant acinetobacter baumannii infection in two hospitals in central Brazil: the role of ST730 and ST162 in clinical outcomes. *J. Med. Microbiol.* 68, 31–40. doi: 10.1099/jmm.0.000853

Deng, M., Zhu, M. H., Li, J. J., Bi, S., Sheng, Z. K., Hu, F. S., et al. (2014). Molecular epidemiology and mechanisms of tigecycline resistance in clinical isolates of acinetobacter baumannii from a Chinese university hospital. *Antimicrob. Agents Chemother.* 58, 297–303. doi: 10.1128/AAC.01727-13

Espinal, P., Marti, S., and Vila, J. (2012). Effect of biofilm formation on the survival of acinetobacter baumannii on dry surfaces. *J. Hosp Infect.* 80, 56–60. doi: 10.1016/j.jhin.2011.08.013

Freire, M. P., de Oliveira Garcia, D., Garcia, C. P., Campagnari Bueno, M. F., Camargo, C. H., Kono Magri, A. S. G., et al. (2016). Bloodstream infection caused by extensively drug-resistant acinetobacter baumannii in cancer patients: high mortality associated with delayed treatment rather than with the degree of neutropenia. *Clin. Microbiol. Infect.* 22, 352–358. doi: 10.1016/j.cmi.2015.12.010

Giannouli, M., Antunes, L. C., Marchetti, V., Triassi, M., Visca, P., and Zarrilli, R. (2013). Virulence-related traits of epidemic acinetobacter baumannii strains belonging to the international clonal lineages I-III and to the emerging genotypes ST25 and ST78. *BMC Infect. Dis.* 13, 282. doi: 10.1186/1471-2334-13-282

Glickman, M. E., Rao, S. R., and Schultz, M. R. (2014). False discovery rate control is a recommended alternative to bonferroni-type adjustments in health studies. *J. Clin. Epidemiol.* 67, 850–857. doi: 10.1016/j.jclinepi.2014.03.012

Greene, C., Vadlamudi, G., Newton, D., Foxman, B., and Xi, C. (2016). The influence of biofilm formation and multidrug resistance on environmental survival of clinical and environmental isolates of acinetobacter baumannii. *Am. J. Infect. Control* 44, e65–e71. doi: 10.1016/j.ajic.2015.12.012

Greene, C., Wu, J., Rickard, A. H., and Xi, C. (2016). Evaluation of the ability of acinetobacter baumannii to form biofilms on six different biomedical relevant surfaces. *Lett. Appl. Microbiol.* 63, 233–239. doi: 10.1111/lam.12627

Hall, B. G., Acar, H., Nandipati, A., and Barlow, M. (2014). Growth rates made easy. *Mol. Biol. Evol.* 31, 232–238. doi: 10.1093/molbev/mst187

Harding, C. M., Hennon, S. W., and Feldman, M. F. (2018). Uncovering the mechanisms of acinetobacter baumannii virulence. *Nat. Rev. Microbiol.* 16, 91–102. doi: 10.1038/nrmicro.2017.148

Imperi, F., Antunes, L. C., Blom, J., Villa, L., Iacono, M., Visca, P., et al. (2011). The genomics of acinetobacter baumannii: insights into genome plasticity, antimicrobial resistance and pathogenicity. *IUBMB Life* 63, 1068–1074. doi: 10.1002/iub.531

Jacobs, A. C., Sayood, K., Olmsted, S. B., Blanchard, C. E., Hinrichs, S., Russell, D., et al. (2012). Characterization of the acinetobacter baumannii growth phase-dependent and serum responsive transcriptomes. *FEMS Immunol. Med. Microbiol.* 64, 403–412. doi: 10.1111/j.1574-695X.2011.00926.x

Joly-Guillou, M. L. (2005). Clinical impact and pathogenicity of acinetobacter. *Clin. Microbiol. Infect.* 11, 868–873. doi: 10.1111/j.1469-0691.2005.01227.x

Kenyon, J. J., and Hall, R. M. (2013). Variation in the complex carbohydrate biosynthesis loci of acinetobacter baumannii genomes. *PLoS One* 8, e62160. doi: 10.1371/journal.pone.0062160

Lee, C. R., Lee, J. H., Park, M., Park, K. S., Bae, I. K., Kim, Y. B., et al. (2017). Biology of acinetobacter baumannii: Pathogenesis, antibiotic resistance mechanisms, and prospective treatment options. *Front. Cell Infect. Microbiol.* 7, 55. doi: 10.3389/fcimb.2017.00055

Maragakis, L. L., and Perl, T. M. (2008). Acinetobacter baumannii: epidemiology, antimicrobial resistance, and treatment options. *Clin. Infect. Dis.* 46, 1254–1263. doi: 10.1086/529198

Ning, N. Z., Liu, X., Bao, C. M., Chen, S. M., Cui, E. B., Zhang, J. L., et al. (2017). Molecular epidemiology of bla OXA-23 -producing carbapenem-resistant acinetobacter baumannii in a single institution over a 65-month period in north China. *BMC Infect. Dis.* 17, 14. doi: 10.1186/s12879-016-2110-1

Norton, M. D., Spilkia, A. J., and Godoy, V. G. (2013). Antibiotic resistance acquired through a DNA damage-inducible response in acinetobacter baumannii. *J. Bacteriol* 195, 1335–1345. doi: 10.1128/JB.02176-12

Ophir, T., and Gutnick, D. L. (1994). A role for exopolysaccharides in the protection of microorganisms from desiccation. *Appl. Environ. Microbiol.* 60, 740–745. doi: 10.1128/aem.60.2.740-745.1994

Overhage, J., Lewenza, S., Marr, A. K., and Hancock, R. E. (2007). Identification of genes involved in swarming motility using a pseudomonas aeruginosa PAO1 mini-Tn5-lux mutant library. *J. Bacteriol* 189, 2164–2169. doi: 10.1128/JB.01623-06

Penwell, W. F., DeGrace, N., Tentarelli, S., Gauthier, L., Gilbert, C. M., Arivett, B. A., et al. (2015). Discovery and characterization of new hydroxamate siderophores, baumannoferrin a and b, produced by acinetobacter baumannii. *Chembiochem* 16, 1896–1904. doi: 10.1002/cbic.201500147

Repizo, G. D., Gagne, S., Foucault-Grunenwald, M. L., Borges, V., Charpentier, X., Limansky, A. S., et al. (2015). Differential role of the T6SS in acinetobacter baumannii virulence. *PLoS One* 10, e0138265. doi: 10.1371/journal.pone.0138265

Runci, F., Gentile, V., Frangipani, E., Rampioni, G., Leoni, L., Lucidi, M., et al. (2019). Contribution of active iron uptake to acinetobacter baumannii pathogenicity. *Infect. Immun.* 87, e00755–18. doi: 10.1128/IAI.00755-18

Russo, T. A., Luke, N. R., Beanan, J. M., Olson, R., Sauberan, S. L., MacDonald, U., et al. (2010). The K1 capsular polysaccharide of acinetobacter baumannii strain 307-0294 is a major virulence factor. *Infect. Immun.* 78, 3993–4000. doi: 10.1128/IAI.00366-10

Sanchez-Larrayoz, A. F., Elhosseiny, N. M., Chevrette, M. G., Fu, Y., Giunta, P., Spallanzani, R. G., et al. (2017). Complexity of complement resistance factors expressed by acinetobacter baumannii needed for survival in human serum. *J. Immunol.* 199, 2803–2814. doi: 10.4049/jimmunol.1700877

Schultz, M. B., Pham Thanh, D., Tran Do Hoan, N., Wick, R. R., Ingle, D. J., Hawkey, J., et al. (2016). Repeated local emergence of carbapenem-resistant acinetobacter baumannii in a single hospital ward. *Microb. Genom* 2, e000050. doi: 10.1099/mgen.0.000050

Simpson, B. W., and Trent, M. S. (2019). Pushing the envelope: LPS modifications and their consequences. *Nat. Rev. Microbiol.* 17, 403–416. doi: 10.1038/s41579-019-0201-x

Smedley, J. G.3rd, Jewell, E., Roguskie, J., Horzempa, J., Syboldt, A., Stolz, D. B., et al. (2005). Influence of pilin glycosylation on pseudomonas aeruginosa 1244 pilus function. *Infect. Immun.* 73, 7922–7931. doi: 10.1128/IAI.73.12.7922-7931.2005

Son, H. J., Cho, E. B., Bae, M., Lee, S. C., Sung, H., Kim, M. N., et al. (2020). Clinical and microbiological analysis of risk factors for mortality in patients with carbapenem-resistant acinetobacter baumannii bacteremia. *Open Forum Infect. Dis.* 7, ofaa378. doi: 10.1093/ofid/ofaa378

Thompson, M. G., Black, C. C., Pavlicek, R. L., Honnold, C. L., Wise, M. C., Alamneh, Y. A., et al. (2014). Validation of a novel murine wound model of acinetobacter baumannii infection. *Antimicrob. Agents Chemother.* 58, 1332–1342. doi: 10.1128/AAC.01944-13

Tipton, K. A., Chin, C. Y., Farokhyfar, M., Weiss, D. S., and Rather, P. N. (2018). Role of capsule in resistance to disinfectants, host antimicrobials, and desiccation in acinetobacter baumannii. *Antimicrob. Agents Chemother.* 62, e00188-18. doi: 10.1128/AAC.01188-18

Wang, H., and Cronan, J. E. (2004). Functional replacement of the FabA and FabB proteins of escherichia coli fatty acid synthesis by enterococcus faecalis FabZ and FabF homologues. *J. Biol. Chem.* 279, 34489–34495. doi: 10.1074/jbc.M403874200

Weber, B. S., Hennon, S. W., Wright, M. S., Scott, N. E., de Berardinis, V., Foster, L. J., et al. (2016). Genetic dissection of the type VI secretion system in acinetobacter and identification of a novel peptidoglycan hydrolase, TagX, required for its biogenesis. *mBio* 7, e01253. doi: 10.1128/mBio.01253-16

World Health Organization. *WHO priority pathogens list for research and development of new antibiotics*. World Health Organization (WHO). Availbale at: https://www.who.int/news/item/27-02-2017-who-publishes-list-of-bacteriafor-which-new-antibiotics-are-urgently-needed(2 June 2018).

Xiao, S. Z., Chu, H. Q., Han, L. Z., Zhang, Z. M., Li, B., Zhao, L., et al. (2016). Resistant mechanisms and molecular epidemiology of imipenem-resistant acinetobacter baumannii. *Mol. Med. Rep.* 14, 2483–2488. doi: 10.3892/mmr.2016.5538

Yoon, E. J., Kim, D., Lee, H., Lee, H. S., Shin, J. H., Uh, Y., et al. (2019). Counter clinical prognoses of patients with bloodstream infections between causative acinetobacter baumannii clones ST191 and ST451 belonging to the international clonal lineage II. *Front. Public Health* 7, 233. doi: 10.3389/fpubh.2019.00233

Zahra, R., Javeed, S., Malala, B., Babenko, D., and Toleman, M. A. (2018). Analysis of escherichia coli STs and resistance mechanisms in sewage from Islamabad, Pakistan indicates a difference in e. coli carriage types between south Asia and Europe. *J. Antimicrob. Chemother.* 73, 1781–1785. doi: 10.1093/jac/dky109

Zhang, Y. M., and Rock, C. O. (2008). Membrane lipid homeostasis in bacteria. *Nat. Rev. Microbiol.* 6, 222–233. doi: 10.1038/nrmicro1839

Zhou, K., Tang, X., Wang, L., Guo, Z., Xiao, S., Wang, Q., et al. (2018). An emerging clone (ST457) of acinetobacter baumannii clonal complex 92 with enhanced virulence and increasing endemicity in south China. *Clin. Infect. Dis.* 67, S179–S188. doi: 10.1093/cid/ciy691

frontiers | Frontiers in Cellular and Infection Microbiology

TYPE Original Research
PUBLISHED 13 March 2023
DOI 10.3389/fcimb.2023.1147585

OPEN ACCESS

EDITED BY
Adline Princy Solomon,
SASTRA University, India

REVIEWED BY
Vijay Antharam,
Methodist University, United States
Tamia Alisha Harris-Tryon,
University of Texas Southwestern Medical Center, United States

*CORRESPONDENCE
Reham Wasfi
rwasfi@msa.edu.eg

SPECIALTY SECTION
This article was submitted to Biofilms, a section of the journal Frontiers in Cellular and Infection Microbiology

RECEIVED 18 January 2023
ACCEPTED 17 February 2023
PUBLISHED 13 March 2023

CITATION
Hammouda ZK, Wasfi R and Abdeltawab NF (2023) Hormonal drugs: Influence on growth, biofilm formation, and adherence of selected gut microbiota. *Front. Cell. Infect. Microbiol.* 13:1147585. doi: 10.3389/fcimb.2023.1147585

Hormonal drugs: Influence on growth, biofilm formation, and adherence of selected gut microbiota

Zainab K. Hammouda[1], Reham Wasfi[1]* and Nourtan F. Abdeltawab[2]

[1]Department of Microbiology and Immunology, Faculty of Pharmacy, October University for Modern Sciences and Arts (MSA), Giza, Egypt, [2]Department of Microbiology and Immunology, Faculty of Pharmacy, Cairo University, Cairo, Egypt

Many studies have reported the influence of hormonal drugs on gut microbiota composition. However, the underlying mechanism of this interaction is still under study. Therefore, this study aimed to evaluate the possible *in vitro* changes in selected members of gut bacteria exposed to oral hormonal drugs used for years. Selected members of gut bacteria were *Bifidobacterium longum, Limosilactobacillus reuteri, Bacteroides fragilis, and Escherichia coli* representing the four main phyla in the gut. Selected hormonal drugs used for a long time were estradiol, progesterone, and thyroxine. The effect of intestinal concentrations of these drugs on the selected bacterial growth, biofilm formation, and adherence to Caco-2/HT-29 cell line was assessed. Short-chain fatty acids (SCFAs) have been included in host functions including the gut, immune and nervous functions; thus, the drug's effects on their production were assayed using High- Performance Liquid Chromatography. Sex steroids significantly increased the growth of all tested bacteria except *B. longum*, similarly, thyroxine increased the growth of tested Gram-negative bacteria however reducing that of tested Gram-positive bacteria. The effect of drugs on biofilm formation and bacterial adherence to cell lines cocultures was variable. Progesterone decreased the biofilm formation of tested Gram-positive bacteria, it nevertheless increased *L. reuteri* adherence to Caco-2/HT-29 cell line cell lines coculture. By contrast, progesterone increased biofilm formation by Gram-negative bacteria and increased adherence of *B. fragilis* to the cell lines coculture. Moreover, thyroxine and estradiol exhibited antibiofilm activity against *L. reuteri*, while thyroxine increased the ability of *E. coli* to form a biofilm. Moreover, hormones affected bacterial adherence to cell lines independently of their effect on hydrophobicity suggesting other specific binding factors might contribute to this effect. Tested drugs affected SCFAs production variably, mostly independent of their effect on bacterial growth. In conclusion, our results showed that the microbiota signature associated with some hormonal drug consumption could be the result of the direct effect of these drugs on bacterial growth, and adherence to enterocytes besides the effect of these drugs on the host tissue targets. Additionally, these drugs affect the production of SCFAs which could contribute to some of the side effects of these drugs.

KEYWORDS

gut microbiota, hormones, *Bacteroides fragilis*, *Bifidobacterium longum*, *Escherichia coli*, *Limosilactobacillus reuteri*, short-chain fatty acids (SCFAs)

1 Introduction

Gut bacteria play an important role in maintaining human health through metabolic, protective, and trophic mechanisms; however, altering their composition has been linked to the development of certain diseases such as irritable bowel disease (IBD), colorectal cancer, obesity, diabetes, autism, etc. (Prakash et al., 2011; DeGruttola et al., 2016). Among the important functions played by the gut bacteria is the production of short-chain fatty acids (SCFAs) as the end products of the metabolism of complex carbohydrates. SCFAs have several effects on maintaining the health and integrity of the human body besides being an energy source for colonocytes, having a strong anti-inflammatory effect, maintaining the integrity of the blood-brain barrier (BBB), and reducing the oxidative stress in the colon. The most abundant SCFAs produced in the colon are acetate, butyrate, and propionate. (Prakash et al., 2011; Valdes-Varela et al., 2016; Silva et al., 2020).

Different types of microorganisms, including bacteria, yeast, and viruses, make up the gut microbiota. *Bacteroidetes* and *Firmicutes* account for 90% of the intestinal bacteria, and *Proteobacteria, Actinobacteria*, and *Verrucomicrobia* comprise the other major phyla that constitute the gut (Scotti et al., 2017; Rinninella et al., 2019). Microbiota composition and functions are exposed to dysbiosis by host factors and environmental pressure (Thursby and Juge, 2017). Among these factors contributing to possible dysbiosis is drug intake (Nicholson et al., 2012; Hasan and Yang, 2019).

Research in population-based cohorts has revealed a connection between various non-antibiotic drug classes and specific gut microbiome signatures highlighting that this interaction might contribute to the development of diseases in addition to the change in drug metabolism by gut microbiota (Vich Vila et al., 2020). Among the drugs that have drawn the attention of researchers to study their effect on gut microbiota are hormonal drugs because they are usually used for a long time ranging from 3 months to a lifetime (Benvenga et al., 2017; Clabaut et al., 2021; Gong et al., 2021). However, the direct effect of these drugs on the growth, adherence, and production of SCFAs by gut bacteria was not studied *in vitro* except for a few studies that utilized concentrations higher than the estimated intestinal concentrations. Therefore, this study aimed to study the impact of hormonal drugs at the intestinal concentration on the growth, adherence, and production of SCFAs and lactic acid by selected members of the gut microbiota to explain the *in vivo* changes in gut microbiota upon consumption of hormonal drugs.

2 Materials and methods

2.1 Bacterial strains and culturing condition

Four bacterial strains were used including *Bacteroides fragilis* (ATCC 25285), *Bifidobacterium longum* (ATCC 15707), *Escherichia coli* (ATCC 8739), and *Limosilactobacillus reuteri* (ATCC 23272) representing the 4 main phyla *Bacteroidetes, Actinobacteria, Proteobacteria*, and *Firmicutes*, respectively, which comprise the gut microbiota.

All strains were cultured in their recommended media: De Man, Rogosa & Sharpe (MRS) broth and lactobacillus selective (LBS) agar for *L. reuteri*; Brain-heart infusion supplemented (BHIS) broth and neomycin anaerobic blood agar (NABA) for *Bacteroides fragilis*; Reinforced clostridial media (RCM) broth and MRS agar supplemented with 0.05% cysteine for *Bifidobacterium longum*; Luria Bertani (LB) broth and MacConkey agar for *E. coli*. All the previous cultures were incubated under anaerobic conditions (BBL anaerobic jar, Gas pack Anaerobic system, Franklin, New Jersey, USA) at 37°C. Strains were preserved in glycerol stock at −20°C.

2.2 Preparation of drug stock solutions

Steroid sex hormones of ethinyl estradiol and progesterone were obtained from Qinhuangdao Zizhu Pharmaceutical (Hebei, China) and Zhejiang Shenzhou Pharmaceutical Co (Zhejiang, China), respectively, while L-thyroxine hormone was supplied by Azico Biophore Ltd (Pradesh, India). Stock solution (100x intestinal concentration) of each drug compound was prepared by dissolving drugs using the least amount of Dimethyl Sulfoxide (DMSO) and diluted with sterile distilled water. Drug stocks were stored at -20°C.

The intestinal concentrations used were previously calculated by Maier and colleagues (2018) and the used final concentrations were 0.562, 211.99, and 0.0481μM for ethinyl estradiol, progesterone and L-thyroxine, respectively (Maier et al., 2018).

2.3 Screening the effect of hormonal drugs on bacterial growth

This assay was carried out according to Maier et al. (2018) with some modifications. The bacterial strains were cultured on their specific medium, and then one isolated colony was allowed to grow overnight on modified Gifu anaerobic (mGAM) broth at 37°C under anaerobic conditions and that was repeated twice to ensure that the culture was robust and consistent. The bacterial overnight culture was adjusted to reach starting OD_{600} of 0.02. Two controls were used simultaneously along with the test for this experiment. Control (1) bacteria in medium, control (2) bacteria in medium containing DMSO at a final concentration as in diluted drugs. The effect of DMSO at final concentrations on the growth of bacterial strains was monitored using controls (1) and (2).

The drug stocks were thawed, and an aliquot was diluted to reach 2x intestinal concentrations. In a 96-well flat bottom plate (Greiner Bio-one®, Germany), 50 µl of the adjusted bacterial suspension (OD_{600} = 0.02) were added to 50 µl of the drug concentration (2x). Plates were incubated at 37°C under anaerobic conditions. For the viable count of bacterial growth at zero and 24 hours, tenfold serial dilutions (10^{-1}-10^{-6}) were performed. An aliquot (10 µl) was spotted on NABA, MRS supplemented with cystine (MRS-C), MacConkey agar, and LBS for the enumeration of *B. fragilis, B. longum, E. coli*, and *L. reuteri*,

respectively. The plates were incubated at 37°C under anaerobic conditions for 48 hours. Following incubation, colonies were counted and used to calculate the number of colonies per ml (CFU/ml) (Wang et al., 2017; Maier et al., 2018).

2.4 Screening the effect of hormonal drugs on auto-aggregation and cell surface hydrophobicity

The tendency of identical bacterial cells for self-adherence (auto-aggregation) and cell surface hydrophobicity (CSH) are two independent traits that influence bacterial adhesion ability to surfaces (Rahman et al., 2008).

2.4.1 Preparation of bacterial inoculum

L. reuteri, B. fragilis, *B. longum*, and *E. coli* were grown in a 5 ml broth of MRS, BHIS, RCM, and LB, respectively, with different drugs at their intestinal concentrations. Tubes were incubated under anaerobic conditions for 18 hours at 37°C. Positive control was run simultaneously where bacteria were cultured in media with a DMSO concentration equivalent to that used in dissolving the drugs. Bacterial pellets were harvested by centrifugation at 9500 rpm for 10 min at 18°C followed by washing twice with ice-cold phosphate buffer saline to be used in the auto-aggregation and cell surface hydrophobicity (Botes et al., 2008).

2.4.2 Auto-aggregation

Bacterial cells were suspended in saline and adjusted to OD_{600} of 0.3. One milliliter of the adjusted bacterial suspension was transferred into a sterile eppendorf tube, then centrifuged at 2000 rpm for 2 min (Botes et al., 2008). The supernatant's optical density (OD_{600}) was measured immediately (A_0) and after one hour (A_{60}) (Botes et al., 2008). Auto-aggregation percentage was calculated using the following equation:

$$\%\ Autoaggregation = \left[\frac{(A0) - (A60)}{(A0)}\right] \text{x } 100$$

2.4.3 Cell surface hydrophobicity

The assay of microbial adhesion to hydrocarbons was used to characterize microbial hydrophobicity according to Lather and his colleagues (2016) with some modifications. Bacterial cells were suspended in saline and adjusted to OD_{600} = 0.5. In a glass tube, 0.8 ml volume of xylene was added to 4.8 ml of the adjusted bacterial suspension. The mixture was shaken vigorously for 1 min and allowed to separate at room temperature for 60 min. Bacterial cells were distributed between aqueous and organic phases according to bacterial hydrophobicity. The aqueous phase was removed with caution using a micropipette and measured by spectrophotometer at wavelength 500 nm (A) (Lather et al., 2016). Percentage hydrophobicity was calculated using the following equation:

$$\%\ Hydrophobicity = \left(1 - \frac{A}{A0}\right) x\ 100$$

A0 is the absorbance before the addition of xylene while A is the absorbance in the aqueous phase after the addition of xylene.

2.5 Screening the drug activity on biofilm formation

The effect of drugs on biofilm formation was measured by crystal violet assay. A selective medium supplemented with 1% glucose was used for the incubation of each bacterium at 37°C for 24 hours under anaerobic conditions. Peptone yeast glucose (PYG), LB, BHIS, and RCM were used for the assessment of *L. reuteri*, *E. coli*, *B. fragilis*, and *B. longum*, respectively. The cell density of bacterial suspension was adjusted to OD600 = 1, followed by dilution 1:100 using the selective fresh medium for each bacterium. In a 96-well flat bottom plate (Greiner Bio-one®, Germany), 100 µl of the bacterial cell suspensions were inoculated with 100 µl of drugs (2x) in each well, incubated for 48 hours at 37° C under anaerobic conditions. After incubation, the bacterial growth was measured using a microtiter plate reader (STAT FAX 2200, Awareness Technology, Florida, USA) at a wavelength of 630 nm. Adhered cells were washed and then stained with 0.1% crystal violet for 30 min followed by washing and solubilization. The colored solution was measured at wavelength 545 nm. The readings were used to calculate the biofilm formation index (Kwasny and Opperman, 2010; Coffey and Anderson, 2014; Woo et al., 2017; Jang et al., 2020). Five technical replicates were used for each bacterial strain to compensate for variability and three biological replicates were performed. A positive control with bacteria in addition to DMSO was used simultaneously along with the test.

$$Biofilm\ \ formation\ \ index = \frac{(OD\ \ 545 - OD\ \ control)}{(OD\ \ 630 - OD\ \ control)}$$

OD 545 is colorimetric absorbance of stained bacteria, OD 630 is absorbance of bacterial growth, and OD control is absorbance of negative control.

2.6 Screening the effect of selected drugs on bacterial adherence to cell lines

Co-culture cells of Caco-2/HT29 (90:10) was used to simulate intestinal tissue which was prepared according to the method described by Kleiveland, (2015).

2.6.1 Cytotoxicity assay of tested drug on cell line

The effect of drugs and DMSO on cell line viability was measured using 3, -4,5 dimethyithiazol-2,5 diphenyl tetrazolium

bromide (MTT) assay. Co-culture cells of Caco-2/HT29 were seeded in 96 well microtiter flat bottom plate (Greiner Bio-one®, Germany) using Roswell Park Memorial Institute (RPMI) medium supplemented with 2% Fetal bovine serum (FBS) and incubated overnight in 5% CO_2 at 37°C. Following incubation, 100 µl of each drug in their working dilution was added to co-culture cells (three technical replicates for each concentration). A control was run simultaneously: a negative control with DMSO concentrations equivalent to that in drug solution. The plates were sealed and incubated overnight in 10% CO_2 at 37°C. MTT was dissolved in fresh medium at concentration 0.05%, added to each well, and incubated for 2 hours under the same conditions. After incubation, the medium was aspirated, and 100 µl of DMSO was used for solubilization. Color was measured at wavelength 545 nm and readings were used to calculate percentage viability (Mueller et al., 2004).

$$\%\ Cell\ \ Viability = \frac{Average\ \ OD\ \ of\ \ Drugs\ \ or\ \ DMSO\ \ treated\ \ cell\ \ lines\ \ coculture}{Average\ \ OD\ \ of\ \ untreated\ \ cell\ \ lines\ \ coculture} \times 100$$

2.6.2 Adherence to cell line assay

The bacterial strains were cultured on their specific media for 20 hours under anaerobic conditions at 37°C. Bacterial cells were centrifuged at 6000 rpm for 5 min at 4°C, the pellet was washed twice with PBS and the cell density for each bacterium was adjusted to $1x10^8$ CFU/ml using PBS. In a 24 well flat bottom plate (Greiner Bio-one®, Germany), Caco-2/HT-29 co-culture was grown and maintained using RPMI medium except for *E. coli* where DMEM medium was used. On plates seeded with cell line coculture, 100 µl of adjusted bacterial suspension and 100 µl of drugs (2x intestinal concentration) were added. Thus, final concentration of the drugs in each well will be equivalent to intestinal concentration (1x). Plates were sealed and incubated at 37°C for 2 hours in 5% CO_2. Following incubation, the medium was removed, and wells were washed using 200 µl of fresh medium to remove non-adherent cells. The cells were then lysed by adding 100 µl of 0.1% Triton X-100 for 10 min at room temperature, then the reaction was stopped by addition of 900 µl of fresh medium. Viable bacterial cells were enumerated by spreading 10µl of diluted bacterial culture (drop plate technique) on their selective medium prior to incubation with cell line (CFU of initial inoculum) and after incubation for 2 hours (CFU of adhered cells)(Letourneau et al., 2011; Gagnon et al., 2013; Reddy and Austin, 2017). The count was recorded and used to calculate the percentage of adhered bacteria.

$$\%\ adhered\ \ cells = \frac{CFU\ \ of\ \ adhered\ \ cells\ \ (2\ \ hours)}{CFU\ \ of\ \ initial\ \ incoulum\ \ (0\ \ hour)} \times 100$$

2.6.3 Imaging of cell adherence to CaCo-2/HT29 co-culture using scanning electron microscope

The same steps of adherence assay were followed for preparation of samples in a 12 well flat bottom plate (Greiner Bio-one®, Germany) for imaging the cell adherence using scanning electron microscope. After incubation for 2 hours, the plate was washed with phosphate buffer saline (PBS) twice, and 5% glutaraldehyde (prepared in 0.1M sodium cacodylate) was added for 2 hours for fixation. The wells were dehydrated by passing them through graded ethanol (25, 50, 70, 80, and 90%) for 10 min in each concentration at room temperature. The last concentration used for dehydration was 100% for 15 min. The wells were coated with gold and examined using scanning electron microscope (Quanta 250 FEG, West Bengal, India) with a magnification power of 5000x and 10000x (Heckman et al., 2007; Ude et al., 2019).

2.7 Measurement of the change in Short Chain Fatty Acids and lactic acid production by bacteria under the effect of hormonal drugs using high performance liquid chromatography (HPLC)

Strict anaerobic bacteria are known for their ability to produce short-chain fatty acids by the saccharolytic fermentation of complex polysaccharides (Nogal et al., 2021), therefore the effect of hormonal drugs on production of SCFA by *B. fragilis* and *B. longum* were studied. Analytical samples were prepared by inoculating colonies of *B. fragilis* and *B. longum* in BHIS broth and MRS broth, respectively for 48 hours at 37°C under anaerobic conditions. The bacterial OD was adjusted to 0.01 at 600 nm and incubated with the intestinal concentration of the three hormonal drugs at 37°C for 16 hours under anaerobic conditions. The suspension was then centrifuged at 9500 rpm for 15 min at 4°C and the supernatant was collected. The analytical sample was injected into the HPLC system (Smart line, Knauer, Germany) using the autosampler after its conditions was set. The HPLC system was equipped with Rezex™ column (Phenomenex, California, USA) for organic acid analysis. The flow rate was set at 0.6 ml/min, UV detector set at 214 nm, column oven temperature kept constant at 65°C, and the mobile phase was 0.005M H_2SO_4. To create the standard curve, a standard solution containing lactic, acetic, propionic, and butyric acids was prepared at concentrations of 1, 10, 100, 500, and 1000 ppm. The SCFA quantities were determined using the standard curves' appropriate linear regression equations ($R^2 \geq 0.99$). The response factor is a measurement of the analyte's relative spectral response to its external standard at the specified retention time, followed by calculation of SCFAs in ppm. Positive control was prepared by growing bacteria in media containing DMSO in concentrations equivalent to their final concentration in drug solution. The data was integrated by clarity chrom software (DataApex, Praha, Czechia)

2.8 Statistical analysis

GraphPad Prism 9.1.1 (GraphPad Software Inc., CA, USA) was used for statistical analysis. Multiple unpaired t-tests and multiple comparisons using the Holm-Šídák method were used to compare auto-aggregation, hydrophobicity, and formation of biofilm in the presence and absence of drugs. For statistical analysis of the viable count of the microorganisms in the screening of the antibacterial

activity of drugs and adherence assay to cell lines coculture, the Mann-Whitney t-test was used. An unpaired t-test was used for the statistical analysis of the effect of drug on the viability of the intestinal cell lines. The readings were considered significant at $p<0.05$.

3 Results

3.1 Alteration in bacterial growth under the effect of hormonal drugs

B. longum was the most affected bacteria in presence of the three tested hormonal drugs showing reduction in viable count by 3, 2, and 4 logs in presence of progesterone, estradiol, thyroxine, respectively (Figure 1C). The growth of Gram-negative bacteria was enhanced by hormonal treatment showing increase by 1 to 2 logs by *B. fragilis* (Figure 1A) and *E. coli* (Figure 1B). The effect on the growth of *L. reuteri* was variable where the steroid hormones increased its growth by 2 to 3 logs while thyroxine reduced its growth by one log (Figure 1D).

3.2 Progesterone changed the auto-aggregation of tested bacteria

Progesterone was the only hormonal drug under test that showed an effect on bacterial auto-aggregation (Figures 2A–D) as it caused a significant increase ($P=0.0008$, $\alpha=0.05$) in the auto-aggregation of *E.coli* from 5.5% in control to 10% in presence of drug (Figure 2C). On the other hand, progesterone remarkably reduced ($P=0.007$, $\alpha=0.05$) the auto-aggregation of *L. reuteri* cells to 5% compared to the control (Figure 2D).

3.3 Hormonal drugs change cell surface hydrophobicity of tested bacteria

The hydrophobicity of *B. fragilis* increased significantly ($P<0.01$) in the presence of the three hormonal drugs (Figure 3A). Estradiol reduced significantly ($P<0.01$) the hydrophobicity of *B. longum* and *L. reuteri* while progesterone reduction to hydrophobicity was limited to *L. reuteri* (Figures 3C, D). *E. coli* did not show significant change in hydrophobicity in presence of the three drugs (Figure 3B).

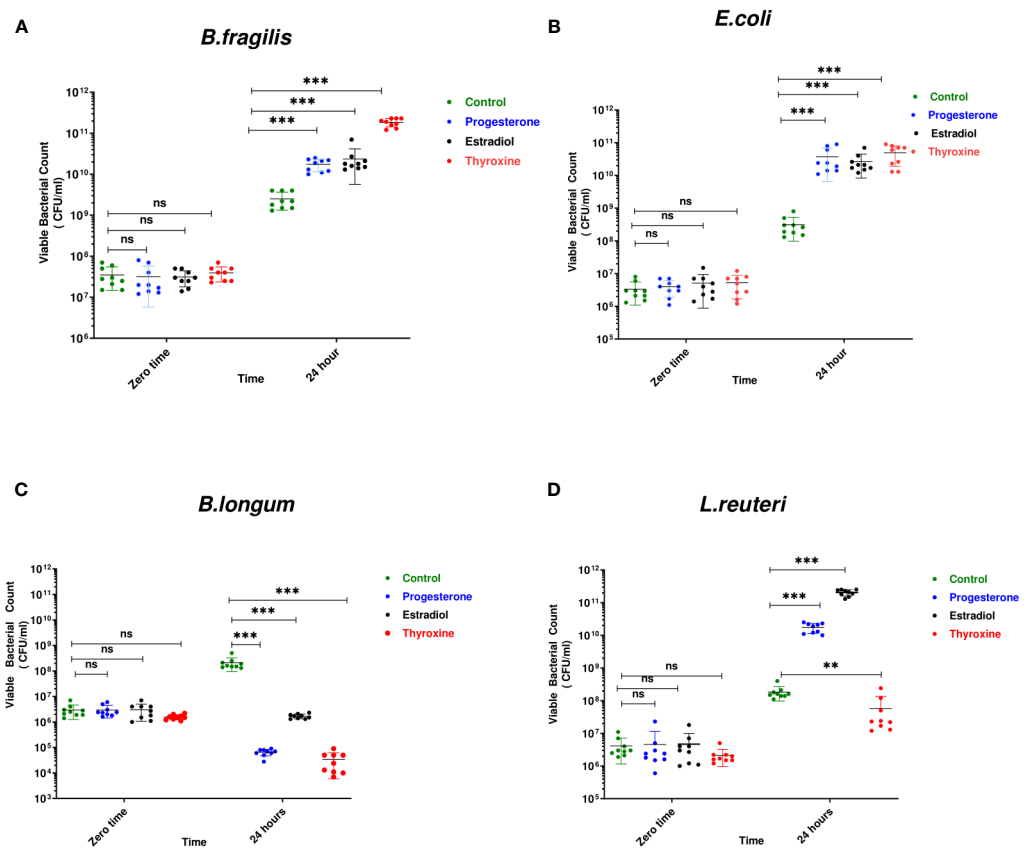

FIGURE 1
Growth of bacteria under the effect of hormonal drugs. Effect of hormonal drugs on the growth of: Gram-negative bacteria **(A)** *Bacteroid fragilis*, **(B)** *Escherichia coli*, and Gram-positive bacteria **(C)** *Bifidobacterium longum*, **(D)** *Limosilactobacillus reuteri* represented as viable count (CFU/ml). Tested hormonal drugs include progesterone, ethinyl estradiol, and L-thyroxine in their intestinal concentrations, 211.99, 0.562, and 0.0481μM, respectively. Control represents the growth of bacteria in addition to DMSO. Mann-Whitney t-test was used to statistically compare the effect on bacterial growth. Significance level of **(P<0.001), ***(P<0.0001). ns, non significant.

3.4 Hormonal drugs changed biofilm formation ability of tested bacteria

B. longum showed the highest biofilm index among tested isolates. Hormonal drugs increased biofilm formation by Gram-negative bacteria (Figures 4A, B) but reduced the ability of Gram-positive bacteria to form biofilm (Figures 4C, D).

3.5 Effect of tested drugs on bacterial adherence to Caco-2/HT-29 coculture cell lines

An unpaired t-test was used to compare the difference in cell viability in presence of drugs compared with the untreated coculture cell lines and no significant effect was observed on coculture viability when treated with the three drugs in their intestinal concentrations (data not shown).

The effect of hormonal drugs on adherence of tested bacteria was variable. No growth of *B. fragilis* was observed on NABA after 2 hours of incubation in both control and drug-treated samples except with progesterone which showed relatively low adherence of 0.13% (Figure 5A). Progesterone reduced the adherence of *E. coli* and *B. longum* while increasing the adherence of *L. reuteri* (Figures 5B–D). Thyroxine remarkably increased the percentage of adhered *E. coli* and *B. longum* to cell lines coculture while reducing adherence of *L. reuteri* when compared to control. Ethinyl estradiol reduced the adherence of *E. coli* and increased the adherence of *B. longum* and *L. reuteri*.

3.6 Scanning electron microscope

The influence of hormonal drugs on bacterial adherence was confirmed by SEM images. As shown in Figure 6A, untreated *B. fragilis* showed no visible bacterial attachment to the extracellular

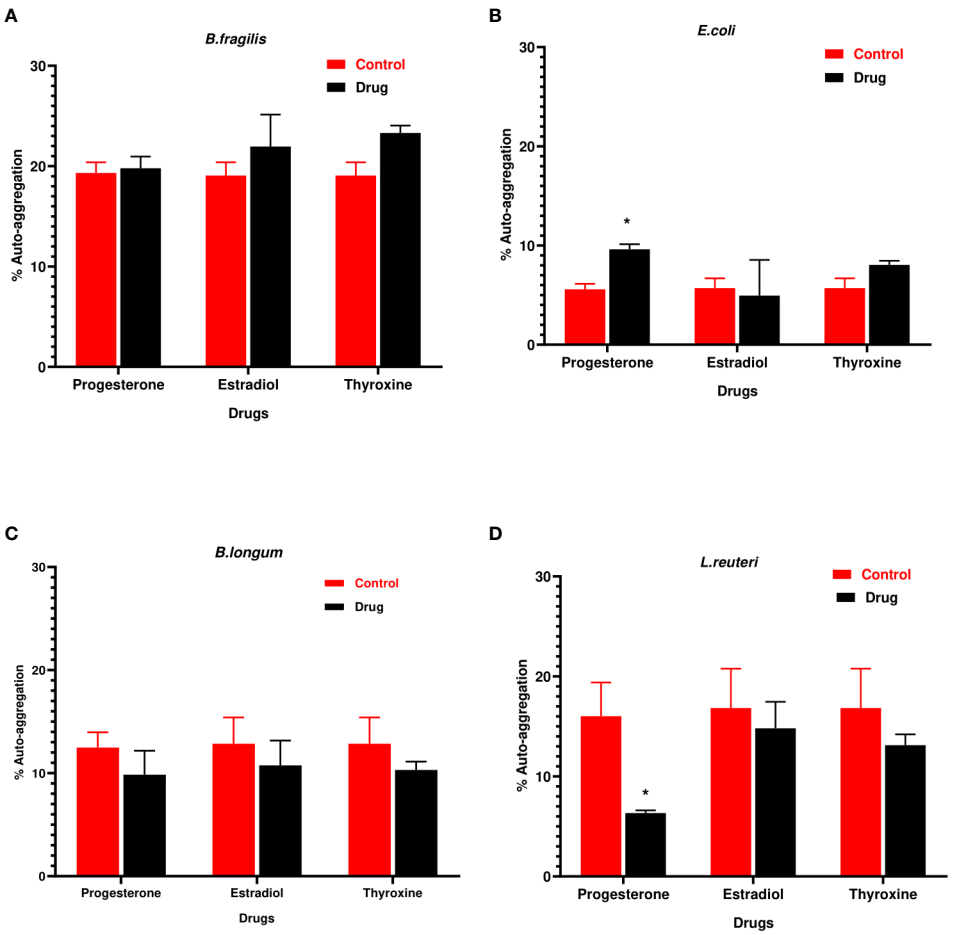

FIGURE 2
Auto-aggregation of bacteria with hormonal drugs. Change in percentage auto- aggregation of **(A)** *B. fragilis*; **(B)** *E. coli;* **(C)** *B. longum;* **(D)** *L. reuteri* after incubation with hormonal drugs at 37°C for 60 min. Values were expressed as the mean of the percentage of three experiments with error bars (SE). Tested hormonal drugs include progesterone, ethinyl estradiol, and L-thyroxine in their intestinal concentrations, 211.99, 0.562, and 0.0481μM, respectively. Control represents the bacteria in addition to DMSO. Multiple unpaired t-tests along with Holm-Šídák for multiple corrections were used to statistically compare the effect of different drugs on bacterial auto-aggregation. * Significant difference ($p<0.05$).

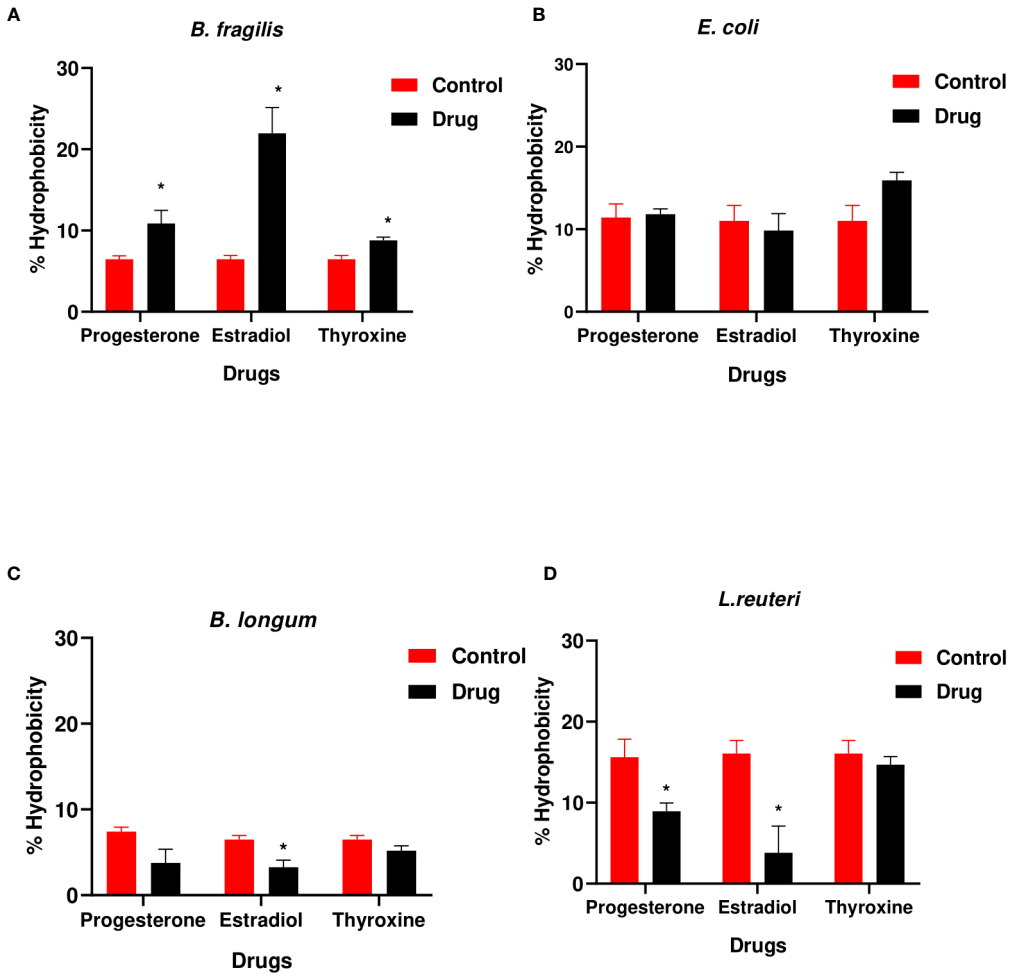

FIGURE 3
Hydrophobicity of bacteria under the effect of hormonal drugs. Change in percentage hydrophobicity of **(A)** *B. fragilis*; **(B)** *E. coli;* **(C)** *B. longum;* **(D)** *L. reuteri* with hormonal drugs after incubation at 37 °C for 60 min. Values were expressed as the mean of the percentage of three experiments with error bars (SE). Tested hormonal drugs include progesterone, ethinyl estradiol, and L-thyroxine in their intestinal concentrations, 211.99, 0.562, and 0.0481μM, respectively. Control represents the bacteria in addition to DMSO. Multiple unpaired t-test along with Holm-Šídák for multiple corrections was used to statistically compare the effect of different drugs on bacterial hydrophobicity. * Significant difference ($p<0.05$).

matrix, while exposure to progesterone increased adherence to the cell line which appeared as few longitudinal rods attaching to the cell line co-culture in Figure 6B. Ethinyl estradiol increased the number of *B. longum* bacteria adhering to cell line coculture (Figure 6D) when compared to the control (Figure 6C). The effect of progesterone on the adherence of *L. reuteri* in the presence (Figure 6F) and absence of the drug (Figure 6E) where a visible slight increase in the number of *L. reuteri* was observed in treated cells.

3.7 Alteration in SCFAs and lactic acid production by *B. fragilis* and *B. longum* in presence of hormonal drugs

The reference chromatograms obtained from the standard solution revealed that SCFAs and lactic acid were detected at different retention times: 13.100, 14.876, 17.967, and 20 min; for lactic, acetic, propionic and butyric acids, respectively. The amount of butyric acid produced wasn't detected in treated and untreated samples under the test conditions. The response factor was calculated for each SCFA, which represented the measurement of the analyte's relative spectral response to its external standard. The highest acid produced by *B. fragilis* was acetic acid followed by lactic acid then propionic acid. The interpretation of chromatogram (Supplementary Figure 1 and Supplementary Table 1) showed a reduction in the amount of both lactic acid and propionic acid and an increase in the amount of acetic acid produced by *B. fragilis* in presence of progesterone (Table 1). The concentration of lactic acid and acetic acid produced by *B. fragilis* was reduced after being treated with ethinyl estradiol, conversely an increase in the amount of propionic acid was observed under the effect of the same drug. Both lactic acid and propionic acid produced by *B. fragilis* increased in amount when the bacteria were treated with thyroxine hormone while acetic acid levels were reduced under the same conditions.

Propionic and butyric acid weren't detected in *B. longum* control or drug-treated samples. The chromatogram

(Supplementary Figure 2 and Supplementary Table 2) showed a reduction in the amount of both lactic acid and acetic acid produced by *B. longum* when treated with progesterone. *Bifidobacterium longum* produced higher levels of both lactic acid and acetic acid after being treated with ethinyl estradiol. Both lactic acid and butyric acid produced by *B. longum* increased in amount when the bacteria were treated with thyroxine hormone (Table 2).

4 Discussion

The human gastrointestinal (GI) tract is a niche to a complex and dynamic community of bacteria known as the gut microbiota, which has a significant impact on the host during health and disease (Thursby and Juge, 2017). The composition and function of the gut microbiome are also influenced by different factors including the use of medications (Wen and Duffy, 2017).

In our study, the steroid hormones such as ethinyl estradiol and progesterone significantly increased the growth of *B. fragilis*, *E. coli*, and *L. reuteri* whereas decreasing the growth of *B. longum*. Conversely, previous studies reported the antibacterial effect of steroid derivatives by preventing the normal development of the cell membrane integrity and permeability. Thus, it is thought that the reason for the antibacterial effect of steroid bile acids is due to their binding to phospholipids in bacterial membranes resulting in membrane destruction and ultimately cell death (DoĞAn et al., 2017; Bustos et al., 2018; Vollaro et al., 2020; Crowley et al., 2022). The resistance of the selected gut bacteria to the deleterious effect of steroids could be due to the presence of bile salt hydrolase enzyme in these genera which protect them from the damaging effect of steroid bile acids (Staley et al., 2017). Another explanation for the resistance of *L. reuteri* to bile salts was the protective effect of this bacteria against steroids as bile acids arising from precipitation of the deconjugated bile salts and physical binding of bile salts by a bacterium, so rendering the detrimental bile salts accessible (De Boever et al., 2000). The increase in growth of *B. fragilis* could be explained by the study carried out by Kornman and Loesche (1982) using labeled C^{14} steroid hormones who proved the uptake of these hormones by *Bacteroides* bacteria and explained their ability to substitute vitamin K compounds, an essential growth factor, with progesterone and ethinyl estradiol resulting in an increased growth curve (Kornman and Loesche,

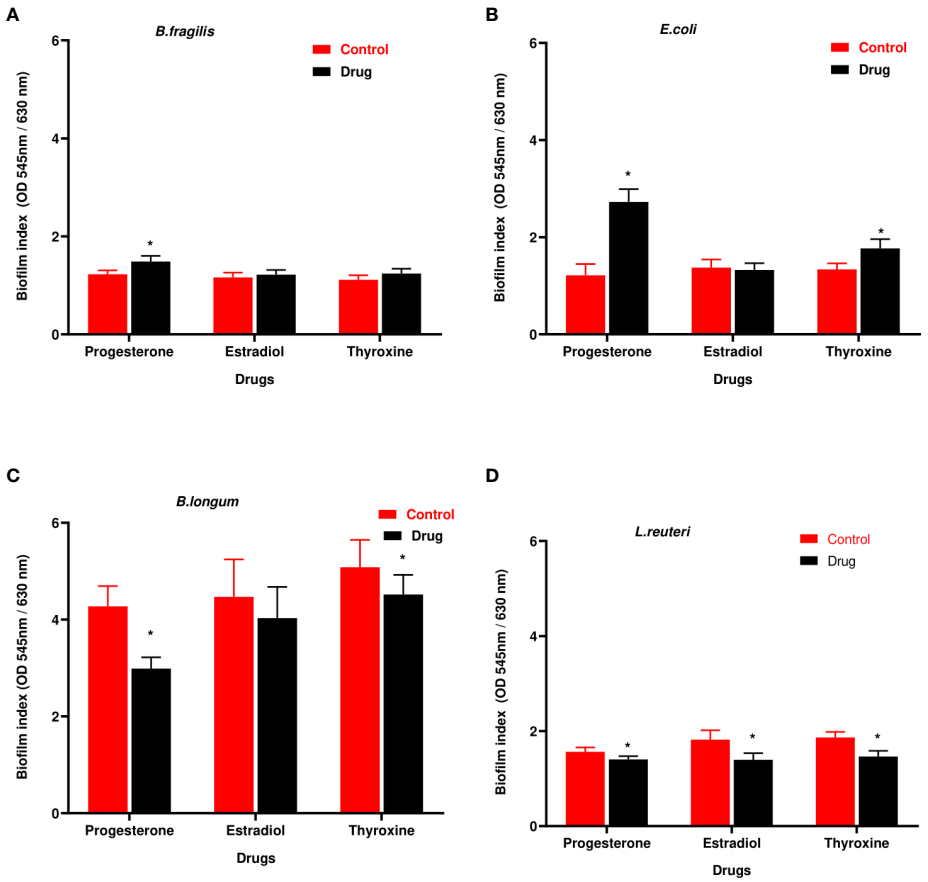

FIGURE 4
Biofilm formation ability of selected bacteria under the effect of hormonal drugs. Change in biofilm formation index by **(A)** *B. fragilis*; **(B)** *E. coli* **(C)**; *B. longum;* **(D)** *L. reuteri* with hormonal drugs. Values were expressed as the mean of the percentage of three experiments with error bars (SE). Tested hormonal drugs include progesterone, ethinyl estradiol, and L-thyroxine in their intestinal concentrations, 211.99, 0.562, and 0.0481μM, respectively. Control represents the bacteria grown in culture with DMSO. Multiple unpaired t-test along with Holm-Šídák for multiple corrections was used to statistically compare the effect of different drugs on bacterial biofilm. * Significant difference ($p<0.05$).

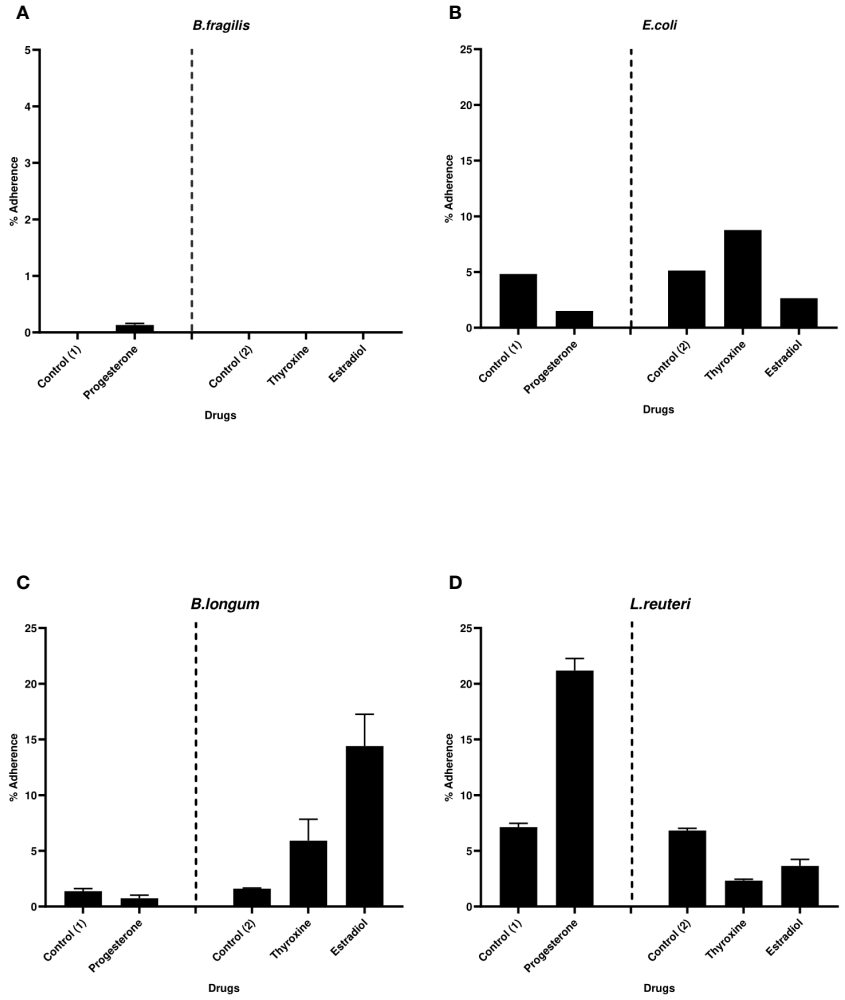

FIGURE 5
Bacterial adherence to Caco-2/HT-29 co-culture under the effect of hormonal drugs. Change in the percentage of adhered bacterial cells **(A)** *B. fragilis*; **(B)** *E. coli*; **(C)** *B. longum*; **(D)** *L. reuteri* under the effect of hormonal drugs: progesterone, ethinyl estradiol, and thyroxine in their intestinal concentrations 211.99, 0.562, and 0.0481μM, respectively. Values were expressed as the mean of the percentage of three experiments with error bars (SE). Positive control with bacteria and DMSO at different concentrations equivalent to that used to dissolve drug (control (1): DMSO 1% and Control (2):DMSO 0.001%).

1982). Both steroid hormones had a significant effect in reducing the growth of *B. longum* in this study supported by findings of previous studies on Gram-positive bacteria, which demonstrated that different steroids reduce *in vitro* growth and increase cell leakage (Souza et al., 2021). *B. longum* growth was reduced under the same treatment which could be attributed to their lower resistance to bile acids compared to other *Bifidobacterium* species (Ibrahim and Bezkorovainy, 1993; Clark and Martin, 1994; Dunne et al., 2001). Many cross sectional studies for the influence of sex steroids on gut bacteria have proved the existence of correlation between sex hormone levels and microbiota composition despite the inevitable interfering factors, including genetics and environment (Santos-Marcos et al., 2018; Shin et al., 2019; Zhao et al., 2019; He et al., 2021). Researchers reported that lower levels of estradiol in postmenopausal women and men is accompanied by increase in *Bacteroidetes* sp. and depletion of *Lactobacillus* sp. Compared to women with higher levels of sex hormones (Santos-Marcos et al., 2018; Zhao et al., 2019). Likewise, the direct effect of the estradiol hormone on the growth of *L. reuteri* has been proved in our study. Treatment of sex steroid deficient mice with *Lactobacillus rhamnosus* could avoid bone loss which indicates the importance of this bacterium in preserving bone density (Li et al., 2016). The effect of sex steroids on gut bacteria *in vivo* could not be compared by their effect *in vitro* because, in some cases, hormonally related microbial shifts result from endogenous steroid-induced tissue and immunological changes rather than from steroids' direct effect on bacteria (Lester and Hechter, 1958; Feraco et al., 2016).

While studying the effect of L-thyroxine on the viability of gut microbiota, results revealed a significant increase in the growth of Gram-negative *B. fragilis* and *E. coli* and a significant reduction in the growth of Gram-positive *B. longum* and *L. reuteri*. The results withstood the previous findings by Garber and Lupowitz-Donenfeld (1973) that L-thyroxine had an inhibitory effect on the growth of Gram-positive bacteria however, it has no significant effect on Gram-negative bacteria. The inhibition of Gram-positive bacteria by L-thyroxine was reduced by cations such as Mn^{2+}, Fe^{2+}, and Ca^{2+} which support the hypothesis that L-thyroxine chelating effect is

10.3389/fcimb.2023.1147585

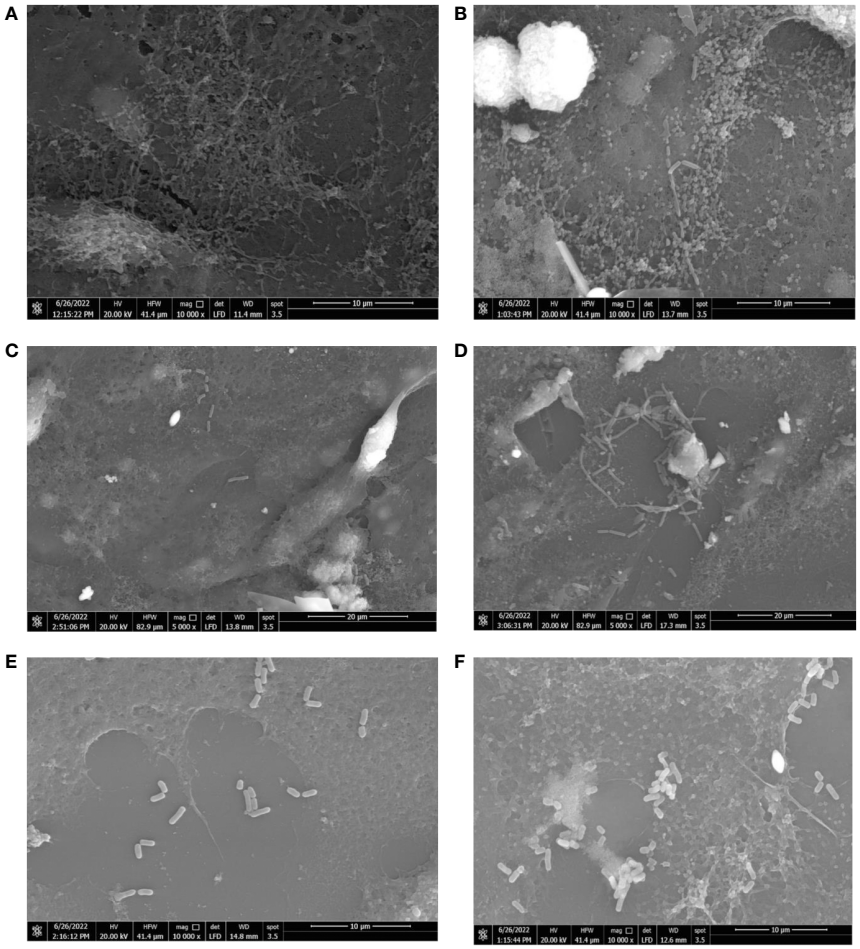

FIGURE 6
Scanning electron micrograph showing the effect of hormonal drugs on adherence of bacteria to Caco-2/HT-29 co-culture. Effect of progesterone on *B. fragilis* adherence **(A)** Control untreated bacterial cells **(B)** Drug-treated bacterial cells (Magnification power 10000x); *B longum* **(C)** Control untreated bacterial cells **(D)** Drug-treated bacterial cells (Magnification power 5000x); *L. reuteri* **(E)** Control with bacterial cells **(F)** Drug-treated cells bacterial cells (Magnification power 10000x). The adherence assay was carried out using RPMI medium in 5% CO_2 at 37°C, and imaging was performed using a scanning electron microscope (Quanta 250 FEG, West Bengal, India).

TABLE 1 The concentration of SCFAs and lactic acid produced by *Bacteroides fragilis* under the effect of hormonal drugs (progesterone, ethinyl estradiol, and thyroxine) measured by HPLC.

Drugs	Compound	Concentration (ppm)	
		Control*	Sample
Progesterone	Lactic acid	1738.136	411.882 ↓
	Acetic acid	5661.760	5809.819 ↑
	Propionic acid	409.485	253.075 ↓
Ethinyl estradiol	Lactic acid	986.53	376.539 ↓
	Acetic acid	5138.918	4933.959 ↓
	Propionic acid	347.249	497.194 ↑
Thyroxine	Lactic acid	986.53	1218.416 ↑
	Acetic acid	5138.918	4512.039 ↑
	Propionic acid	347.249	403.225 ↓

* Positive control of bacteria in media containing DMSO in concentrations equivalent to their final concentration in drug solution.
↑increase production compared to control.
↓lower production compared to control.

TABLE 2 The concentration of SCFAs and lactic acid produced by *Bifidobacterium longum* under the effect of hormonal drugs (progesterone, ethinyl estradiol, and thyroxine) measured by HPLC.

Drugs	Compound	Concentration (ppm)	
		Control*	Sample
Progesterone	Lactic acid	315.68	116.640 ↓
	Acetic acid	7994.02	7296.440 ↓
Ethinyl estradiol	Lactic acid	289.266	331.122 ↑
	Acetic acid	8133.807	8405.94 ↑
Thyroxine	Lactic acid	986.53	309.830 ↓
	Acetic acid	5138.918	8322.263 ↑

* Positive control of bacteria in media containing DMSO in concentrations equivalent to their final concentration in drug solution.
↑increase production compared to control.
↓lower production compared to control.

one of the factors contributing to its inhibitory effect (Garber and Lupowitz-Donenfeld, 1973; Benvenga et al., 2017). Metagenomic analysis of gut microbiome in hyperthyroidism patients showed as a significant decline in *Bifidobacterium* and *Lactobacillus* (Zhou et al., 2014). Similarly, reduction in these two genera was detected in our study under the influence of L-thyroxine which also explain the need for probiotic supplement in hypothyroidism patients treated with L-thyroxine to keep bone density and optimizing thyroid function (Knezevic et al., 2020).

The process of bacterial adhesion to different surfaces is a complex process that involves contact between bacterial membranes and interacting surfaces. Specific and nonspecific binding are the two essentially distinct strategies that cause bacterial adhesion (Piette and Idziak, 1992). Electrostatic or hydrophobic interactions have a major role in the non-specific binding and considerably affect adhesion strength (Piette and Idziak, 1992). Two factors were assessed in this study to understand the influence of their changes in altering bacterial adherence in the presence of hormones. The auto-aggregation and cell surface hydrophobicity assays were carried out to evaluate the effect of the drugs on non-specific binding of these bacteria to different surfaces. Previous study showed that biofilm formation is correlated with hydrophobicity (Krasowska and Sigler, 2014) however this correlation was detected in *L. reuteri* under the effect of tested drugs where reduction in hydrophobicity was accompanied by the reduction in biofilm formation ability of this bacterium. Conversely, hydrophobicity was not correlated to bacteria adherence to Caco-2/HT-29 co-culture. Similarly, some previous studies showed that the correlation between hydrophobicity and adhesion to hydrophobic mucosal cells was strain specific (Kos et al., 2003; Muñoz-Provencio et al., 2009). This has suggested that nonspecific binding factors such as hydrophobicity is not an accurate measure of adhesive potential to enterocytes (Van Tassell and Miller, 2011) and interactions between microbes and hosts depend greatly on the structure of the cell surface rather than nonspecific binding (Nishiyama et al., 2021). Many studies have shown that, components of a protein nature such as mucus adhesins in *L. reuteri* (Vélez et al., 2007; Sánchez et al., 2008) and *B. longum* (Izquierdo et al., 2008) as well as capsular polymer in *B. fragilis* (Nakano et al., 2008; Reis et al., 2014) are primarily important for bacterial adherence to intestinal mucin types and/or epithelial cells beside saccharide moieties and lipoteichoic acid.

A previous study linked hormonal drugs' impact on bacterial growth with its impact on bacterial biofilm (Fteita et al., 2014). Similarly, in our results, a change in bacterial growth under the effect of the drug was associated with a similar change in biofilm formation except *L. reuteri* showing a reduction in biofilm in presence of sex steroids despite the increase in growth and this could be explained by the increased production of biosurfactant by *Lactobacillus* species in the presence of sex steroids thus decreasing biofilm formation (Clabaut et al., 2021). Additionally, the effect of progesterone on quorum sensing has been reported for some bacteria which could affect phenotypes that depend on cell-to-cell communication (Cadavid et al., 2018).

The gut microbiota makes use of SCFAs as a source of carbon by cross-feeding, but SCFAs can be harmful to some gut bacterial species when present in high concentrations (Feng et al., 2018). The amount of SCFAs produced by the anaerobic bacteria *B. fragilis* and *B. longum* was measured using HPLC. Surprisingly we did not detect butyric acid after incubation of *B. longum* for 48 hours despite being known as butyric acid producer (Aguirre et al., 2016). Additionally, propionate was not detected in *B. longum* culture and similar result was obtained by Rios-Covian et al. (2017). The effect of the tested drug compounds in this study on SCFAs production was variable and mostly independent of their effect on bacterial growth, in contrast to earlier studies' results that a change in abundance of gut bacteria owing to drug usage was correlated to a similar effect on SCFAs production (Hojo et al., 2018). Notably, numerous studies reveal that *Bacteroidetes* are the main producers of propionate in the human gut (Salonen et al., 2014; Aguirre et al., 2016) and this SCFA is known for its ability to suppress inflammation and the increase in its level is associated with cognitive decline in elderly (Kawasoe et al., 2022; Neuffer et al., 2022) while low level of propionic acid and acetate was linked to autism(Tetel et al., 2018). Progesterone and L-thryoxine reduced the production of propionic acid by *B. fragilis*. A key organic acid in the fermentation of prebiotics is lactic acid, which is generated in the GIT by the bacteria *Lactobacilli* and *Bifidobacteria*. Lactic acid does not significantly accumulate in the intestinal lumen, and it is

further metabolized by cross-feeding species, particularly with the butyrate-producing bacteria, to acetate or butyrate, or propionate.

5 Conclusion

Oral hormonal drugs can affect the growth, biofilm formation and adherence of gut bacteria at intestinal concentrations *in vitro* which can explain specific microbiome signatures associated with long term use of these drugs. Steroid hormones increase the growth of *B. fragilis*, *E. coli*, and *L. reuteri* while reducing the growth *B. longum*. However, thyroxine increased the growth of Gram-negative bacteria and reduced the growth of Gram-positive one. The effect of these drugs on biofilm formation by selected bacteria was linked to their effect on growth except *L. reuteri* where steroid hormones reduced biofilm formation by this bacterium despite increasing bacterial growth. The effect of hormonal drugs on bacterial adherence to Caco-2/HT-28 coculture was not solely dependent on the change in hydrophobicity but other specific binding factors might contribute to their effect. The effect of the tested drug compounds on SCFAs and lactic acid production was variable and mostly independent of their effect on bacterial growth.

Data availability statement

The original contributions presented in the study are included in the article/Supplementary Material. Further inquiries can be directed to the corresponding author.

Author contributions

NA and RW conceptualized the work. ZH performed the experiments.NA, RW, and ZH analyzed the results. All authors contributed to the article and approved the submitted version.

Conflict of interest

The authors declare that the research was conducted in the absence of any commercial or financial relationships that could be construed as a potential conflict of interest.

Publisher's note

All claims expressed in this article are solely those of the authors and do not necessarily represent those of their affiliated organizations, or those of the publisher, the editors and the reviewers. Any product that may be evaluated in this article, or claim that may be made by its manufacturer, is not guaranteed or endorsed by the publisher.

Supplementary material

The Supplementary Material for this article can be found online at: https://www.frontiersin.org/articles/10.3389/fcimb.2023.1147585/full#supplementary-material

References

Aguirre, M., Eck, A., Koenen, M. E., Savelkoul, P. H., Budding, A. E., and Venema, K. (2016). Diet drives quick changes in the metabolic activity and composition of human gut microbiota in a validated *in vitro* gut model. *Res. Microbiol.* 167 (2), 114–125. doi: 10.1016/j.resmic.2015.09.006

Benvenga, S., Di Bari, F., and Vita, R. (2017). Undertreated hypothyroidism due to calcium or iron supplementation corrected by oral liquid levothyroxine. *Endocrine* 56 (1), 138–145. doi: 10.1007/s12020-017-1244-2

Botes, M., Loos, B., van Reenen, C. A., and Dicks, L. M. (2008). Adhesion of the probiotic strains enterococcus mundtii ST4SA and lactobacillus plantarum 423 to caco-2 cells under conditions simulating the intestinal tract, and in the presence of antibiotics and anti-inflammatory medicaments. *Arch. Microbiol.* 190 (5), 573–584. doi: 10.1007/s00203-008-0408-0

Bustos, A. Y., Font de Valdez, G., Fadda, S., and Taranto, M. P. (2018). New insights into bacterial bile resistance mechanisms: the role of bile salt hydrolase and its impact on human health. *Food Res. Int.* 112, 250–262. doi: 10.1016/j.foodres.2018.06.035

Cadavid, E., Robledo, S. M., Quiñones, W., and Echeverri, F. (2018). Induction of biofilm formation in klebsiella pneumoniae ATCC 13884 by several drugs: the possible role of quorum sensing modulation. *Antibiotics* 7 (4), 103. doi: 10.3390/antibiotics7040103

Clabaut, M., Suet, A., Racine, P.-J., Tahrioui, A., Verdon, J., Barreau, M., et al. (2021). Effect of 17β-estradiol on a human vaginal lactobacillus crispatus strain. *Sci. Rep.* 11 (1), 7133. doi: 10.1038/s41598-021-86628-x

Clark, P. A., and Martin, J. H. (1994). Selection of bifidobacteria for use as dietary adjuncts in cultured dairy foods. III. tolerance to simulated bile concentrations of human small intestines. *Cultured dairy products J.* 29 (3), 18. doi: 10.12938/bifidus.23.93

Coffey, B. M., and Anderson, G. G. (2014). "Biofilm formation in the 96-well microtiter plate," in *Pseudomonas methods and protocols*. Eds. A. Filloux and J.-L. Ramos (New York, NY: Springer New York), 631–641.

Crowley, J., Withana, M., and Deplazes, E. (2022). The interaction of steroids with phospholipid bilayers and membranes. *Biophys. Rev.* 14 (1), 163–179. doi: 10.1007/s12551-021-00918-2

De Boever, P., Wouters, R., Verschaeve, L., Berckmans, P., Schoeters, G., and Verstraete, W. (2000). Protective effect of the bile salt hydrolase-active lactobacillus reuteri against bile salt cytotoxicity. *Appl. Microbiol. Biotechnol.* 53 (6), 709–714. doi: 10.1007/s002530000330

DeGruttola, A. K., Low, D., Mizoguchi, A., and Mizoguchi, E. (2016). Current understanding of dysbiosis in disease in human and animal models. *Inflammatory bowel Dis.* 22 (5), 1137–1150. doi: 10.1097/MIB.0000000000000750

DoĞAn, A., Otlu, S., Çelebi, Ö., Aksu Kiliçle, P., Gülmez Sağlam, A., DoĞAn, A., et al. (2017). An investigation of antibacterial effects of steroids. *Turkish J. Of Veterinary And Anim. Sci.* 41, 302–305. doi: 10.3906/vet-1510-24

Dunne, C., O'Mahony, L., Murphy, L., Thornton, G., Morrissey, D., O'Halloran, S., et al. (2001). *In vitro* selection criteria for probiotic bacteria of human origin: correlation with *in vivo* findings. *Am. J. Clin. Nutr.* 73 (2 Suppl), 386s–392s. doi: 10.1093/ajcn/73.2.386s

Feng, W., Ao, H., and Peng, C. (2018). Gut microbiota, short-chain fatty acids, and herbal medicines. *Front. Pharmacol.* 9. doi: 10.3389/fphar.2018.01354

Feraco, D., Blaha, M., Khan, S., Green, J. M., and Plotkin, B. J. (2016). Host environmental signals and effects on biofilm formation. *Microbial pathogenesis* 99, 253–263. doi: 10.1016/j.micpath.2016.08.015

Fteita, D., Könönen, E., Söderling, E., and Gürsoy, U. K. (2014). Effect of estradiol on planktonic growth, coaggregation, and biofilm formation of the prevotella intermedia group bacteria. *Anaerobe* 27, 7–13. doi: 10.1016/j.anaerobe.2014.02.003

Gagnon, M., Zihler Berner, A., Chervet, N., Chassard, C., and Lacroix, C. (2013). Comparison of the caco-2, HT-29 and the mucus-secreting HT29-MTX intestinal cell models to investigate salmonella adhesion and invasion. *J. Microbiol. Methods* 94 (3), 274–279. doi: 10.1016/j.mimet.2013.06.027

Garber, N., and Lupowitz-Donenfeld, B. (1973). The effect of thyroxine and triiodothyronine on bacterial growth. *Canadian Journal of Microbiology* 19 (1), 1401–1405. doi: 10.1139/m73-226%M4203514

Gong, B., Wang, C., Meng, F., Wang, H., Song, B., Yang, Y., et al. (2021). Association between gut microbiota and autoimmune thyroid disease: A systematic review and meta-analysis. *Front. Endocrinol.* 12. doi: 10.3389/fendo.2021.774362

Hasan, N., and Yang, H. (2019). Factors affecting the composition of the gut microbiota, and its modulation. *PeerJ* 7, e7502–e7502. doi: 10.7717/peerj.7502

He, S., Li, H., Yu, Z., Zhang, F., Liang, S., Liu, H., et al. (2021). The gut microbiome and sex hormone-related diseases. *Frontiers in Microbiology* 12, 2699. doi: 10.3389/fmicb.2021.711137

Heckman, C., Kanagasundaram, S., Cayer, M., and Paige, J. (2007). Preparation of cultured cells for scanning electron microscope. *Protocol Exchange*. doi: 10.1038/nprot.2007.504

Hojo, M., Asahara, T., Nagahara, A., Takeda, T., Matsumoto, K., Ueyama, H., et al. (2018). Gut microbiota composition before and after use of proton pump inhibitors. *Digestive Dis. Sci.* 63 (11), 2940–2949. doi: 10.1007/s10620-018-5122-4

Ibrahim, S. A., and Bezkorovainy, A. (1993). Survival of bifidobacteria in the presence of bile salt. *Journal of the Science of Food and Agriculture* 62 (4), 351–354. doi: 10.1002/jsfa.2740620407

Izquierdo, E., Medina, M., Ennahar, S., Marchioni, E., and Sanz, Y. (2008). Resistance to simulated gastrointestinal conditions and adhesion to mucus as probiotic criteria for bifidobacterium longum strains. *Curr. Microbiol.* 56 (6), 613–618. doi: 10.1007/s00284-008-9135-7

Jang, H.-I., Rhee, K.-J., and Eom, Y.-B. (2020). Antibacterial and antibiofilm effects of α-humulene against bacteroides fragilis. *Can. J. Microbiol.* 66 (6), 389–399. doi: 10.1139/cjm-2020-0004

Kawasoe, J., Uchida, Y., Kawamoto, H., Miyauchi, T., Watanabe, T., Saga, K., et al. (2022). Propionic acid, induced in gut by an inulin diet, suppresses inflammation and ameliorates liver ischemia and reperfusion injury in mice. *Frontiers in Immunol.* 13. doi: 10.3389/fimmu.2022.862503

Kleiveland, C. R.. (2015). Co-cultivation of Caco-2 and HT-29MTX. In: K. Verhoeckx, P. Cotter, I. López-Expósito, et al editors. *The Impact of Food Bioactives on Health:* in vitro *and ex vivo models [Internet]*. Cham (CH): Springer. Chapter 13. doi: 10.1007/978-3-319-16104-4_13

Knezevic, J., Starchl, C., Tmava Berisha, A., and Amrein, K. (2020). Thyroid-Gut-Axis: How does the microbiota influence thyroid function? *Nutrients* 12 (6), 1769. doi: 10.3390/nu12061769

Kornman, K. S., and Loesche, W. J. (1982). Effects of estradiol and progesterone on bacteroides melaninogenicus and bacteroides gingivalis. *Infection Immun.* 35 (1), 256–263. doi: 10.1128/iai.35.1.256-263.1982

Kos, B., Susković, J., Vuković, S., Simpraga, M., Frece, J., and Matosić, S. (2003). Adhesion and aggregation ability of probiotic strain lactobacillus acidophilus M92. *J. Appl. Microbiol.* 94 (6), 981–987. doi: 10.1046/j.1365-2672.2003.01915.x

Krasowska, A., and Sigler, K. (2014). How microorganisms use hydrophobicity and what does this mean for human needs? *Front. Cell. Infection Microbiol.* 4. doi: 10.3389/fcimb.2014.00112

Kwasny, S. M., and Opperman, T. J. (2010). Static biofilm cultures of gram-positive pathogens grown in a microtiter format used for anti-biofilm drug discovery. *Curr. Protoc. Pharmacol.* 50 (1), 13A.18.11–13A.18.23. doi: 10.1002/0471141755.ph13a08s50

Lather, P., Mohanty, A. K., Jha, P., and Garsa, A. K. (2016). Contribution of cell surface hydrophobicity in the resistance of staphylococcus aureus against antimicrobial agents. *Biochem. Res. Int.* 2016, 1091290. doi: 10.1155/2016/1091290

Lester, G., and Hechter, O. (1958). Effect of deoxycorticosterone on the growth of microorganisms. *J. Bacteriology* 76 (4), 365–367. doi: 10.1128/jb.76.4.365-367.1958

Letourneau, J., Levesque, C., Berthiaume, F., Jacques, M., and Mourez, M. (2011). *In vitro* assay of bacterial adhesion onto mammalian epithelial cells. *J. Vis. Exp.* 51, e2783. doi: 10.3791/2783

Li, J.-Y., Chassaing, B., Tyagi, A. M., Vaccaro, C., Luo, T., Adams, J., et al. (2016). Sex steroid deficiency–associated bone loss is microbiota dependent and prevented by probiotics. *J. Clin. Invest.* 126 (6), 2049–2063. doi: 10.1172/JCI86062

Maier, L., Pruteanu, M., Kuhn, M., Zeller, G., Telzerow, A., Anderson, E. E., et al. (2018). Extensive impact of non-antibiotic drugs on human gut bacteria. *Nature* 555 (7698), 623–628. doi: 10.1038/nature25979

Mueller, H., Kassack, M. U., and Wiese, M. (2004). Comparison of the usefulness of the MTT, ATP, and calcein assays to predict the potency of cytotoxic agents in various human cancer cell lines. *J. biomolecular screening* 9 (6), 506–515. doi: 10.1177/1087057104265386

Muñoz-Provencio, D., Llopis, M., Antolín, M., de Torres, I., Guarner, F., Pérez-Martínez, G., et al. (2009). Adhesion properties of lactobacillus casei strains to resected intestinal fragments and components of the extracellular matrix. *Arch. Microbiol.* 191 (2), 153–161. doi: 10.1007/s00203-008-0436-9

Nakano, V., Piazza, R. M. F., Cianciarullo, A., Bueris, V., Santos, M., Menezes, M., et al. (2008). Adherence and invasion of bacteroidales isolated from the human intestinal tract. *Clin. Microbiol. infection* 14 (10), 955–963. doi: 10.1111/j.1469-0691.2008.02069.x

Neuffer, J., González-Domínguez, R., Lefèvre-Arbogast, S., Low, D. Y., Driollet, B., Helmer, C., et al. (2022). Exploration of the gut-brain axis through metabolomics identifies serum propionic acid associated with higher cognitive decline in older persons. *Nutrients* 14 (21), 4688. doi: 10.3390/nu14214688

Nicholson, J. K., Holmes, E., Kinross, J., Burcelin, R., Gibson, G., Jia, W., et al. (2012). Host-gut microbiota metabolic interactions. *Science* 336 (6086), 1262. doi: 10.1126/science.1223813

Nishiyama, K., Yokoi, T., Sugiyama, M., Osawa, R., Mukai, T., and Okada, N. (2021). Roles of the cell surface architecture of bacteroides and bifidobacterium in the gut colonization. *Front. Microbiol.* 12, 3115. doi: 10.3389/fmicb.2021.754819

Nogal, A., Valdes, A. M., and Menni, C. (2021). The role of short-chain fatty acids in the interplay between gut microbiota and diet in cardio-metabolic health. *Gut Microbes* 13 (1), 1–24. doi: 10.1080/19490976.2021.1897212

Piette, J. P., and Idziak, E. S. (1992). A model study of factors involved in adhesion of pseudomonas fluorescens to meat. . *Appl. Environ. Microbiol* 58 (9), 2783–2791. doi: 10.1128/aem.58.9.2783-2791.1992

Prakash, S., Rodes, L., Coussa-Charley, M., and Tomaro-Duchesneau, C. (2011). Gut microbiota: next frontier in understanding human health and development of biotherapeutics. . *Biologics: Targets Ther* 5, 71–86. doi: 10.2147/BTT.S19099

Rahman, M., Kim, W.-S., Kumura, H., and Shimazaki, K.-I. (2008). Autoaggregation and surface hydrophobicity of bifidobacteria. *World J. Microbiol. Biotechnol* 24 (8), 1593–1598. doi: 10.1007/s11274-007-9650-x

Reddy, S., and Austin, F. (2017). Adhesion and invasion assay procedure using caco-2 cells for listeria monocytogenes. *Bio Protoc.* 7 (9), e2267. doi: 10.21769/BioProtoc.2267

Reis, A. C., Silva, J. O., Laranjeira, B. J., Pinheiro, A. Q., and Carvalho, C. B. (2014). Virulence factors and biofilm production by isolates of bacteroides fragilis recovered from dog intestinal tracts. *Braz. J. Microbiol.* 45 (2), 647–650. doi: 10.1590/s1517-83822014000200037

Rinninella, E., Raoul, P., Cintoni, M., Franceschi, F., Miggiano, G. A. D., Gasbarrini, A., et al. (2019). What is the healthy gut microbiota composition? a changing ecosystem across age, environment, diet, and diseases. *Microorganisms* 7 (1), 14. doi: 10.3390/microorganisms7010014

Rios-Covian, D., Salazar, N., Gueimonde, M., and de Los Reyes-Gavilan, C. G. (2017). Shaping the metabolism of intestinal bacteroides population through diet to improve human health. *Front. Microbiol.* 8. doi: 10.3389/fmicb.2017.00376

Salonen, A., Lahti, L., Salojärvi, J., Holtrop, G., Korpela, K., Duncan, S. H., et al. (2014). Impact of diet and individual variation on intestinal microbiota composition and fermentation products in obese men. *ISME J.* 8 (11), 2218–2230. doi: 10.1038/ismej.2014.63

Sánchez, E., Nadal, I., Donat, E., Ribes-Koninckx, C., Calabuig, M., and Sanz, Y. (2008). Reduced diversity and increased virulence-gene carriage in intestinal enterobacteria of coeliac children. *BMC Gastroenterol.* 8 (1), 50. doi: 10.1186/1471-230X-8-50

Santos-Marcos, J. A., Rangel-Zuñiga, O. A., Jimenez-Lucena, R., Quintana-Navarro, G. M., Garcia-Carpintero, S., Malagon, M. M., et al. (2018). Influence of gender and menopausal status on gut microbiota. *Maturitas* 116, 43–53. doi: 10.1016/j.maturitas.2018.07.008

Scotti, E., Boué, S., Sasso, G. L., Zanetti, F., Belcastro, V., Poussin, C., et al. (2017). Exploring the microbiome in health and disease: Implications for toxicology. *Toxicol. Res. Appl.* 1, 2397847317741884. doi: 10.1177/2397847317741884

Shin, J.-H., Park, Y.-H., Sim, M., Kim, S.-A., Joung, H., and Shin, D.-M. (2019). Serum level of sex steroid hormone is associated with diversity and profiles of human gut microbiome. *Res. Microbiol.* 170 (4), 192–201. doi: 10.1016/j.resmic.2019.03.003

Silva, Y. P., Bernardi, A., and Frozza, R. L. (2020). The role of short-chain fatty acids from gut microbiota in gut-brain communication. *Front. Endocrinol.* 11. doi: 10.3389/fendo.2020.00025

Souza, C., Barbosa, C. D., Coelho, H. I., Santos Júnior, M. N., Barbosa, E. N., Queiroz, E. C., et al. (2021). Effects of 17β-estradiol on Monocyte/Macrophage response to staphylococcus aureus: An in vitro study. *Front. Cell. infection Microbiol.* 11, 701391. doi: 10.3389/fcimb.2021.701391

Staley, C., Weingarden, A. R., Khoruts, A., and Sadowsky, M. J. (2017). Interaction of gut microbiota with bile acid metabolism and its influence on disease states. *Appl. Microbiol. Biotechnol.* 101 (1), 47–64. doi: 10.1007/s00253-016-8006-6

Tetel, M. J., de Vries, G. J., Melcangi, R. C., Panzica, G., and O'Mahony, S. M. (2018). Steroids, stress and the gut microbiome-brain axis. *J. Neuroendocrinol* 30 (2), e12548. doi: 10.1111/jne.12548

Thursby, E., and Juge, N. (2017). Introduction to the human gut microbiota. *Biochem. J.* 474 (11), 1823–1836. doi: 10.1042/bcj20160510

Ude, V. C., Brown, D. M., Stone, V., and Johnston, H. J. (2019). Using 3D gastrointestinal tract *in vitro* models with microfold cells and mucus secreting ability to assess the hazard of copper oxide nanomaterials. *J. Nanobiotechnology* 17 (1), 70. doi: 10.1186/s12951-019-0503-1

Valdes-Varela, L., Hernandez-Barranco, A. M., Ruas-Madiedo, P., and Gueimonde, M. (2016). Effect of bifidobacterium upon clostridium difficile growth and toxicity when Co-cultured in different prebiotic substrates. *Front. Microbiol.* 7. doi: 10.3389/fmicb.2016.00738

Van Tassell, M. L., and Miller, M. J. (2011). Lactobacillus adhesion to mucus. *Nutrients* 3 (5), 613–636. doi: 10.3390/nu3050613

Vélez, M. P., De Keersmaecker, S. C., and Vanderleyden, J. (2007). Adherence factors of lactobacillus in the human gastrointestinal tract. *FEMS Microbiol. Lett.* 276 (2), 140–148. doi: 10.1111/j.1574-6968.2007.00908.x

Vich Vila, A., Collij, V., Sanna, S., Sinha, T., Imhann, F., Bourgonje, A. R., et al. (2020). Impact of commonly used drugs on the composition and metabolic function of the gut microbiota. *Nat. Commun.* 11 (1), 362. doi: 10.1038/s41467-019-14177-z

Vollaro, A., Esposito, A., Antonaki, E., Iula, V. D., D'Alonzo, D., Guaragna, A., et al. (2020). Steroid derivatives as potential antimicrobial agents against staphylococcus aureus planktonic cells. *Microorganisms* 8 (4), 468. doi: 10.3390/microorganisms8040468

Wang, J., Woo, M., and Yan, C. (2017). Spot plating assay for the determination of survival and plating efficiency of escherichia coli in sub-MIC levels of antibiotics. *JEMI Methods* 1, 26–29.

Wen, L., and Duffy, A. (2017). Factors influencing the gut microbiota, inflammation, and type 2 diabetes. *J. Nutr.* 147 (7), 1468s–1475s. doi: 10.3945/jn.116.240754

Woo, S.-G., Lee, S.-M., Lee, S.-Y., Lim, K.-H., Ha, E.-J., Kim, S.-H., et al. (2017). The effectiveness of anti-biofilm and anti-virulence properties of dihydrocelastrol and dihydrocelastryl diacetate in fighting against methicillin-resistant staphylococcus aureus. *Arch. Microbiol.* 199 (8), 1151–1163. doi: 10.1007/s00203-017-1386-x

Zhao, H., Chen, J., Li, X., Sun, Q., Qin, P., and Wang, Q. (2019). Compositional and functional features of the female premenopausal and postmenopausal gut microbiota. *FEBS letters* 593 (18), 2655–2664. doi: 10.1002/1873-3468.13527

Zhou, L., Li, X., Ahmed, A., Wu, D., Liu, L., Qiu, J., et al. (2014). Gut microbe analysis between hyperthyroid and healthy individuals. *Curr. Microbiol.* 69 (5), 675–680. doi: 10.1007/s00284-014-0640-6

frontiers | Frontiers in Cellular and Infection Microbiology

TYPE Original Research
PUBLISHED 14 March 2023
DOI 10.3389/fcimb.2023.1138588

OPEN ACCESS

EDITED BY
Adline Princy Solomon,
SASTRA University, India

REVIEWED BY
Sahana Vasudevan,
Institute for Stem Cell Science and Regenerative Medicine (inStem), India
Rekha Arya,
Sungkyunkwan University, Republic of Korea

*CORRESPONDENCE
Jing Zhao
Zhaojing-722@sina.com
Baohua Xu
zryhbaohuaxu@163.com

SPECIALTY SECTION
This article was submitted to Biofilms, a section of the journal Frontiers in Cellular and Infection Microbiology

RECEIVED 05 January 2023
ACCEPTED 27 February 2023
PUBLISHED 14 March 2023

CITATION
An J, Song Y, Zhao J and Xu B (2023) Antifungal efficiency and cytocompatibility of polymethyl methacrylate modified with zinc dimethacrylate. *Front. Cell. Infect. Microbiol.* 13:1138588. doi: 10.3389/fcimb.2023.1138588

Antifungal efficiency and cytocompatibility of polymethyl methacrylate modified with zinc dimethacrylate

Jiali An, Yunpeng Song, Jing Zhao* and Baohua Xu*

Dental Medical Center, China-Japan Friendship Hospital, Beijing, China

Objectives: Considering the high incidence rates of denture stomatitis, research that providing dental biomaterials with antifungal property are essential for clinical dentistry. The objectives of the present study were to investigate the effect of zinc dimethacrylate (ZDMA) modification on the antifungal and cytotoxic properties, as well as the variance in surface characteristics and other physicochemical properties of polymethyl methacrylate (PMMA) denture base resin.

Methods: PMMA with various mass fraction of ZDMA (1 wt%, 2.5 wt% and 5 wt%) were prepared for experimental groups, and unmodified PMMA for the control. Fourier-transform infrared spectroscopy (FTIR) was applied for characterization. Thermogravimetric analysis, atomic force microscopy and water contact angle were performed to investigate the thermal stability and surface characteristics (n=5). Antifungal capacities and cytocompatibility were evaluated with Candida albicans (*C. albicans*) and human oral fibroblasts (HGFs), respectively. Colony-forming unit counting, crystal violet assay, live/dead biofilm staining and scanning electron microscopy observation were performed to assess antifungal effects, and the detection of intracellular reactive oxygen species production was applied to explore the possible antimicrobial mechanism. Finally, the cytotoxicity of ZDMA modified PMMA resin was evaluated by the 3-(4,5-dimethyl-thiazol-2-yl)-2,5-diphenyl-tetrazolium bromide (MTT) assay and live/dead double staining.

Results: The FTIR analyses confirmed some variation in chemical bonding and physical blend of the composites. Incorporation of ZDMA significantly enhanced the thermal stability and hydrophilicity compared with unmodified PMMA ($p < 0.05$). The surface roughness increased with the addition of ZDMA while remained below the suggested threshold (≤ 0.2 μm). The antifungal activity significantly improved with ZDMA incorporation, and cytocompatibility assays indicated no obvious cytotoxicity on HGFs.

Conclusions: In the present study, the ZDMA mass fraction up to 5 wt% in PMMA performed better thermal stability, and an increase in surface roughness and hydrophilicity without enhancing microbial adhesion. Moreover, the ZDMA modified PMMA showed effective antifungal activity without inducing any cellular side effects.

KEYWORDS

polymethyl methacrylate (PMMA), zinc dimethacrylate (ZDMA), surface characteristics, antifungal, cytocompatibility

1 Introduction

As the population aged, improving the quality of life among them has caused great concern due to the difficulty aged people faced on a day-to-day basis. One of the most common issues in aged individuals is the teeth loss. Restorative dentistry has been the outstanding solution to restore such oral functions, and resin-based polymeric systems are widely applied in this area (Kostić et al., 2022). Poly methyl methacrylate (PMMA) is one of the most widely utilized of resin-based polymeric material due to its unique properties, including cost-effectiveness, well cytocompatibility, aesthetics, ease of manipulation, etc (Zafar, 2020). However, there are a number of concerns in the application of PMMA resin, such as its high porosity, surface hydrophobic and roughness (Matsuo et al., 2015; Walczak et al., 2020), which are susceptible to lead dental plaque deposition. In addition, poor denture hygiene contributes to inflammation in oral mucosa. All of these drawbacks are prone to lead denture stomatitis.

Denture stomatitis is a multifactorial oral disease, mainly caused by Candida albicans (*C. albicans*) infection. Candida-associated denture stomatitis has been found in up to 60% of denture wearers, being the most common oral mucosal issue related with denture base. To overcome such undesirable deficiency, considerable research about PMMA denture base resin modification have been studied, including incorporating nanoparticles, fibers or other fillers, utilizing copolymers to polymerize with PMMA resin matrix and curing in different conditions, etc (Gad et al., 2020; Karatepe and Ozdemir, 2020; Aati et al., 2022). The modified methods of PMMA based denture resin with monomer additives have been reported before (Kanie et al., 2004; Elzahar et al., 2022). For instance, the quaternary ammonium salts (QAS) monomer was a successful approach used in the restorative dentistry to overcome biofilm formation (Melo et al., 2014; Cao et al., 2018).

In addition to this, a novel metal-containing methacrylate monomer has been applied in dental materials recently. The incorporation of metal methacrylate including silver, zinc, calcium and dibutyltin-containing methacrylate into dental resin matrix allowed the materials to exert novel bioactive properties (Rubin Cocco et al., 2018; da Silva Barboza et al., 2021). The ability of these monomers to become immobilized in the main polymer chain and antibacterial effects contribution by metallic elements make them possess potential application value in resin-based polymeric dental material modification. Previous studies have demonstrated that zinc-based dental materials performed broad-spectrum antibacterial activity and biological safety, and thus it is expected that zinc-containing methacrylate will show a feasible antimicrobial effect against oral pathogenic bacterial without impacting biocompatibility. Zinc dimethacrylate (ZDMA), existing in the form of homopolymerized polysalt particles with diameters around 20 ~ 100 nm (Ambrožič et al., 2011), is a kind of metal crosslinking monomer with unsaturated carboxylic groups (the molecular structure of ZDMA was displayed in Figure 1) (Chen et al., 2013a). Two methacrylate (MAA-) groups are connected to the divalent Zn^{2+} through ionic bonds, and under certain conditions (such as in the presence of oxidation reduction or peroxide), the C=C bonds in MAA- groups can polymerize both with the matrix and itself (Xu et al., 2016; Wu et al., 2022). The ZDMA monomer has showed remarkable performance in clinical dentistry as modification ingredients of composites (Henn et al., 2011; Cocco et al., 2020). For instance, dental resin adhesive containing ZDMA performed great capacities of matrix metalloproteinase 2 (MMP-2) inhibition without impacting resin bond strength (Henn et al., 2012). In our previous study, ZDMA was incorporated into PMMA denture base resin and it demonstrated that modified PMMA resin containing mass fraction of ZDMA less than 5 wt% showed enhanced mechanical properties and also displayed great antibacterial property against Streptococcus mutans (*S. mutans*). However, there is still a limited information about its antifungal performance, physicochemical characters, surface characteristics and cytocompatibility of such modification.

Therefore, the aim of this study was to further evaluate the effect of ZDMA at various mass fraction (1 wt%, 2.5 wt% and 5 wt%) on the thermal stability, surface roughness and hydrophilic/hydrophobic properties, antifungal and cytocompatibility performance of PMMA denture base resin. It was hypothesized that 1) incorporating ZDMA into PMMA resin would increase the surface roughness and hydrophilicity compared with unmodified PMMA; 2) incorporation of ZDMA will provide effective antifungal activity without inducing any cellular side effects.

2 Materials and methods

2.1 Preparation of specimens

The PMMA resin (Nissin, China) and ZDMA particles (Sigma-Aldrich, USA) used in this study were all commercially available. PMMA resin were prepared using the room temperature denture base polymerizing acrylic powder and liquid following the manufacturer's instructions. To develop the new metal methacrylate modified PMMA resin, ZDMA was added at 1 wt%, 2.5 wt%, and 5 wt% to the PMMA monomer. Mass fraction greater than 5 wt% of ZDMA were eliminated considering that the preliminary study (An et al., 2022) has indicated a significant decrease in mechanical properties. Therefore, PMMA modified with ZDMA (1 wt%, 2.5 wt% and 5 wt%) were applied for the experimental groups, and unmodified PMMA for the control. In total, four groups were performed in this study. The manufacturing methods of the specimens for each group are described briefly below. Different mass fraction of ZDMA was added into acrylic powder and mixed with turbine mixer. After completely mix, acrylic

FIGURE 1
Molecular structure of zinc dimethacrylate.

liquid was added into the combined powder to form a paste which was then used to fabricate specimens for experimental groups. The acrylic powder and liquid were directly mixed to fabricate specimens for control group.

2.2 Characterization

2.2.1 Fourier transform infrared spectroscopy (FTIR)

To investigate the effect of the ZDMA incorporation on the PMMA resin, the infrared spectra of transmittance of the specimens selected randomly from each group and ZDMA were recorded using FTIR (Nicolet iS5, Thermo Fisher Scientific, USA) with an attenuated total reflectance (ATR) sampling accessory. The wavenumber was set in the range of 550 to 4000 cm^{-1}. For each spectrum 32 scans were recorded with resolution at 4 cm^{-1}.

2.2.2 Thermogravimetric analysis (TGA)

TGA (Q-50, TA instrument, USA) was applied for thermal stability characterization. The thermal stability of each sample was observed from ambient temperature to 500°C under nitrogen flow at a heating rate of 10°C/min. The weight loss experienced by the specimens as a function of temperature provided the kinetic data, thermal degradation behavior and rate of degradation.

2.2.3 Surface roughness

Specimens (n=5 per group) with dimension of 2 mm in thickness and 10 mm in diameter were prepared for surface roughness examination. Atomic force microscopy (AFM, Multimode 8, Bruker Daltonics Inc, USA) was performed to detect the surface topography and roughness. AFM was used at a high resolution with a sharp silicon tip (0.5 N/m) in tapping mode. The surface topography of the specimens was obtained over an area 10 × 10 μm. The surface roughness of the specimens from each group was obtained with a systemic software (NanoScope Analysis 1.7, Bruker Daltonics Inc), and the data of arithmetic roughness (Ra) were compared. Ra represented the average distance from the roughness profile to the center plane of the profile.

2.2.4 Water contact angle

The water contact angle of the specimens (n = 5) was measured using contact angle goniometer (OCAH200, Dataphysics, Germany) by quickly recording (less than 1 min) the images of ultrapure water droplets (3.5 μL) on the flat surface at 20°C. Contact angle measurements were repeated three times at different positions for each sample to obtain average values.

2.3 Antifungal activity

2.3.1 Biofilm formation

For antifungal experiments, the specimens were fabricated as PMMA discs (diameter = 10 mm, thickness = 2mm) and prior to test, specimens were disinfected using 70% ethanol, washed in triplicate with phosphate buffered saline (PBS) and then placed under UV light for 30 mins. The antifungal activities of the specimens were evaluated by using *C. albicans* (ATCC 10231). *C. albicans* were provided by the China-Japan Friendship Hospital of Clinical Microbiology Laboratory, which were cultured in a Sabouraud Dextrose (SD) broth at 37 °C. Each PMMA disc was placed at the bottom of a 24-well plate and around 2 mL of *C. albicans* suspension (optical density, OD = 0.02, equivalent to 2×10^4 CFU/mL) was added in each well and incubated for 24 h in a humid environment at 37°C under 95% air and 5% CO_2 to form mature fungi biofilm on the surface of the samples.

2.3.2 Colony-forming unit (CFU) counting

Following incubation, the specimens (n=5 per group) were washed twice with PBS to remove nonadherent fungi. The *C. albicans* biofilms adherent to the specimens were collected by scraping and sonication. The obtained biofilm suspensions were serially diluted, and 20 μL of diluted suspension was dropped onto SD solid medium plate and then incubated at 37°C for 24 h in anaerobic conditions. After 24 h, the colonies on the plate were counted for data analysis.

2.3.3 Crystal violet (CV) assay for biofilm biomass

CV assay is the most commonly used quantitative technique for detecting biomass accumulation in microplate method. Specimens (n=5 per group) with *C. albicans* biofilms were rinsed with PBS to remove nonadherent fungi and then air dried for 20 min. The air-dried specimens were submerged in 100% methyl alcohol for 15 min for fixation and then stained with 0.1% CV solution (C8470, Solarbio, China) for 15 mins. The bound dye was extracted from the stained cells with 95% ethanol solution. Biomass accumulation was then quantified by measuring the optical density of the CV/ethanol extract at a wavelength of 600 nm in a microplate reader (SpectraMax M5, Molecular Devices, USA).

2.3.4 Live/dead biofilm staining assay

The biofilm-coated specimens (n = 5 per group) were washed with sterile deionized water to remove non-adhered fungi. After rinsing with deionized water, the specimens with adhered *C. albicans* biofilms were stained with the LIVE/DEAD Yeast Viability kit (L7009, Thermo Fisher Scientific Inc, USA), followed by rinsing with deionized water to remove unnecessary fluorescence dye. The stained specimens were examined using an inverted epifluorescence microscope (Eclipse TE2000-S, Nikon, USA).

2.3.5 Scanning electron microscopy (SEM)

The biofilm-coated specimens (n = 5 per group) were employed to observe *C. albicans* adhesion population and biofilm morphology by SEM (Phenom ProX, Thermo Fisher Scientific Inc, USA). Each specimen was fixed with 2.5% glutaraldehyde at 4°C overnight, and then rinsed with PBS. After fixation, the samples were dehydrated in a graded series of ethanol solutions (30%, 50%, 70%, 80%, 90% and 100%), desiccation, sputter coated with Au–Pd alloy and then inspected by SEM.

2.3.6 Detection of intracellular reactive oxygen species (ROS) production

Intracellular ROS levels in *C. albicans* adhering to the specimen surface were measured by a fluorometric kit (Solarbio, China) using 2,7-dichlorofluorescein diacetate (DCFH-DA) probe as a ROS indicator as previously described (Pourhajibagher et al., 2020). Briefly, the *C. albicans* biofilms attached to the surface of specimens (n = 10 per group) were collected, washed with PBS for three times and then resuspended in PBS by adjusting the cell density to 10^6 CFU/mL. DCFH-DA at concentration of 10 μmol/L was added to the fungus suspension and incubated for 20 mins at 37 °C. The microbial cells were then collected by centrifugation at 12000 g for 5 mins and washed with PBS to remove any unnecessary DCFH-DA. The fluorescence spectrophotometer (Thermo Fisher Scientific Inc, USA) at an emission wavelength of 535 nm and an excitation wavelength of 488 nm was used to determine the fluorescence intensity of the target cells and the inverted epifluorescence microscope was applied for fluorescence observation.

2.4 Cytotoxicity

2.4.1 Cell culture

Human oral fibroblasts (HGFs; PCS-201–030, ATCC, USA) were cultured in fibroblast basal medium (FBM; SC 2301, WHELAB, USA) supplemented with 2% fetal bovine serum, 1% penicillin/streptomycin and 1% fibroblast growth supplement. The culture was incubated with 5% CO_2 at 37°C under saturated humidity until 95% confluence was achieved. Cells between the 4 and 6 passages were used for subsequent experimental procedures.

2.4.2 Preparation of the extract

In total, 10 specimens were prepared for each group, leading to a total surface area of 13.2 cm^2. The ratio of the specimen surface to the medium volume was 1.25 cm^2/mL. The specimens were sterilized and then eluted with fresh FBM at 37°C for 24, 48 and 72 h. The obtained extracts were passed through 0.22 μm filters for the next cytotoxicity tests.

2.4.3 Detection of cell viability

To evaluate the cell viability of the new metal monomer modified PMMA, a 3-(4,5-dimethyl-thiazol-2- yl) -2,5-diphenyl-tetrazolium bromide (MTT) kit (M1020, Solarbio, China) was used according to ISO 10993. The cells were collected and seeded at a density of 10^5 cells/mL in 24-well plates. After proliferation, 100 μL aliquots of the various extracts obtained from each group were added to 96-well plates. After 24 h of cell culturing, the medium was removed and MTT solution was added. The incubation was cultured at 37°C for 4 h, and the OD value of the formazan product at 450 nm was measured using a microplate reader, since the absorbance of formazan reflects the cell metabolism. Cells without the extracts were cultured as negative control and the extracts containing medium and MTT solution without cells were cultured as blank group. The cell viability value was calculated using the following equation:

$$\text{Cell Viability} = [OD_{(t)} - OD_{(blank)}]/[OD_{(nc)} - OD_{(blank)}] \times 100\,\%$$

where $OD_{(t)}$ is the OD value of the extracts from all groups, $OD_{(blank)}$ is the OD value of the blank group, and $OD_{(nc)}$ is the OD value of the negative control group.

2.4.4 Live/dead double staining

HGFs were seeded at a density of 10^5 cells/well in 24-well plate. The extract from each group was added after 4 h of proliferation. After 24 h of incubation, a live/dead staining kit (L10119, Thermo Fisher Scientific Inc, USA) was utilized to assess the cytotoxicity of the extracts. Calcein-AM was a staining reagent for fluorescently labeling living cells with green fluorescence, and its working concentration was 1 μM. In addition, PI (3 μM) only stained dead cells and excited red fluorescence. Finally, dyed cells were visualized through inverted epifluorescence microscope.

2.5 Statistical analysis

The statistical data are expressed as the mean ± standard deviation. Statistical analysis was performed by using a statistical software program (IBM SPSS Statistics, v22.0 for Windows, IBM Corp, USA). Dependent variables were evaluated by one-way analysis of variance (ANOVA) followed by the Tukey honestly significant difference *post hoc* test (α=.05) for this study, given that the data were consistent with a normal distribution and variance homogeneity.

3 Results

3.1 Characterization

3.1.1 FTIR

Figure 2 shows the FTIR spectra (550 - 4000 cm^{-1}) of the unmodified PMMA, ZDMA modified PMMA and ZDMA particles. The spectra of all groups were similar which exhibited the characteristic absorption peaks of PMMA (Karatepe and Ozdemir, 2020; Akhtar et al., 2021), such as the IR peaks at 2996.53 cm^{-1} and 2948.95 cm^{-1} representing the C-H asymmetric and symmetric stretching absorption peaks, that at 2849.52 cm^{-1} and 1730.77 cm^{-1} representing the CH_2 and C=O stretching vibration absorption peak respectively. After ZDMA incorporation, ZDMA modified PMMA exhibited the characteristic absorption peaks of ZDMA, including the IR peaks at 1655.48 cm^{-1}, 1610.36 cm^{-1} and 1425.38 cm^{-1}, etc. The infrared spectra about ZDMA can be described that, the C=O and C-O have been homogenized due to the existence of Zn^{2+} which leading the two chemical bonds move to the absorption peaks of 1537.12 cm^{-1} and 1425.38 cm^{-1}, and C=C bonds move its position to 1655.48 cm^{-1} due to conjugated with C=O (Ambrožič et al., 2011; Chen et al., 2013a). In addition, certain effects were noticed after ZDMA modification, such as transmittance being modified due to the cross-linking and physical blend leading the formation of new chemical bonds. One of the noteworthy IR peaks among the

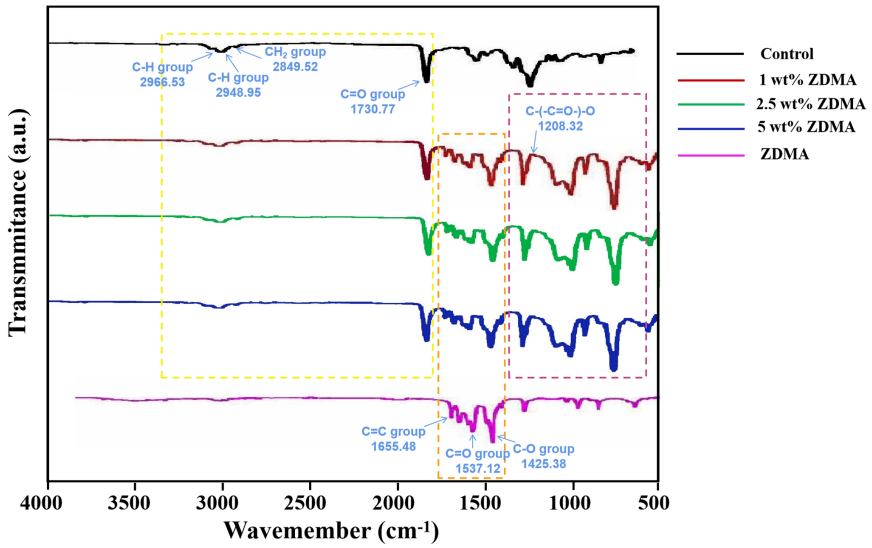

FIGURE 2
FTIR spectra of unmodified PMMA, ZDMA modified PMMA and ZDMA.

transmittance was the stretching vibration peak at 1208.32 cm^{-1}. The generation of IR peak at 1208.32 cm^{-1} was due to the open of C=C double bond in ZDMA which confirmed the cross linking of ZDMA in the composite (Ambrožič et al., 2011; Chen et al., 2013b).

3.1.2 TGA

In order to evaluate the thermal stability of each sample, TGA analysis has been carried out up to 500°C at the heating rate of 10°C/min in nitrogen atmosphere. The weight loss curves are shown in Figure 3 and the comparative study of TGA data for each group are displayed in Table 1. The thermogram of all samples displayed a three-step thermal degradation behavior (Adnan et al., 2021). The first weak weight loss step corresponds to chain scission resulting from hydrogen bonds. The second step is attributed to the scissions of the chains at the unsaturated ends while the later beginning of weight loss is due to the polymeric chain random scission. It is noticeable that the decomposing stage of ZDMA modified PMMA were significantly postponed compared with the unmodified PMMA. As shown in Table 1, the degradation temperature range in the three-step weight loss of ZDMA modified PMMA were all higher than that of the unmodified PMMA, and with the ZDMA mass fraction increased, the degradation temperature range increased gradually. T_5, T_{10} and T_{50} representative the temperature of mass loss fraction at 5 wt%, 10 wt% and 50 wt%, respectively. In order to evaluate thermal stability, a reference point was selected as criterion, usually, at 5 wt% mass loss according to literature (Vedhanayagam et al., 2020). The TGA results indicated that T_5 of ZDMA modified PMMA were all higher than unmodified PMMA and increased with the ZDMA mass fraction, implying that the thermal stability of ZDMA modified PMMA had been improved.

3.1.3 Surface roughness

The surface roughness was examined *via* AFM, and Figure 4 illustrates representative images and Ra values of each group. The control group showed the lowest Ra value (107.2 ± 2.76 nm). Compared with the control group, ZDMA modified PMMA groups have shown higher Ra values, 108.8 ± 2.59 nm, 110.1 ± 2.24 nm and 110.8 ± 1.63 nm, and there was an absence of statistically significant difference among these three experimental groups ($p > 0.05$). The 5 wt% ZDMA group (110.8 ± 1.63 nm) displayed the highest Ra values and significantly higher than the control group ($p < 0.05$).

3.1.4 Water contact angle

The water contact angles of each group are exhibited in Figure 5. The control group showed the highest hydrophobicity with a contact angle of around 72.1 ± 1.4°. After ZDMA was incorporated into PMMA, as the mass fraction increased (1 wt%, 2.5 wt% and 5 wt%), the contact angle decreased gradually. The contact angle of 5 wt% ZDMA group (59.57 ± 1.53°) was the lowest among these groups and significantly lower than other groups ($p < 0.001$).

3.2 Antifungal activity

3.2.1 CFU

The amount of *C. albicans* colonies (CFU/ml) from each group are shown in Figure 6. The *C. albicans* colonies of the control group were much denser than those of other experimental groups ($p < 0.001$). For the specimens with ZDMA added, those with 5 wt% ZDMA mass fraction PMMA showed the lowest number of colonies among all groups, about 2-fold lower than the control.

3.2.2 Crystal violet assay

The *C. albicans* biomass accumulation was indicated by CV assay and the results are shown in Figure 7. The variance of the *C. albicans* biomass accumulation for each group was similar to the

10.3389/fcimb.2023.1138588

TABLE 1 Comparative study of TGA data for each group.

Groups	Stage	Temperature Range (°C)	Weight Loss	T_5 (°C)	T_{10} (°C)	T_{50} (°C)
Control	I	195.81 ~ 292.35	11 wt%	257.04	291.67	366.28
	II	292.35 ~ 386.84	75 wt%			
	III	386.84 ~ 438.23	97 wt%			
1 wt% ZDMA	I	194.67 ~ 292.04	9 wt%	264.05	298.09	380.14
	II	319.37 ~ 388.29	59 wt%			
	III	388.29 ~ 460.26	96 wt%			
2.5 wt% ZDMA	I	192.51 ~ 323.31	12 wt%	266.67	314.37	380.17
	II	323.31 ~ 389.55	60 wt%			
	III	389.55 ~ 466.16	96 wt%			
5 wt% ZDMA	I	202.29 ~ 324.74	10 wt%	275.96	324.74	381.29
	II	324.74 ~ 387.69	56 wt%			
	III	387.69 ~ 483.82	93 wt%			

CFU results. Compared with the control group (2.67 ± 0.01), the biomass accumulation reduced with the ZDMA incorporation. When the mass fraction of ZDMA up to 5 wt%, the biomass accumulation was the lowest (2.07 ± 0.06), reduced significantly compared with the control group ($p < 0.05$).

3.2.3 Live/dead staining

Representative live/dead staining images of the *C. albicans* biofilm on the surface from each group are shown in Figure 8. The live microbial cells were stained green while the microbial cells with compromised membranes were stained red, and the overlap of live and compromised membranes were stained orange. The control group was primarily covered with live microbial cells with green staining, while the proportion of red staining significantly increased in ZDMA modified PMMA groups, indicating that dead microbial cells obviously increased.

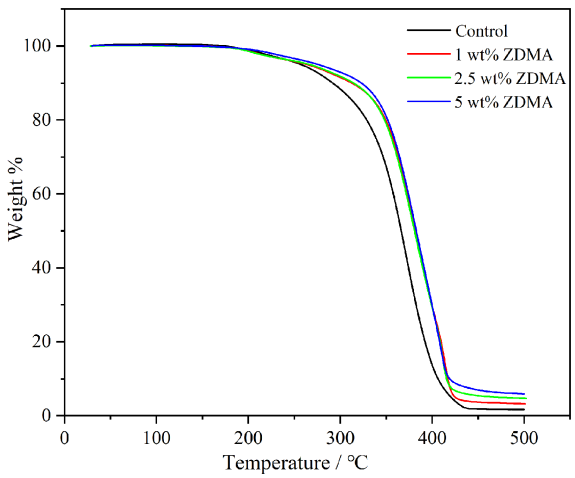

FIGURE 3
TGA weight loss curves of each group.

3.2.4 SEM observation

The morphology and distribution of the *C. albicans* adhered to the surface of each group observed by SEM are shown in Figure 9 and it is obvious that the biofilm of the control group was much denser than those in experimental groups. The *C. albicans* in the control group shrank less, exhibited a more complete plump shape and formed more contiguous and thicker biofilm covering the entire acrylic surface. The amounts of adhered *C. albicans* on the ZDMA modified PMMA surface reduced significantly and decreased as the mass fraction of ZDMA increased. Compared with the control group, ZDMA modified PMMA displayed a sparse and less *C. albicans* compact biofilm distributed on its surface.

3.2.5 Detection of intracellular ROS production

The levels of intracellular ROS in *C. albicans* were detected by DCFH-DA fluorescent probe in the present study. DCFH-DA itself has no fluorescence and it can pass through the cell membrane freely. Once inside, DCFH-DA is first hydrolyzed into DCFH by lipase, and then be oxidized to DCF, with strong fluorescence, by ROS. Accordingly, the production of ROS in cells can be examined by the DCF fluorescence intensity. The fluorescence intensity and representative staining images of each group are displayed in Figure 10. As shown in Figure 10A, there was almost no fluorescence production when the co-culture of *C. albicans* with unmodified PMMA. In the experimental groups, the fluorescence amount and intensity significantly increased with the incorporation of ZDMA. The data of fluorescence intensity detecting by fluorescence spectrophotometer are shown in Figure 10B. No fluorescence expression detected in the control group. The ROS fluorescence intensity in *C. albicans* adhering to the specimen

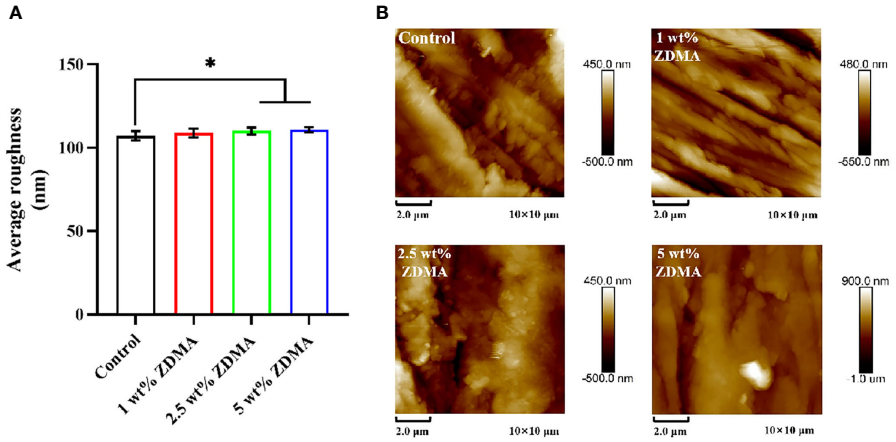

FIGURE 4
Surface roughness of each group. **(A)** Means ± standard deviations for Ra values of each group (*p < 0.05). **(B)** Representative AFM image of each group.

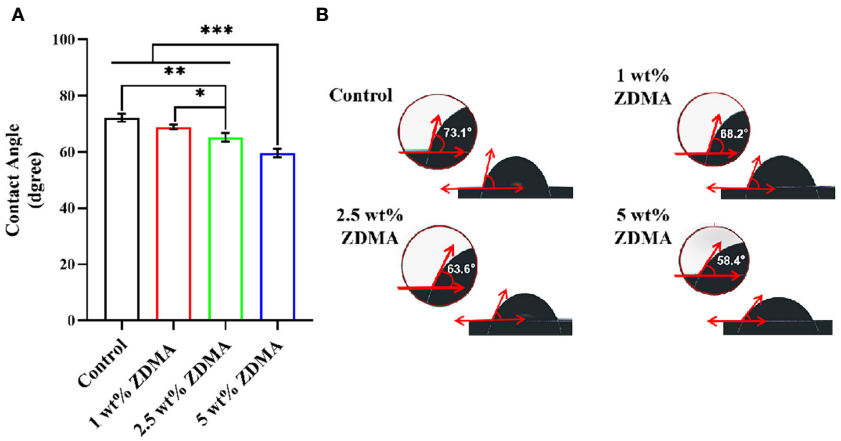

FIGURE 5
The water contact angle measurements of different specimens. **(A)** Means ± standard deviations for contact angle of each group (*p < 0.05, **p < 0.01, ***p < 0.001). **(B)** Representative contact angle image of each group.

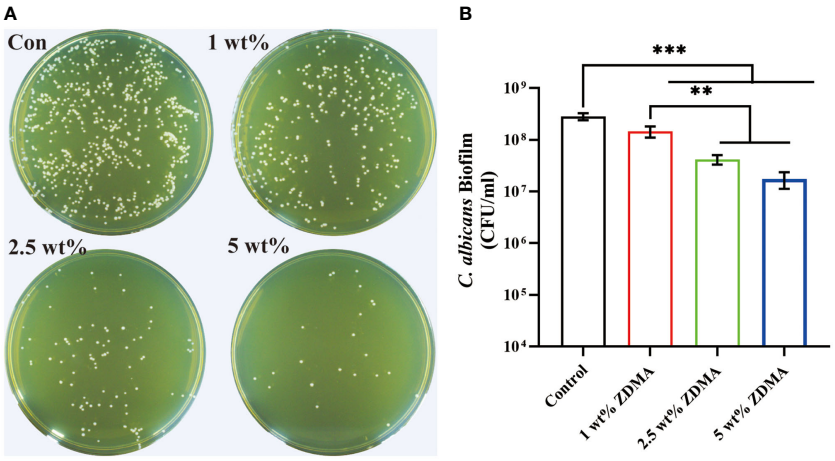

FIGURE 6
The number of *C. albicans* colonies detached from each group. **(A)** Representative images of *C. albicans* colonies of each group. **(B)** Means ± standard deviations for *C. albicans* colonies of each group (**p < 0.01, ***p < 0.001).

10.3389/fcimb.2023.1138588

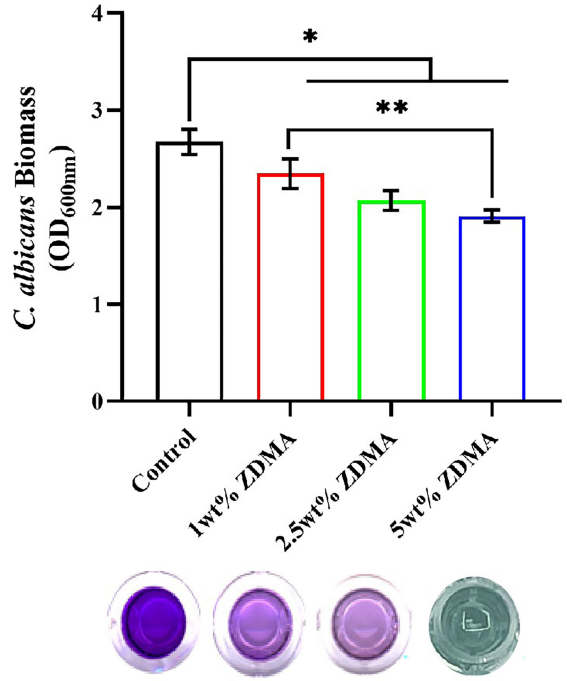

FIGURE 7
The visualization of *C. albicans* biofilm formation and means ± standard deviations for *C. albicans* biomass accumulation of the specimens for each group (*p < 0.05, **p < 0.01).

surface of experimental groups was in direct proportionate to the increased mass fraction of ZDMA. The fluorescence intensity of 5 wt% ZDMA group was the highest, significantly higher than 1 wt% ZDMA group ($p < 0.01$).

3.3 Cytotoxicity

The *in vitro* cell viability and cytotoxic effect of the extracts from each group against HGFs were measured and imaged as shown in Figure 11. The relative cell viability reduced with the mass fraction of ZDMA increased among the experimental groups compared with the control group. The 5 wt% ZDMA group exhibited the lowest cytocompatibility, decreased by 19.1% at most and significantly lower than the control group ($p < 0.05$). With the extension of extracting time, the relative cell viability of each group all decreased. In the present study, the relative cell viabilities were all greater than 90%. The effect of the extracts from each group in different experimental time on HGFs cell proliferation activity were determined by live/dead cell staining kit, and live cells were dyed green with calcein AM while dead cells displayed red due to propidium iodide. Live/Dead double staining assay (Figure 11B) presented that the live cells (green) accounted for more than 90% of the total cells in all groups, but it was obvious that with the increase of mass fraction of ZDMA, the proportion of dead cells (red) increased significantly, particular in 5 wt% ZDMA group.

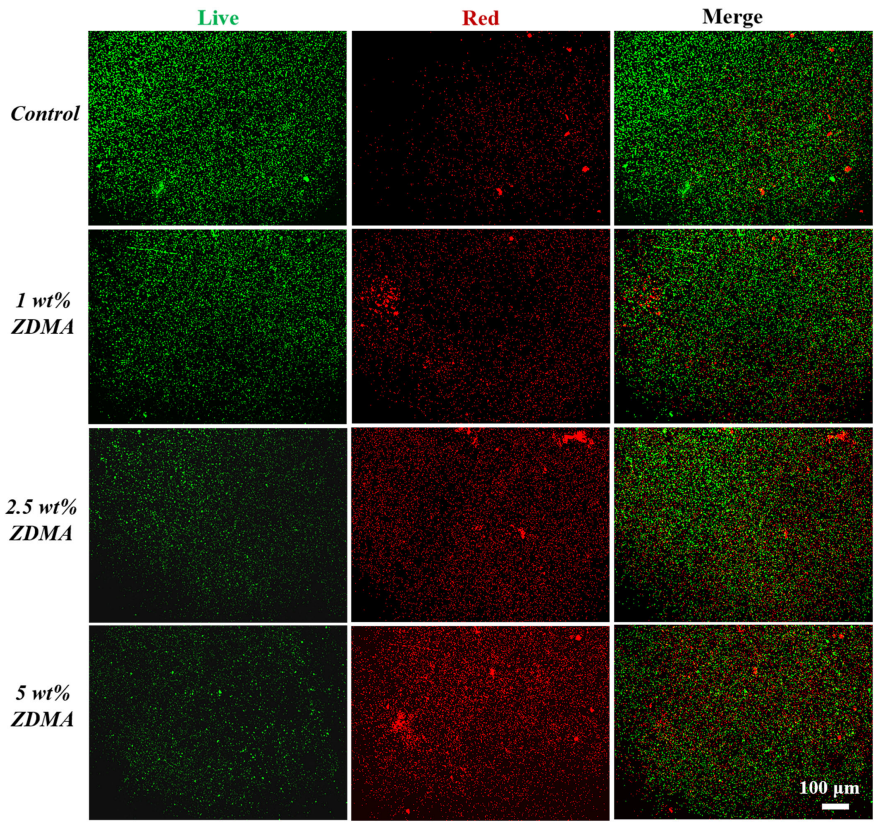

FIGURE 8
Representative live/dead staining images of *C. albicans* biofilms on specimens of each group.

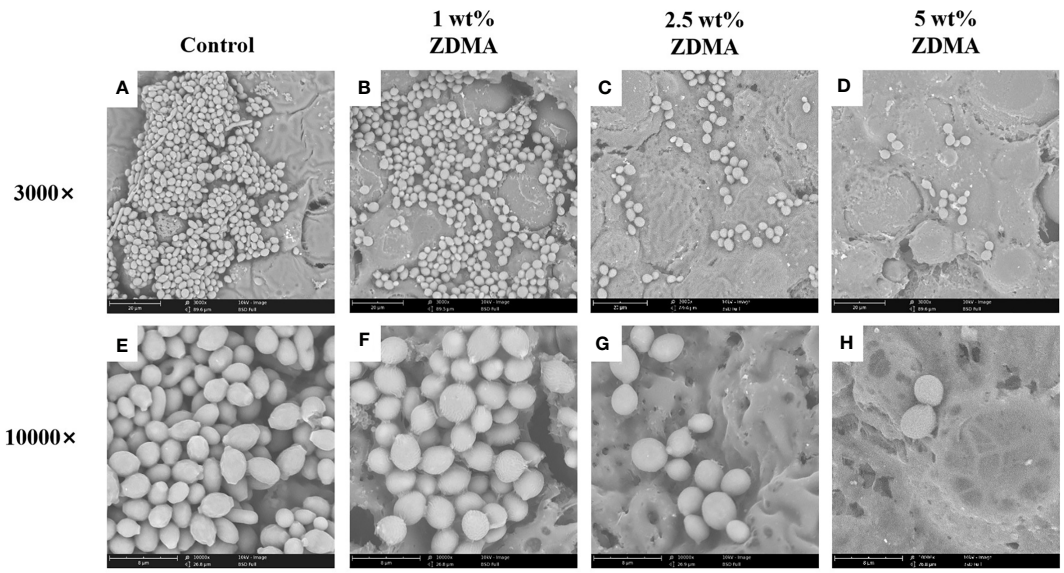

FIGURE 9
Representative scanning electron microscopy images showing morphologic changes of *C. albicans* on the specimens of each group: Images **(A–D)** represent SEM observation at 3000 magnifications. Images **(E–H)** represent SEM observation at 10000 magnifications.

4 Discussion

PMMA is the most commonly utilized polymers in clinical dentistry due to its great physiochemical properties and cytocompatibility (Zafar, 2020). However, the use of PMMA resin in the oral provides more surfaces for microorganism adhesion and alters biofilms distribution, impacting its application and oral health (Gad et al., 2017). Many attempts have been proposed to overcome such deficiency, such as incorporating QAS monomer into PMMA resin matrix. Such quaternary ammonium compound incorporation was reported to be cytotoxic and impacting mechanical properties (Beyth et al., 2008; Pei et al., 2018). To address these issues, in our previous study, ZDMA, a versatile crosslinker, was incorporated into PMMA matrix to generate a novel kind of metal methacrylate modified PMMA resin, and it was found that when the mass fraction of ZDMA was no more than 5 wt %, ZDMA provided modified PMMA antibacterial action against *S. mutans* and mechanical properties enhancement. In this study, surface characteristics, antifungal property, cytocompatibility and other physiochemical properties were further detected, and the results indicated that the incorporation of ZDMA significantly affected *C. albicans* adhesion and activity, without impacting its cytocompatibility.

FTIR results in Figure 2 displayed that all groups contained the characteristic absorption peaks of PMMA, demonstrated that the main structural component of all specimens is the PMMA polymer (Muhammad et al., 2022). The appearance of new absorption peaks in experimental groups at 1425.38 cm^{-1}, 1537.12 cm^{-1} and 1655.48

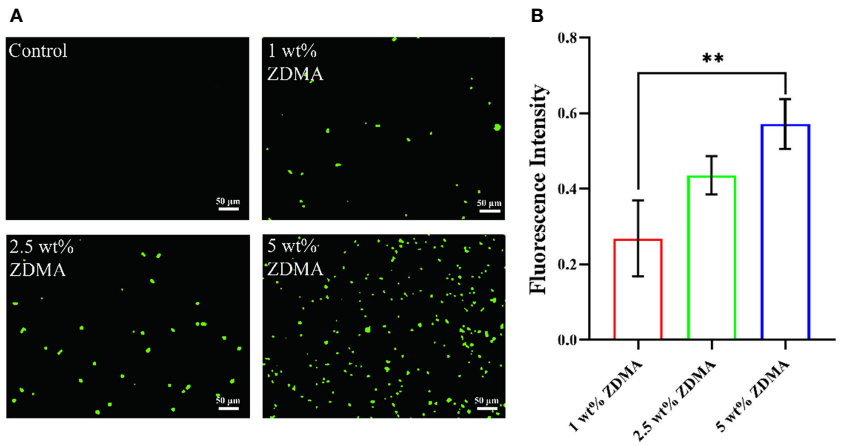

FIGURE 10
The expression of intracellular ROS in *C. albicans*. **(A)** Representative ROS fluorescence staining images from each group. **(B)** Means ± standard deviations for fluorescence intensity of each group (**p < 0.01).

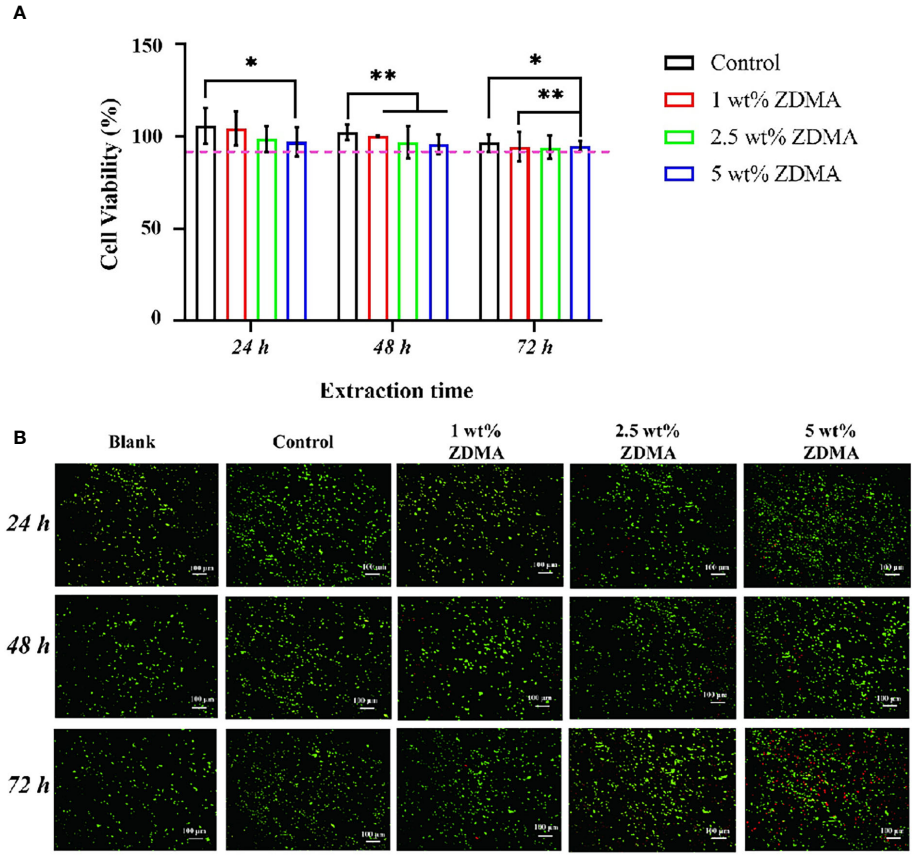

FIGURE 11
Cytotoxicity results of the extracts from each group. **(A)** The cytotoxicity of the extracts from each group determined by MTT assay (*p < 0.05, **p < 0.01). **(B)** Representative images of live/dead double staining of HGFs seeded with the extracts for each group and different extracting time.

cm^{-1} related to ZDMA (Chen et al., 2013a) also confirmed itself blend modification with PMMA matrix. The resulting modified PMMA resin not only have both PMMA and ZDMA characteristic chemical bonds information, but also showing some new absorption peaks in the range of 1400 cm^{-1} to 550 cm^{-1}. The appearance of these new transmittance revealed some chemical bonding and physical blend between ZDMA and PMMA in those modified composites (Elmergawy et al., 2021). One of the noteworthy IR peaks among the transmittance was the stretching vibration peak at 1208.32 cm^{-1}. The C=C double bond of ZDMA opened and then the single bond C-(-C=O-)-O generated (Ambrožič et al., 2011; Chen et al., 2013b). The stretching vibration peak around 1208 cm^{-1} represented the generation of the single bond C-(-C=O-)-O. In the present FTIR spectrum (Figure 2), the appearance of IR peak at 1208.32 cm^{-1} revealed cross linking of ZDMA monomer in the composite. However, the FITR spectrum only confirmed the generation of cross linking in ZDMA, more specific results about cross linking degree or efficiency should be justified by other characteristic tests.

The thermal characteristics enhancement of the ZDMA modified PMMA resin could be observed studying the TGA results. ZDMA, a kind of ionic crystalline solid, is high in melting point and stable in chemical structure due to the strong interaction between positive and negative charges of the two ionic crosslink bonds (Xia et al., 2021). As it turns out that the second and third stage of the thermal degradation in all ZDMA modified specimens postponed, and the delay degradation stage may result from the incorporation of ZDMA which could increase the bond energy and stability of the composites (Chrysafi et al., 2020). Water contact angle is often used as an indicator for hydrophilic/hydrophobic properties of polymers surfaces. As illustrated in Figure 5, the contact angle of ZDMA modified PMMA were significantly lower compared with the unmodified PMMA, implying the incorporation of ZDMA increase the surface hydrophilicity of the composites. This may be partly attributed to the molecular structure of ZDMA. The hydrophilic functional groups, including carboxyl, hydroxy, carboxylate and acylamino groups, etc, impart hydrophilicity to the polymers (Zimudzi et al., 2018). ZDMA is a kind of unsaturated metal carboxylates, containing two unsaturated carboxylate groups (Chen et al., 2013b; Xia et al., 2021) (its structure was shown in Figure 1). The incorporation of ZDMA provided more hydrophilic groups than unmodified PMMA which may result in the hydrophilicity increase (Nonkumwong et al., 2018).

The application of PMMA denture base resin placing into oral changes the oral environment as well promotes the microbials formation and attachment on the composites surface. The most

common isolated oral microorganisms from PMMA denture base resin are *C. albicans*, which is primarily leading to denture stomatitis, and *S. mutans*, which is mainly responsible for dental caries (Lapinska et al., 2020). Some studies have reported that *S. mutans* have a close association with increasing *C. albicans* biofilm formation (Pereira-Cenci et al., 2008). Therefore, it is crucial for ZDMA modified PMMA denture base resin to detect the potential antibacterial and antifungal effect against *S. mutans* and *C. albicans*. In our previous study, ZDMA modified PMMA has been proved to process antibacterial property against *S. mutans* while this study evaluated the antifungal effect on *C. albicans*. The amount of adherent and the activity of *C. albicans* on the ZDMA modified PMMA surface was significantly reduced by the addition of ZDMA, especially with the ZDMA mass fraction increased (as shown in Figures 5–8). The antifungal activity of ZDMA modified PMMA resin against *C. albicans* could be generally considered to be the contribution of the divalent Zn^{2+} connected with two methacrylate groups in ZDMA molecular structure. Zinc-containing dental materials, such as zinc oxide-eugenol cements and zinc ion coating implants, have been reported to show great antimicrobial performance against microbial strains (Arun et al., 2020; Yin et al., 2021). The ROS formation activated by Zn^{2+} is the key in microorganism inhibition (Wu et al., 2009). The excited electron catalyzed by Zn^{2+} react with the oxygen absorbed on the Zn^{2+}, and then reduce the oxygen into ROS or hydroxyl radicals. Such ROS or hydroxyl radicals with strong redox activity would lead to the cell membrane and protease structure damage, microbial cell dysfunction, and ultimately exerting antimicrobial effects (Vedhanayagam et al., 2020; Yang et al., 2021). In the present study, the intracellular ROS fluorescence intensity were detected in *C. albicans* adhering to ZDMA modified PMMA surface but no fluorescence intensity in *C. albicans* on unmodified PMMA surface. These results uncovered that the ZDMA modified PMMA exerts its antifungal activity through Zn^{2+} induced ROS accumulation in *C. albicans*.

Moreover, apart from the active antimicrobial ingredients, another primary influence upon microorganism adhesion were the physicochemical property of the dental material surface, including van der Waals force, surface energy, hydrophobicity and roughness, etc (Lee et al., 2018; Kallem et al., 2021). Surface roughness is one of the key determinant factors in dental materials application. There are many previous studies have reported that surface roughness could substantially affect bacterial adhesion on the surface of polymers, susceptible to cause oral health issues (Zou et al., 2017). It was determined that the Ra value over 0.2 μm leading to an increase of microorganism attachment (Al-Harbi et al., 2019). In the present study, the surface of each sample remained unpolished to make the comparison even handed between groups. The AFM results in Figure 4 showed that the Ra values of ZDMA modified PMMA increased with the mass fraction of ZDMA increase. Among these experimental groups, the Ra values of 5 wt % ZDMA group increased by 3.4% compared with unmodified PMMA. Although, ZDMA incorporation increased the surface roughness of modified PMMA resin, it remained significantly below the suggested threshold of dental materials ($Ra \leq 0.2$ μm) to avoid negative impact in application, such as microorganism adhesion and accumulation. In addition, an associated change with surface characteristic was the hydrophilicity enhancement in ZDMA modified PMMA resin. The hydrophilicity/hydrophobicity significantly influence the microorganism adherence and accumulation on materials surface (Hamid et al., 2021). The hydrophobic interaction occurs between the microbial surface and PMMA resin, leading the microbial cells to overcome the initial electrostatic repulsive forces between them (Krasowska and Sigler, 2014; Aati et al., 2022), thereby enhancing microbial biofilm adherence over the substrates. Another plausible explanation could be that hydrophobic surfaces favors proteins accumulation which provide specific binding sites for microbiomes and thus accelerating and facilitating their adhesion as well (An and Friedman, 1998). The surface hydrophilicity enhancement would lead to the formation of a tight water layer that create a physical barrier and then inhibit microbial adhesion. The results in the present study were consistent with the aforementioned studies, the amount of *C. albicans* adherence to the surface of the modified PMMA reduced significantly with the surface hydrophilicity enhancement, that confirmed by the CFU counting, biomass accumulation examining by CV assay, and the evident biofilm observation through SEM. The incorporation of ZDMA into PMMA matrix increased the composites hydrophilicity and then reduced the *C. albicans* attachment on its surface.

Biocompatibility of dental materials is a critical consideration for application in clinical (Caldas et al., 2019). In the present study, the inhibition about HGFs cell viability with ZDMA modified PMMA enhanced with the ZDMA mass fraction increase and the extension of extracting time. This may partly result from the incomplete cured residual monomer (Ausiello et al., 2013), including MMA and ZDMA, leaching out from resin matrix. The unpolymerized monomer can induce adverse effects in biological tissues through cell DNA damage, inhibiting cell cycle, et al (Issa et al., 2004). Apart from this, ZDMA modified PMMA resin can not only induce *C. albicans* to generate ROS to exerts its antifungal activity but also induce normal cells to product ROS leading to itself apoptosis, and this may impact biocompatibility. The results of cytotoxicity in the present study supports our inference about the inhibition in cell viability. In general, despite an inhibition in cell viability compared the unmodified PMMA resin, it was still all above 90% in all ZDMA modified PMMA, considered well biocompatibility according to the International Organization for Standardization (ISO) 10993-5 standard (Walters et al., 2016).

The achieved results in the present study verified the hypotheses that incorporating ZDMA into PMMA resin increased the hydrophilicity and roughness without enhancing microbial adhesion compared with unmodified PMMA; incorporating ZDMA into PMMA resin achieved great antifungal effects and without inducing any cellular side effects.

5 Conclusion

A novel metal methacrylate monomer modified PMMA denture base resin was developed in the present study. With the ZDMA mass fraction increased (up to 5 wt%), the thermal stability

and surface hydrophilicity enhanced significantly, and the surface roughness also increased while remained below the recommended threshold. Moreover, ZDMA modified PMMA resin showed great antifungal activities without inducing any cytotoxic effects. Therefore, the modification of PMMA denture base resin with ZDMA monomer holds a promising future in clinical dentistry.

Data availability statement

The raw data supporting the conclusions of this article will be made available by the authors, without undue reservation.

Author contributions

JA contributed to the conceptualization, data curation, formal analysis, investigation, methodology, validation, visualization and writing - original draft. YS contributed to the investigation, methodology, software and validation. JZ contributed to the data curation, project administration, resources, validation and visualization. BX contributed to the conceptualization, data curation, project administration, resources, supervision, validation, visualization and writing - review & editing. All authors contributed to the article and approved the submitted version.

Acknowledgments

The authors appreciate the China-Japan Friendship Hospital of Clinical Microbiology Laboratory for the guidance in this study.

Conflict of interest

The authors declare that the research was conducted in the absence of any commercial or financial relationships that could be construed as a potential conflict of interest.

Publisher's note

References

Aati, S., Shrestha, B., and Fawzy, A. (2022). Cytotoxicity and antimicrobial efficiency of ZrO2 nanoparticles reinforced 3D printed resins. *Dent. Mater.* 38 (8), 1432–1442. doi: 10.1016/j.dental.2022.06.030

Adnan, M., Rahman, T. U., Bahadur, A., Zeb, M. A., Liaqat, W., Akitsu, T., et al. (2021). The effect of AlI_3 nanoadditive on the thermal behavior of PMMA subjected to thermoanalytical py-GC-MS technique. *Materials (Basel).* 14 (22), 7036. doi: 10.3390/ma14227036

Akhtar, A. N., Murtaza, G., Shafique, M. A., and Haidyrah, A. S. (2021). Effect of Cu ions implantation on structural, electronic, optical and dielectric properties of polymethyl methacrylate (PMMA). *Polymers (Basel).* 13 (6), 973. doi: 10.3390/polym13060973

Al-Harbi, F. A., Abdel-Halim, M. S., Gad, M. M., Fouda, S. M., Baba, N. Z., AlRumaih, H. S., et al. (2019). Effect of nanodiamond addition on flexural strength, impact strength, and surface roughness of PMMA denture base. *J. Prosthodont.* 28 (1), e417–e425. doi: 10.1111/jopr.12969

Ambrožič, G., Škapin, S. D., Žigon, M., and Crnjak Orel, Z. (2011). Poly (zinc dimethacrylate) as a precursor in the low-temperature formation of ZnO nanoparticles. *J. Colloid Interface Sci.* 360 (2), 370–376. doi: 10.1016/j.jcis.2011.05.025

An, J., Ding, N., and Zhang, Z. (2022). Mechanical and antibacterial properties of polymethyl methacrylate modified with zinc dimethacrylate. *J. Prosthet Dent.* 128 (1), 100.e1–100.e8. doi: 10.1016/j.prosdent.2022.04.029

An, Y. H., and Friedman, R. J. (1998). Concise review of mechanisms of bacterial adhesion to biomaterial surfaces. *J. Biomed. Mater. Res.* 43 (3), 338–348. doi: 10.1002/(sici)1097-4636(199823)43:3<338::aid-jbm16>3.0.co;2-b

Arun, D., Adikari Mudiyanselage, D., Gulam Mohamed, R., Liddell, M., Monsur Hassan, N. M., and Sharma, D. (2020). Does the addition of zinc oxide nanoparticles improve the antibacterial properties of direct dental composite resins? a systematic review. *Materials (Basel).* 14 (1), 40. doi: 10.3390/ma14010040

Ausiello, P., Cassese, A., Miele, C., Beguinot, F., Garcia-Godoy, F., Di Jeso, B., et al. (2013). Cytotoxicity of dental resin composites: An *in vitro* evaluation. *J. Appl. Toxicol.* 33 (6), 451–457. doi: 10.1002/jat.1765

Beyth, N., Houri-Haddad, Y., Baraness-Hadar, L., Yudovin-Farber, I., Domb, A. J., and Weiss, E. I. (2008). Surface antimicrobial activity and biocompatibility of incorporated polyethylenimine nanoparticles. *Biomaterials.* 29 (31), 4157–4163. doi: 10.1016/j.biomaterials.2008.07.003

Caldas, I. P., Alves, G. G., Barbosa, I. B., Scelza, P., de Noronha, F., and Scelza, M. Z. (2019). *In vitro* cytotoxicity of dental adhesives: A systematic review. *Dent. Mater.* 35 (2), 195–205. doi: 10.1016/j.dental.2018.11.028

Cao, L., Xie, X., Wang, B., Weir, M. D., Oates, T. W., Xu, H. H. K., et al. (2018). Protein-repellent and antibacterial effects of a novel polymethyl methacrylate resin. *J. Dent.* 79, 39–45. doi: 10.1016/j.jdent.2018.09.007

Chen, Y., Xu, C., Cao, L., Wang, Y., and Fang, L. (2013a). Morphology study of peroxide-induced dynamically vulcanized polypropylene/ethylene-propylene-diene monomer/zinc dimethacrylate blends during tensile deformation. *J. Phys. Chem. B.* 117 (25), 7819–7825. doi: 10.1021/jp403293b

Chen, Y., Xu, C., Liang, X., and Cao, L. (2013b). *In situ* reactive compatibilization of polypropylene/ethylene-propylene-diene monomer thermoplastic vulcanizate by zinc dimethacrylate *via* peroxide-induced dynamic vulcanization. *J. Phys. Chem. B.* 117 (36), 10619–10628. doi: 10.1021/jp404427w

Chrysafi, I., Kontonasaki, E., Anastasiou, A. D., Patsiaoura, D., Papadopoulou, L., Vourlias, G., et al. (2020). Mechanical and thermal properties of PMMA resin composites for interim fixed prostheses reinforced with calcium β-pyrophosphate. *J. Mech. Behav. BioMed. Mater.* 112, 104094. doi: 10.1016/j.jmbbm.2020.104094

Cocco, A. R., Cuevas-Suárez, C. E., Liu, Y., Lund, R. G., Piva, E., and Hwang, G. (2020). Anti-biofilm activity of a novel pit and fissure self-adhesive sealant modified with metallic monomers. *Biofouling.* 36 (3), 245–255. doi: 10.1080/08927014.2020.1748603

da Silva Barboza, A., Fang, L. K., Ribeiro, J. S., Cuevas-Suárez, C. E., Moraes, R. R., and Lund, R. G. (2021). Physicomechanical, optical, and antifungal properties of polymethyl methacrylate modified with metal methacrylate monomers. *J. Prosthet Dent.* 125 (4), 706.e1–706.e6. doi: 10.1016/j.prosdent.2020.12.039

Elmergawy, F. H., Nassif, M. S., El-Borady, O. M., Mabrouk, M., and El-Korashy, D. I. (2021). Physical and mechanical evaluation of dental resin composite after modification with two different types of montmorillonite nanoclay. *J. Dent.* 112, 103731. doi: 10.1016/j.jdent.2021.103731

Elzahar, H. B., El-Okaily, M. S., Khedr, M. H., Amgad Kaddah, M., and El-Shahawy, A. A. G. (2022). Novel cold cure acrylic denture base with recycled zirconia nano-fillers that were functionalized by HEMA agent incorporation: Using the sprinkle approach. *Int. J. Nanomedicine.* 17, 4639–4658. doi: 10.2147/IJN.S374258

Gad, M. M., Al-Thobity, A. M., Fouda, S. M., Näpänkangas, R., and Raustia, A. (2020). Flexural and surface properties of PMMA denture base material modified with thymoquinone as an antifungal agent. *J. Prosthodont.* 29 (3), 243–250. doi: 10.1111/jopr.12967

Gad, M. M., Fouda, S. M., Al-Harbi, F. A., Näpänkangas, R., and Raustia, A. (2017). PMMA denture base material enhancement: A review of fiber, filler, and nanofiller addition. *Int. J. Nanomedicine.* 12, 3801–3812. doi: 10.2147/IJN.S130722

Hamid, S. K., Alghamdi, L. A., Alshahrani, F. A., Khan, S. Q., Matin, A., and Gad, M. M. (2021). *In vitro* assessment of artificial aging on the antifungal activity of PMMA denture base material modified with ZrO_2 nanoparticles. *Int. J. Dent.* 2021, 5560443. doi: 10.1155/2021/5560443

Henn, S., de Carvalho, R. V., Ogliari, F. A., de Souza, A. P., Line, S. R., da Silva, A. F., et al. (2012). Addition of zinc methacrylate in dental polymers: MMP-2 inhibition and ultimate tensile strength evaluation. *Clin. Oral. Investig.* 16 (2), 531–536. doi: 10.1007/s00784-011-0551-x

Henn, S., Nedel, F., de Carvalho, R. V., Lund, R. G., Cenci, M. S., Pereira-Cenci, T., et al. (2011). Characterization of an antimicrobial dental resin adhesive containing zinc methacrylate. *J. Mater Sci. Mater Med.* 22 (8), 1797–1802. doi: 10.1007/s10856-011-4364-x

Issa, Y., Watts, D. C., Brunton, P. A., Waters, C. M., and Duxbury, A. J. (2004). Resin composite monomers alter MTT and LDH activity of human gingival fibroblasts *in vitro*. *Dent. Mater.* 20 (1), 12–20. doi: 10.1016/s0109-5641(03)00053-8

Kallem, P., Bharath, G., Rambabu, K., Srinivasakannan, C., and Banat, F. (2021). Improved permeability and antifouling performance of polyethersulfone ultrafiltration membranes tailored by hydroxyapatite/boron nitride nanocomposites. *Chemosphere.* 268, 129306. doi: 10.1016/j.chemosphere.2020.129306

Kanie, T., Arikawa, H., Fujii, K., and Inoue, K. (2004). Physical and mechanical properties of PMMA resins containing gamma-methacryloxypropyltrimethoxysilane. *J. Oral. Rehabil.* 31 (2), 166–171. doi: 10.1111/j.1365-2842.2004.01043.x

Karatepe, U. Y., and Ozdemir, T. (2020). Improving mechanical and antibacterial properties of PMMA *via* polyblend electrospinning with silk fibroin and polyethyleneimine towards dental applications. *Bioact. Mater.* 5 (3), 510–515. doi: 10.1016/j.bioactmat.2020.04.005

Kostić, M., Igić, M., Gligorijević, N., Nikolić, V., Stošić, N., and Nikolić, L. (2022). The use of acrylate polymers in dentistry. *Polymers.* 14 (21), 4511. doi: 10.3390/polym14214511

Krasowska, A., and Sigler, K. (2014). How microorganisms use hydrophobicity and what does this mean for human needs? *Front. Cell. Infect. Microbiol.* 4. doi: 10.3389/fcimb.2014.00112

Lapinska, B., Szram, A., Zarzycka, B., Grzegorczyk, J., Hardan, L., Sokolowski, J., et al. (2020). An *In vitro* study on the antimicrobial properties of essential oil modified resin composite against oral pathogens. *Materials (Basel).* 13 (19), 4383. doi: 10.3390/ma13194383

Lee, J. H., Jo, J. K., Kim, D. A., Patel, K. D., Kim, H. W., and Lee, H. H. (2018). Nano-graphene oxide incorporated into PMMA resin to prevent microbial adhesion. *Dent. Mater.* 34 (4), e63–e72. doi: 10.1016/j.dental.2018.01.019

Matsuo, H., Suenaga, H., Takahashi, M., Suzuki, O., Sasaki, K., and Takahashi, N. (2015). Deterioration of polymethyl methacrylate dentures in the oral cavity. *Dent. Mater J.* 34 (2), 234–239. doi: 10.4012/dmj.2014-089

Melo, M. A., Wu, J., Weir, M. D., and Xu, H. H. (2014). Novel antibacterial orthodontic cement containing quaternary ammonium monomer dimethylaminododecyl methacrylate. *J. Dent.* 42 (9), 1193–1201. doi: 10.1016/j.jdent.2014.07.006

Muhammad, N., Sarfraz, Z., Zafar, M. S., Liaqat, S., Rahim, A., Ahmad, P., et al. (2022). Characterization of various acrylate based artificial teeth for denture fabrication. *J. Mater. Sci. Mater. Med.* 33 (2), 17. doi: 10.1007/s10856-022-06645-8

Nonkumwong, J., Erasquin, U. J., Sy Piecco, K. W., Premadasa, U. I., Aboelenen, A. M., Tangonan, A., et al. (2018). Successive surface reactions on hydrophilic silica for modified magnetic nanoparticle attachment probed by sum-frequency generation spectroscopy. *Langmuir.* 34 (43), 12680–12693. doi: 10.1021/acs.langmuir.8b01333

Pei, Y., Liu, H., Yang, Y., Yang, Y., Jiao, Y., Tay, F. R., et al. (2018). Biological activities and potential oral applications of n-acetylcysteine: Progress and prospects. *Oxid. Med. Cell Longev.* 2018, 2835787. doi: 10.1155/2018/2835787

Pereira-Cenci, T., Deng, D. M., Kraneveld, E. A., Manders, E. M., Del Bel Cury, A. A., Ten Cate, J. M., et al. (2008). The effect of streptococcus mutans and candida glabrata on candida albicans biofilms formed on different surfaces. *Arch. Oral. Biol.* 53 (8), 755–764. doi: 10.1016/j.archoralbio.2008.02.015

Pourhajibagher, M., Rahimi Esboei, B., Hodjat, M., and Bahador, A. (2020). Sonodynamic excitation of nanomicelle curcumin for eradication of streptococcus mutans under sonodynamic antimicrobial chemotherapy: Enhanced anti-caries activity of nanomicelle curcumin. *Photodiagnosis Photodyn. Ther.* 30, 101780. doi: 10.1016/j.pdpdt.2020.101780

Rubin Cocco, A., de Oliveira da Rosa, W. L., Luque Peralta, S., Timm Maske, T., da Silva, A. F., Andrade Hartwig, C., et al. (2018). New adhesive system based in metals cross-linking methacrylate. *J. Mech. Behav. BioMed. Mater.* 77, 519–526. doi: 10.1016/j.jmbbm.2017.10.010

Vedhanayagam, M., Anandasadagopan, S., Nair, B. U., and Sreeram, K. J. (2020). Polymethyl methacrylate (PMMA) grafted collagen scaffold reinforced by PdO-TiO_2 nanocomposites. *Mater. Sci. Eng. C Mater. Biol. Appl.* 108, 110378. doi: 10.1016/j.msec.2019.110378

Walczak, K., Schierz, G., Basche, S., Petto, C., Boening, K., and Wieckiewicz, M. (2020). Antifungal and surface properties of chitosan-salts modified PMMA denture base material. *Molecules.* 25 (24), 5899. doi: 10.3390/molecules25245899

Walters, N. J., Xia, W., Salih, V., Ashley, P. F., and Young, A. M. (2016). Poly (propylene glycol) and urethane dimethacrylates improve conversion of dental composites and reveal complexity of cytocompatibility testing. *Dent. Mater.* 32 (2), 264–277. doi: 10.1016/j.dental.2015.11.017

Wu, X. Z., Cheng, A. X., Sun, L. M., Sun, S. J., and Lou, H. X. (2009). Plagiochin e, an antifungal bis(bibenzyl), exerts its antifungal activity through mitochondrial dysfunction-induced reactive oxygen species accumulation in candida albicans. *Biochim. Biophys. Acta* 1790 (8), 770–777. doi: 10.1016/j.bbagen.2009.05.002

Wu, M., Yang, L., Zheng, Z., Wan, F., Teng, X., and Xu, C. (2022). Strengthened self-healable natural rubber composites based on carboxylated cellulose nanofibers participated in ionic supramolecular network. *Int. J. Biol. Macromol* 222 (Pt A), 587–598. doi: 10.1016/j.ijbiomac.2022.09.192

Xia, L., Meng, J., Ma, Y., and Zhao, P. (2021). Facile fabrication of eucommia rubber composites with high shape memory performance. *Polymers (Basel).* 13 (20), 3479. doi: 10.3390/polym13203479

Xu, C., Cao, L., Lin, B., Liang, X., and Chen, Y. (2016). Design of self-healing supramolecular rubbers by introducing ionic cross-links into natural rubber *via* a controlled vulcanization. *ACS Appl. Mater Interfaces.* 8 (27), 17728–17737. doi: 10.1021/acsami.6b05941

Yang, Y., Zheng, M., Jia, Y. N., Li, J., Li, H. P., and Tan, J. G. (2021). Time-dependent reactive oxygen species inhibit streptococcus mutans growth on zirconia after a helium cold atmospheric plasma treatment. *Mater Sci. Eng. C Mater Biol. Appl.* 120, 111633. doi: 10.1016/j.msec.2020.111633

Yin, S., Sun, N., Jiang, F., Lu, Y., Yang, G., Wu, X., et al. (2021). The translation from *In vitro* bioactive ion concentration screening to *In vivo* application for preventing peri-implantitis. *ACS Appl. Mater Interfaces.* 13 (4), 5782–5794. doi: 10.1021/acsami.0c19698

Zafar, M. S. (2020). Prosthodontic applications of polymethyl methacrylate (PMMA): An update. *Polymers.* 12 (10), 2299. doi: 10.3390/polym12102299

Zimudzi, T. J., Feldman, K. E., Sturnfield, J. F., Roy, A., Hickner, M. A., and Stafford, C. M. (2018). Quantifying carboxylic acid concentration in model polyamide desalination membranes *via* Fourier transform infrared spectroscopy. *Macromolecules.* 51, 6623–6629. doi: 10.1021/acs.macromol.8b01194

Zou, F., Zhou, H., Jeong, D. Y., Kwon, J., Eom, S. U., Park, T. J., et al. (2017). Wrinkled surface-mediated antibacterial activity of graphene oxide nanosheets. *ACS Appl. Mater Interfaces.* 9 (2), 1343–1351. doi: 10.1021/acsami.6b15085

frontiers | Frontiers in Cellular and Infection Microbiology

TYPE Review
PUBLISHED 06 April 2023
DOI 10.3389/fcimb.2023.1137947

OPEN ACCESS

EDITED BY
Adline Princy Solomon,
SASTRA University, India

REVIEWED BY
Selvaraj Anthonymuthu,
University of California, Irvine,
United States
Saravanan Periasamy,
Rajalakshmi Engineering College, India

*CORRESPONDENCE
Yipin Liu
yipinliu@163.net

SPECIALTY SECTION
This article was submitted to Biofilms, a section of the journal Frontiers in Cellular and Infection Microbiology

RECEIVED 07 January 2023
ACCEPTED 09 March 2023
PUBLISHED 06 April 2023

CITATION
Zhao A, Sun J and Liu Y (2023) Understanding bacterial biofilms: From definition to treatment strategies. *Front. Cell. Infect. Microbiol.* 13:1137947. doi: 10.3389/fcimb.2023.1137947

Understanding bacterial biofilms: From definition to treatment strategies

Ailing Zhao[1], Jiazheng Sun[2] and Yipin Liu[1*]

[1]Department of Gastroenterology, Yantai Affiliated Hospital of Binzhou Medical University, Yantai, Shandong, China, [2]Department of Vasculocardiology, Jinzhou Medical University, Jinzhou, Liaoning, China

Bacterial biofilms are complex microbial communities encased in extracellular polymeric substances. Their formation is a multi-step process. Biofilms are a significant problem in treating bacterial infections and are one of the main reasons for the persistence of infections. They can exhibit increased resistance to classical antibiotics and cause disease through device-related and non-device (tissue) -associated infections, posing a severe threat to global health issues. Therefore, early detection and search for new and alternative treatments are essential for treating and suppressing biofilm-associated infections. In this paper, we systematically reviewed the formation of bacterial biofilms, associated infections, detection methods, and potential treatment strategies, aiming to provide researchers with the latest progress in the detection and treatment of bacterial biofilms.

KEYWORDS

bacterial biofilms, infection, antibiotic resistance, biofilm detection, treatment

1 Introduction

Bacterial biofilms have become an essential contributor to global health problems due to antibiotic resistance, the host's immune defense system, and other external pressures. Biofilms are commonly found on the surface of hospital instruments and body tissue, in industry, food processing units, and natural environments (Schulze et al., 2021). Almost all bacteria can form biofilms.

Bacterial biofilms are usually defined as fixed microbial communities encased in extracellular polymeric substances (EPS). It is characterized by changes in the irreversible adhesion of microbial cells to surfaces or substrates or each other, embedded in EPS, and exhibiting specific phenotypes in terms of gene transcription and growth rates. A bacterial biofilm is composed of a single microorganism or a mixture of bacteria, fungi, archaea, protozoa, and yeasts. It has a channel structure that controls the release of gases, nutrients, and antimicrobials.

Free-floating bacterial cells can also aggregate to form biofilms, which exhibit similar characteristics to medical device-related biofilms (Hall-Stoodley et al., 2012). With the improvement of medical technology, the widespread use of medical devices, and the

pursuit of high quality of life for patients, medical device-associated biofilms pose a severe threat to the life and health of patients. Microorganisms can adhere to almost all medical devices and cause medical device-associated biofilm infections. Device-associated infections usually occur during treatment, where some microorganisms originate from the host. When these microorganisms attach and colonize the surface of a medical device, they can form a biological container. The pathogenesis of medical device-associated infections is related to microorganisms in complex communities that adhere to and grow on device surfaces. Medical device-related biofilms can consist of single or multiple species, depending primarily on the type of device and the time it is left in the patient's body. In most cases, device-associated infections are associated with biofilm formation on device surfaces. When floating bacteria come into contact with the surface of a medical device, they secrete polymers that create a three-dimensional matrix, which eventually sticks to the surface of the device, forming a biofilm structure. When the biofilm on the surface of implanted medical devices reaches a critical level, it can induce an inflammatory response in the host and may even cause implant failure. The most common microorganisms for medical device-associated infections are *Staphylococcus aureus* and *Staphylococcus epidermidis*. Multi-resistant gram-negative bacteria (e.g., *Escherichia coli*, *Klebsiella pneumoniae*, *Pseudomonas aeruginosa*, and *Acinetobacter baumannii*) can also cause medical device-associated infections in complex hospital settings (Niveditha et al., 2012). In addition, microorganisms can adhere to various tissue surfaces in the body (e.g., skin, connective tissue, intestinal mucosa, vascular endothelium, oral cavity, airway, bone tissue, and vagina), which in turn can cause non-device (tissue) -associated biofilm infections and lead to various diseases (Wi and Patel, 2018). When microorganisms in the oral cavity attach to enamel, dentin, and mucosal epithelial tissues, they can form a dental plaque, which is influenced by the nature of the attachment surface, the intraoral environment, and the state of oral health.

When stimulated by the harsh environment, the exopolysaccharides, fibrins and lipoproteins secreted by bacteria adhere to the surface of inert objects and form microbial substances. EPS is conducive to bacterial adhesion and promotes the formation of a biofilm matrix composed of extracellular polysaccharides, exogenous DNA, proteins, and lipids (Schilcher and Horswill, 2020; Chiba et al., 2022). The EPS matrix reduces the effect of antibiotics by neutralizing antimicrobial agents or limiting diffusion using extracellular polysaccharides. EPS facilitates intercellular communication, protects cells from chemical damage, provides oxygen diffusion, releases extracellular enzymes for nutrition and, in turn, stimulates the spread of bacteria within the biofilm (Costa et al., 2018; Galdiero et al., 2019). Bacterial biofilms are highly structured, functional, specific and coordinated. Various substances in biofilms coordinate to complete several life activities, such as bacterial biofilms' morphological diversity, adhesion and protective barrier function. Taking *P. aeruginosa* as an example, Table 1 shows the main components and basic functions of biofilms.

Bacterial biofilms are communities of microorganisms derived from single or multiple bacterial strains. Compared with single-species biofilms, multi-species biofilms showed the following new characteristics through interspecies interactions: increased biofilm mass, increased community cell count, enhanced metabolic activity of community members, increased antimicrobial tolerance, and changes in spatial organization and structure (Sadiq et al., 2021). Multispecies biofilms exhibit new characteristics different from their floating state, resulting from competition or cooperation. The interactions among bacteria of multiple species are synergy, mutual benefit, cooperation, utilization, antagonism, and competition (Liu et al., 2016). Among them, synergistic interactions play an important role in regulating bacterial microbial activity and constructing complex spatial structures of multispecies biofilms. The cooperation and competition between bacterial cells promote the formation of multispecies biofilms. Multispecies biofilms are found in many natural environments, such as the oral cavity, implantable medical devices, and mammalian intestines. The physical interactions, co-adhesion, and metabolic cooperation among bacterial cells promote the formation of multispecies biofilms in natural environments. Until now, research has focused on single-species biofilms. But now microbiologists are paying more attention to multispecies biofilms and cell interactions between communities. The early stage of multispecies biofilm formation is the adhesion and aggregation of microbial cells. Different biofilm-forming abilities and strategies of various bacteria and microorganisms lead to the formation of multiple types of biofilm (Yao et al., 2022). Multispecies biofilms are associated with developing various diseases, such as cystic fibrosis, diabetic foot ulcers, chronic wounds, and otitis media (Chan et al., 2017; Loera-Muro et al., 2021). The development and outcome of multispecies biofilm-associated diseases are related to the physiological organization and distribution of biofilms.

TABLE 1 Main components and basic functions of *P. aeruginosa* biofilm.

Components	Percentage (%)	Functions	Authors
Exopolysaccharides	1-2	Maintaining the structure and stability of biofilm matrix	Rather et al., 2021
Proteins (including enzymes)	<1-2	Maintaining the stability of biofilm matrix and surface colonization; Maintaining the structural integrity of biofilm	Fong and Yildiz, 2015
Extracellular DNA	<1-2	Promoting biofilm formation; Protecting the integrity of bacterial biofilms; Maintaining structural stability; Protecting the host immune system	Okshevsky and Meyer (2015)
Water	Up to 97	Keeping the biofilm hydrated to prevent it from drying out	Flemming and Wingender (2010)

Due to species diversity, the various stages of bacterial biofilm formation vary but are generally close. The formation of bacterial biofilms is a multi-step process, as shown in Figure 1, including molecular attachment to the surface of an object, bacterial adhesion and secretion of extracellular polymeric substances, maturation of the biofilm through the formation of colonies, and bacterial cell escape and dispersion and formation of a new biofilm structure (Kranjec et al., 2021). The process of bacterial biofilm formation is detailed below.

The attachment of bacterial microorganisms to a surface is the first stage of bacterial biofilm formation. The bacterial cells are transported to the object's surface by convection, Brownian motion, or sedimentation (Palmer et al., 2007). Chemotaxis is prevalent in bacterial microorganisms and refers to the ability of planktonic bacterial cells in fluids to move along a distribution of material concentrations towards chemically induced substances (i.e., sugars and amino acids) or nutrient sources. It promotes interaction between bacterial cells and the surface of an object, which in turn stimulates the colonization and growth of planktonic bacteria on the surface. When planktonic bacteria reach the surface of an object, the sum of the attractive or repulsive forces between the cell surface and the object's surface determines the interaction between the two characters. When the repulsive force is greater than the attractive force, bacteria cannot adhere to the surface; conversely, when the attractive force is greater than the repulsive force, bacteria can stick to the surface (Carniello et al., 2018). Planktonic bacteria adhere to the surface of objects by non-specific physical forces such as van der Waals forces, electrostatic forces, and hydrophobic interactions (Carniello et al., 2018), and planktonic microbial cells are transformed into stable cells. Still, the process is reversible, and the adhesion is weak. Reversible bacterial cells can maintain a two-dimensional structure Brownian motion and can separate from the surface of an object by their mobility and shear effects. The substrate required for bacterial biofilm growth refers to all substrates that come into contact with planktonic bacteria. Physico-chemical properties such as the substrate surface's roughness, hydrophobicity, film modulation, and surface charge can influence the efficiency of planktonic bacterial colonization and biofilm formation.

Hydrophobicity plays a vital role in the attachment of bacterial microorganisms to surfaces. A hydrophobic surface is more conducive to bacterial microbial colonization than a hydrophilic material, probably due to the hydrophobic effect, which reduces the repulsion between the bacterial cell surface and the substrate. Yu et al. (2016) suggest that *Streptococcus mutants*' attachment can influence the hydrophobicity and roughness of the substrate. Bacterial cell surface hydrophobicity is influenced by multiple factors such as bacterial species, growth rate, and culture medium. Hydrophobicity affects the attachment of bacterial microorganisms to surfaces, and when the surface of a bacteria or object is more hydrophobic, the stronger the adhesion between the two. The structural and physicochemical properties of bacterial cells and object surfaces determine whether bacteria attach to hydrophilic or hydrophobic surfaces. Another physical factor affecting bacterial microorganisms' attachment surface is the surface charge. Many amino, carboxyl, and phosphate groups in most bacterial cells give them a negative surface charge. A positively charged surface facilitates the attachment of planktonic bacteria, while a negative charge hinders the attachment of bacteria (Tuson and Weibel, 2013). The surface charge of bacterial cells is influenced by bacterial species, age, environmental pH, ionic strength, and culture medium. The regulatory film is an integral part of the bacterial adherent surface. Almost all planktonic bacteria come into contact with the regulatory film as they transit from the medium to the surface. It is formed as a nutrient adsorbed onto the surface of an object, resulting in a change in the physicochemical properties of the material surface, which in turn affects the attachment of bacterial cells.

The second phase is irreversible adhesion, where microbial cell surface components can recognize bacterial adhesion molecules and consolidate bacterial interconnections (Nourbakhsh and Namvar, 2016). This phase is accomplished through bacterial cell surface hydrophobicity, hydrogen bonding, covalent bonding, ionic bonding, and dipole-dipole interactions. As bacterial cell surface

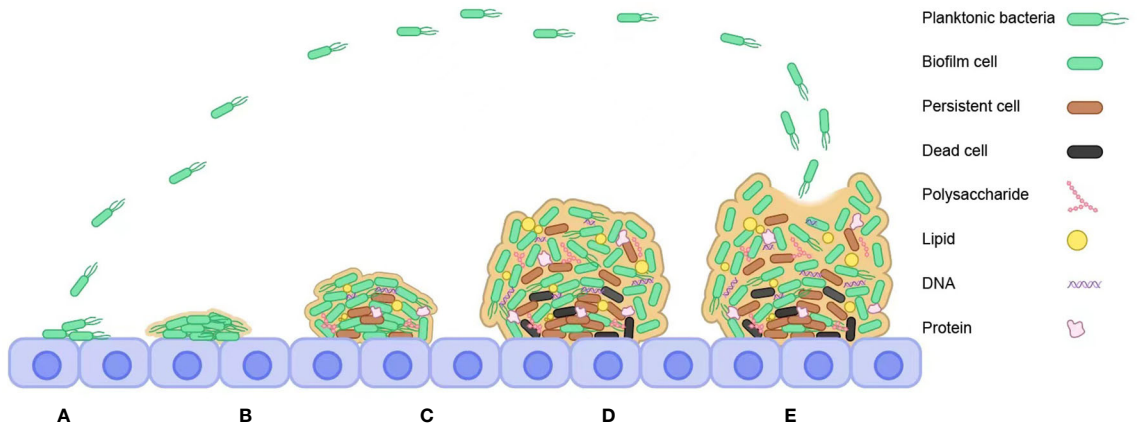

FIGURE 1
Steps to bacterial biofilm formation. **(A)** Reversible attachment. **(B)** Irreversible attachment. **(C)** Bacterial cells synthesize and secrete EPS. **(D)** Maturation. **(E)** Dispersal.

adhesion structures, flagella and fimbriae can form bacterial biofilms and contribute to the physical contact of planktonic bacteria with the substrate (Carniello et al., 2018). Flagella can swim in liquid substances and swarm on the surface of wet solid substances. Through these two forms of movement, various species of bacterioplankton direct cell adhesion to surfaces and transfer to favorable environments. Flagella initiate the adhesion of planktonic bacterial cells to surfaces, primarily because of the ability of flagella to overcome the resistance that prevents cell-surface interactions. Fimbriae also contribute to the early adhesion of bacterial cells to surfaces and each other. *P. aeruginosa* generates bacterial cell surface motility through fimbriae in a manner known as twitching motility. As an intercellular signaling mechanism, the Quorum sensing (QS) system also significantly facilitates the formation of bacterial biofilms in single cells (Abraham, 2016). Bacterial cells use means through QS to synthesize and release first messengers, such as chemical signals, to enable communication between bacterial flora. Both Gram-positive and Gram-negative bacilli affect the formation of bacterial biofilms. Gram-positive bacilli utilize oligopeptides, while Gram-negative bacilli utilize acyl homoserine lactones (Muhammad et al., 2020).

Bacterial cell synthesis and secretion of EPS is the third stage of bacterial biofilm formation. EPS substrate is hydrophobic and ion bridging, which can promote bacterial condensation and biofilm adhesion. EPS can affect surface adhesion, bacterial biofilm formation, biofilm internal structure, mutual recognition between cells, signal transduction system, nutrient acquisition, cell maintenance, and genetic information exchange, playing a crucial role in various aspects (Costa et al., 2018). The second messenger, c-di-GMP, can stimulate bacterial adhesion from a reversible to irreversible state, mainly due to its ability to produce the EPS matrix and form bacterial cell surface structures. As an essential component of the EPS matrix, extracellular polysaccharides are necessary for most bacteria to form biofilms and promote their development. EPS is also rich in proteins (i.e., enzymes)and protein structures (i.e., fimbriae). At the same time, eDNA and lipids are also components of the EPS matrix. The former can connect to bacterial cells, while the latter can affect the attachment of *Thiobacillus ferrooxidans* (Flemming et al., 2016).

The maturation of bacterial biofilms is the fourth stage of biofilm development. Bacterial biofilms mature as bacteria replicate and multiply in the EPS matrix, forming small microbial colonies and generating three-dimensional structures. As the EPS matrix accumulates and bacterial colonies form, this leads to altered gene expression, and the induction products of these genes can be used for EPS matrix generation. When the matrix is formed, water channels can be generated, which act by a mechanism similar to the body's circulatory system to deliver available nutrients to the cell community while rejecting extraneous products.

The process of dispersal of bacterial biofilms is the final stage of biofilm development. After a while, the mature bacterial biofilm may suffer damage, and the biofilm structure evolves. Still, the released bacterial microorganisms can infect other parts of the organism and form new biofilm structures. The mechanisms of dispersal are different due to the specificity of the bacteria. Still, all broadly involve the following three standard processes: detachment of bacterial cells from small colonies, transfer of bacterial cells to other substrates, and attachment of bacterial cells to new substrates (Shen et al., 2018). The process of detachment of bacterial biofilms can be either active or passive behavior. Active behavior refers to seeding dispersion, where bacterial cells in the biofilm undergo their detachment to adapt to environmental changes when the bacterial biofilm is subjected to matrix-degrading enzymes, antimicrobials, and nutrient deprivation. Passive behavior refers to shedding and erosion dispersion mediated by external forces (e.g., shear). Shedding dispersion refers to the abrupt shedding of a large proportion of the bacterial biofilm, and erosion dispersion refers to releasing a portion of bacterial cells in a bacterial biofilm. Low expression levels of c-di-GMP can inhibit the formation of bacterial biofilms and promote biofilm separation (Kaplan, 2010). Thus, inhibition of the c-di-GMP signaling pathway can effectively disperse bacterial biofilms. Changes in environmental factors such as temperature, pH, oxygen, and nutrient content can also affect the dispersion process of bacterial biofilms. For example, low-oxygen environments can facilitate bacterial biofilm dispersion by accelerating the rate of c-di-GMP degradation. Increased glucose levels can reduce the amount of c-di-GMP in the organism and promote flagellar synthesis, which slows down the progress of separation (Lee and Yoon, 2017).

The process of bacterial biofilm formation is influenced by temperature and blood pH changes, nutrient content, quorum sensing, Brownian motion, and surface properties. At the same time, different strains and signal transduction also affect the formation of bacterial biofilm. The structure of mature biofilm is a matrix layer, regulatory layer, connective layer and bacterial biofilm layer from inside to outside.

Microorganisms can form biofilms on the surface of the device, causing the development of infectious diseases in the organism. Medical implants have brought hope to the medical revolution and provided new opportunities for human life and health progress. Still, they also increase the risk of infections in the body tissues. Bacterial adhesion is the first step in forming biofilms for device-related infections and is divided into two stages: initial non-specific reversible adhesion and specific irreversible adhesion. *S. aureus* and *S. epidermidis* are the main strains (Pietrocola et al., 2022). These microorganisms can come from the patient's skin, the healthcare worker's skin, or the environment. *S. epidermidis* adheres to each other and medical devices by using adhesins. *S. aureus* relies on adhesin ligands (fibronectin, fibrinogen, and collagen) for its adhesion (Darouiche, 2001). The prerequisite for device-related biofilm formation is the coating of the medical device with plasma proteins (Arciola et al., 2018). The type and amount of plasma proteins adhered to the device surface are mainly determined by the surface's physicochemical properties and the plasma proteins' characteristics. When *S. aureus* sticks to the surface of a medical device, it can interact through adhesins. Adhesins specifically recognize plasma proteins coated on the surface of the device. *S. aureus* can then proliferate and produce EPS composed of extracellular polysaccharides, proteins, and eDNA. The final stage is when the *S. aureus* community disperses and spreads the infection (Pietrocola et al., 2022). Inhibition of EPS production, enzyme-promoted EPS degradation, and surfactants all

contribute to the bacterial dispersion process (Solano et al., 2014). The characteristic change of biofilm dispersion in *S. aureus* is the formation of phenol-soluble modulins (PSM) and extracellular enzymes. PSM plays an essential role in the diffusion stage of biofilm. It disrupts the non-covalent binding forces that strengthen the biofilm matrix, helping to form channels for transporting nutrients to deeper biofilm layers (Peschel and Otto, 2013).

Biofilms are a persistent cause of infection in implanted medical devices. The formation of device-related biofilms is closely related to the interactions between microbial cells. The common microorganisms that can form biofilms on the surface of equipment include *S. aureus*, *S. epidermidis*, *E. coli*, *P. aeruginosa*, *K. pneumoniae*, and *Enterococcus faecalis*. When a medical device is contaminated with these microorganisms, the formation of biofilms depends on several factors. First, the microorganisms must adhere to the exposed surface of the implant long enough to reach the irreversible attachment stage. The adhesion speed of microbial cells on the surface of the device mainly depends on the content and types of bacterial cells in the liquid exposed by the equipment, the liquid's flow speed, and the physical and chemical properties of the surface. At the same time, the composition of the fluid can change the properties of the device's surface and affect the rate of cell attachment. When microbial cells irreversibly adhere to the surface of a medical device and produce EPS to form a biofilm, the rate of growth and development is influenced by the flow rate, nutrient content, antimicrobial concentration, ambient temperature, and pH (Donlan, 2001). In the absence of antimicrobial agents, when a medical device is implanted in a host, the surface of the device is immediately surrounded by multiple fluids (e.g., blood, saliva, urine, and other fluids). Mucopolysaccharides, glycoproteins, and metal ions then appear within minutes. These substances can penetrate and adhere to the surface of the device. The bacterial cells can use their surface-specific adhesion molecules to recognize the device surface receptors and thus undergo the adhesion process. Once the microorganism adheres to the device surface, the gene expression level is immediately affected. During the growth and reproduction phase, bacterial cells can synthesize EPS, form microbial communities, and then form biofilms (Huang et al., 2022).

Microorganisms colonize almost all central venous catheters implanted in patients. The most common microorganisms that form catheter biofilms are *S. aureus*, *S. epidermidis*, *P. aeruginosa*, and *K. pneumoniae* (Elliott et al., 1997). These microorganisms can move outward from the skin or inward from the port along the outer surface of the central venous catheter. Colonization of the catheter surface by microorganisms can occur within 24 hours. Biofilms can commonly form on the surface of central venous catheters, but the location and extent of bacterial biofilm formation are influenced by the time of catheter implantation. When the catheter is implanted <10 days, more biofilms can form on the external surface of the catheter. When implanted >30 days, biofilms are more likely to form in the catheter lumen (Raad et al., 1993). Common contaminating microorganisms on urinary catheters are *S. epidermidis*, *E. faecalis*, *E. coli*, *P. aeruginosa*, and *K. pneumoniae*. When the catheter is implanted in the body, these microorganisms tend to form biofilms on the internal and external surfaces. The longer the catheter is left in place, the greater the ability of these microorganisms to form biofilms and the greater the likelihood of causing urinary tract infections.

Microorganisms can form biofilms on non-device (tissue) surfaces. There are several stages of dental plaque biofilm formation. First, the tooth's surface is covered with an organic "membrane" composed of immunoglobulins, carbohydrates, and glycoproteins. These substances can adhere to the surface of hydroxyapatite through electrostatic interactions. This interaction is generated between Ca2+, phosphate, and molecular groups with opposite charges in saliva. Among other things, carbohydrates comprise intracellularly stored polysaccharides and other intracellularly present polysaccharides. Water-insoluble glucans and fructans promote the attachment of bacterial cells to the tooth surface (Jakubovics et al., 2021). Bacterial cells can bind to surface organic membranes, leading to interactions between adhesion factors and fimbriae, capsules, and complementary receptors. Subsequently, the bacterial cells adhering to the tooth surface can produce various exopolymers to synthesize biofilm EPS (Mirzaei et al., 2020). Maturation and dispersion of dental plaque biofilm is the final stage. During the initial process of dental plaque biofilm formation, the source of nutrition for microbial cells is through the breakdown of salivary substrates (e.g., mucins and other glycoproteins) (Jakubovics, 2015). *P. aeruginosa* is the leading cause of death in patients with cystic fibrosis combined with *P. aeruginosa* infection due to its high virulence factor, biofilm formation, and resistance to antimicrobials. High levels of c-di-GMP expression generally promote matrix production and biofilm formation. In contrast, low levels of c-di-GMP expression down-regulate matrix production and can lead to a bacterial planktonic lifestyle. Carbon starvation and nitric oxide signaling can affect phosphodiesterase activity in *P. aeruginosa* cells, reducing the intracellular expression of c-di-GMP in the cells (Bjarnsholt et al., 2010). *P. aeruginosa* can produce a small molecule that can induce the dispersion of mature biofilms (Davies and Marques, 2009).

Bacterial biofilms provide an excellent and stable homeostasis environment that prevents host immune cells and antibiotics from entering the bacterial biofilm community while protecting bacterial microorganisms from the effects of blood pH, osmotic pressure, and nutrient deficiency. Thus, by providing a physical barrier for bacteria and microorganisms, bacteria can communicate with each other and co-exist, even in harsh conditions. This communication mechanism, called the quorum sensing system, comprises extracellular chemical signals (known as autoinducers). The QS system can help bacteria and microorganisms sense population density and influence biofilm formation and maturation, antibiotic resistance, bacterial communities, and bacterial-host interactions (Whiteley et al., 2017; Paluch et al., 2020). At the same time, some signaling molecules in bacterial microorganisms, such as c-di-GMP, can affect bacterial behavior, including cell cycle, cell movement, pili synthesis, RNA regulation, stress response, and bacterial virulence (Loera-Muro et al., 2021). Bacterial biofilms have specific immune escape mechanisms, including inhibition of immune cell function, alteration of gene expression, obstruction of immune recognition, and mechanical protection (Campoccia et al., 2019; de Vor et al., 2020). When

bacterial organisms accumulate on the surface and form biofilms, the clearance function of immune cells is impaired, a phenomenon known as impaired phagocytosis (Urwin et al., 2020).

To provide additional research on bacterial biofilms, we review bacterial biofilm-associated infections, describe current methods used to detect biofilms and effective strategies for treating bacterial biofilms, and give an outlook on the development and future of bacterial biofilms.

2 Biofilm-associated infection

Bacterial biofilms can cause serious infections, such as multidrug-resistant, broad-spectrum drug-resistant, and complete drug-resistant bacteria. Currently, more than 80% of bacterial infections are caused by the formation of bacterial biofilms (Fleming and Rumbaugh, 2017). Bacterial biofilms can cause disease in the body through device-related and non-device-related infections. The following will describe the biofilm infections in terms of both and the relationship of bacterial microorganisms to infectious diseases and adhesive surfaces.

2.1 Device-related infections

The use of medical devices improves the quality of life for patients. Still, suppose bacterial biofilms form on the surfaces of medical implants (e.g., dental devices, catheters, heart valves, ventricular shunts, joint prostheses). In that case, they may cause bloodstream and urinary tract infections, posing a severe threat to global health. Medical device-associated infections are closely linked to biofilm formation, and the bacterial biofilm on the surface of most devices is composed of a variety of bacteria. Bacterial organisms first attach to the surface of the medical device or the surrounding tissue of the breakage. Bacterial cells proliferate, develop, and form a bacterial biofilm, which is then encapsulated in the EPS. At the same time, the bacterial cells are released from the bacterial biofilm. They can be transmitted through the bloodstream leading to infection or recurrence of localized lesions elsewhere in the body.

Cardiac implants, including pacemakers, artificial heart valves, cardioverter-defibrillators, and cardiovascular implantable electronic devices, are associated with higher morbidity and mortality due to infections (Habib et al., 2013). Gastrointestinal devices are associated with a wide range of microorganisms. A study using scanning electron microscopy showed defects in percutaneous endoscopic gastrostomy cannulas (PEGs), which can provide suitable sites for the attachment of bacterial microorganisms and biofilm formation (Dautle et al., 2003). The study found that bacterial biofilms were present on the surfaces of all devices included in the examination and that PEGs are a risk factor for colonization of the gastrointestinal tract by drug-resistant bacterial microorganisms and the formation of bacterial biofilms. Orthopedic implant surgery is often a safe and efficient treatment modality that restores hip and knee function and enhances patient well-being. However, there are still postoperative complications, the most common of which is an artificial joint infection, on top of which the formation of a combined bacterial biofilm may lead to osteomyelitis.

Neurosurgical implants include cerebrospinal fluid shunts, extra-ventricular cerebrospinal fluid drains, and neurostimulators. The main microorganisms in cerebrospinal fluid shunts are *S. epidermidis* and *S. aureus* (Fux et al., 2006). The microorganisms capable of forming biofilms on extra-ventricular cerebrospinal fluid drains are mainly *S. aureus*, followed by *Propionibacterium acnes* (Strahm et al., 2018). In neurostimulator-associated infections, common pathogenic microorganisms include *S. aureus*, *P. aeruginosa*, and *P. acnes* (Conen et al., 2017). The incidence of infection with these devices is 3-15%, with a higher incidence of infection with extra-ventricular cerebrospinal fluid drains (Caldara et al., 2022). These infections can be fatal to patients and increase morbidity and mortality. Permanent or temporary urinary catheters, nephrostomy tubes, penile implants, and ureteral stents are the most commonly used devices in the genitourinary system. Bacterial biofilms can be found on the surfaces of all these devices. In most clinical situations, infections from implanted stents occur, with fever and urinary tract infections being the most common complications, and even bacteremia and death may occur (Kehinde et al., 2002). Endovascular devices commonly used in clinical practice include intravenous infusions, hemodialysis, haemodilution, and parenteral nutrition. The risk of infection is increased by irregular disinfection, environmental contamination, and incomplete biofilm removal from the surface of implanted devices. To reduce the risk of infection, we should improve disinfection protocols and procedures in the future and detect the propensity for contamination of all types of implanted devices. Breast implants can be used for breast reconstruction and cosmetic surgery, helping improve patients' quality of life. However, breast implants are susceptible to complications such as infection, hematoma, contracture of the envelope, and scar formation. Contracture can lead to the removal or revision of the implant, causing discomfort and swelling of the breast and affecting its appearance. The researchers detected bacteria in 85% of the breast implants that developed periosteal contracture. They examined them using scanning electron microscopy and found bacterial biofilms in over half of the implants (Pajkos et al., 2003). *P. acnes*, *Streptococcus* spp., *Lactobacillus* spp., *Bacillus* spp., and *Mycobacterium* spp. can survive in the environment around breast implants and form a bacterial biofilm.

Bacteria in the mouth are closely linked to diabetes, heart disease, lung inflammation, and systemic diseases. Prevention and treatment Kalamaraof oral diseases can help prevent these diseases. Oral implants can be used to restore the normal function of the mouth. When bacterial microorganisms colonize the surface of these materials, a solid bacterial biofilm usually forms, leading to inflammation around the implant, which may damage healthy gums. The microorganisms can degrade the composite resin, and the bacteria can invade the implant and tooth interface, leading to severe consequences. Clinicians can apply prophylactic antibiotic treatment to avoid this outcome. At the same time, proper treatment planning, proper implant placement, attention to changes in condition, medication history, and monitoring of

underlying health conditions (e.g., diabetes, hypertension, obesity, osteoporosis) are essential to prevent implant failure. Bacterial keratitis is a cornea infection characterized by forming a bacterial biofilm on the eye's surface. If patients do not receive timely and effective treatment, it will likely lead to vision loss or even loss of vision. Bacterial keratitis is associated with various risk factors, such as corneal trauma, contact lens wear, surgical treatment of the eye, and immunocompromised systemic disease (Ng et al., 2015). Corneal trauma is a significant risk factor for bacterial keratitis in developing countries. Contact lenses are the primary source of bacterial keratitis infection in more developed countries. It can alter the corneal epithelium and carry bacterial organisms to the eye's surface. Bacterial keratitis is associated with the formation of a variety of bacterial biofilms. The lens materials (e.g., water retention, hydrophobicity) and contact lenses' physical and chemical properties can influence the colonization of bacterial biofilms. We should follow up with a vigorous search for novel materials to prevent implantable device-related biofilm infections. The most common bacterial organisms on the surface of medical devices are described in detail in Supplementary Table 1. In conclusion, medical device implant-related biofilm infections increase morbidity and mortality in patients, especially hospitalized patients, and pose a severe threat to their quality of life. We should pay more attention to the composition of different bacterial microorganisms on the surface of specific medical devices, continue to study biofilms *in vivo*, and systematically describe the interrelationship between bacteria on device surfaces and the surrounding environment of implants.

2.2 Non-device-related infections

Non-device-related infections also have a significant impact on health problems. Dental plaque (Rabe et al., 2022), urinary tract infections (Singh et al., 2022), cystic fibrosis (Vandeplassche et al., 2020), otitis media (Bair et al., 2020), infective endocarditis (Han and Poma, 2022), tonsillitis (Klagisa et al., 2022), periodontitis (Prado et al., 2022), necrotizing fasciitis (Grier et al., 2021), osteomyelitis (Huang et al., 2022), infective kidney stones (Fayez Hassan et al., 2021), chronic inflammatory diseases (Wu et al., 2015), bacterial vaginitis (Arroyo-Moreno et al., 2022), and bladder infections (Mirzaei et al., 2020) are all examples of non-device-related bacterial biofilm infections.

The human oral environment, with its favorable temperature and humidity and rich in micro-nutrients, can provide adequate conditions for bacterial growth, survival, and the formation and maturation of dental plaque biofilms. The most common microbial cell grouping in the oral cavity is the bacterial cell, followed by various fungi, viruses, and protozoa. Oral microorganisms co-exist with each other, maintain mutually beneficial relationships with their hosts, and generally do not cause disease. If this community changes, the symbiotic and mutually beneficial balance will be disrupted, leading to various conditions, such as dental caries. Bacterial microorganisms in the mouth can enter the circulation, affect the heart's function, and bind fatty plaque in the coronary arteries. Dental biofilms can cause periodontitis and gingivitis and even lead to tooth decay. Chronic bacterial infections cause almost all periodontal diseases. Periodontal infections increase the incidence of inflammation, promote the formation of plaque, and lead to edema in the coronary arteries. During the maturation of bacterial biofilms, anaerobes are the main colonizing bacteria in the human mouth. Several studies have shown that dental biofilms can cause not only the development of periodontitis but also various systemic diseases such as diabetes mellitus, infective endocarditis, and rheumatoid arthritis (Larsen and Fiehn, 2017; Marsh and Zaura, 2017). The main bacteria that play a role include *Porphyromonas gingivalis*, *Bacteroides forsythus*, and *Aggregatibacter actinomycetemcomitans*.

Lactobacillus strains can be associated with health problems by producing lactic acid to maintain a low pH environment in the vagina, thereby protecting the female genitourinary tract from bacterial microorganisms not of its origin. *Lactobacillus* spp. can play a role in maintaining the homeostasis of the vaginal environment while preventing bacterial microbes from colonizing and infecting it. Women are more prone to urinary tract infections than men because of the proximity of the female urethra to the anus, vagina, and rectum. Disturbances in the body's vaginal bacterial microbiota also increase women's risk of urinary tract infections. Estrogen plays a role in maintaining a low pH environment in the vagina, and post-menopausal women are more likely to develop urinary tract infections than younger women due to a lack of estrogen. The most common pathogenic bacteria for urinary tract infections in adult women is *E. coli*. Uropathogenic *E. coli* (UPEC) strains may evade the body's immune response by stimulating a pro-inflammatory reaction or obscuring the immunogenic bacterial component. Bacterial biofilms may play a key role in maintaining the sustainability of UPEC strains in the bladder and vagina. The second most common pathogen of urinary tract infections is *Proteus* spp. When they first adhere to surfaces, *Proteus mirabilis* can proliferate, develop and form biofilms, enhancing the antimicrobial properties of bacterial microbes and protecting the bacteria from the body's immune function. Bacterial biofilms are an essential factor in the persistence and existence of bacterial infections, and their diversity can influence the viability and survival of bacterial microorganisms (Delcaru et al., 2016). In addition, bacterial biofilms play an important role in renal pathology and can affect renal stones and the dialysis system. Pathogenic bacteria invade renal tissue and can cause chronic pyelonephritis and bacterial prostatitis. Most of the *E. coli* strains isolated from bacterial prostatitis exhibit the potential to form bacterial biofilms.

Bacterial vaginitis is the most common vaginal infection worldwide and severely impacts the quality of life of women who suffer from it. It is characterized by increased vaginal discharge, usually accompanied by a specific irritating odor. Various bacterial biofilms are present on the surface of the vaginal epithelium. *Gardnerella vaginalis* is associated with bacterial vaginitis infections and has been shown in several studies to produce bacterial biofilms on vaginal tissue and enhance the expression of various virulence factors (Castro et al., 2015; Gaspar et al., 2021).

Cystic fibrosis responds poorly to medications and is one of the chronic inflammatory diseases. Several studies have shown that

most people with cystic fibrosis are susceptible to *P. aeruginosa* infections (Harrison, 2007; Filkins and O'Toole, 2015). *P. aeruginosa* infections in combination with cystic fibrosis are challenging to cure, mainly due to the formation of bacterial biofilms in the lungs of patients with cystic fibrosis. *P. aeruginosa* can colonize, develop and form bacterial biofilms in the lungs of people with cystic fibrosis due to the excessive release of mucus in the airways, providing an environment with low oxygen levels. Chronic *P. aeruginosa* infection can lead to complications such as epithelial tissue damage, mucus obstruction of the airways, respiratory dysfunction, and even accelerated death.

Infective endocarditis is a refractory disease that severely threatens human life and health. Although medical technology has been refined, the mortality rate of patients with co-infected endocarditis during hospitalization is still higher than 20% (Beynon et al., 2006). The ability to generate bacterial biofilms is critical in the virulence of bacterial microbes associated with infective endocarditis. Studies (Elgharably et al., 2016; Polewczyk et al., 2017) have confirmed that many bacterial microorganisms can form infectious neoplasms on the surface of the heart, which can lead to the development of infectious endocarditis. These neoplasms are essentially large bacterial biofilms. Using immunofluorescence staining techniques and electron microscopy, Bosio et al. (2012) found *Mycobacterium fortuitum* biofilms on infected artificial biological heart valves. Bacterial microorganisms shed from biofilm structures and enter the blood circulation, and the body will develop bacteremia and sepsis manifestations. Of these, bacteremia is controlled by the collective immune defense system and antimicrobials. Although bacteremia can be effectively prevented or even eliminated with aggressive treatment, the deeper biofilm and neoplasm structures can provide a "hideout" for the ever-present bacterial biofilm cells. When bacterial cells in biofilm structures are repeatedly shed, it is easy to develop septic embolism in the distal limb (Mirzaei et al., 2020).

Otitis media is a complex inflammatory disease, and its complications are a major cause of hearing loss. Approximately 75% of infants under three years suffer from middle ear-associated infections. Bacteria capable of forming biofilm in the middle ear are the leading cause of chronic bacterial infections. Using molecular methods, researchers have demonstrated that the DNA of *Haemophilus influenzae*, *Moraxella catarrhalis*, and *Streptococcus pneumoniae* can be detected in up to 80% of infants with otitis media (Otsuka et al., 2013).

The formation of bacterial biofilms can lead to severe chronic inflammatory and autoimmune diseases in the body. L-type pathogens and chronic biofilm infections can cause the development of inflammatory diseases. The vitamin D receptor is an alkaline substance that regulates the activity of immune cells and is the primary defense against bacterial microbial infections. Specific L-type and biofilm-forming pathogens can produce a substance that adheres to and kills the vitamin D receptor. Thus, as chronic bacterial biofilms and L-type pathogens accumulate in the body, most bacterial microorganisms can produce substances that inactivate the vitamin D receptor and severely compromise the body's immune defenses. Supplementary Table 2 describes non-device-related biofilm infections.

2.3 Bacterial biofilm cause tissue related and device associated infections

S. aureus and *S. epidermidis* can form biofilms on the surfaces of central venous catheters, heart valves, suture devices, and prostheses, in turn, can cause nosocomial infections, endocarditis, mucus cysts, and otitis media (Qu et al., 2010; Arciola et al., 2012). *P. aeruginosa* forms biofilms on the surface of contact lenses, central venous catheter, middle ear, and prosthesis, which can cause nosocomial infection, cystic fibrosis, and otitis media (Wiley et al., 2012; Huse et al., 2013). Bacterial biofilms formed by *S. aureus*, *E. coli* and *Streptococcus agalactiae* can cause mastitis (Loera-Muro et al., 2021). *E. coli* can form biofilms on medical devices such as catheters (Zhang et al., 2019), ultrasonic instruments (Khatoon et al., 2018), and contact lenses (El-Ganiny et al., 2017). The relationship between bacterial microbes adhering to surfaces to form bacterial biofilms and thus causing disease is detailed in Supplementary Table 3. The formation of bacterial biofilms will increase mortality in hospitalized patients (Batoni et al., 2016; Evans and Bolz, 2019). Multiple biofilm infections may exhibit different antibiotic sensitivities. Although the specific details of bacterial interactions in numerous microorganisms are not yet precise, there are metabolic links and spatial organization among bacteria, which may result in quorum sensing and resistance gene transfer to produce more antibiotic-resistant biofilms (Røder et al., 2020; Sadiq et al., 2021).

The three-dimensional structure of bacterial biofilm can act as a natural barrier to antibiotics and reduce the sensitivity of biofilm to antibiotics. Bacterial biofilm resistance to antibiotics is known to be 10–1000 times higher than planktonic bacteria (Ning et al., 2014), which may be related to the different antibacterial mechanisms between them. Biofilm communities produce antibacterial target mutations, efflux pumps, higher transverse transfer frequency, reduced cell permeability, and drug-neutralizing proteins (Kumar et al., 2013; Lata et al., 2015; Sharma et al., 2015; Sharma et al., 2016). In addition, there is a particular type of bacterial cell phenotype in biofilms – persistent cells, which can survive under the action of a powerful immune defense system and powerful antibiotics. These cells have metabolic inertia, slow growth and replication, and can regulate virus-antitoxic systems and enhance antioxidant and DNA repair systems. They show an inability to respond to antibiotics (Rather et al., 2021). Anoxia, nutrient deficiencies, antibiotic modification enzymes, and oxidative stress can also lead to antibiotic resistance in bacterial biofilms (Hall and Mah, 2017). Due to the phenotypic diversity of bacterial biofilms, the content of antimicrobials entering the biofilms will be reduced, and the microenvironment within the biofilms will be changed, causing the biofilms' resistance mechanism to antibiotics (Sharma et al., 2019), making it difficult to eradicate. In addition, genetic mutations can also lead to antimicrobial resistance in bacterial biofilms. As a result, the effect of antibiotics commonly used in clinical practice on bacterial biofilms is insignificant.

In recent years, due to the increasing incidence of iatrogenic bacterial biofilm-associated infections, long-term infections are difficult to cure, which will pose a new challenge to preventing and controlling infectious diseases caused by biofilms. In addition,

bacterial biofilms can avoid the scavenging action of conventional antibiotics and the killing effect of the body's immune system and become a possible source of infection. Currently, methods for detecting, inhibiting and treating biofilm-associated infections are inadequate, and managing bacterial biofilm-associated infections remains a significant challenge. In addition, due to the specific environment within the biofilm, we cannot treat biofilm-associated infections with traditional antibiotics, and researchers must propose new antimicrobial or anti-biofilm-associated treatment strategies.

3 Methods for detecting bacterial biofilms

3.1 Nuclear medical imaging technology

Nuclear medicine imaging remains the standard method for detecting infectious diseases (Salmanoglu et al., 2018). As radionuclides, technetium-99m, indium-111, and iodine-125 have been shown to be useful for radio-labelling compounds. Still, some drawbacks exist, such as low expression of target receptors on the bacteria studied, non-specific adsorption, and complex radiochemical synthesis (Eggleston and Panizzi, 2014). A recent study found that as a metabolic product of bacteria, the maltodextrin transport system can also radially label compounds and trace them to detect bacterial biofilm infection (Auletta et al., 2019). Nuclear medicine imaging technology also has certain disadvantages, such as the need for specialized equipment and instruments, operator training, and patient exposure to radiation (Cruz et al., 2021).To further improve the sensitivity of nuclear medicine imaging, relevant researchers have developed an MH18F nuclear imaging agent, which can participate in the metabolism of bacterial carbohydrates and be internalized by maltodextrin transporter specific to bacteria (Auletta et al., 2019), contributing to the early detection of bacterial biofilms.

3.2 Ultrasonic technology

Ultrasonic technology can monitor dirt on instrument surfaces in real-time and has been shown to monitor the formation and growth of some bacterial microbial colonies (Kujundzic et al., 2007). Combined with other methods, it can enhance the detection strategy of bacterial biofilms (Vaidya et al., 2014). Ultrasound echo enhancers and microbubble contrast agents have opened up new avenues in diagnostic ultrasound medicine (Calliada et al., 1998). Ultrasonic medical imaging technology has matured with the application of contrast media, which contributes to the accuracy of medical diagnosis. The application of targeted ultrasonic contrast media is conducive to determining the difference between healthy and infected tissues (Unnikrishnan and Klibanov, 2012). The acoustic impedance of bacterial biofilms is similar to that of human tissue, making detection and *in vivo* targeting of bacterial biofilm substrates difficult. The combination of ultrasound and targeted ultrasound contrast agents can aid in the early detection and identification of bacterial biofilms and can help to improve therapeutic efficacy. Ligand-targeted ultrasound contrast agents can be a non-invasive imaging method for detecting early and late-stage bacterial biofilms. These agents can target, image, and detect the formation of the *S. aureus* biofilm matrix *in vitro* (Anastasiadis et al., 2014).

3.3 Crystal violet staining method

Crystal violet (CV) is the most commonly used staining method for the quantitative determination of microtiters of biofilms grown *in vitro* in polystyrene pore plates (Hassan et al., 2011). After CV staining, the structure of the biofilm can be observed directly by scanning electron microscopy. However, this staining method also has certain limitations, as it can reduce the number of bacterial biofilms after multiple washing (Hou et al., 2022), and the incubation time is longer. It is unsuitable for the rapid detection of biofilms. Castro et al. (2022) found that CV staining was highly effective for single-species biofilm detection. Still, in bacterial vaginosis, there might be bias in evaluating the formation of multiple bacterial biofilms.

3.4 Other detection methods

Bioluminescence analysis, tissue culture plate method, and percentage transfer method are also used to detect bacterial biofilms. Certain imaging techniques, such as infrared spectroscopy, reflection spectroscopy, optical fluorescence imaging, confocal laser scanning microscopy, target fluorescence imaging, and fluorescence *in situ* hybridization of peptide nucleic acid, can also be used to detect the formation of biofilms and provide spatial information on the distribution of strains and biofilms (Roy et al., 2018; Cruz et al., 2021). However, these imaging techniques depend on clear samples and are unsuitable for *in situ* bacterial biofilm detection. Raman and surface-enhanced spectroscopy offer high sensitivity and are non-invasive molecular detection techniques (Xu Y. et al., 2020). Laser capture micro-cutting technology has a high resolution, which can help researchers quickly separate or sample the required cells from solid tissue by laser beam, which is helpful for the detection of living biofilms. Ultra-wide-spectrum imaging is a labeling-free detection method showing bacterial biofilms in natural and wound environments.

One of the components of bacterial biofilm is protein, which is related to the types of pathogens and the stages of biofilm development and virulence. Several different proteins are listed below for their role in forming and maintaining biofilm structures. *S. epidermidis* expresses a variety of cell wall-anchored surface proteins that promote the formation of biofilms on the surface of medical devices, aid in binding to the EPS, and are a significant determinant of the virulence of *S. epidermidis*. For example, SdrG/Fbe protein can promote adhesion to the surface of conditioned biomaterials. SdrF protein enhances the adhesion between bacteria and fixed collagen. Embp protein can promote bacterial adherence to fixed fibronectin. Sesl protein may promote adhesion between bacteria and non-living surfaces. Sbp protein can

promote the formation of amyloid protein and maintain biofilm integrity (Foster, 2020). McCourt et al. (2014) found that surface-bound fibronectin FnBPA and FnBPB could mediate the formation of methicillin-resistant *S. aureus* (MRSA) biofilm, increase bacterial aggregation, promote initial microbial adhesion on the surface, and facilitate biofilm accumulation. Manfiolli et al. (2018) showed that MAP kinases (MpkA, MpkC, and SakA) and phosphatases could regulate the *Aspergillus fumigatus* cell wall composition and affect cell adhesion and EPS production, as well as have essential effects on signaling pathways during biofilm formation. Liang et al. (2011) identified a novel cell surface protein, BapA1, from *Streptococcus parasanguinis* FW213 and found that it can affect biofilm formation. The BapA1 protein contains multiple putative fimbriae isopeptide junction structural domains that promote the aggregation of bacterial fimbriae in Gram-positive bacteria and is a novel streptococcal adhesin. When the BapA1 protein is deficient, it can inhibit the auto-aggregation of bacterial cells. Ye et al. (2018) found that outer membrane protein W (OmpW) contributed to the survival of *Cronobacter sakazakii* cells in a planktonic mode under the stress of NaCl and that the ability of cells to survive and form biofilms increased with increasing OmpW concentration.

Quantitative proteomics technology based on iTRAQ is helpful for the detection of bacterial biofilms and the search for promising targets for biofilm elimination (Sauer, 2003). The meta-proteomic analysis is an important technique for showing the interactions and functional roles of individual members of bacterial microbial communities. The areas of proteomics include protein function, expression level, post-translational modification, localization, stability, and adequate genome sequencing. Proteomic patterns are responses to the physiological state of cells and can elucidate bacterial biofilm phenotypes (Khemiri et al., 2016). Through the proteomic analysis of *Burkholderia pseudomallei* in the floating state and biofilm state, Khan et al. (2019) found that the change of proteome contributed to the survival of the biofilm by increasing the abundance of pressure proteins and reducing the presence of metabolic proteins. Ali Mohammed et al. (2021) used proteomic analysis to determine the proteome of *Fusobacterium nucleatum* and *P. gingivalis* expressed in the planktonic or biofilm state. The results showed that *P. gingivalis* produces fewer proteins due to the presence of *F. nucleatum* in the mouth. Resolution and dynamic range limit the initial development of proteomics techniques based on electrophoresis. The addition of transcriptomic analysis has led to the rapid development of proteomics because of its ability to detect solid structures capable of detecting functional cells. Charlebois et al. (2016) confirmed that by RNA transcriptional sequencing technology, 25.7% of genes were different between *Clostridium perfringens* biofilms and planktonic cells. About 12.9% of genes in biofilm cells were down-regulated, and about 12.8% were up-regulated. After leptospira forms a mature biofilm, some fundamental biological processes, such as DNA replication and cell division, are down-regulated. Transcriptome-based sequencing techniques can focus on transcriptional changes associated with leptospirosis biofilm formation and maturation (Iraola et al., 2016). *Fusobacterium nucleatum* stain ATCC 25586 at the planktonic cell and biofilm stages by RNA sequencing. It was confirmed that 110 genes of the *F. nucleatum* biofilm state differed from those of planktonic cells. The 85 down-regulated genes in the biofilm state are mainly related to cell proliferation, division, and oxidative stress. The 25 up-regulated genes are primarily associated with amino acid and carbohydrate metabolism (Zhao et al., 2022).

Metabolites are generated in the presence of metabolic enzymes and are the end products of gene expression processes. Many of the life activities in microbial cells (e.g., energy release, cellular signal release, and intercellular communication) are regulated by metabolites. Metabolites can reflect the microenvironment in which a bacterial cell is located and are also closely related to the nutritional status of the cell, the effects of drugs, contaminants, and other external factors. Several metabolites are listed below for their functions in biofilms formed by bacterial pathogens. Glucose, as the primary carbon source and metabolite, can upregulate the expression of extracellular polysaccharide-related gene pslA, which is conducive to promoting the formation of *P. aeruginosa* biofilms and changing metabolic pathways. Glucose could lead to decreased expression of 18 metabolites (including inositol, glutamine, 4-acetyl butyrate, myristic acid, and β-alanine) and increased expression of 7 metabolites (including fructose, 3-hydroxy propionic acid, and glucose-6-phosphate) in *P. aeruginosa* biofilms (She et al., 2019). Guanosine 59-diphosphate 39-diphosphate is also a metabolite that regulates the expression of a large number of genes and plays a vital role in the formation of biofilms of *E. coli*, *E. faecalis*, and *S. mutans* (de la Fuente-Núñez et al., 2014). Short-chain fatty acids, including butyrate, are also strongly associated with the pathogenesis of the periodontal disease. In the initial stage of biofilm formation, butyrate can promote early *Actinomyces oris*-dependent colonization and stimulate biofilm formation (Barbour et al., 2022). *Bacillus subtilis* can produce a variety of specific metabolites. Most of these metabolites (e.g., bacteriolysin, subtilisin A, surfactin, spore-killing factors) are associated with antimicrobial properties (Kalamara and Stanley-Wall, 2021). Schoenborn et al. (2021) investigated the role of nine specific metabolites in biofilm formation. They found that most of them (surfactin A, ComX, subtilin A, spore delaying protein, spore killing factor) could promote biofilm formation.

Metabolomics analysis techniques can reveal the processes of bacterial cell metabolism and are the study of metabolites (e.g., carbohydrates, amino acids, and lipids), intermediate metabolites, and other signaling molecules. The technique emphasizes discrete altered metabolic pathways and highlights biological small molecule metabolites. The Metabolite group is a complete assemblage of all metabolites in the tissues, organs, and compartments of biological cells that are extracted from cells or expressed as bodily fluids (Zhang and Powers, 2012). Metabolomics techniques focus on the broad or total analysis of cellular metabolites through high-throughput detection methods rather than localized and targeted analysis of specific numbers of individual metabolites (Fiehn, 2002). Many metabolic pathways between planktonic bacterial cells and biofilms were changed. Through instrumental analysis, bioinformatics, stoichiometry, and cell biology, metabolomics analysis can show the status of the overall metabolites, simplify the process of metabolite detection, and cover almost all metabolic changes of major pathways. Metabolomics analysis provides a systematic method for characterizing complex bacterial

communities, showing the behavior of bacterial cells in biofilms, and contributing to the understanding of biofilms. In addition, biofilms' strain type and antimicrobial resistance are phenotypic by their differences from the metabolome. Shen et al. (2020) showed that carnosol could inhibit the formation of *S. aureus* biofilm by metabonomics analysis technique.

The fiber optic biosensor is capable of monitoring the growth quality of bacterial biofilms, quantifying analytes, and displaying biofilm properties. It works by monitoring the environment around the sensing element through changes in the refractive index. The sensor offers the following advantages: lightweight construction, compact size, biocompatibility, low fabrication costs, and real-time monitoring. The spherical resonance sensor is highly sensitive and can detect changes in the surface of bacterial cells, such as planktonic cells attached to the surface of an object, and has great potential for early detection of the presence of bacterial biofilms (Rakhimbekova et al., 2022). SiNW-FET, as a new nanosensor, can be combined with microfluidic technology to realize real-time, rapid, and fully automated detection of bacterial biofilms. It can reveal the biological and metabolic processes occurring in bacterial biofilms and has the advantages of high sensitivity, low consumption, non-invasive and traceless (Yeor-Davidi et al., 2020). Dai et al. (2022) reported a PH-responsive branched polymer [poly(MBA-AEPZ)-AEPZ-NA] capable of reducing the dose of antibiotics and overcoming antimicrobial resistance. It can emit intense green light rays in the local bacterial biofilm microenvironment (pH 5.5) to detect biofilm formation in real time. AmyGreen, a water-soluble amino ketone fuel, is a stain that enables the visualization of the amyloid component of the extracellular polymeric substances of bacterial biofilms. It can detect pathological amyloid proteins *in vitro* as a potent fluorescent dye. The application of the AmyGreen stain effectively reduced the risk of false positives when measuring the amyloidogenic fibrils of biofilms. In combination with other stains can be used for confocal fluorescence microscopy (Moshynets et al., 2020). Pandit et al. (2021) have developed a simple sensor of raw, non-functional graphene that is simple to manufacture and can be powerful without the need for precise species identification. It can distinguish and detect different bacterial types according to different growth dynamics, adhesion density, adhesion pattern, and colony formation between bacterial cells, which is helpful for the early detection of bacterial microbial colonization and biofilm formation. A new diagnostic kit is the product of a combination of two reagents, one that relies on a substance that promotes hydrogen peroxide to produce oxygen through catalase and the other a mobile biosensor. The kit can detect *P. aeruginosa* infection in sputum with high sensitivity and specificity within 8 minutes (Clemente et al., 2020). Bacterial biofilms attached to the mucous membranes of the mouth are difficult to visualize with the naked eye. Quantitative light-induced fluorescence (QLF) can detect bacterial infections in the oral cavity and the formation of dental biofilms. Park et al. (2022) demonstrated using QLF to detect and remove pathological biofilms from oral mucosa in elderly patients during hospitalization. The test tube method and Congo red agar technique can help detect biofilm formation by obtaining isolates of bacterial biofilm formation from contact lenses, the conjunctiva of contact lens wearers, and decorative contact lens cases (Raksha et al., 2020). Kouijzer et al. (2021) demonstrated that microvesicles in vancomycin-modified bacteria could detect the formation of *S. aureus* biofilms and could potentially treat *S. aureus* biofilm-associated infections.

Artificial intelligence technologies have also been found to be beneficial for detecting bacterial biofilms due to their powerful computational and learning capabilities. For example, biosensors based on electrochemical impedance spectroscopy can be used to detect *E. coli* biofilms (Xu et al., 2022). Convolutional neural network (CNN) can be used to detect the presence of biofilms and the formation of multiple biofilms through deep learning, with a CNN accuracy of up to 90%. Oh et al. (2022) have developed a material capable of precisely guiding the diagnosis and removal of bacterial biofilms. The material is a magnetic field-directed assembly of nanomaterials into surface topography adaptive robotic superstructures (STARS). It can adapt to complex bacterial surface topography and use automatic motion patterns to target the complex three-dimensional structure of human teeth to detect dental biofilm content with high accuracy while the effect of removing formed biofilm.

Currently, non-invasive techniques used in clinical practice have yet to provide the best method for detecting biofilms. Low practicability, low resolution and low cost-effectiveness limit the development of biofilm detection tools. Therefore, there is an urgent need to develop more accurate and practical detection techniques and diagnostic tools.

4 Strategies against bacterial biofilm removal

Bacterial biofilm inhibition is mainly achieved by physical, chemical or biological methods. Supplementary Figure 1 shows the different therapeutic strategies that inhibit bacterial biofilm formation. Physical methods include ionizing and ultraviolet radiation, damaging instruments and affecting material quality (Galié et al., 2018). Ultrasonic treatment is also one of the physical methods. Its mechanism of action is mainly through chemical and mechanical energy, including pressure, vibration, shear stress, shock waves and agitation. Stable pressure and cavitation can produce multidirectional acoustic microjets, which can damage proximal bacterial microorganisms and their biofilms. Relevant studies have confirmed the effect of plasma technology on therapeutic biofilms (Govaert et al., 2019; Patange et al., 2019). The influence of plasma on bacterial biofilms is mediated by biological activators, such as charged particles, ions, electrons, electric fields, and ultraviolet rays (Lu et al., 2016). Cold plasma can kill bacterial microorganisms and destroy the biofilm matrix. Still, the specific mechanism remains unclear, which may be related to ROS/RNS penetrating bacterial cells, oxidizing and nitrosating lipids and proteins, and then lipid peroxidation, inhibiting enzyme function, and changing DNA structure (Van Impe et al., 2018). Patange et al. (2021) found that atmospheric plasma and acoustic ultrasonic treatment technology can destroy the integrity of bacterial biofilm

structure and effectively inactivate *E.coli* and *Listeria innocua* biofilm. They also found that atmospheric plasma was more effective than aeroacoustic ultrasound in treating both early and mature biofilms. When applied in combination, the two technologies have the potential to enhance the inactivation effect. The main mechanisms of atmospheric plasma damage to bacterial biofilms include cell membrane damage, structural changes, and biological and genetic changes. Future studies are needed to understand further the distribution of active particles in atmospheric plasma and acoustic ultrasonic techniques and the detailed mechanism of inactivating bacterial biofilms.

Microneedles (MNs) are an effective and minimally invasive method for the treatment of bacterial biofilms. MNs can not only destroy the tight physical barrier of EPS and directly penetrate the antibacterial agent into the biofilm, but also provide a large specific surface area to promote the diffusion of antibiotics in the biofilm. Yi et al. (2021) combined chitosan and zinc nitrate with MNs structure to produce CS-Zn[II] MNs. This substance has good cytocompatibility, rich acicular design and a large specific surface area, and is conducive to eradicating *S. aureus* and *E.coli* biofilms.

Chemical methods are unstable, cannot play a role in mild conditions, and the price of chemistry is relatively high, prone to producing toxic byproducts. Therefore, it is not usually the preferred method for eradicating bacterial biofilms.

Biological methods have higher inhibition efficiency, which is a relatively new method against biofilm, including the application of bacteriophage, bacteriocin and enzyme treatment of bacterial biofilm. In recent years, emerging anti-biofilm preparations have been developed to limit the adhesion of bacteria on the surface to eliminate the biofilm grown or replace cells from the established biofilm (Batoni et al., 2016). The EPS matrix in biofilms plays a crucial role in evaluating the drug resistance mechanism of biofilms. The ideal anti-biofilm preparation is characterized by its unique structure, antibacterial activity, restriction of EPS accumulation, facilitation of EPS penetration into cells, interference with communication mechanisms between cells, and synergistic action with other antibacterial agents (Wiens et al., 2014).

4.1 Antimicrobial peptide

Novel antimicrobial peptides (AMPs), as a kind of cation, can down-regulate biofilm formation genes, prevent bacteria from adhering to the cell-matrix surface, down-regulate QS system signals, and produce a wide range of antibacterial activities against bacterial microorganisms (Yazici et al., 2018). When used alone or in combination with antibiotics, AMPs can effectively inhibit the formation of biofilms or even destroy mature biofilms (Mulani et al., 2019) and can be used to treat biofilm-associated infections. AMPs bind rapidly to cell membranes, reducing bacterial load while circumventing the development of resistance, and it has strong antibacterial, fungal, and viral properties (Pontes et al., 2022). One of the mechanisms of action of AMPs against bacterial biofilms is the down-regulation of gene expression and inhibition of the biological behavior of bacterial cells (e.g., synthesis of DNA, RNA, proteins, and cell walls) (Graf and Wilson, 2019). At the same time, AMPs can interact with signaling molecules, which can control the maturation process of bacterial biofilm and cooperate with antibiotics to resist bacterial microorganisms.

Heinonen et al. (2021) proposed that AMP TAT-RasGAP 317-326 could effectively inhibit the formation and development of biofilms of *P. aeruginosa* and *A. baumannii*, and had little anti-biofilm activity against *S. aureus*. In the human oral environment, AMPs are widely present in the oral mucosa and salivary glands of the epidermal cells and neutrophils (Dale and Fredericks, 2005). AMPs are small in shape and have a positively charged amphiphilic structure, which can enter bacterial microbial cells through transmembrane pores and cause their cracking. AMPs are a potentially effective treatment for bacterial biofilm-associated oral infections due to their extensive antibacterial activity, low drug resistance, and ubiquity in the oral cavity. LL-37 is one of the most widely studied AMPs, which can modulate the immune response, regulate the inflammatory response, accelerate angiogenesis, promote wound healing, and help in oral defense against bacterial biofilms (Wuersching et al., 2021b). Levels of LL-37 are associated with various chronic inflammatory diseases, such as periodontal disease, gingivitis, systemic lupus erythematosus, and psoriasis (Pahar et al., 2020). Lactoferrin peptides are functional AMPs hydrolyzed by pepsin and are an effective anti-biofilm preparation. Wuersching et al. (2021a) demonstrated that LL-37 and human lactoferrin could interfere with the planktonic growth of anaerobic bacteria and the formation of bacterial biofilms, thus reducing the incidence of dental caries and periodontitis. Lactoferrin chimeras have a wide range of antibacterial activities. Ruangcharoen et al. (2017) proved that, compared with minocycline hydrochloride and chlorhexidine digluconate, lactoferrin chimeric could better inhibit the formation of oral multispecies biofilms *in vitro*, and it could reduce the activity of various bacterial cells in the biofilms. Antimicrobials depend on active cells, whereas AMPs are less specific for targeting molecules and can even target metabolically dormant cells in most regions of the mature bacterial biofilm.

At present, treating cystic fibrosis combined with *P. aeruginosa* infection remains difficult. Metal AMP piscidin 1 and piscidin 3 showed activity against *P. aeruginosa* biofilm infection, mainly due to their ability to tolerate an acidic environment and high ionic strength and to cut eDNA in the presence of Cu^2+. Metal AMP Gaduscidin-1 (Gad-1) is a broad-spectrum AMP that binds Cu^2+ efficiently in acidic and neutral environments. Holo-Gad-1 can eradicate mature bacterial biofilms and prevent the formation of new biofilms, mainly because eDNA is required for adhesion during the formation of nascent biofilms (Whitchurch et al., 2002). Portelinha and Angeles-Boza (2021) demonstrated that Gad-1 has multiple forms of action and can effectively remove *P. aeruginosa* biofilms in acidic, neutral, and high-salinity environments. When GaD-1 is combined with several commonly used antibiotics (e.g., Kanamycin and ciprofloxacin) to treat bacterial and microbial infections, it can play a synergistic role and improve the survival outcome of patients. This paper lists the acting bacteria and mechanisms of several peptides with antibiofilm activity in Supplementary Table 4.

Most AMPs can be combined with antibiotics to enhance the role of antimicrobials in preventing bacterial biofilm formation and killing mature biofilms. Antimicrobial peptides are expected to improve the antibiofilm effect and reduce the dosage of antibacterial agents. However, there are limitations to the application of AMPs. Because AMPs are trapped by anionic biofilms, are easily broken down by enzymes in the biofilms, and may even cause acute hemolytic and toxic reactions.

4.2 Nanoparticles

Nanomaterials can reduce the adhesion of bacterial biofilms, promote the delivery of antimicrobial agents, improve the permeability of antibiotics, maintain the stability of antibiotics, and directly produce resistance to biofilms through specific mechanisms without antibiotic treatment. Due to their unique physical and chemical properties, namely biological response, surface charge and small-scale effect, nanomaterials can acquire a variety of antibacterial modes and perform multi-potency interactions with bacterial cells. Nanomaterials are effective carriers of antibacterial agents and inhibit the growth of biofilms through thermal damage, oxidative stress, and physical damage, which is conducive to the treatment of bacterial biofilm infection (Makabenta et al., 2021), and are not prone to drug resistance (Pelgrift and Friedman, 2013). Because of their special structure, nanomaterials can increase antibacterial activity in the following four ways. The surface charge of nanomaterials can enhance the interaction with bacterial microbial cells and lipid molecules, thus extending the exposure time of bacterial cells to antibiotics. Some nanomaterials reduce the generation of bacterial drug resistance through the self-cracking mechanism. Nanomaterials can enhance antimicrobials' solubility, prolong antimicrobials' life cycle, maintain the effective release of antimicrobials at the target site, and deliver multiple antimicrobials to the same target site to achieve combined therapy (e.g., photothermal and photodynamic therapy). Some nanovesicles inhibit the pre-degradation or release of drugs and deliver antimicrobials to designated targets *via* membrane fusion mode (He et al., 2022). Supplementary Figure 2 shows the mechanism of action of nanomaterials for inhibiting bacterial biofilm formation.

It is known that most organic nanoparticles can improve the dispersion performance of bacterial biofilms and have good biocompatibility, which is an important research direction in the field of antibacterial biofilms. Nanomaterials provide a new idea for the treatment of bacterial biofilms in the future, which can effectively improve the therapeutic efficiency of antibiotics and reduce the drug resistance caused by biofilms. The therapeutic effect of nanomaterials in the treatment of bacterial biofilms is mainly affected by their unique physical and chemical properties and the characteristics of biofilms. The combined application of organic nanomaterials with different functions can improve the efficacy of anti-biofilm. New composites composed of organic nanomaterials and other materials with antibacterial biofilm activity can significantly enhance the ability to resist biofilms and are currently the most widely used antibacterial substances.

Nanoparticle-based therapeutic regimens are expected to be effective for removing bacterial biofilms because of their advantages: functional versatility, selectivity, traceability, high loading efficacy, and controlled drug release (Datta et al., 2018; Khan et al., 2018). Unlike conventional antimicrobials, the activated nanoparticles can be designed to work in the presence of only a trigger, which reduces the side effects of being off-target (Schwartz-Duval et al., 2020). Therefore, the active development of nanomaterials for treating bacterial biofilm-associated infections has important research implications (Gao et al., 2020M; Yu et al., 2020). Ostadhossein et al. (2021) proposed a "particle-in-particle" treatment scheme for the first time. In the absence of antibiotics, they can deliver small therapeutic nanoparticles through simple chemical methods, which can target the characteristic pH of EPS, promote the killing of bacteria mediated by bacterial biofilm pH, and then use nanoparticles to kill caries pathogen S. Under the low pH value, the metabolic state of dental biofilm can produce pathogenicity. Targeting this factor can stabilize the original ecological balance and inhibit harmful pathogenic microorganisms. Particle-in-particle therapeutic approaches have been shown to provide excellent drug delivery, especially during oncology treatment (Xu F. et al., 2020; Zhang et al., 2020). Carbon dots (CDots), a new class of carbon-based nanoparticles, have the advantages of a simple fabrication process, adjustable luminescence function, and wealthy off-energy groups (Nguyen et al., 2020), which can provide unique conditions for antibacterial biofilms. One study confirmed that CDots could reduce the amount of caries pathogen S while killing bacterial biofilm EPS. *In vivo*, nanoparticles can effectively kill *S. mutans* and balance the oral environment (Ostadhossein et al., 2021).

Nanomaterials are effective in preventing the formation of bacterial biofilms on the surface of implantable medical devices. Metal nanoparticles are the key types of nanoparticles that have intrinsic anti-biofilm activity. Some metallic nanomaterials interact with the EPS of bacterial biofilms through surface charge interactions, and they can release soluble ions targeting bacterial microorganisms or EPS (Hiebner et al., 2020). Silver is one of the metal nanoparticles with high sterilization capacity. Silver nanoparticles (Ag-NPs) effectively prevented biofilm formation of *S. aureus* and oral mixed flora (*Streptococcus oralis*, *P. gingivalis*, and *Actinomyces naeslundii*) biofilm formation. Ag-NPs with maximum antibacterial activity after three repeated irradiations (Pérez-Tanoira et al., 2022). Habimana et al. (2018) developed a substance (GNP+PK) that treated gold nanoparticles (GNP) with the enzyme protease K (PK). They treated the bacterial biofilm on the surface of medical devices for 24 hours with enzyme protease K, gold particle, and GNP+PK, respectively. The total biomass of *Pseudomonas fluorescens* biofilm decreased by 40%, 77%, and 74%, while the thickness was reduced by 52%, 72%, and 78%, respectively. This study confirmed that GNP+PK particles could kill cells in *P. fluorescens* biofilm, mechanically separate cells in suspension, and damage the structure of bacterial biofilm, showing better anti-biofilm efficacy than PK or GNP. Slomberg et al. (2013) combined NO and silica nanoparticles to examine the effects of these materials on *S. aureus* and *P. aeruginosa* biofilms. In this process, the bacterial biofilm was first placed in a biological

reaction incubator for 48 hours and then treated the biofilm with nanoparticles for 24 hours. They found that the morphology and volume of nanoparticles both affected the effectiveness of bacterial biofilm elimination. Chitosan (CS) carries a positive charge on its surface and can adsorb to the surface of bacterial microorganisms. It binds to the surface of bacterial cells carrying a negative charge using electrostatic interaction, and the permeability of bacterial cell membrane changes, leading to apoptosis (Rashki et al., 2021). At the same time, chitosan can penetrate the bacterial cell membrane and interact with nucleic acids to interfere with the DNA/RNA synthesis process, triggering intracellular reactions that lead to cell death. Pan et al. (2022) combined CS with artificial nano enzymes. They found that the conjugate is an efficient, economical, and environmentally friendly antibiofilm preparation, which may eventually become an effective alternative to eradicate bacterial biofilms.

Nanosponges can prevent the formation of biofilms or eliminate biofilms those already formed and exhibit broad-spectrum antimicrobial membrane activity against pathogenic single and double-species biofilms, with no toxicity to mammals. Nabawy et al. (2021) reported the ability of biodegradable polymer-stabilized oil-in-water nanosponges to inhibit methicillin-resistant *S. aureus* and *P. aeruginosa* biofilms. Raj et al. (2022) synthesized chitosan-gum arabic-coated liposomes-alizarin nanocarriers. They found that this material can eliminate the biofilm formed by *S. aureus* and *Candia albicans*, which helps improve drug penetration and release in biofilm cells. However, low stability and water solubility limit the broad application of nanomaterials. At present, a new method has been proposed for the treatment of biofilm-associated infections, namely "nanoscale bacterial debridement", which can separate bacteria from biofilm in a specific way, effectively kill bacteria, and reduce the biomass of biofilm (Li et al., 2021). However, as a new type of nanomaterial, "nanoscale bacterial debridement" has received little relevant research. Biofilm removal by separating bacteria and biofilm has broad research prospects and needs further investigation. Most nanomaterials have been shown to be effective solutions for preventing bacterial biofilm formation (Baelo et al., 2015; Cheeseman et al., 2020). Since biofilms exhibit a high antibacterial bacterial microbial community embedded in EPS, not all nanoparticles will be able to destroy bacterial biofilms. Although organic nanomaterials play an excellent role in inhibiting the formation of bacterial biofilms, they are less effective against stationary and persistent bacteria (Li et al., 2021). The cytotoxicity and abnormal distribution of complex tissues are common problems in nanomaterials application. Therefore, more in-depth research is needed to focus on the overlooked aspects of bacterial biofilm processing.

4.3 Catabolite control protein A inhibitor

Catabolite control protein A (CcpA) is the primary regulator of the trans-activation of carbon catabolite repression. It can induce and stimulate the upregulation of cidA and icaA gene expression. The cidA and icaA genes can play a role in synthesizing polysaccharide intercellular adhesins. They can be involved in encoding cave proteins that are involved in lysing bacterial cells and releasing eDNA (Sadykov et al., 2019). At the same time, CcpA can inhibit small noncoding RNA RsaI transcription and then affect bacterial biofilm formation (Bronesky et al., 2019; Bulock et al., 2022). CcpA of *S. aureus* (SaCcpA) can also affect bacterial biofilm formation, antimicrobial resistance development, and virulence factor expression. Catabolite control protein A inhibitor can inhibit the DNA-binding ability of SaCcpA, which is expected to eliminate the virulence factor of *S. aureus* strains. Silver, as an inhibitor, can target SaCcpA, eliminate alpha-hemolysin expression in bacterial cells, and reduce bacterial virulence (Liao et al., 2017). However, silver ions are toxic, and silver-containing preparations (e.g., silver sulfadiazine) are generally used only as topical treatments. Huang et al. (2020) identified a specific small molecule inhibitor that disrupts the SaCcpA-DNA complex product and reduces the expression of α-hemolysin encoded by the hla gene. The Sak gene is a staphylokinase that can convert plasminogen into plasmin (Tam and Torres, 2019). It can inhibit the formation and development of biofilms and separate mature biofilms by activating plasminogen and splitting fibrin from the host. After treatment with the Sak gene, *C. albicans* and *S. aureus* biofilms integrity and biomass decreased (Liu et al., 2019). Zheng et al. (2022) proposed that CcpA can bind to the promoter region of the Sak gene and inhibit Sak gene expression, thus regulating the formation and development of bacterial biofilms. This method has low cost and minor side effects and is expected to be a drug for treating *S. aureus*-related biofilm infections.

4.4 Bacteriophage

Bacteriophage is a virus that can infect and kill bacteria. Compared to common antibiotics, bacteriophage has the advantages of functional specificity, more robust tolerance, higher safety, narrower scope of action, and cost-effectiveness (Principi et al., 2019), and it cannot infect human or animal cells. Bacteriophages can penetrate the structure of bacterial biofilm and eradicate or prevent bacterial biofilm (Łusiak-Szelachowska et al., 2020), which is expected to be an alternative therapy for antibiotics. Supplementary Figure 3 shows the multiple mechanisms by which bacteriophages counteract bacterial biofilm formation. Haemolysinase is a phage-derived enzyme that can hydrolyze the peptidoglycan of the cell wall, which in turn can disrupt the structure of bacterial biofilms (Gray et al., 2018; Sharma et al., 2018). Bacteriophage infection of host cells mainly involves the following steps: (i) adhesion to the bacterial cell surface using phage receptor binding proteins; (ii) the phage genome enters the cytoplasm; (iii) phage for protein assembly; (iv) release of progeny phage (Tian et al., 2021).

Novel phage Φ 15 produces a polysaccharide depolymerase that hydrolyzes the EPS of a single species of single-species *Pseudomonas putida* and inhibits biofilm formation (Cornelissen et al., 2011). Rai et al. (2020) used CV staining to determine the biofilm content. They found that phage PD1 and PE2 could effectively prevent the formation of *S. aureus* biofilms, while PD1, PE1, and P3 could disperse mature biofilms. Phage Φ29 and phage T4 could inhibit the formation of *S. aureus* biofilms (Sybesma et al.,

2016). Phages from the order Caudovirales, Myoviridae family, could reduce the proliferation of *P. aeruginosa* in the floating state. At the same time, this phage could also reduce the metabolic activity of endotracheal cannula-associated biofilm and destroy the already-formed *P. aeruginosa* biofilms (Oliveira et al., 2020). The phage mixture (LPSTLL, LPST94, LPST153) has a wide host range and lytic activity, which can play a role in reducing the biofilm of *Salmonella* spp. (Islam et al., 2019).

Combining bacteriophage and antibiotics can improve the therapeutic effect of bacterial biofilms and achieve reduced phage resistance without increasing the toxicity of antimicrobials. For example, the combination of bacteriophage T4 and tobramycin can significantly reduce *E. coli* tolerance to tobramycin (Hemmati et al., 2021). Combining specific phage and amoxicillin can improve the synergistic effect on *K. pneumoniae* B5055 biofilm (Bedi et al., 2009). Bacteriophages can be used alone or in combination with various bacteriophages in treating bacterial biofilms. Phage mixtures are effective in preventing the formation of bacterial biofilms and removing mature biofilms because they produce fewer types of phage resistance and significantly increase the host spectrum compared to phage alone. However, bacteriophage therapy also has limitations: for example, bacteriophages increase antibiotic resistance, bacteriophage DNA replication and protein synthesis need to interfere with bacteria metabolism, and bacteriophages are related to the growth conditions of bacterial microorganisms (Tagliaferri et al., 2019; Łusiak-Szelachowska et al., 2020). Since bacteriophages are viruses and pathogenic factors, there may be potential hazards. Therefore, when combining phages and antibiotics for treating bacterial biofilms, we should fully consider the possible adverse effects to prevent contraindications to the pairing.

4.5 Quorum sensing inhibitors

The communication mechanism between bacteria and microorganisms is called the quorum sensing system, which can control the expression of various virulence genes at different stages of bacterial biofilm formation and development (Dijkshoorn et al., 2007). Inhibition of this system can impair the formation of bacterial biofilm. As a small signal molecule, an autoinducer can mediate the communication between bacteria and microorganisms in the QS system to coordinate the development of bacterial cells. Significant changes in intracellular gene expression levels may occur when bacterial population densities reach concentration thresholds set by autoinducer agents while under the influence of the external environment (Hemmati et al., 2020). Gene expression level can induce or inhibit various virulence factors in bacterial cells and affect biofilm formation. Autoinducer peptides (AIP), Autoinducer-2 (AI-2), and N-acyl-homoserine lactones (AHLs) are three of the most studied QS signaling molecules (Muras et al., 2022). AIP is synthesized by Gram-positive bacteria. It cannot penetrate bacterial cells but binds to specific transmembrane receptors in cell membranes or cells to stimulate signal transduction pathways and promote the transcription of target genes. AHLs are usually produced by Gram-negative bacteria and can spread into bacterial cells to bind to specific receptor proteins that activate corresponding transcription factors and regulate gene expression (Duplantier et al., 2021). Blocking the production of AHLs can reduce the biological activity of AHL synthase and decrease the concentration of AHLs, which in turn interferes with the QS system. The AI-2 molecule is an autoinducer that mediates the signaling process between Gram-negative and Gram-positive bacteria, which is influenced by osmotic pressure and pH. The signaling molecule will be broken down when exposed to low osmotic pressure. AI-2 signaling molecules can affect bacterial biofilm formation, antibiotic resistance, virulence factor secretion, and cell motility Li and Zhao (2020).

Quorum sensing inhibitors (QSI) are produced by prokaryotes or eukaryotes. It can block the quorum sensing system, which may reduce efflux pump expression and destroy bacterial biofilm formation (Hemmati et al., 2020). QSI has been shown to interfere with AI-2 and the Competence Stimulation Peptide system to prevent the formation of oral bacterial biofilms (Muras et al., 2020). Non-steroidal anti-inflammatory drugs (e.g., Meloxicam and aspirin) can be used as potential QS inhibitors, which can affect the QS signaling molecules of *P. aeruginosa* and the formation and maturation of its biofilm (Almeida et al., 2018). Some commonly used antimicrobials (e.g., erythromycin, azithromycin, piperacillin-tazobactam, streptomycin, and ciprofloxacin) have high levels of QSI activity (Skindersoe et al., 2008). Natural products, antibiotics and compounds can affect the function of QSI. Bacteria may be resistant to a single QSI preparation, reducing its effective biological activity. Bacteria may be resistant to a single QSI preparation, reducing its effective biological activity. Therefore, it is recommended to combine the application of QSI and antibiotics to inhibit resistance to QSI without increasing the toxicity of antibiotics (Wang et al., 2016), which can effectively improve the therapeutic effect. When resveratrol was combined with aminoglycoside antibiotics (gentamicin, streptomycin, amikacin) to treat bacterial microorganisms, it significantly reduced the formation of bacterial biofilms compared with various substances alone (Zhou et al., 2018). Therefore, QSI can target the quorum sensing system in bacteria and may be a potential therapeutic solution for bacterial biofilms.

4.6 Enzymes involved in biofilm degradation

Enzymes are involved in ESP generation, intercellular communication, maturation and dispersion of biofilms, with high specificity. It can remove specific components from biofilms, helping to inhibit the extracellular matrix and quorum-sensing system of bacterial microorganisms (Ivanova et al., 2015). Enzymes capable of hydrolyzing ESP components have anti-biofilm activity, including oxidase (Nguyen and Burrows, 2014), polysaccharide degrading enzyme (Saggu et al., 2019), and proteolytic enzyme (Wille and Coenye, 2020). Therefore, enzymes are preferred among biological methods for inhibiting biofilms (Tan et al., 2020). Table 2 shows several enzymes and their mechanisms of action.

Soluble enzymes are unstable under different biofilm growth conditions and are not reusable. Enzyme immobilization can achieve enzyme stability, improve utilization, and reduce activity

loss (Perwez et al., 2017). The immobilization includes adsorption, crosslinking, embedding, encapsulation and covalent coupling. Perwez et al. (2021) proposed m-combi-Cross linked Enzyme Aggregate (m-combi-CLEA), a novel biofilm inhibition method that can inhibit the biofilms of *E. coli* and *S. aureus*. The bacterial biofilms treated with enzyme mixtures in the form of CLEA showed inhibition rates could reach 75-78%, promising an alternative to antibiotics. The magnetic effect of CLEA helps achieve enzyme recirculation.

4.7 Aptamers

Aptamers are single-stranded oligonucleotide molecules or peptides produced *in vitro*. Because of its specific three-dimensional structure can select target molecules (e.g., cells, proteins, antimicrobial agents, small molecules, and metal ions) by specific linkage and high affinity. These properties make the aptamers highly active against bacterial biofilms and antimicrobials. Their antibacterial effects may be generated through the depolarization of cell walls of bacterial microorganisms. Aptamers may be an effective alternative to inhibit the development of biofilms (Shatila et al., 2020). Supplementary Figure 4 briefly shows the primary mechanism of action of aptamers in inhibiting bacterial biofilm formation. Aptamers are suitable alternative substances in the treatment of biofilms due to their flexible diagnostic and therapeutic properties. Mao et al. (2018) developed an aptamer-targeted graphene oxide (GO) therapeutic strategy against bacterial biofilms, defining the coupling as aptamer-GO. They found it can inhibit 93.5 ± 3.4% of *Salmonella typhimurium* biofilms, showing superior antibacterial biofilm properties and effectively becoming a long-term therapeutic option for treating bacterial biofilms. As a special targeting agent, aptamers are expected to improve the effective concentration of antibiotics and reduce the possibility of missing targets, which can be used to treat bacterial microbial infections. The synergistic action of aptamers and antibiotics may affect more bacterial microbial cells (Ning et al., 2015).

Shatila et al. (2020) demonstrated the inhibitory effect of DNA aptamer of *Salmonella* spp. invasion protein A (Apt177) on bacterial biofilms. They found that Apt177 could alter the three-dimensional structure of biofilms and was effective in reducing bacterial biofilm formation when applied alone or in combination with ampicillin. Enteropathogenic *E. coli* (EPEC) is a biological agent that causes diarrhea by forming a bacterial biofilm. It was found that the nucleic acid aptamer SELEX 10 Colony 5 could reduce the motion diameter of EPEC K1.1 and showed the highest biofilm inhibition effect. This aptamer can reduce the mRNA expression level of bacterial biofilm formation genes (e.g., curli gene, interaction, and motility), hinder EPEC K1.1's motility, and prevent bacterial biofilm formation (Oroh et al., 2020). Sengupta et al. (2020) reported the effectiveness of aptamer-DNA template silver nanocluster (Ag-NC) for inhibiting *P. aeruginosa* biofilm formation, and Ag-NC as a sensor is expected to be a new way to detect planktonic cells and biofilm formation. Ning et al. (2022) found that simultaneous delivery of penicillin-binding protein 2a-specific DNA aptamer and berberine *via* graphene oxide effectively inhibited the formation of MRSA biofilms, and this complex could potentially be an effective strategy for the treatment of chronic infections caused by MRSA biofilms. *P. gingivalis* can cause the occurrence of periodontitis. DNA-aptamer-nanographene oxide (NGO) achieves real-time, *in situ* detection and removal of *P. gingivalis* biofilm. The DNA-Aptamer-NGO complex serves as an antimicrobial photodynamic therapy and is a promising method that may inhibit the formation of bacterial biofilms (Pourhajibagher et al., 2022). Therefore, aptamers combined with other reagents can improve targeting specificity and inhibit the formation and development of bacterial biofilms, which is considered an ideal measure for antibacterial biofilms.

4.8 Peptide nucleic acid

Peptide nucleic acids (PNA) is a synthetic analogue of nucleic acid, composed of nucleic acid and peptide, similar in structure to DNA or RNA, and identical in physical and chemical properties to

TABLE 2 Enzymes with antibacterial biofilm activity.

Enzyme	Mechanism of action	Bacteria	Authors
Trypsin	Hydrolysis of the peptide bond on the carboxyl side of protein arginine and lysine residues	Inhibition of biofilm formation in *P. aeruginosa* and *Erysipelas rubbery* C208	(Gilan and Sivan, 2013; Banar et al., 2016)
Cellulase	Hydrolyses the β-1, 4 glycosidic bonds of hemicellulose and cellulose	Decomposition of EPS in *P. aeruginosa* biofilms	(Ibrahim et al., 2021)
α-amylase	Hydrolysis of α-1,4 glycosidic bonds in glycogen and starch		(Fleming et al., 2017)
Pectinex ultra clear	Contains polygalacturonase, pectin ester, hemicellulase and cellulase activity		(Perwez et al., 2021)
Disintegrin B produced by Aggregatibacter actinomycetem-comitans	Hydrolysis of glycosidic bonds in polysaccharides	Decomposing the mature *Staphylococcus* spp. biofilms	(Donelli et al., 2007)
Alginate lyase	Resistant alginate substances in *P. aeruginosa* biofilm substrates	*P. aeruginosa*	(Franklin et al., 2011)

protein. PNA has a high affinity and specific binding ability, showing great potential in removing drug-resistant bacteria (Lee et al., 2019), and can hinder the formation of bacterial biofilms. Combined with conventional antibiotics, it can improve the antibacterial efficacy of antibiotics and anti-biofilm activity. There are two main reasons why pre-PNA has yet to be widely used. One is that PNA is hydrophobic and not easily dissolved in an aqueous solution. Second, due to the lack of effective carriers to transport PNA to biofilms, bacterial biofilms have low permeability to PNA (Wojciechowska et al., 2020). Meanwhile, components of bacterial cells, such as lipopolysaccharide and peptidoglycan, are also major barriers that restrict PNA entry into biofilms (Kurupati et al., 2007). Various methods have been proposed to increase the penetration of PNAs into biofilm cells: chemical changes in the structure of PNAs can enhance the hydrophilicity of PNA. Some cell-penetrating peptides (e.g., chloroquine, photochemical internalization, cationic lipids) can covalently bind to PNAs. This process helps PNAs form complementary base pairs with bacterial DNA. Filamenting temperature-sensitive mutant Z (FtsZ) remains silent in numerous bacterial cells and is one of the essential structures involved in the bacterial division process, making ftsZ a potential target for developing new antimicrobial agents. Narenji et al. (2020) showed that antisense PNAs targeting the efaA gene could reduce the formation of *Enterococcus* spp. biofilms, that anti-ftsZ materials could inhibit bacterial cell growth by interfering with *E. coli* division, and that PNAs were shown to inhibit the function of ftsZ. AcpP-PNA14-5'L is a PNA peptide based on targeting the acpP gene with a 5' membrane penetrating peptide and junction. It exhibits efficient antibacterial activity against *H. influenzae* in both planktonic and biofilm states and is not susceptible to drug resistance (Otsuka et al., 2017). Castillo et al. (2018) found that PNA can directly block the transcription of mRNAs encoding acyl carrier proteins. Certain antibiotics (such as polymyxin B) can interfere with cell wall formation and, when used in combination with PNA, are effective in preventing the formation of biofilms from Enterohemorrhagic *E. coli* 0157: H7. The combination of PNA with conventional antimicrobials has the potential to be an effective therapeutic option for the treatment of Gram-negative bacteria. In conclusion, PNA is expected to be an effective way to increase anti-biofilm activity.

4.9 Vaccine

Currently, vaccines formulated using biofilm-derived antigens are an effective way to prevent infectious diseases, which can improve the protective efficacy of existing vaccines (Loera-Muro et al., 2021). The outer membrane vesicles (OMV) derived from *Bordetella pertussis* can effectively prevent the colonization of bacterial cells in the lung of mice. Carriquiriborde et al. (2021) used OMV from the planktonic state (OMVplank) and biofilm state (OMVbiof) to create a vaccine. The OMVbiof vaccine was more affinity and immunogenic than the OMVplank vaccine in antibody induction. In addition, the *B. pertussis* biofilm-derived vaccine was found to be more protective and immunoreactive against bacterial strains with defective pertactin antigen expression than the OMVplank vaccine. Zurita et al. (2019) found that the OMVs vaccine induced respiratory CD4 tissue-resident memory cells with long-lasting protection against *B. pertussis*. It caused a durable immune response, making it an excellent alternative to third-generation pertussis vaccines. The treatment of pathogens with biofilm-derived vaccines is still in the research stage and may help treat biofilm infections. More advanced technologies are needed to identify bacterial biofilm-derived antigens in the future.

5 Conclusion and prospect

Clinically, most chronic infections are associated with biofilms of bacterial microorganisms, which are resistant to antibiotics and can grow and mature even under poor survival conditions. Biofilm-associated infection is a significant clinical problem. Biofilms can form on the surface of devices and non-devices, increasing patient morbidity and mortality and seriously threatening human life and health. In addition, the increased spread of multidrug-resistant bacteria has made biofilm infections a significant threat to hospitalized patients. Although many studies have been done to elucidate devices and non-devices surface biofilm formation, they are mainly limited to a few surfaces and specific bacterial microorganisms. Therefore, it is critical to focus on bacterial biofilm infections and work to raise awareness of the different microbial populations present on device and non-device surfaces to develop strategies for detecting and treating bacterial biofilms. Early detection of bacterial biofilms can improve treatment effectiveness and reduce medical costs. There are many strategies to resist biofilms, but relatively few to clinical treatment. In the future, we should also focus on more efficient, durable, and environmentally friendly methods and further study the safety and effectiveness of each strategy.

Author contributions

Conceptualization- YL; collecting data- AZ and JS; writing and editing- AZ; supervision- YL. All authors contributed to the article and approved the submitted version.

Conflict of interest

The authors declare that the research was conducted in the absence of any commercial or financial relationships that could be construed as a potential conflict of interest.

Publisher's note

Supplementary material

The Supplementary Material for this article can be found online at: https://www.frontiersin.org/articles/10.3389/fcimb.2023.1137947/full#supplementary-material

SUPPLEMENTARY FIGURE 1
Different therapeutic strategies for inhibiting bacterial biofilm formation.

SUPPLEMENTARY FIGURE 2
Mechanism of action of nanomaterials against biofilms.

SUPPLEMENTARY FIGURE 3
Mechanism of action of bacteriophages with anti-biofilm activity.

SUPPLEMENTARY FIGURE 4
Mechanism of action of aptamers with anti-biofilm activity.

SUPPLEMENTARY TABLE 1
Most common bacterial organisms on the surface of medical devices.

SUPPLEMENTARY TABLE 2
Non-device-related biofilm infections.

SUPPLEMENTARY TABLE 3
Microbial and bacterial biofilm-associated infections and their adhesion surfaces.

SUPPLEMENTARY TABLE 4
Mechanism of action of antimicrobial peptide.

References

Abraham, W. R. (2016). Going beyond the control of quorum-sensing to combat biofilm infections. *Antibiotics (Basel)* 5 (1), 3. doi: 10.3390/antibiotics5010003

Ali Mohammed, M. M., Pettersen, V. K., Nerland, A. H., Wiker, H. G., and Bakken, V. (2021). Label-free quantitative proteomic analysis of the oral bacteria fusobacterium nucleatum and porphyromonas gingivalis to identify protein features relevant in biofilm formation. *Anaerobe* 72, 102449. doi: 10.1016/j.anaerobe.2021.102449

Almeida, F. A., Vargas, E. L. G., Carneiro, D. G., Pinto, U. M., and Vanetti, M. C. D. (2018). Virtual screening of plant compounds and nonsteroidal anti-inflammatory drugs for inhibition of quorum sensing and biofilm formation in salmonella. *Microb. Pathog.* 121, 369–388. doi: 10.1016/j.micpath.2018.05.014

Anastasiadis, P., Mojica, K. D., Allen, J. S., and Matter, M. L. (2014). Detection and quantification of bacterial biofilms combining high-frequency acoustic microscopy and targeted lipid microparticles. *J. Nanobiotechnol.* 12, 24. doi: 10.1186/1477-3155-12-24

Arciola, C. R., Campoccia, D., and Montanaro, L. (2018). Implant infections: adhesion, biofilm formation and immune evasion. *Nat. Rev. Microbiol.* 16 (7), 397–409. doi: 10.1038/s41579-018-0019-y

Arciola, C. R., Campoccia, D., Speziale, P., Montanaro, L., and Costerton, J. W. (2012). Biofilm formation in staphylococcus implant infections. a review of molecular mechanisms and implications for biofilm-resistant materials. *Biomaterials* 33 (26), 5967–5982. doi: 10.1016/j.biomaterials.2012.05.031

Arroyo-Moreno, S., Cummings, M., Corcoran, D. B., Coffey, A., and McCarthy, R. R. (2022). Identification and characterization of novel endolysins targeting gardnerella vaginalis biofilms to treat bacterial vaginosis. *NPJ biofilms microbiomes* 8 (1), 29. doi: 10.1038/s41522-022-00285-0

Auletta, S., Varani, M., Horvat, R., Galli, F., Signore, A., and Hess, S. (2019). PET radiopharmaceuticals for specific bacteria imaging: A systematic review. *J. Clin. Med.* 8 (2), 197. doi: 10.3390/jcm8020197

Baelo, A., Levato, R., Julián, E., Crespo, A., Astola, J., Gavaldà, J., et al. (2015). Disassembling bacterial extracellular matrix with DNase-coated nanoparticles to enhance antibiotic delivery in biofilm infections. *J. Control Release* 209, 150–158. doi: 10.1016/j.jconrel.2015.04.028

Bair, K. L., Shafirstein, G., and Campagnari, A. A. (2020). *In vitro* photodynamic therapy of polymicrobial biofilms commonly associated with otitis media. *Front. Microbiol.* 11. doi: 10.3389/fmicb.2020.558482

Banar, M., Emaneini, M., Satarzadeh, M., Abdellahi, N., Beigverdi, R., Leeuwen, W. B., et al. (2016). Evaluation of mannosidase and trypsin enzymes effects on biofilm production of *Pseudomonas aeruginosa* isolated from burn wound infections. *PloS One* 11 (10), e0164622. doi: 10.1371/journal.pone.0164622

Barbour, A., Elebyary, O., Fine, N., Oveisi, M., and Glogauer, M. (2022). Metabolites of the oral microbiome: important mediators of multikingdom interactions. *FEMS Microbiol. Rev.* 46 (1), fuab039. doi: 10.1093/femsre/fuab039

Batoni, G., Maisetta, G., and Esin, S. (2016). Antimicrobial peptides and their interaction with biofilms of medically relevant bacteria. *Biochim. Biophys. Acta* 1858 (5), 1044–1060. doi: 10.1016/j.bbamem.2015.10.013

Bedi, M. S., Verma, V., and Chhibber, S. (2009). Amoxicillin and specific bacteriophage can be used together for eradication of biofilm of klebsiella pneumoniae B5055. *World J. Microbiol. Biotechnol.* 25, 1145. doi: 10.1007/s11274-009-9991-8

Beynon, R. P., Bahl, V. K., and Prendergast, B. D. (2006). Infective endocarditis. *BMJ* 333 (7563), 334–339. doi: 10.1136/bmj.333.7563.334

Bjarnsholt, T., Tolker-Nielsen, T., Høiby, N., and Givskov, M. (2010). Interference of pseudomonas aeruginosa signalling and biofilm formation for infection control. *Expert Rev. Mol. Med.* 12, e11. doi: 10.1017/S1462399410001420

Bosio, S., Leekha, S., Gamb, S. I., Wright, A. J., Terrell, C. L., and Miller, D. V. (2012). Mycobacterium fortuitum prosthetic valve endocarditis: a case for the pathogenetic role of biofilms. *Cardiovasc. Pathol.* 21 (4), 361–364. doi: 10.1016/j.carpath.2011.11.001

Bronesky, D., Desgranges, E., Corvaglia, A., François, P., Caballero, C. J., Prado, L., et al. (2019). A multifaceted small RNA modulates gene expression upon glucose limitation in *Staphylococcus aureus*. *EMBO J.* 38 (6), e99363. doi: 10.15252/embj.201899363

Bulock, L. L., Ahn, J., Shinde, D., Pandey, S., Sarmiento, C., Thomas, V. C., et al. (2022). Interplay of CodY and CcpA in regulating central metabolism and biofilm formation in *Staphylococcus aureus*. *J. Bacteriol.* 204 (7), e0061721. doi: 10.1128/jb.00617-21

Caldara, M., Belgiovine, C., Secchi, E., and Rusconi, R. (2022). Environmental, microbiological, and immunological features of bacterial biofilms associated with implanted medical devices. *Clin. Microbiol. Rev.* 35 (2), e0022120. doi: 10.1128/cmr.00221-20

Calliada, F., Campani, R., Bottinelli, O., Bozzini, A., and Sommaruga, M. G. (1998). Ultrasound contrast agents: basic principles. *Eur. J. Radiol.* 27 (Suppl 2), S157–S160. doi: 10.1016/s0720-048x(98)00057-6

Campoccia, D., Mirzaei, R., Montanaro, L., and Arciola, C. R. (2019). Hijacking of immune defences by biofilms: a multifront strategy. *Biofouling* 35 (10), 1055–1074. doi: 10.1080/08927014.2019.1689964

Carniello, V., Peterson, B. W., van der Mei, H. C., and Busscher, H. J. (2018). Physico-chemistry from initial bacterial adhesion to surface-programmed biofilm growth. *Adv. Colloid Interface Sci.* 261, 1–14. doi: 10.1016/j.cis.2018.10.005

Carriquiriborde, F., Martin Aispuro, P., Ambrosis, N., Zurita, E., Bottero, D., Gaillard, M. E., et al. (2021). Pertussis vaccine candidate based on outer membrane vesicles derived from biofilm culture. *Front. Immunol.* 12, 730434. doi: 10.3389/fimmu.2021.730434

Castillo, J. I., Równicki, M., Wojciechowska, M., and Trylska, J. (2018). Antimicrobial synergy between mRNA targeted peptide nucleic acid and antibiotics in e. coli. *Bioorg Med. Chem. Lett.* 28 (18), 3094–3098. doi: 10.1016/j.bmcl.2018.07.037

Castro, J., Alves, P., Sousa, C., Cereija, T., França, Â., Jefferson, K. K., et al. (2015). Using an *in-vitro* biofilm model to assess the virulence potential of bacterial vaginosis or non-bacterial vaginosis gardnerella vaginalis isolates. *Sci. Rep.* 5, 11640. doi: 10.1038/srep11640

Castro, J., Lima, Â., Sousa, L. G. V., Rosca, A. S., Muzny, C. A., and Cerca, N. (2022). Crystal violet staining alone is not adequate to assess synergism or antagonism in multi-species biofilms of bacteria associated with bacterial vaginosis. *Front. Cell Infect. Microbiol.* 11. doi: 10.3389/fcimb.2021.795797

Chan, C. L., Richter, K., Wormald, P. J., Psaltis, A. J., and Vreugde, S. (2017). Alloiococcus otitidis forms multispecies biofilm with haemophilus influenzae: Effects on antibiotic susceptibility and growth in adverse conditions. *Front. Cell. infection Microbiol.* 7. doi: 10.3389/fcimb.2017.00344

Charlebois, A., Jacques, M., and Archambault, M. (2016). Comparative transcriptomic analysis of clostridium perfringens biofilms and planktonic cells. *Avian Pathol.* 45 (5), 593–601. doi: 10.1080/03079457.2016.1189512

Cheeseman, S., Christofferson, A. J., Kariuki, R., Cozzolino, D., Daeneke, T., Crawford, R. J., et al. (2020). Antimicrobial metal nanomaterials: From passive to stimuli-activated applications. *Adv. Sci. (Weinh)* 7 (10), 1902913. doi: 10.1002/advs.201902913

Chiba, A., Seki, M., Suzuki, Y., Kinjo, Y., Mizunoe, Y., and Sugimoto, S. (2022). *Staphylococcus aureus* utilizes environmental RNA as a building material in specific polysaccharide-dependent biofilms. *NPJ Biofilms Microbiomes* 8 (1), 17. doi: 10.1038/s41522-022-00278-z

Clemente, A., Alba-Patiño, A., Rojo-Molinero, E., Russell, S. M., Borges, M., Oliver, A., et al. (2020). Rapid detection of *Pseudomonas aeruginosa* biofilms *via* enzymatic liquefaction of respiratory samples. *ACS Sens* 5 (12), 3956–3963. doi: 10.1021/acssensors.0c01618

Conen, A., Fux, C. A., Vajkoczy, P., and Trampuz, A. (2017). Management of infections associated with neurosurgical implanted devices. *Expert Rev. anti-infective Ther.* 15 (3), 241–255. doi: 10.1080/14787210.2017.1267563

Cornelissen, A., Ceyssens, P. J., T'Syen, J., Van Praet, H., Noben, J. P., Shaburova, O. V., et al. (2011). The T7-related pseudomonas putida phage φ15 displays virion-associated biofilm degradation properties. *PloS One* 6 (4), e18597. doi: 10.1371/journal.pone.0018597

Costa, O. Y. A., Raaijmakers, J. M., and Kuramae, E. E. (2018). Microbial extracellular polymeric substances: Ecological function and impact on soil aggregation. *Front. Microbiol.* 9. doi: 10.3389/fmicb.2018.01636

Cruz, A., Condinho, M., Carvalho, B., Arraiano, C. M., Pobre, V., and Pinto, S. N. (2021). The two weapons against bacterial biofilms: Detection and treatment. *Antibiotics (Basel)* 10 (12), 1482. doi: 10.3390/antibiotics10121482

Dai, X., Xu, Q., Yang, L., Ma, J., and Gao, F. (2022). pH-responsive fluorescent polymer-drug system for real-time detection and *In situ* eradication of bacterial biofilms. *ACS Biomater Sci. Eng.* 8 (2), 893–902. doi: 10.1021/acsbiomaterials.1c01520

Dale, B. A., and Fredericks, L. P. (2005). Antimicrobial peptides in the oral environment: expression and function in health and disease. *Curr. Issues Mol. Biol.* 7 (2), 119–133. doi: 10.1093/jac/dki103

Darouiche, R. O. (2001). Device-associated infections: a macroproblem that starts with microadherence. *Clin. Infect. Dis.* 33 (9), 1567–1572. doi: 10.1086/323130

Datta, S., Misra, S. K., Saha, M. L., Lahiri, N., Louie, J., Pan, D., et al. (2018). Orthogonal self-assembly of an organoplatinum(II) metallacycle and cucurbit[8]uril that delivers curcumin to cancer cells. *Proc. Natl. Acad. Sci. U.S.A.* 115 (32), 8087–8092. doi: 10.1073/pnas.1803800115

Dautle, M. P., Wilkinson, T. R., and Gauderer, M. W. (2003). Isolation and identification of biofilm microorganisms from silicone gastrostomy devices. *J. Pediatr. Surg.* 38 (2), 216–220. doi: 10.1053/jpsu.2003.50046

Davies, D. G., and Marques, C. N. (2009). A fatty acid messenger is responsible for inducing dispersion in microbial biofilms. *J. bacteriol* 191 (5), 1393–1403. doi: 10.1128/JB.01214-08

de la Fuente-Núñez, C., Reffuveille, F., Haney, E. F., Straus, S. K., and Hancock, R. E. (2014). Broad-spectrum anti-biofilm peptide that targets a cellular stress response. *PloS Pathog.* 10 (5), e1004152. doi: 10.1371/journal.ppat.1004152

Delcaru, C., Alexandru, I., Podgoreanu, P., Grosu, M., Stavropoulos, E., Chifiriuc, M. C., et al. (2016). Microbial biofilms in urinary tract infections and prostatitis: Etiology, pathogenicity, and combating strategies. *Pathogens* 5 (4), 65. doi: 10.3390/pathogens5040065

de Vor, L., Rooijakkers, S. H. M., and van Strijp, J. A. G. (2020). Staphylococci evade the innate immune response by disarming neutrophils and forming biofilms. *FEBS Lett.* 594 (16), 2556–2569. doi: 10.1002/1873-3468.13767

Dijkshoorn, L., Nemec, A., and Seifert, H. (2007). An increasing threat in hospitals: multidrug-resistant acinetobacter baumannii. *Nat. Rev. Microbiol.* 5 (12), 939–951. doi: 10.1038/nrmicro1789

Donelli, G., Francolini, I., Romoli, D., Guaglianone, E., Piozzi, A., Ragunath, C., et al. (2007). Synergistic activity of dispersin b and cefamandole nafate in inhibition of staphylococcal biofilm growth on polyurethanes. *Antimicrob. Agents Chemother.* 51 (8), 2733–2740. doi: 10.1128/AAC.01249-06

Donlan, R. M. (2001). Biofilms and device-associated infections. *Emerging Infect. Dis.* 7 (2), 277–281. doi: 10.3201/eid0702.010226

Duplantier, M., Lohou, E., and Sonnet, P. (2021). Quorum sensing inhibitors to quench *P. aeruginosa* pathogenicity. *Pharm. (Basel)* 14 (12), 1262. doi: 10.3390/ph14121262

Eggleston, H., and Panizzi, P. (2014). Molecular imaging of bacterial infections *in vivo*: the discrimination of infection from inflammation. *Inf. (MDPI)* 1 (1), 72–99. doi: 10.3390/informatics101007

El-Ganiny, A. M., Shaker, G. H., Aboelazm, A. A., and El-Dash, H. A. (2017). Prevention of bacterial biofilm formation on soft contact lenses using natural compounds. *J. Ophthalmic Inflammation Infect.* 7 (1), 11. doi: 10.1186/s12348-017-0129-0

Elgharably, H., Hussain, S. T., Shrestha, N. K., Blackstone, E. H., and Pettersson, G. B. (2016). Current hypotheses in cardiac surgery: Biofilm in infective endocarditis. *Semin. Thorac. Cardiovasc. Surg.* 28 (1), 56–59. doi: 10.1053/j.semtcvs.2015.12.005

Elliott, T. S., Moss, H. A., Tebbs, S. E., Wilson, I. C., Bonser, R. S., Graham, T. R., et al. (1997). Novel approach to investigate a source of microbial contamination of central venous catheters. *Eur. J. Clin. Microbiol. Infect. Dis.* 16 (3), 210–213. doi: 10.1007/BF01709583

Evans, J. J., and Bolz, D. D. (2019). Regulation of virulence and antibiotic resistance in gram-positive microbes in response to cell wall-active antibiotics. *Curr. Opin. Infect. Dis.* 32 (3), 217–222. doi: 10.1097/QCO.0000000000000542

Fayez Hassan, N., Khaled Ibrahim, M., Yousef El Tablawy, S., and Abd Allah Farrag, H. (2021). Characterization of biofilm producer nanobacteria isolated from kidney stones of some Egyptian patients. *Pakistan J. Biol. Sci.* 24 (9), 953–970. doi: 10.3923/pjbs.2021.953.970

Fiehn, O. (2002). Metabolomics–the link between genotypes and phenotypes. *Plant Mol. Biol.* 48 (1-2), 155–171. doi: 10.1023/A:1013713905833

Filkins, L. M., and O'Toole, G. A. (2015). Cystic fibrosis lung infections: Polymicrobial, complex, and hard to treat. *PloS Pathog.* 11 (12), e1005258. doi: 10.1371/journal.ppat.1005258

Fleming, D., Chahin, L., and Rumbaugh, K. (2017). Glycoside hydrolases degrade polymicrobial bacterial biofilms in wounds. *Antimicrob. Agents Chemother.* 61 (2), e01998-16. doi: 10.1128/AAC.01998-16

Fleming, D., and Rumbaugh, K. P. (2017). Approaches to dispersing medical biofilms. *Microorganisms* 5 (2), 15. doi: 10.3390/microorganisms5020015

Flemming, H. C., and Wingender, J. (2010). The biofilm matrix. nature reviews. *Microbiology* 8 (9), 623–633. doi: 10.1038/nrmicro2415

Flemming, H. C., Wingender, J., Szewzyk, U., Steinberg, P., Rice, S. A., and Kjelleberg, S. (2016). Biofilms: an emergent form of bacterial life. *Nat. Rev. Microbiol.* 14 (9), 563–575. doi: 10.1038/nrmicro.2016.94

Fong, J. N. C., and Yildiz, F. H. (2015). Biofilm matrix proteins. *Microbiol. Spectr.* 3 (2). doi: 10.1128/microbiolspec.MB-0004-2014

Foster, T. J. (2020). Surface proteins of *Staphylococcus epidermidis*. *Front. Microbiol.* 11. doi: 10.3389/fmicb.2020.01829

Franklin, M. J., Nivens, D. E., Weadge, J. T., and Howell, P. L. (2011). Biosynthesis of the *Pseudomonas aeruginosa* extracellular polysaccharides, alginate, pel, and psl. *Front. Microbiol.* 2. doi: 10.3389/fmicb.2011.00167

Fux, C. A., Quigley, M., Worel, A. M., Post, C., Zimmerli, S., Ehrlich, G., et al. (2006). Biofilm-related infections of cerebrospinal fluid shunts. *Clin. Microbiol. infection* 12 (4), 331–337. doi: 10.1111/j.1469-0691.2006.01361.x

Galdiero, E., Lombardi, L., Falanga, A., Libralato, G., Guida, M., and Carotenuto, R. (2019). Biofilms: Novel strategies based on antimicrobial peptides. *Pharmaceutics* 11 (7), 322. doi: 10.3390/pharmaceutics11070322

Galié, S., García-Gutiérrez, C., Miguélez, E. M., Villar, C. J., and Lombó, F. (2018). Biofilms in the food industry: Health aspects and control methods. *Front. Microbiol.* 9. doi: 10.3389/fmicb.2018.00898

Gao, Y, Wang, J, Chai, M, Li, X, Deng, Y, Jin, Q, et al (2020). Size and charge adaptive clustered nanoparticles targeting the biofilm microenvironment for chronic lung infection management. *ACS Nano* 14 (5), 5686–5699. doi: 10.1021/acsnano.0c00269

Gaspar, C., Rolo, J., Cerca, N., Palmeira-de-Oliveira, R., Martinez-de-Oliveira, J., and Palmeira-de-Oliveira, A. (2021). Dequalinium chloride effectively disrupts bacterial vaginosis (BV) *Gardnerella* spp. biofilms. *Pathogens* 10 (3), 261. doi: 10.3390/pathogens10030261

Gilan, I., and Sivan, A. (2013). Effect of proteases on biofilm formation of the plastic-degrading actinomycete rhodococcus ruber C208. *FEMS Microbiol. Lett.* 342 (1), 18–23. doi: 10.1111/1574-6968.12114

Govaert, M., Smet, C., Vergauwen, L., Ećimović, B., Walsh, J., Baka, M., et al. (2019). Influence of plasma characteristics on the efficacy of cold atmospheric plasma (CAP) for inactivation of listeria monocytogenes and salmonella typhimurium biofilms. *Innov. Food Sci. Emerg.* 52, 376–386. doi: 10.1016/j.ifset.2019.01.013

Graf, M., and Wilson, D. N. (2019). Intracellular antimicrobial peptides targeting the protein synthesis machinery. *Adv. Exp. Med. Biol.* 1117, 73–89. doi: 10.1007/978-981-13-3588-4_6

Gray, J. A., Chandry, P. S., Kaur, M., Kocharunchitt, C., Bowman, J. P., and Fox, E. M. (2018). Novel biocontrol methods for listeria monocytogenes biofilms in food production facilities. *Front. Microbiol.* 9. doi: 10.3389/fmicb.2018.00605

Grier, J. T., Arivett, B. A., Ramírez, M. S., Chosed, R. J., Bigner, J. A., Ohneck, E. J., et al. (2021). Two acinetobacter baumannii isolates obtained from a fatal necrotizing fasciitis infection display distinct genomic and phenotypic characteristics in comparison to type strains. *Front. Cell. infection Microbiol.* 11. doi: 10.3389/fcimb.2021.635673

Habib, A., Le, K. Y., Baddour, L. M., Friedman, P. A., Hayes, D. L., Lohse, C. M., et al. (2013). Predictors of mortality in patients with cardiovascular implantable electronic device infections. *Am. J. Cardiol.* 111 (6), 874–879. doi: 10.1016/j.amjcard.2012.11.052

Habimana, O., Zanoni, M., Vitale, S., O'Neill, T., Scholz, D., Xu, B., et al. (2018). One particle, two targets: A combined action of functionalised gold nanoparticles, against *Pseudomonas* fluorescens biofilms. *J. Colloid Interface Sci.* 526, 419–428. doi: 10.1016/j.jcis.2018.05.014

Hall, C. W., and Mah, T. F. (2017). Molecular mechanisms of biofilm-based antibiotic resistance and tolerance in pathogenic bacteria. *FEMS Microbiol. Rev.* 41 (3), 276–301. doi: 10.1093/femsre/fux010

Hall-Stoodley, L., Stoodley, P., Kathju, S., Høiby, N., Moser, C., Costerton, J. W., et al. (2012). Towards diagnostic guidelines for biofilm-associated infections. *FEMS Immunol. Med. Microbiol.* 65 (2), 127–145. doi: 10.1111/j.1574-695X.2012.00968.x

Han, J., and Poma, A. (2022). Molecular targets for antibody-based anti-biofilm therapy in infective endocarditis. *Polymers* 14 (15), 3198. doi: 10.3390/polym14153198

Harrison, F. (2007). Microbial ecology of the cystic fibrosis lung. *Microbiol. (Reading)* 153 (Pt 4), 917–923. doi: 10.1099/mic.0.2006/004077-0

Hassan, A., Usman, J., Kaleem, F., Omair, M., Khalid, A., and Iqbal, M. (2011). Evaluation of different detection methods of biofilm formation in the clinical isolates. *Braz. J. Infect. Dis.* 15 (4), 305–311. doi: 10.1590/S1413-86702011000400002

He, J., Hong, M., Xie, W., Chen, Z., Chen, D., and Xie, S. (2022). Progress and prospects of nanomaterials against resistant bacteria. *J. Control Release* 351, 301–323. doi: 10.1016/j.jconrel.2022.09.030

Heinonen, T., Hargraves, S., Georgieva, M., Widmann, C., and Jacquier, N. (2021). The antimicrobial peptide TAT-RasGAP317-326 inhibits the formation and expansion of bacterial biofilms *in vitro*. *J. Glob Antimicrob. Resist.* 25, 227–231. doi: 10.1016/j.jgar.2021.03.022

Hemmati, F., Rezaee, M. A., Ebrahimzadeh, S., Yousefi, L., Nouri, R., Kafil, H. S., et al. (2021). Novel strategies to combat bacterial biofilms. *Mol. Biotechnol.* 63 (7), 569–586. doi: 10.1007/s12033-021-00325-8

Hemmati, F., Salehi, R., Ghotaslou, R., Samadi Kafil, H., Hasani, A., Gholizadeh, P., et al. (2020). Quorum quenching: A potential target for antipseudomonal therapy. *Infect. Drug Resist.* 13, 2989–3005. doi: 10.2147/IDR.S263196

Hiebner, D. W., Barros, C., Quinn, L., Vitale, S., and Casey, E. (2020). Surface functionalization-dependent localization and affinity of SiO2 nanoparticles within the biofilm EPS matrix. *Biofilm* 2, 100029. doi: 10.1016/j.bioflm.2020.100029

Hou, C., Yin, F., Wang, S., Zhao, A., Li, Y., and Liu, Y. (2022). Helicobacter pylori biofilm-related drug resistance and new developments in its anti-biofilm agents. *Infect. Drug Resist.* 15, 1561–1571. doi: 10.2147/IDR.S357473

Huang, K., Lin, B., Liu, Y., Ren, H., and Guo, Q. (2022). Correlation analysis between chronic osteomyelitis and bacterial biofilm. *Stem Cells Int.* 2022, 9433847. doi: 10.1155/2022/9433847

Huang, Q., Zhang, Z., Li, H., Guo, Y., Liao, X., Li, H., et al. (2020). Identification of a novel inhibitor of catabolite control protein a from *Staphylococcus aureus*. *ACS Infect. Dis.* 6 (3), 347–354. doi: 10.1021/acsinfecdis.9b00465

Huse, H. K., Kwon, T., Zlosnik, J. E., Speert, D. P., Marcotte, E. M., and Whiteley, M. (2013). *Pseudomonas aeruginosa* enhances production of a non-alginate exopolysaccharide during long-term colonization of the cystic fibrosis lung. *PloS One* 8 (12), e82621. doi: 10.1371/journal.pone.0082621

Ibrahim, A. M., Hamouda, R. A., El-Naggar, N. E., and Al-Shakankery, F. M. (2021). Bioprocess development for enhanced endoglucanase production by newly isolated bacteria, purification, characterization and *in-vitro* efficacy as anti-biofilm of *Pseudomonas aeruginosa*. *Sci. Rep.* 11 (1), 9754. doi: 10.1038/s41598-021-87901-9

Iraola, G., Spangenberg, L., Lopes Bastos, B., Graña, M., Vasconcelos, L., Almeida, Á., et al. (2016). Transcriptome sequencing reveals wide expression reprogramming of basal and unknown genes in leptospira biflexa biofilms. *mSphere* 1 (2), e00042–e00016. doi: 10.1128/mSphere.00042-16

Islam, M. S., Zhou, Y., Liang, L., Nime, I., Liu, K., Yan, T., et al. (2019). Application of a phage cocktail for control of salmonella in foods and reducing biofilms. *Viruses* 11 (9), 841. doi: 10.3390/v11090841

Ivanova, K., Fernandes, M. M., Francesko, A., Mendoza, E., Guezguez, J., Burnet, M., et al. (2015). Quorum-quenching and matrix-degrading enzymes in multilayer coatings synergistically prevent bacterial biofilm formation on urinary catheters. *ACS Appl. Mater Interfaces* 7 (49), 27066–27077. doi: 10.1021/acsami.5b09489

Jakubovics, N. S. (2015). Saliva as the sole nutritional source in the development of multispecies communities in dental plaque. *Microbiol. Spectr.* 3 (3), MBP-0013-2014. doi: 10.1128/microbiolspec.MBP-0013-2014

Jakubovics, N. S., Goodman, S. D., Mashburn-Warren, L., Stafford, G. P., and Cieplik, F. (2021). The dental plaque biofilm matrix. *Periodontol 2000* 86 (1), 32–56. doi: 10.1111/prd.12361

Kalamara, M., and Stanley-Wall, N. R. (2021). The intertwined roles of specialized metabolites within the bacillus subtilis biofilm. *J. bacteriol* 203 (22), e0043121. doi: 10.1128/JB.00431-21

Kaplan, J. B. (2010). Biofilm dispersal: mechanisms, clinical implications, and potential therapeutic uses. *J. Dent. Res.* 89 (3), 205–218. doi: 10.1177/0022034509359403

Kehinde, E. O., Rotimi, V. O., Al-Awadi, K. A., Abdul-Halim, H., Boland, F., Al-Hunayan, A., et al. (2002). Factors predisposing to urinary tract infection after J ureteral stent insertion. *J. Urol.* 167 (3), 1334–1337. doi: 10.1016/S0022-5347(05)65294-9

Khan, M. M., Chattagul, S., Tran, B. Q., Freiberg, J. A., Nita-Lazar, A., Shirtliff, M. E., et al. (2019). Temporal proteomic profiling reveals changes that support burkholderia biofilms. *Pathog. Dis.* 77 (2), ftz005. doi: 10.1093/femspd/ftz005

Khan, M. S., Dighe, K., Wang, Z., Srivastava, I., Daza, E., Schwartz-Dual, A. S., et al. (2018). Detection of prostate specific antigen (PSA) in human saliva using an ultra-sensitive nanocomposite of graphene nanoplatelets with diblock-co-polymers and au electrodes. *Analyst* 143 (5), 1094–1103. doi: 10.1039/c7an01932g

Khatoon, Z., McTiernan, C. D., Suuronen, E. J., Mah, T. F., and Alarcon, E. I. (2018). Bacterial biofilm formation on implantable devices and approaches to its treatment and prevention. *Heliyon* 4 (12), e01067. doi: 10.1016/j.heliyon.2018.e01067

Khemiri, A., Jouenne, T., and Cosette, P. (2016). Proteomics dedicated to biofilmology: What have we learned from a decade of research? *Med. Microbiol. Immunol.* 205 (1), 1–19. doi: 10.1007/s00430-015-0423-0

Klagisa, R., Racenis, K., Broks, R., Balode, A. O., Kise, L., and Kroica, J. (2022). Analysis of microorganism colonization, biofilm production, and antibacterial susceptibility in recurrent tonsillitis and peritonsillar abscess patients. *Int. J. Mol. Sci.* 23 (18), 10273. doi: 10.3390/ijms231810273

Kouijzer, J. J. P., Lattwein, K. R., Beekers, I., Langeveld, S. A. G., Leon-Grooters, M., Strub, J. M., et al. (2021). Vancomycin-decorated microbubbles as a theranostic agent for *Staphylococcus aureus* biofilms. *Int. J. Pharm.* 609, 121154. doi: 10.1016/j.ijpharm.2021.121154

Kranjec, C., Morales Angeles, D., Torrissen Mårli, M., Fernández, L., García, P., Kjos, M., et al. (2021). Staphylococcal biofilms: Challenges and novel therapeutic perspectives. *Antibiotics (Basel)* 10 (2), 131. doi: 10.3390/antibiotics10020131

Kujundzic, E., Fonseca, A. C., Evans, E. A., Peterson, M., Greenberg, A. R., and Hernandez, M. (2007). Ultrasonic monitoring of early-stage biofilm growth on polymeric surfaces. *J. Microbiol. Methods* 68 (3), 458–467. doi: 10.1016/j.mimet.2006.10.005

Kumar, B., Sharma, D., Sharma, P., Katoch, V. M., Venkatesan, K., and Bisht, D. (2013). Proteomic analysis of mycobacterium tuberculosis isolates resistant to kanamycin and amikacin. *J. Proteomics* 94, 68–77. doi: 10.1016/j.jprot.2013.08.025

Kurupati, P., Tan, K. S., Kumarasinghe, G., and Poh, C. L. (2007). Inhibition of gene expression and growth by antisense peptide nucleic acids in a multiresistant beta-lactamase-producing klebsiella pneumoniae strain. *Antimicrob. Agents Chemother.* 51 (3), 805–811. doi: 10.1128/AAC.00709-06

Kusumoto, F. M., Schoenfeld, M. H., Wilkoff, B. L., Berul, C. I., Birgersdotter-Green, U. M., Carrillo, R., et al. (2017). 2017 HRS expert consensus statement on cardiovascular implantable electronic device lead management and extraction. *Heart Rhythm.* 14 (12), e503–e551. doi: 10.1016/j.hrthm.2017.09.001

Larsen, T., and Fiehn, N. E. (2017). Dental biofilm infections - an update. *APMIS: Acta pathologica microbiologica immunologica Scandinavica* 125 (4), 376–384. doi: 10.1111/apm.12688

Lata, M., Sharma, D., Deo, N., Tiwari, P. K., Bisht, D., and Venkatesan, K. (2015). Proteomic analysis of ofloxacin-mono resistant mycobacterium tuberculosis isolates. *J. Proteomics* 127 (Pt A), 114–121. doi: 10.1016/j.jprot.2015.07.031

Lee, H. T., Kim, S. K., and Yoon, J. W. (2019). Antisense peptide nucleic acids as a potential anti-infective agent. *J. Microbiol.* 57 (6), 423–430. doi: 10.1007/s12275-019-8635-4

Lee, K., and Yoon, S. S. (2017). *Pseudomonas aeruginosa* biofilm, a programmed bacterial life for fitness. *J. Microbiol. Biotechnol.* 27 (6), 1053–1064. doi: 10.4014/jmb.1611.11056

Lew, D. P., and Waldvogel, F. A. (2004). Osteomyelitis. *Lancet (London England)* 364 (9431), 369–379. doi: 10.1016/S0140-6736(04)16727-5

Li, X., Chen, D., and Xie, S. (2021). Current progress and prospects of organic nanoparticles against bacterial biofilm. *Adv. Colloid Interface Sci.* 294, 102475. doi: 10.1016/j.cis.2021.102475

Li, T., Zhang, Z., Wang, F., He, Y., Zong, X., Bai, H., et al. (2020). Antimicrobial susceptibility testing of metronidazole and clindamycin against gardnerella vaginalis in planktonic and biofilm formation. *Can. J. Infect. Dis. Med. Microbiol.* 2020, 1361825. doi: 10.1155/2020/1361825

Liang, X., Chen, Y. Y., Ruiz, T., and Wu, H. (2011). New cell surface protein involved in biofilm formation by streptococcus parasanguinis. *Infection Immun.* 79 (8), 3239–3248. doi: 10.1128/IAI.00029-11

Liao, X., Yang, F., Wang, R., He, X., Li, H., Kao, R. Y. T., et al. (2017). Identification of catabolite control protein a from *Staphylococcus aureus* as a target of silver ions. *Chem. Sci.* 8 (12), 8061–8066. doi: 10.1039/c7sc02251d

Liu, H., Chen, H., Sun, Y., Zhang, X., Lu, H., Li, J., et al. (2019). Characterization of the mechanism and impact of staphylokinase on the formation of candida albicans and staphylococcus aureus polymicrobial biofilms. *J. Med. Microbiol.* 68 (3), 355–367. doi: 10.1099/jmm.0.000914

Liu, W., Røder, H. L., Madsen, J. S., Bjarnsholt, T., Sørensen, S. J., and Burmølle, M. (2016). Interspecific bacterial interactions are reflected in multispecies biofilm spatial organization. *Front. Microbiol.* 7. doi: 10.3389/fmicb.2016.01366

Loera-Muro, A., Guerrero-Barrera, A., Tremblay D N, Y., Hathroubi, S., and Angulo, C. (2021). Bacterial biofilm-derived antigens: a new strategy for vaccine development against infectious diseases. *Expert Rev. Vaccines* 20 (4), 385–396. doi: 10.1080/14760584.2021.1892492

Lu, X., Naidis, G., Laroussi, M., Reuter, S., Graves, D., and Ostrikov, K. (2016). Reactive species in non-equilibrium atmospheric-pressure plasmas: Generation, transport, and biological effects. *Phys. Rep.* 630, 1–84. doi: 10.1016/j.physrep.2016.03.003

Łusiak-Szelachowska, M., Weber-Dąbrowska, B., and Górski, A. (2020). Bacteriophages and lysins in biofilm control. *Virol. Sin.* 35 (2), 125–133. doi: 10.1007/s12250-019-00192-3

Makabenta, J. M. V., Nabawy, A., Li, C. H., Schmidt-Malan, S., Patel, R., and Rotello, V. M. (2021). Nanomaterial-based therapeutics for antibiotic-resistant bacterial infections. *Nat. Rev. Microbiol.* 19 (1), 23–36. doi: 10.1038/s41579-020-0420-1

Manfiolli, A. O., Dos Reis, T. F., de Assis, L. J., de Castro, P. A., Silva, L. P., Hori, J. I., et al. (2018). Mitogen activated protein kinases (MAPK) and protein phosphatases are

involved in *Aspergillus fumigatus* adhesion and biofilm formation. *Cell surface (Amsterdam Netherlands)* 1, 43–56. doi: 10.1016/j.tcsw.2018.03.002

Mao, B., Cheng, L., Wang, S., Zhou, J., and Deng, L. (2018). Combat biofilm by bacteriostatic aptamer-functionalized graphene oxide. *Biotechnol. Appl. Biochem.* 65 (3), 355–361. doi: 10.1002/bab.1631

Marsh, P. D., and Zaura, E. (2017). Dental biofilm: ecological interactions in health and disease. *J. Clin. Periodontol* 44 Suppl 18, S12–S22. doi: 10.1111/jcpe.12679

McCourt, J., O'Halloran, D. P., McCarthy, H., O'Gara, J. P., and Geoghegan, J. A. (2014). Fibronectin-binding proteins are required for biofilm formation by community-associated methicillin-resistant staphylococcus aureus strain LAC. *FEMS Microbiol. Lett.* 353 (2), 157–164. doi: 10.1111/1574-6968.12424

Mirzaei, R., Mohammadzadeh, R., Alikhani, M. Y., Shokri Moghadam, M., Karampoor, S., Kazemi, S., et al. (2020). The biofilm-associated bacterial infections unrelated to indwelling devices. *IUBMB Life* 72 (7), 1271–1285. doi: 10.1002/iub.2266

Moshynets, O., Chernii, S., Chernii, V., Losytskyy, M., Karakhim, S., Czerwieniec, R., et al. (2020). Fluorescent β-ketoenole AmyGreen dye for visualization of amyloid components of bacterial biofilms. *Methods Appl. Fluoresc* 8 (3), 035006. doi: 10.1088/2050-6120/ab90e0

Muhammad, M. H., Idris, A. L., Fan, X., Guo, Y., Yu, Y., Jin, X., et al. (2020). Beyond risk: Bacterial biofilms and their regulating approaches. *Front. Microbiol.* 11. doi: 10.3389/fmicb.2020.00928

Mulani, M. S., Kamble, E. E., Kumkar, S. N., Tawre, M. S., and Pardesi, K. R. (2019). Emerging strategies to combat ESKAPE pathogens in the era of antimicrobial resistance: A review. *Front. Microbiol.* 10. doi: 10.3389/fmicb.2019.00539

Muras, A., Mallo, N., Otero-Casal, P., Pose-Rodríguez, J. M., and Otero, A. (2022). Quorum sensing systems as a new target to prevent biofilm-related oral diseases. *Oral. Dis.* 28 (2), 307–313. doi: 10.1111/odi.13689

Muras, A., Otero-Casal, P., Blanc, V., and Otero, A. (2020). Acyl homoserine lactone-mediated quorum sensing in the oral cavity: a paradigm revisited. *Sci. Rep.* 10 (1), 9800. doi: 10.1038/s41598-020-66704-4

Nabawy, A., Makabenta, J. M., Li, C. H., Park, J., Chattopadhyay, A. N., Schmidt-Malan, S., et al. (2021). Activity of biodegradable polymeric nanosponges against dual-species bacterial biofilms. *ACS Biomater Sci. Eng.* 7 (5), 1780–1786. doi: 10.1021/acsbiomaterials.0c01433

Narenji, H., Teymournejad, O., Rezaee, M. A., Taghizadeh, S., Mehramuz, B., Aghazadeh, M., et al. (2020). Antisense peptide nucleic acids againstftsZ andefaA genes inhibit growth and biofilm formation of enterococcusfaecalis. *Microb. Pathog.* 139, 103907. doi: 10.1016/j.micpath.2019.103907

Ng, A. L., To, K. K., Choi, C. C., Yuen, L. H., Yim, S. M., Chan, K. S., et al. (2015). Predisposing factors, microbial characteristics, and clinical outcome of microbial keratitis in a tertiary centre in Hong Kong: A 10-year experience. *J. Ophthalmol.* 2015, 769436. doi: 10.1155/2015/769436

Nguyen, U. T., and Burrows, L. L. (2014). DNase I and proteinase K impair listeria monocytogenes biofilm formation and induce dispersal of pre-existing biofilms. *Int. J. Food Microbiol.* 187, 26–32. doi: 10.1016/j.ijfoodmicro.2014.06.025

Nguyen, H. A., Srivastava, I., Pan, D., and Gruebele, M. (2020). Unraveling the fluorescence mechanism of carbon dots with Sub-Single-Particle resolution. *ACS Nano* 14 (5), 6127–6137. doi: 10.1021/acsnano.0c01924

Ning, Y., Cheng, L., Ling, M., Feng, X., Chen, L., Wu, M., et al. (2015). Efficient suppression of biofilm formation by a nucleic acid aptamer. *Pathog. Dis.* 73 (6), ftv034. doi: 10.1093/femspd/ftv034

Ning, X., Seo, W., Lee, S., Takemiya, K., Rafi, M., Feng, X., et al. (2014). PET imaging of bacterial infections with fluorine-18-labeled maltohexaose. *Angew Chem. Int. Ed Engl.* 53 (51), 14096–14101. doi: 10.1002/anie.201408533

Ning, Y., Wang, X., Chen, P., Liu, S., Hu, J., Xiao, R., et al. (2022). Targeted inhibition of methicillin-resistant staphylococcus aureus biofilm formation by a graphene oxide-loaded aptamer/berberine bifunctional complex. *Drug Delivery* 29 (1), 1675–1683. doi: 10.1080/10717544.2022.2079768

Niveditha, S., Pramodhini, S., Umadevi, S., Kumar, S., and Stephen, S. (2012). The isolation and the biofilm formation of uropathogens in the patients with catheter associated urinary tract infections (UTIs). *J. Clin. Diagn. Res.* 6 (9), 1478–1482. doi: 10.7860/JCDR/2012/4367.2537

Nourbakhsh, F., and Namvar, A. E. (2016). Detection of genes involved in biofilm formation in *Staphylococcus aureus* isolates. *GMS Hyg Infect. Control* 11, Doc07. doi: 10.3205/dgkh000267

Oh, M. J., Babeer, A., Liu, Y., Ren, Z., Wu, J., Issadore, D. A., et al. (2022). Surface topography-adaptive robotic superstructures for biofilm removal and pathogen detection on human teeth. *ACS Nano* 16 (8), 11998–12012. doi: 10.1021/acsnano.2c01950

Okshevsky, M., and Meyer, R. L. (2015). The role of extracellular DNA in the establishment, maintenance and perpetuation of bacterial biofilms. *Crit. Rev. Microbiol.* 41 (3), 341–352. doi: 10.3109/1040841X.2013.841639

Oliveira, V. C., Bim, F. L., Monteiro, R. M., Macedo, A. P., Santos, E. S., Silva-Lovato, C. H., et al. (2020). Identification and characterization of new bacteriophages to control multidrug-resistant pseudomonas aeruginosa biofilm on endotracheal tubes. *Front. Microbiol.* 11. doi: 10.3389/fmicb.2020.580779

Oroh, S. B., Mustopa, A. Z., Budiarti, S., and Budiarto, B. R. (2020). Inhibition of enteropathogenic escherichia coli biofilm formation by DNA aptamer. *Mol. Biol. Rep.* 47 (10), 7567–7573. doi: 10.1007/s11033-020-05822-8

Ortega-Loubon, C., Muñoz-Moreno, M. F., Andrés-García, I., Álvarez, F. J., Gómez-Sánchez, E., Bustamante-Munguira, J., et al. (2019). Nosocomial vs. community-acquired infective endocarditis in Spain: Location, trends, clinical presentation, etiology, and survival in the 21st century. *J. Clin. Med.* 8 (10), 1755. doi: 10.3390/jcm8101755

Ostadhossein, F., Moitra, P., Altun, E., Dutta, D., Sar, D., Tripathi, I., et al. (2021). Function-adaptive clustered nanoparticles reverse streptococcus mutans dental biofilm and maintain microbiota balance. *Commun. Biol.* 4 (1), 846. doi: 10.1038/s42003-021-02372-y

Otsuka, T., Brauer, A. L., Kirkham, C., Sully, E. K., Pettigrew, M. M., Kong, Y., et al. (2017). Antimicrobial activity of antisense peptide-peptide nucleic acid conjugates against non-typeable haemophilus influenzae in planktonic and biofilm forms. *J. Antimicrob. Chemother.* 72 (1), 137–144. doi: 10.1093/jac/dkw384

Otsuka, T., Kitami, O., Kondo, K., Ota, H., Oshima, S., Tsuchiya, A., et al. (2013). Incidence survey of acute otitis media in children in sado island, Japan–sado otitis media study (SADOMS). *PloS One* 8 (7), e68711. doi: 10.1371/journal.pone.0068711

Pahar, B., Madonna, S., Das, A., Albanesi, C., and Girolomoni, G. (2020). Immunomodulatory role of the antimicrobial LL-37 peptide in autoimmune diseases and viral infections. *Vaccines (Basel)* 8 (3), 517. doi: 10.3390/vaccines8030517

Pajkos, A., Deva, A. K., Vickery, K., Cope, C., Chang, L., and Cossart, Y. E. (2003). Detection of subclinical infection in significant breast implant capsules. *Plast. reconstructive Surg.* 111 (5), 1605–1611. doi: 10.1097/01.PRS.0000054768.14922.44

Palmer, J., Flint, S., and Brooks, J. (2007). Bacterial cell attachment, the beginning of a biofilm. *J. Ind. Microbiol. Biotechnol.* 34 (9), 577–588. doi: 10.1007/s10295-007-0234-4

Paluch, E., Rewak-Soroczyńska, J., Jędrusik, I., Mazurkiewicz, E., and Jermakow, K. (2020). Prevention of biofilm formation by quorum quenching. *Appl. Microbiol. Biotechnol.* 104 (5), 1871–1881. doi: 10.1007/s00253-020-10349-w

Pan, T., Chen, H., Gao, X., Wu, Z., Ye, Y., and Shen, Y. (2022). Engineering efficient artificial nanozyme based on chitosan grafted fe-doped-carbon dots for bacteria biofilm eradication. *J. Hazard Mater* 435, 128996. doi: 10.1016/j.jhazmat.2022.128996

Pandit, S., Li, M., Chen, Y., Rahimi, S., Mokkapati, V., Merlo, A., et al. (2021). Graphene-based sensor for detection of bacterial pathogens. *Sensors (Basel)* 21 (23), 8085. doi: 10.3390/s21238085

Park, S., Lee, E. S., Jung, H. I., and Kim, B. I. (2022). Optical detection of oral biofilm in hospitalized geriatric patients using quantitative light-induced fluorescence technology. *Photodiagnosis Photodyn. Ther.* 39, 102962. doi: 10.1016/j.pdpdt.2022.102962

Patange, A., Lu, P., Boehm, D., Cullen, P. J., and Bourke, P. (2019). Efficacy of cold plasma functionalised water for improving microbiological safety of fresh produce and wash water recycling. *Food Microbiol.* 84, 103226. doi: 10.1016/j.fm.2019.05.010

Patange, A. D., Simpson, J. C., Curtin, J. F., Burgess, C. M., Cullen, P. J., and Tiwari, B. K. (2021). Inactivation efficacy of atmospheric air plasma and airborne acoustic ultrasound against bacterial biofilms. *Sci. Rep.* 11 (1), 2346. doi: 10.1038/s41598-021-81977-z

Pelgrift, R. Y., and Friedman, A. J. (2013). Nanotechnology as a therapeutic tool to combat microbial resistance. *Adv. Drug Delivery Rev.* 65 (13-14), 1803–1815. doi: 10.1016/j.addr.2013.07.011

Pérez-Tanoira, R., Fernández-Arias, M., Potel, C., Carballo-Fernández, R., Pérez-Castro, S., Boutinguiza, M., et al. (2022). Silver nanoparticles produced by laser ablation and re-irradiation are effective preventing peri-implantitis multispecies biofilm formation. *Int. J. Mol. Sci.* 23 (19), 12027. doi: 10.3390/ijms231912027

Perwez, M., Ahmad, R., and Sardar, M. (2017). A reusable multipurpose magnetic nanobiocatalyst for industrial applications. *Int. J. Biol. Macromol* 103, 16–24. doi: 10.1016/j.ijbiomac.2017.05.029

Perwez, M., Mazumder, J. A., Noori, R., and Sardar, M. (2021). Magnetic combi CLEA for inhibition of bacterial biofilm: A green approach. *Int. J. Biol. Macromol* 186, 780–787. doi: 10.1016/j.ijbiomac.2021.07.091

Peschel, A., and Otto, M. (2013). Phenol-soluble modulins and staphylococcal infection. *Nat. Rev. Microbiol.* 11 (10), 667–673. doi: 10.1038/nrmicro3110

Pietrocola, G., Campoccia, D., Motta, C., Montanaro, L., Arciola, C. R., and Speziale, P. (2022). Colonization and infection of indwelling medical devices by *Staphylococcus aureus* with an emphasis on orthopedic implants. *Int. J. Mol. Sci.* 23 (11), 5958. doi: 10.3390/ijms23115958

Polewczyk, A., Jachec, W., Tomaszewski, A., Brzozowski, W., Czajkowski, M., Polewczyk, A. M., et al. (2017). Lead-related infective endocarditis: factors influencing the formation of large vegetations. *Europace* 19 (6), 1022–1030. doi: 10.1093/europace/euw121

Pontes, J. T. C., Toledo Borges, A. B., Roque-Borda, C. A., and Pavan, F. R. (2022). Antimicrobial peptides as an alternative for the eradication of bacterial biofilms of multi-drug resistant bacteria. *Pharmaceutics* 14 (3), 642. doi: 10.3390/pharmaceutics14030642

Portelinha, J., and Angeles-Boza, A. M. (2021). The antimicrobial peptide gad-1 clears *Pseudomonas aeruginosa* biofilms under cystic fibrosis conditions. *Chembiochem* 22 (9), 1646–1655. doi: 10.1002/cbic.202000816

Pourhajibagher, M., Etemad-Moghadam, S., Alaeddini, M., Miri Mousavi, R. S., and Bahador, A. (2022). DNA-Aptamer-nanographene oxide as a targeted bio-theragnostic

system in antimicrobial photodynamic therapy against porphyromonas gingivalis. *Sci. Rep.* 12 (1), 12161. doi: 10.1038/s41598-022-16310-3

Prado, M. M., Figueiredo, N., Pimenta, A. L., Miranda, T. S., Feres, M., Figueiredo, L. C., et al. (2022). Recent updates on microbial biofilms in periodontitis: An analysis of *In vitro* biofilm models. *Adv. Exp. Med. Biol.* 1373, 159–174. doi: 10.1007/978-3-030-96881-68

Principi, N., Silvestri, E., and Esposito, S. (2019). Advantages and limitations of bacteriophages for the treatment of bacterial infections. *Front. Pharmacol.* 10. doi: 10.3389/fphar.2019.00513

Qu, Y., Daley, A. J., Istivan, T. S., Rouch, D. A., and Deighton, M. A. (2010). Densely adherent growth mode, rather than extracellular polymer substance matrix build-up ability, contributes to high resistance of staphylococcus epidermidis biofilms to antibiotics. *J. Antimicrob. Chemother.* 65 (7), 1405–1411. doi: 10.1093/jac/dkq119

Røder, H. L., Olsen, N. M. C., Whiteley, M., and Burmølle, M. (2020). Unravelling interspecies interactions across heterogeneities in complex biofilm communities. *Environ. Microbiol.* 22 (1), 5–16. doi: 10.1111/1462-2920.14834

Raad, I., Costerton, W., Sabharwal, U., Sacilowski, M., Anaissie, E., and Bodey, G. P. (1993). Ultrastructural analysis of indwelling vascular catheters: a quantitative relationship between luminal colonization and duration of placement. *J. Infect. Dis.* 168 (2), 400–407. doi: 10.1093/infdis/168.2.400

Rabe, A., Gesell Salazar, M., Michalik, S., Kocher, T., Below, H., Völker, U., et al. (2022). Impact of different oral treatments on the composition of the supragingival plaque microbiome. *J. Oral. Microbiol.* 14 (1), 2138251. doi: 10.1080/20002297.2022.2138251

Rai, A., Vittal, R., and Mohan Raj, J. (2020). Isolation, characterization, and comparison of efficiencies of bacteriophages to reduce planktonic and biofilm-associated staphylococcus aureus. *J. Hlth All Sci-India* 10 (03), 102–108. doi: 10.1055/s-0040-1715773

Raj, V., Kim, Y., Kim, Y. G., Lee, J. H., and Lee, J. (2022). Chitosan-gum arabic embedded alizarin nanocarriers inhibit biofilm formation of multispecies microorganisms. *Carbohydr. polymers* 284, 118959. doi: 10.1016/j.carbpol.2021.118959

Rakhimbekova, A., Kudaibergenov, B., Moldabay, D., Zharylgap, A., Ajunwa, O. M., Marsili, E., et al. (2022). Biofilm detection by a fiber-tip ball resonator optical fiber sensor. *Biosensors (Basel)* 12 (7), 481. doi: 10.3390/bios12070481

Raksha, L., Gangashettappa, N., Shantala, G. B., Nandan, B. R., and Sinha, D. (2020). Study of biofilm formation in bacterial isolates from contact lens wearers. *Indian J. Ophthalmol.* 68 (1), 23–28. doi: 10.4103/ijo.IJO_947_19

Rashki, S., Asgarpour, K., Tarrahimofrad, H., Hashemipour, M., Ebrahimi, M. S., Fathizadeh, H., et al. (2021). Chitosan-based nanoparticles against bacterial infections. *Carbohydr Polym* 251, 117108. doi: 10.1016/j.carbpol.2020.117108

Rather, M. A., Gupta, K., and Mandal, M. (2021). Microbial biofilm: formation, architecture, antibiotic resistance, and control strategies. *Braz. J. Microbiol.* 52 (4), 1701–1718. doi: 10.1007/s42770-021-00624-x

Roy, R., Tiwari, M., Donelli, G., and Tiwari, V. (2018). Strategies for combating bacterial biofilms: A focus on anti-biofilm agents and their mechanisms of action. *Virulence* 9 (1), 522–554. doi: 10.1080/21505594.2017.1313372

Ruangcharoen, S., Suwannarong, W., Lachica, M. R. C. T., Bolscher, J. G. M., Nazmi, K., Khunkitti, W., et al. (2017). Killing activity of LFchimera on periodontopathic bacteria and multispecies oral biofilm formation *in vitro*. *World J. Microbiol. Biotechnol.* 33 (9), 167. doi: 10.1007/s11274-017-2334-2

Sadiq, F. A., Burmølle, M., Heyndrickx, M., Flint, S., Lu, W., Chen, W., et al. (2021). Community-wide changes reflecting bacterial interspecific interactions in multispecies biofilms. *Crit. Rev. Microbiol.* 47 (3), 338–358. doi: 10.1080/1040841X.2021.1887079

Sadykov, M. R., Windham, I. H., Widhelm, T. J., Yajjala, V. K., Watson, S. M., Endres, J. L., et al. (2019). CidR and CcpA synergistically regulate *Staphylococcus aureus* cidABC expression. *J. bacteriol* 201 (23), e00371–e00319. doi: 10.1128/JB.00371-19

Saggu, S. K., Jha, G., and Mishra, P. C. (2019). Enzymatic degradation of biofilm by metalloprotease from microbacterium sp. SKS10. *Front. Bioeng Biotechnol.* 7. doi: 10.3389/fbioe.2019.00192

Salmanoglu, E., Kim, S., and Thakur, M. L. (2018). Currently available radiopharmaceuticals for imaging infection and the holy grail. *Semin. Nucl. Med.* 48 (2), 86–99. doi: 10.1053/j.semnuclmed.2017.10.003

Sauer, K. (2003). The genomics and proteomics of biofilm formation. *Genome Biol.* 4 (6), 219. doi: 10.1186/gb-2003-4-6-219

Schilcher, K., and Horswill, A. R. (2020). Staphylococcal biofilm development: Structure, regulation, and treatment strategies. *Microbiol. Mol. Biol. Rev.* 84 (3), e00026–e00019. doi: 10.1128/MMBR.00026-19

Schoenborn, A. A., Yannarell, S. M., Wallace, E. D., Clapper, H., Weinstein, I. C., and Shank, E. A. (2021). Defining the expression, production, and signaling roles of specialized metabolites during bacillus subtilis differentiation. *J. bacteriol* 203 (22), e0033721. doi: 10.1128/JB.00337-21

Schulze, A., Mitterer, F., Pombo, J. P., and Schild, S. (2021). Biofilms by bacterial human pathogens: Clinical relevance - development, composition and regulation - therapeutical strategies. *Microb. Cell* 8 (2), 28–56. doi: 10.15698/mic2021.02.741

Schwartz-Duval, A. S., Konopka, C. J., Moitra, P., Daza, E. A., Srivastava, I., Johnson, E. V., et al. (2020). Intratumoral generation of photothermal gold nanoparticles through a vectorized biomineralization of ionic gold. *Nat. Commun.* 11 (1), 4530. doi: 10.1038/s41467-020-17595-6

Sengupta, B., Adhikari, P., Mallet, E., Havner, R., and Pradhan, P. (2020). Spectroscopic study on *Pseudomonas aeruginosa* biofilm in the presence of the aptamer-DNA scaffolded silver nanoclusters. *Mol (Basel Switzerland)* 25 (16), 3631. doi: 10.3390/molecules25163631

Sharma, D., Kumar, B., Lata, M., Joshi, B., Venkatesan, K., Shukla, S., et al. (2015). Comparative proteomic analysis of aminoglycosides resistant and susceptible mycobacterium tuberculosis clinical isolates for exploring potential drug targets. *PloS One* 10 (10), e0139414. doi: 10.1371/journal.pone.0139414

Sharma, D., Lata, M., Singh, R., Deo, N., Venkatesan, K., and Bisht, D. (2016). Cytosolic proteome profiling of aminoglycosides resistant mycobacterium tuberculosis clinical isolates using MALDI-TOF/MS. *Front. Microbiol.* 7. doi: 10.3389/fmicb.2016.01816

Sharma, D., Misba, L., and Khan, A. U. (2019). Antibiotics versus biofilm: an emerging battleground in microbial communities. *Antimicrob. Resist. Infect. Control* 8, 76. doi: 10.1186/s13756-019-0533-3

Sharma, U., Vipra, A., and Channabasappa, S. (2018). Phage-derived lysins as potential agents for eradicating biofilms and persisters. *Drug Discovery Today* 23 (4), 848–856. doi: 10.1016/j.drudis.2018.01.026

Shatila, F., Yaşa, İ., and Yalçın, H. T. (2020). Inhibition of salmonella enteritidis biofilms by salmonella invasion protein-targeting aptamer. *Biotechnol. Lett.* 42 (10), 1963–1974. doi: 10.1007/s10529-020-02920-2

She, P., Wang, Y., Liu, Y., Tan, F., Chen, L., Luo, Z., et al. (2019). Effects of exogenous glucose on pseudomonas aeruginosa biofilm formation and antibiotic resistance. *MicrobiologyOpen* 8 (12), e933. doi: 10.1002/mbo3.933

Shen, F., Ge, C., and Yuan, P. (2020). Metabolomics study reveals inhibition and metabolic dysregulation in staphylococcus aureus planktonic cells and biofilms induced by carnosol. *Front. Microbiol.* 11. doi: 10.3389/fmicb.2020.538572

Shen, D., Langenheder, S., and Jürgens, K. (2018). Dispersal modifies the diversity and composition of active bacterial communities in response to a salinity disturbance. *Front. Microbiol.* 9. doi: 10.3389/fmicb.2018.02188

Singh, N., Mishra, S., Mondal, A., Sharma, D., Jain, N., and Aseri, G. K. (2022). Potential of desert medicinal plants for combating resistant biofilms in urinary tract infections. *Appl. Biochem. Biotechnol.* doi: 10.1007/s12010-022-03950-4

Skindersoe, M. E., Alhede, M., Phipps, R., Yang, L., Jensen, P. O., Rasmussen, T. B., et al. (2008). Effects of antibiotics on quorum sensing in *Pseudomonas aeruginosa*. *Antimicrob. Agents Chemother.* 52 (10), 3648–3663. doi: 10.1128/AAC.01230-07

Slomberg, D. L., Lu, Y., Broadnax, A. D., Hunter, R. A., Carpenter, A. W., and Schoenfisch, M. H. (2013). Role of size and shape on biofilm eradication for nitric oxide-releasing silica nanoparticles. *ACS Appl. Mater Interfaces* 5 (19), 9322–9329. doi: 10.1021/am402618w

Solano, C., Echeverz, M., and Lasa, I. (2014). Biofilm dispersion and quorum sensing. *Curr. Opin. Microbiol.* 18, 96–104. doi: 10.1016/j.mib.2014.02.008

Strahm, C., Albrich, W. C., Zdravkovic, V., Schöbi, B., Hildebrandt, G., and Schlegel, M. (2018). Infection rate after cranial neurosurgical procedures: A prospective single-center study. *World Neurosurg.* 111, e277–e285. doi: 10.1016/j.wneu.2017.12.062

Sybesma, W., Zbinden, R., Chanishvili, N., Kutateladze, M., Chkhotua, A., Ujmajuridze, A., et al. (2016). Bacteriophages as potential treatment for urinary tract infections. *Front. Microbiol.* 7. doi: 10.3389/fmicb.2016.00465

Tagliaferri, T. L., Jansen, M., and Horz, H. P. (2019). Fighting pathogenic bacteria on two fronts: Phages and antibiotics as combined strategy. *Front. Cell Infect. Microbiol.* 9. doi: 10.3389/fcimb.2019.00022

Tam, K., and Torres, V. J. (2019). *Staphylococcus aureus* secreted toxins and extracellular enzymes. *Microbiol. Spectr.* 7 (2). doi: 10.1128/microbiolspec.GPP3-0039-2018

Tan, Y., Ma, S., Leonhard, M., Moser, D., Ludwig, R., and Schneider-Stickler, B. (2020). Co-Immobilization of cellobiose dehydrogenase and deoxyribonuclease I on chitosan nanoparticles against fungal/bacterial polymicrobial biofilms targeting both biofilm matrix and microorganisms. *Mater Sci. Eng. C Mater Biol. Appl.* 108, 110499. doi: 10.1016/j.msec.2019.110499

Tian, F., Li, J., Nazir, A., and Tong, Y. (2021). Bacteriophage - a promising alternative measure for bacterial biofilm control. *Infect. Drug Resist.* 14, 205–217. doi: 10.2147/IDR.S290093

Tuson, H. H., and Weibel, D. B. (2013). Bacteria-surface interactions. *Soft Matter* 9 (18), 4368–4380. doi: 10.1039/C3SM27705D

Unnikrishnan, S., and Klibanov, A. L. (2012). Microbubbles as ultrasound contrast agents for molecular imaging: preparation and application. *AJR Am. J. Roentgenol.* 199 (2), 292–299. doi: 10.2214/AJR.12.8826

Urwin, L., Okurowska, K., Crowther, G., Roy, S., Garg, P., Karunakaran, E., et al. (2020). Corneal infection models: Tools to investigate the role of biofilms in bacterial keratitis. *Cells* 9 (11), 2450. doi: 10.3390/cells9112450

Vaidya, K., Osgood, R., Ren, D., Pichichero, M. E., and Helguera, M. (2014). Ultrasound imaging and characterization of biofilms based on wavelet de-noised radiofrequency data. *Ultrasound Med. Biol.* 40 (3), 583–595. doi: 10.1016/j.ultrasmedbio.2013.11.005

Vandeplassche, E., Sass, A., Ostyn, L., Burmølle, M., Kragh, K. N., Bjarnsholt, T., et al. (2020). Antibiotic susceptibility of cystic fibrosis lung microbiome members in a multispecies biofilm. *Biofilm* 2, 100031. doi: 10.1016/j.bioflm.2020.100031

Van Impe, J., Smet, C., Tiwari, B., Greiner, R., Ojha, S., Stulić, V., et al. (2018). State of the art of nonthermal and thermal processing for inactivation of micro-organisms. *J. Appl. Microbiol.* 125 (1), 16–35. doi: 10.1111/jam.13751

Wang, D., Lin, Z., Ding, X., Hu, J., and Liu, Y. (2016). The Comparison of the Combined Toxicity between Gram-negative and Gram-positive Bacteria: a Case Study of Antibiotics and Quorum-sensing Inhibitors. *Mol Inform.* 35 (2), 54–61. doi: 10.1002/minf.201500061

Whitchurch, C. B., Tolker-Nielsen, T., Ragas, P. C., and Mattick, J. S. (2002). Extracellular DNA required for bacterial biofilm formation. *Science* 295 (5559), 1487. doi: 10.1126/science.295.5559.1487

Whiteley, M., Diggle, S. P., and Greenberg, E. P. (2017). Progress in and promise of bacterial quorum sensing research. *Nature* 551 (7680), 313–320. doi: 10.1038/nature24624

Wi, Y. M., and Patel, R. (2018). Understanding biofilms and novel approaches to the diagnosis, prevention, and treatment of medical device-associated infections. *Infect. Dis. Clinics North America* 32 (4), 915–929. doi: 10.1016/j.idc.2018.06.009

Wiens, J. R., Vasil, A. I., Schurr, M. J., and Vasil, M. L. (2014). Iron-regulated expression of alginate production, mucoid phenotype, and biofilm formation by *Pseudomonas aeruginosa*. *mBio* 5 (1), e01010–e01013. doi: 10.1128/mBio.01010-13

Wiley, L., Bridge, D. R., Wiley, L. A., Odom, J. V., Elliott, T., and Olson, J. C. (2012). Bacterial biofilm diversity in contact lens-related disease: emerging role of achromobacter, stenotrophomonas, and delftia. *Invest. Ophthalmol. Vis. Sci.* 53 (7), 3896–3905. doi: 10.1167/iovs.11-8762

Wille, J., and Coenye, T. (2020). Biofilm dispersion: The key to biofilm eradication or opening pandora's box? *Biofilm* 2, 100027. doi: 10.1016/j.bioflm.2020.100027

Wojciechowska, M., Równicki, M., Mieczkowski, A., Miszkiewicz, J., and Trylska, J. (2020). Antibacterial peptide nucleic acids-facts and perspectives. *Molecules* 25 (3), 559. doi: 10.3390/molecules25030559

Wu, H., Moser, C., Wang, H. Z., Høiby, N., and Song, Z. J. (2015). Strategies for combating bacterial biofilm infections. *Int. J. Oral. Sci.* 7 (1), 1–7. doi: 10.1038/ijos.2014.65

Wuersching, S. N., Huth, K. C., Hickel, R., and Kollmuss, M. (2021a). Inhibitory effect of LL-37 and human lactoferricin on growth and biofilm formation of anaerobes associated with oral diseases. *Anaerobe* 67, 102301. doi: 10.1016/j.anaerobe.2020.102301

Wuersching, S. N., Huth, K. C., Hickel, R., and Kollmuss, M. (2021b). Targeting antibiotic tolerance in anaerobic biofilms associated with oral diseases: Human antimicrobial peptides LL-37 and lactoferricin enhance the antibiotic efficacy of amoxicillin, clindamycin and metronidazole. *Anaerobe* 71, 102439. doi: 10.1016/j.anaerobe.2021.102439

Xu, Y., Dhaouadi, Y., Stoodley, P., and Ren, D. (2020). Sensing the unreachable: challenges and opportunities in biofilm detection. *Curr. Opin. Biotechnol.* 64, 79–84. doi: 10.1016/j.copbio.2019.10.009

Xu, F., Huang, X., Wang, Y., and Zhou, S. (2020). A size-changeable collagenase-modified nanoscavenger for increasing penetration and retention of nanomedicine in deep tumor tissue. *Adv. Mater.* 32 (16), e1906745. doi: 10.1002/adma.201906745

Xu, Y., Li, C., Jiang, Y., Guo, M., Yang, Y., Yang, Y., et al. (2022). Electrochemical impedance spectroscopic detection of e.coli with machine learning. *J. Electrochem. Soc.* 167 (4), 047508. doi: 10.1149/1945-7111/ab732f

Yao, S., Hao, L., Zhou, R., Jin, Y., Huang, J., and Wu, C. (2022). Multispecies biofilms in fermentation: Biofilm formation, microbial interactions, and communication. *Compr. Rev. Food Sci. Food Saf.* 21 (4), 3346–3375. doi: 10.1111/1541-4337.12991

Yazici, A., Ortucu, S., Taskin, M., and Marinelli, L. (2018). Natural-based antibiofilm and antimicrobial peptides from microorganisms. *Curr. Top. Med. Chem.* 18 (24), 2102–2107. doi: 10.2174/1568026618666181112143351

Ye, Y., Ling, N., Gao, J., Zhang, X., Zhang, M., Tong, L., et al. (2018). Roles of outer membrane protein W (OmpW) on survival, morphology, and biofilm formation under NaCl stresses in cronobacter sakazakii. *J. dairy Sci.* 101 (5), 3844–3850. doi: 10.3168/jds.2017-13791

Yeor-Davidi, E., Zverzhinetsky, M., Krivitsky, V., and Patolsky, F. (2020). Real-time monitoring of bacterial biofilms metabolic activity by a redox-reactive nanosensors array. *J. Nanobiotechnol* 18 (1), 81. doi: 10.1186/s12951-020-00637-y

Yi, X., Wang, C., Yu, X., Su, W., and Yuan, Z. (2021). Chitosan/zinc nitrate microneedles for bacterial biofilm eradication. *J. BioMed. Mater. Res. B Appl. Biomater* 109 (6), 911–920. doi: 10.1002/jbm.b.34755

Yu, Q., Deng, T., Lin, F. C., Zhang, B., and Zink, J. I. (2020). Supramolecular assemblies of heterogeneous mesoporous silica nanoparticles to Co-deliver antimicrobial peptides and antibiotics for synergistic eradication of pathogenic biofilms. *ACS Nano* 14 (5), 5926–5937. doi: 10.1021/acsnano.0c01336

Yu, P., Wang, C., Zhou, J., Jiang, L., Xue, J., and Li, W. (2016). Influence of surface properties on adhesion forces and attachment of streptococcus mutans to zirconia *In vitro*. *BioMed. Res. Int.* 2016, 8901253. doi: 10.1155/2016/8901253

Zhang, X., Chen, X., Song, J., Zhang, J., Ren, X., and Zhao, Y. (2020). Size-transformable nanostructures: From design to biomedical applications. *Adv. Mater* 32 (48), e2003752. doi: 10.1002/adma.202003752

Zhang, B., and Powers, R. (2012). Analysis of bacterial biofilms using NMR-based metabolomics. *Future Med. Chem.* 4 (10), 1273–1306. doi: 10.4155/fmc.12.59

Zhang, S., Wang, L., Liang, X., Vorstius, J., Keatch, R., Corner, G., et al. (2019). Enhanced antibacterial and antiadhesive activities of silver-PTFE nanocomposite coating for urinary catheters. *ACS Biomater Sci. Eng.* 5 (6), 2804–2814. doi: 10.1021/acsbiomaterials.9b00071

Zhao, T., Chen, J., Liu, S., Yang, J., Wu, J., Miao, L., et al. (2022). Transcriptome analysis of fusobacterium nucleatum reveals differential gene expression patterns in the biofilm versus planktonic cells. *Biochem. Biophys. Res. Commun.* 593, 151–157. doi: 10.1016/j.bbrc.2021.11.075

Zheng, M., Zhu, K., Peng, H., Shang, W., Zhao, Y., Lu, S., et al. (2022). CcpA regulates *Staphylococcus aureus* biofilm formation through direct repression of staphylokinase expression. *Antibiotics (Basel)* 11 (10), 1426. doi: 10.3390/antibiotics11101426

Zhou, J. W., Chen, T. T., Tan, X. J., Sheng, J. Y., and Jia, A. Q. (2018). Can the quorum sensing inhibitor resveratrol function as an aminoglycoside antibiotic accelerant against *Pseudomonas aeruginosa*? *Int. J. Antimicrob. Agents* 52 (1), 35–41. doi: 10.1016/j.ijantimicag.2018.03.002

Zurita, M. E., Wilk, M. M., Carriquiriborde, F., Bartel, E., Moreno, G., Misiak, A., et al. (2019). A pertussis outer membrane vesicle-based vaccine induces lung-resident memory CD4 T cells and protection against bordetella pertussis, including pertactin deficient strains. *Front. Cell Infect. Microbiol.* 9. doi: 10.3389/fcimb.2019.00125

frontiers | Frontiers in Cellular and Infection Microbiology

TYPE Original Research
PUBLISHED 02 May 2023
DOI 10.3389/fcimb.2023.1142274

OPEN ACCESS

EDITED BY
Ashraf Zarkan,
University of Cambridge, United Kingdom

REVIEWED BY
Roberto Rusconi,
Humanitas University, Italy
María Guembe,
Gregorio Marañón Hospital, Spain
Oana Ciofu,
University of Copenhagen, Denmark

*CORRESPONDENCE
Laia Fernández-Barat
lfernan1@recerca.clinic.cat
Antoni Torres
atorres@clinic.cat

†These authors have contributed equally to this work and share first authorship

SPECIALTY SECTION
This article was submitted to Biofilms, a section of the journal Frontiers in Cellular and Infection Microbiology

RECEIVED 11 January 2023
ACCEPTED 04 April 2023
PUBLISHED 02 May 2023

CITATION
Fernández-Barat L, Vázquez Burgos N, Alcaraz V, Bueno-Freire L, López-Aladid R, Cabrera R, Gabarrús A, Palomeque A, Oscanoa P, Ceccato A, Motos A, Amaro R, Bernardi T, Provot C, Soler-Comas A, Muñoz L, Vila J and Torres A (2023) The value of biofilm testing to guide antimicrobial stewardship in chronic respiratory diseases.
Front. Cell. Infect. Microbiol. 13:1142274.
doi: 10.3389/fcimb.2023.1142274

The value of biofilm testing to guide antimicrobial stewardship in chronic respiratory diseases

Laia Fernández-Barat[1,2*†], Nil Vázquez Burgos[1,2†], Victoria Alcaraz[1,2], Leticia Bueno-Freire[1,2], Ruben López-Aladid[1,2], Roberto Cabrera[1,2], Albert Gabarrús[1,2], Andrea Palomeque[1,2], Patricia Oscanoa[1,2], Adrian Ceccato[1,2], Ana Motos[1,2], Rosanel Amaro[1,2], Thierry Bernardi[3,4], Christian Provot[3,4], Alba Soler-Comas[1,2], Laura Muñoz[5], Jordi Vila[5] and Antoni Torres[1,2*]

[1]Cellex Laboratory, CibeRes (CB06/06/0028)-Instituto de Investigaciones Biomédicas August Pi i Sunyer (IDIBAPS), School of Medicine, University of Barcelona, Barcelona, Spain, [2]Pneumology Service, Respiratory Institute, Hospital Clinic, Barcelona, Spain, [3]BioFilm Pharma SAS, Lyon, France, [4]BioFilm Control SAS, Saint Beauzire, France, [5]Microbiology Service, Hospital Clinic, Barcelona, Spain

Introduction: Biofilm production is an important yet currently overlooked aspect of diagnostic microbiology that has implications for antimicrobial stewardship. In this study, we aimed to validate and identify additional applications of the BioFilm Ring Test® (BRT) for Pseudomonas aeruginosa (PA) isolates from patients with bronchiectasis (BE).

Materials and methods: Sputa were collected from BE patients who had at least one PA positive culture in the previous year. We processed the sputa to isolate both mucoid and non-mucoid PA, and determined their susceptibility pattern, mucA gene status, and presence of ciprofloxacin mutations in QRDR genes. The Biofilm production index (BPI) was obtained at 5 and 24 hours. Biofilms were imaged using Gram staining.

Results: We collected 69 PA isolates, including 33 mucoid and 36 non-mucoid. A BPI value below 14.75 at 5 hours predicted the mucoid PA phenotype with 64% sensitivity and 72% specificity.

Conclusion: Overall, our findings suggest that the fitness-cost associated with the mucoid phenotype or ciprofloxacin resistance is shown through a time-dependent BPI profile. The BRT has the potential to reveal biofilm features with clinical implications.

KEYWORDS

***Pseudomonas aeruginosa*, antimicrobial agents, antimicrobial resistances, biofilm diagnose, biofilm**

1 Introduction

Non-cystic fibrosis (non-CF) bronchiectasis (BE) is a chronic structural and inflammatory respiratory disease characterized by irreversible destruction and dilatation of the bronchi that result in recurrent infections and exacerbations. Physiopathologically, the tissular destruction involves a vicious circle of impaired mucociliary clearance, bronchial infection and chronic inflammation (Cohen and Sahn, 1999; Barker, 2002; King et al., 2006; Hill et al., 2017; Polverino et al., 2017; Flume et al., 2018).. *Haemophilus influenzae* and *Pseudomonas aeruginosa* (PA) are the most frequently isolated microorganisms in non-CF BE exacerbations (Chandrasekaran et al., 2018). Furthermore, PA is an independent factor contributing to a threefold increase in the risk of death. It is also associated with a higher number of exacerbations and hospitalizations, and higher symptomatology perceived by the patient (Finch et al., 2015). Given the relationship between PA and poor clinical outcomes in patients with BE, its early detection and appropriate management are essential (Fernández-Barat et al., 2021).

Early PA colonization is frequently associated with the isolation of the non-mucoid phenotype. However, unless eradicated, the non-mucoid strain can shift to a mucoid PA phenotype through genetic changes such as mutations in mucA gene (Fernández-Barat et al., 2017; Crisafulli et al., 2018; Dhand, 2018). These mutations are considered to play an important role in the genetic adaptive evolution of PA. It has been demonstrated that mutator populations are amplified in the lung by presenting adaptive mutations (Ciofu et al., 2017). Loss-of-function mutations in mucA cause an overproduction of alginate exopolysaccharide, which is characteristic of the mucoid phenotype. The mucoid phenotype has been shown to be a hallmark of chronic infections, higher viscoelasticity of sputum (Alcaraz-Serrano et al., 2019) and biofilm maturation, which impair both the effect of antibiotics and host immune functions (Malhotra et al., 2018). In addition, the metabolic rate of PA within biofilm aggregates is lower than its planktonic counterparts, driving bacterial cells to a dormant state in which some of them become "persister cells" that do not divide and are highly tolerant to antimicrobials (Lewis, 2007; Yang et al., 2008).

It is important to highlight that the Minimum Inhibitory Concentration (MIC) routinely reported by the microbiology laboratories does not reflect the Minimum Biofilm Inhibitory Concentration (MBIC) since the MBIC is often several times greater than the MIC of a planktonic PA strain (Ciofu et al., 2017). Thus, the diagnostic value of biofilm formation is currently underestimated hindering the management of patients with chronic respiratory diseases (Wang et al., 2012; Thieme et al., 2019).

Multiple methods are available to measure bacterial biofilm production, although none of them are currently applied in the routine standard of care (Peeters et al., 2008; Pantanella et al., 2013). The microtiter plate method is extensively used to quantify the *in vitro* biofilm capability of bacteria, but it is limited by the inability to confidently extrapolate those results to *in vivo* scenarios (Fernández-Barat et al., 2018). BioFilm Ring Test® (BRT) is a novel technology developed to determine biofilm formation production by the measurement of the adhesion between bacteria. It has shown increased sensitivity and specificity compared to the traditional crystal violet test. The BRT does not require staining, is easy to handle and the results can be obtained in a few hours, being more suitable for clinical practice than previous techniques (Chavant et al., 2007; Sulaeman et al., 2010; Olivares et al., 2016). The BRT has been recently shown to have a potential application in the selection of antimicrobials in CF (Olivares et al., 2016). However, additional applications of the BRT, such as its correlation with microbiological and clinical features have not been previously reported (Di Domenico et al., 2016). We aimed to validate the BRT assay using a significant number of PA clinical isolates from Non-CF BE patients. We also aimed to investigate additional applications of the BRT by comparing the biofilm production index (BPI) between mucoid and non-mucoid PA isolates, susceptible and resistant PA, presence and absence of biofilm pattern by Gram and intermittent and chronic infection status, in addition to assess the sensitivity and specificity for significant associations. Finally, we correlated the BPI with the mutations in mucA gene.

2 Material and methods

2.1 Definitions

2.1.1 Bronchiectasis

A diagnosis of BE of any cause in the absence of chronic obstructive pulmonary disease (COPD) using high-resolution computed tomography (HRCT) of the chest.

2.1.2 Bronchiectasis with chronic obstructive pulmonary disease

Diagnosis of BE as mentioned above and a diagnosis of COPD (persistent respiratory symptoms and airflow limitation with a history of smoking, according to the GOLD criteria (Vogelmeier et al., 2017).

2.1.3 Chronic infection

≥2 PA isolates in respiratory specimens ≥3 months apart in 1 year (Polverino et al., 2017).

2.1.4 Intermittent infection

PA isolates in respiratory specimens not accomplishing the chronic infection definition (Fernández-Barat et al., 2021).

2.1.5 Exacerbation

Deterioration in three or more key symptoms: cough, sputum volume and/or consistency, sputum purulence, dyspnea and/or exercise tolerance, fatigue or malaise, and hemoptysis, in accordance with European guidelines (Hill et al., 2017).

2.1.6 Slow growing PA

PA with an increased BPI in 24 h of incubation when compared to 5 h of incubation.

2.2 Patients and strains

The studies involving human participants were reviewed and approved by the Internal Review Board of the Hospital Clinic of Barcelona (registry number HCB/0236). Written informed consent was obtained from all patients. The study was carried out in compliance with the Declaration of Helsinki (current version: Fortaleza, Brazil, October 2013) and with the requirements of the 2007 Spanish Biomedical Research Act.

All patients (≥18 years) had BE (confirmed by a CT scan) with or without COPD and had at least one recent positive sputum culture for PA prior to study recruitment. Valid sputa were immersed in 1:1 Dithiothreitol (DTT) solution and sonicated for 5 min at 40KHz in an ultrasonic cleaning equipment (Branson 3510 E-MT; Bransonic, Danbury, CT, USA), before being serially diluted in 0.9% saline solution and cultured both in MacConkey agar and Blood agar (BD). PA strains were isolated and identified by MALDI-TOF. They were classified as mucoid or non-mucoid phenotypes depending on the colony morphology. An extension of each fresh sample was obtained for the Gram staining.

2.3 Imaging PA biofilms by Gram staining

The quality of the sample was evaluated by Gram staining in the area of maximal purulence, according to the criteria of Murray and Washington (1975). To image the Gram staining, an Olympus BX41TF microscope (Olympus, Tokyo, Japan) with a 100X oil immersion lens was used. Gram-negative bacilli susceptible of PA (PA was confirmed in culture from the same sputum sample) were classified into 3 groups: planktonic PA (Gram-negative rods present without aggregates), PA biofilm (Gram-negative rods present in aggregates) and PA alginate (Gram-negative rods in aggregates embedded in alginate).

2.4 Susceptibility testing

Strains were classified as resistant, intermediate or susceptible to amikacin, tobramycin, imipenem, meropenem, ceftazidime, ciprofloxacin, piperacillin-tazobactam, aztreonam, and colistin according to the EUCAST (2017) breakpoints using the disk diffusion method (BD) following the EUCAST protocol. ATCC 27853 was used as quality control. Strains were then categorized as non-multidrug resistant (non-MDR) or resistant strains (including multidrug resistant (MDR) and extensive drug resistant (XDR) strains) according to current definitions (Magiorakos et al., 2012).

2.5 Biofilm ring test

The test was performed using the reagents in the Biofilm Ring Test kit (KIT01) (Biofilm Control, Saint Beauzire, France), following Chavant T. et al. protocol (Chavant et al., 2007). Bead aggregation was analyzed by the BFC Elements 3.0 software (Biofilm reader, Biofilm Control, Saint Beauzire, France). In order to minimize variability on the BPI, 8 intra-assay replicates and inter-assay triplicates were performed. PA were then classified into weak BPI<5, moderate BPI≥5 but <10, strong BPI≥10 but <15 and very strong BPI≥15 biofilm producers based on their BPI. In a subset of 20 mucoid and 9 non-mucoid PA suspected of slow biofilm production at 5h, an extended experiment was performed, using the aforementioned protocol but with a 24h incubation instead of the 5h of the standard protocol in order to elucidate the role of the PA slow growth in the BPI results. We classified the strains showing an increase in BPI from 5 to 24 hours as slow-growing *Pseudomonas aeruginosa* strains. To estimate their growth rate, we used the percentage of the total BPI at 5 hours. We then compared the growth rates between mucoid and non-mucoid strains that exhibited slow growth.

2.6 Mutations in mucA and QRDR genes

The mucA gene of all PA and for quinolone resistant QRDR genes (gyrA, gyrB, parC and parE) for 43 PA isolates included in this study were amplified by PCR. Primers used for amplification and sequencing are reported in Table 1 or previously published (Cabrera et al., 2022). PCR products were sequenced by Sanger methods (Genewiz, Germany), and were analyzed by alignment with the corresponding template sequence of PAO1 mucA at GenBank (Ciofu et al., 2010). PCR was performed in a Veriti PCR Thermal Cycler (Applied Biosystems, France) for 2 min denaturation at 94°C followed by 30 cycles of 1 min at 94°C, 1 min at 60°C and 1 min at 72°C, with a final extension of 7 min at 72°C.

2.7 Statistical analysis

Categorical variables were reported as number (%), while continuous variables were reported as mean ± standard deviation (SD) or median (interquartile range, IQR), if the distribution was normal or non-normal, respectively. Continuous variables between groups were compared using the one-way analysis of variance (ANOVA) followed by a *post-hoc* pairwise Tukey's honestly significant difference (HSD) or Kruskal-Wallis tests, as appropriate. Paired samples were compared with a paired t-test or the nonparametric Wilcoxon signed-rank test when appropriate. Chi-squared test was performed for categorical comparisons.

Receiver operating characteristic (ROC) curves (*) were constructed to determine the best cut-point for BPI to predict the

TABLE 1 Amplification and sequencing primers for mucA.

mucA1	F (5' 3')	CTCTGCAGCCTTTGTTGCGAGAAG
mucA1	R (5' 3')	CTGCCAAGCAAAAGCAACAGGGAGG
mucA2	F (5' 3')	GTGCGTCTGTACAACCAGAACGACG
mucA2	R (5' 3')	GTCGTTCTGGTTGTACAGACGCACG

PA phenotype or resistance to ciprofloxacin. Youden's index (Youden, 1950) was defined for all points along the ROC curve, and the maximum value of the index was used as a criterion for selecting the optimum cut-off point. To determine the predictive capacity of BPI for identification of PA mucoid phenotype or resistance to ciprofloxacin, we determined sensitivity, specificity, positive and negative predictive values (*), along with the 95% confidence intervals (CIs).

All statistical analyses were performed with the SPSS program version 22.0. The level of significance was adjusted at 0.05 (two-tailed).

3 Results

3.1 Patients and strains

Sixty-nine BE patients were included (25 of them with BE-COPD). Forty-eight patients had been chronically infected by PA for a period of 5.5 [2.25-12] years whilst 21 were intermittently colonized. Thirty-three mucoid and 36 non-mucoid PA isolates similarly distributed between the BE-COPD and BE (p=0.78) were found. The distribution of mucoid vs non-mucoid PA strains was different between chronically infected and intermittently colonized patients (94% vs 6% for the mucoid strains and 47.2% vs 52.8% for the non-mucoid strains, respectively, $p < 0.001$).

3.2 Gram visualization

Presence of alginate in sputa Gram stains was observed in 44% of the patients with a chronic PA respiratory infection, but was not found in the non-chronically infected patients ($p = 0.004$). Alginate was more frequently when the mucoid PA was isolated than when the non-mucoid PA was isolated (93.3% vs 6.7%, respectively, $p < 0.001$) and more frequently observed in the non-MDR PA isolates than in the resistant ones (MDR and XDR) (78.6% vs 21.4%, respectively, $p = 0.010$). The presence of alginate in the Gram stains did not show a statistically significant association with differences in the BPI, although the sputum samples with alginate were associated with lower BPI values at 5 h than those without alginate (13.38 [6.98-19.73] vs 16.7 [7.18-20.00], $p = 0.202$) (Figure 1).

3.3 Biofilm ring test

The BPI after 5 h was significantly different between the mucoid and non-mucoid strains, being higher in the non-mucoid isolates (12.36 [5.55-18.74] vs 19.08 [10.63-20.00], respectively, $p = 0.006$) (Figure 2A). In a subset of 22 mucoid and 18 non-mucoid PA strains with slow growth, BPI was compared at 5 h vs 24 h of incubation. The percentage of BPI achieved at 5 h was different between mucoid and non-mucoid strains (35.33 ± 23.78 vs. 68.37 ± 23.07 ± 23.07, $p<0.0001$), which demonstrated that the delay in growth was superior in mucoid than in non-mucoid strains. The BPI increased in a time-dependent manner for mucoids at 5 vs 24h (4.55 [1.18-7.86] vs 19.75 [18.60-20.00], respectively, $p = 0.001$). By contrast, no statistically significant increase in the BPI was found for non-mucoid strains at 5 h vs 24 h (6.84 [6.01-9.05] vs 19.55 [12.09-19.96], respectively, $p = 0.068$) (Figure 2B).

In particular, all the 8 mucoid strains with a low BPI that were weak biofilm producers at 5 h exhibited a strong and very strong biofilm producer phenotype at 24 h based on their BPI (1.98 [0.38-4.19] vs 19.31 [17.13-20.00], respectively, $p = 0.012$). Additionally, the categorical stratification of the BPI (at 5 h) into weak, moderate, strong and very strong biofilm producers presented significant differences when comparing mucoid and non-mucoid PA strains ($p = 0.022$). After 24 hours, 85% of the mucoid vs 56% of the non-mucoid strains demonstrated a strong or very strong ability to produce biofilms (see Table 2). Comparing the BPI of resistant and susceptible strains for all the antimicrobial agents, no significant differences were found in the BPI, except for ciprofloxacin. Ciprofloxacin-resistant strains presented a lower BPI than susceptible strains (12.94 [6.58-19.37] vs 19.38 [9.73-20.00], respectively, $p = 0.039$) (Figure 3).

Although a trend of an increased BPI was found in the PA isolates from intermittently colonized patients compared to those from chronically infected patients, this was not statistically significant (15.27 ± 1.21 vs 13.24 ± 1.00, respectively, $p = 0.20$). PA isolates from patients with BE and from those with BE-COPD did not differ in their BPI (13.47 ± 1.076 vs 14.55 ± 1.09,

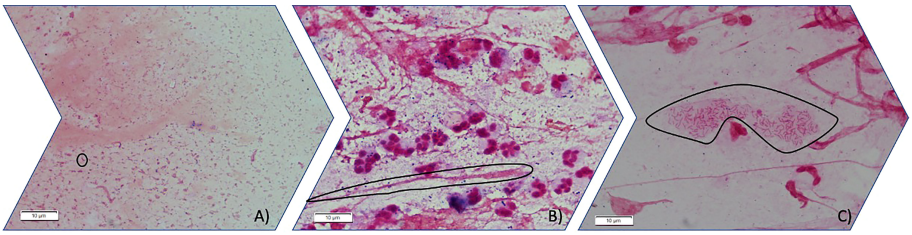

FIGURE 1
Three different stages of PA mode of growth in sputum observed by light microscopy (100X). **(A)** Planktonic stage in which Gram-negative bacilli are seen free floating in planktonic mode of growth (circled an individual gram-negative bacilli). **(B)** Gram-negative bacilli grow aggregated forming immature biofilms. (circled an aggregate of gram-negative bacilli inside mucus) **(C)** Gram-negative bacilli can be found aggregated embedded in an optically distinguishable alginate extracellular matrix circled in the image.

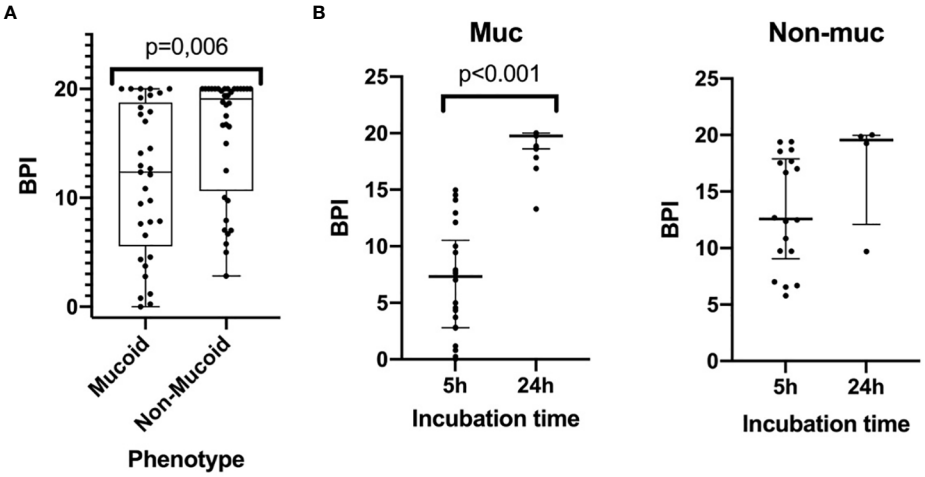

FIGURE 2
The Biofilm index of mucoid and non-mucoid PA phenotypes and its time-dependent increase during incubation. **(A)** Boxplot showing BPI of the 69 PA isolates, by mucoid and non-mucoid PA, read at 5h as recommended by manufacturer. Median and interquartile ratio are represented by the box and whiskers show the maximum and minimum values. The non-mucoid vs mucoid PA phenotype is associated with an increased BPI (19,08 [10,63-20,00] vs 12,36 [5,55-18,74] p=0.006, respectively). **(B)** BPI at 5 vs 24h by phenotype. Median is represented by the central line whilst interquartile ratio is represented by the two lines at the extremes. A statistically significant increase of the BPI can be seen in mucoid strains when incubating at 24 h whilst a greater heterogenous non-statistically significant result is achieved in non-mucoid strains).

respectively, p = 0.49). No differences were found in the categorical stratification of the BPI when comparing the chronicity of infection (intermittent vs chronic PA infection), resistance pattern (MDR or XDR vs non-MDR) or the underlying respiratory disease (BE or BE-COPD).

3.4 MucA mutations

Out of the 67 PA strains tested, 13 had mutations in the mucA gene (mutant mucA), whilst 54 did not (wild-type mucA). The BPI at 5 h of the mutants was lower compared to the wild-type PA strains (7.61 [1.98-19.27] vs 17.79 [9.94-20], respectively, p = 0.028) (Figure 4). In contrast, at 24 h, differences were not statistically significant between the mutants vs. the wild type BPI (20.00 [18.80-20.00] vs 18.64 [15.79-19.59], respectively, p = 0.051).

Interestingly, 50% of the strains that showed slow growth (BPI differed at 5 h vs 24 h) presented mutations in the mucA gene, whilst all the non-slow-growing strains had the wild-type mucA gene (p = 0.005). Wild-type strains presented an increased proportion of resistance compared to the mucA mutant strains (87.9% vs 12.1%, respectively, p = 0.05). In particular, amikacin resistance was higher in the wild-type strains than in the mutant PA strains (84.2% vs 15.8%, p = 0.032).

No differences were found in the distribution of the mucoids vs non-mucoids in mutant and wild-type PA strains, BE vs BE-COPD, intermittent vs chronic PA colonization or the 3 categories of Gram.

3.5 Ciprofloxacin resistance mechanism

Twenty four out of 43 (56%) PA isolates did not present any mutation on QRDR genes and they were quinolone susceptible as confirmed by disc diffusion (group 0). Five out of 43 (12%) presented <3 mutations on QRDR genes (group 1) and they were quinolone resistant as confirmed by disc diffusion with and an average MIC of 9 mg/L. Finally, 14 out of 43 (33%) presented ≥3 mutations on QRDR genes (group 2) and they were quinolone

TABLE 2 Categorical stratification of the BPI among mucoid and non-mucoid *Pseudomonas aeruginosa* strains.

		5h (n=69)		24h (n=29)	
		Phenotype			
		Mucoid	Non-Mucoid	Mucoid	Non-Mucoid
Biofilm production	Weak	8 (24.2%)	2 (5.6%)	0 (0%)	1 (11.1%)
	Moderate	6 (18.2%)	6 (16.2%)	0 (0%)	1 (11.1%)
	Strong	7 (21.2%)	3 (8.3%)	3 (15.0%)	2 (22.2%)
	Very strong	12(36.4%)	25(69.4%)	17 (85.0%)	5 (55.6%)

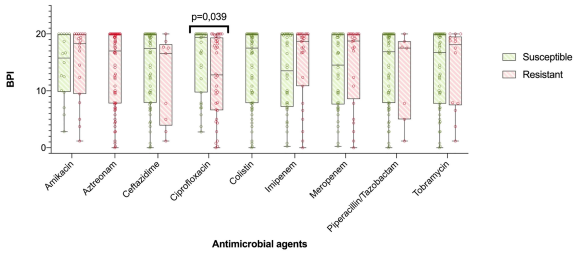

FIGURE 3
BPI in accordance to antibiotic resistance. The boxplot represents median and interquartile ratio, whiskers represent minimum and maximum values. Differences in the BPI in accordance to antibiotic resistance pattern where only statistically significant comparing ciprofloxacin resistant vs. susceptible PA (12,94 [6,58-19,37] vs. 19,38 [9,73-20,00], p=0.039, respectively).

resistant as confirmed by disc diffusion and with an average MIC of 20-32mg/L. Comparing those strains of group 0, group 1 and group 2 we observed that the group 2 ones had the lowest BPI (17.64 [7.68-2.00], 12.67 [10.91-20.00] and 8.20 [3.45-13.88], p=0.030, respectively). Pairwise comparisons found significantly lower BPI in group 2 compared with group 0 (p=0.012) without any other statistically significant differences.

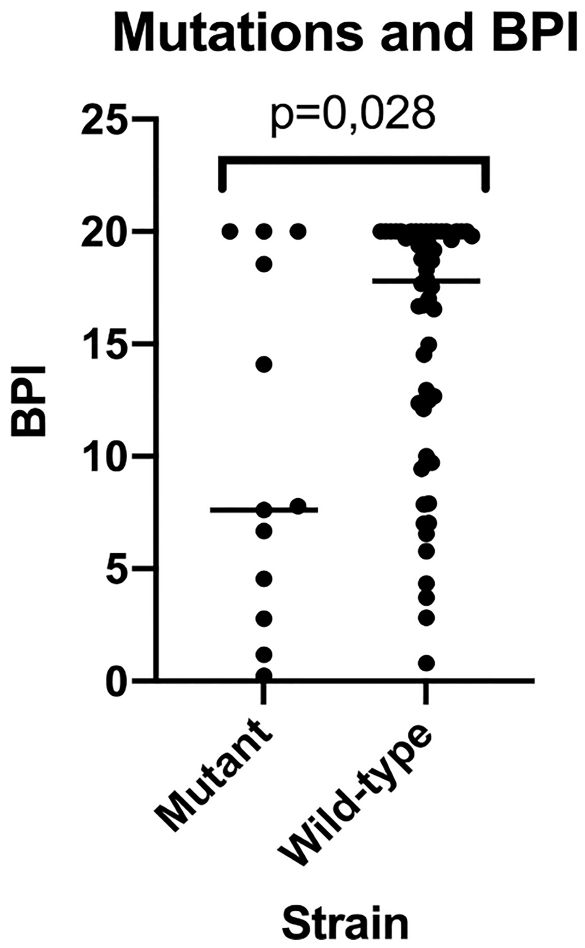

FIGURE 4
BPI of mutant vs wild-type strains for mucA gene. This figure shows how mutant strains present a reduced BPI when compared to wild-type strains being this last population much more heterogeneous in BPI testing results.

3.6 Predictive performance of BPI compared to phenotype or resistance to ciprofloxacin

Following Youden's index methodology, we selected 14.75 as the optimal cut-off point for BPI to predict the PA phenotype (<14.75 = Mucoid, ≥14.75 = Non-mucoid; sensitivity, specificity, positive and negative predictive values were 64% [95% CI 46% to 82%], 72% [95% CI 56% to 88%], 68% [95% CI 50% to 86%], and 68% [95% CI 52% to 85%], respectively), and 19.28 as the optimal cut-off point for BPI in relation to resistance to ciprofloxacin (<19.28 = Ciprofloxacin resistant, ≥19.28 = Ciprofloxacin susceptible; sensitivity, specificity, positive and negative predictive values were 75% [95% CI 59% to 91%], 52% [95% CI 32% to 71%], 64% [95% CI 49% to 80%], and 64% [95% CI 43% to 85%], respectively) (Figure 5).

4 Discussion

To the best of our knowledge, this is the first study that validates BioFilm Ring Test® (BRT) in a significant number of PA strains from patients with bronchiectasis and which describes BioFilm production Index (BPI) associations with microbiology and clinical outcomes. We found that at 5h of incubation, non-mucoid PA and ciprofloxacin susceptible showed higher BPI than mucoid and ciprofloxacin resistant PA strains, respectively; We suggested a new application of BRT using BPI cut off points to predict the mucoid (<14.75) or Ciprofloxacin resistant (<19.28) phenotype, two outcomes of clinical interest in the context of chronic respiratory diseases. In addition, the presence of alginate in Gram images was associated with the mucoid phenotype, non-MDR PA strains and with the chronic respiratory infection status of the patient. Considering the current lack of routine methods in hospital settings to diagnose biofilm and their clinical implications, this translational approach reveals new diagnostic applications for BRT.

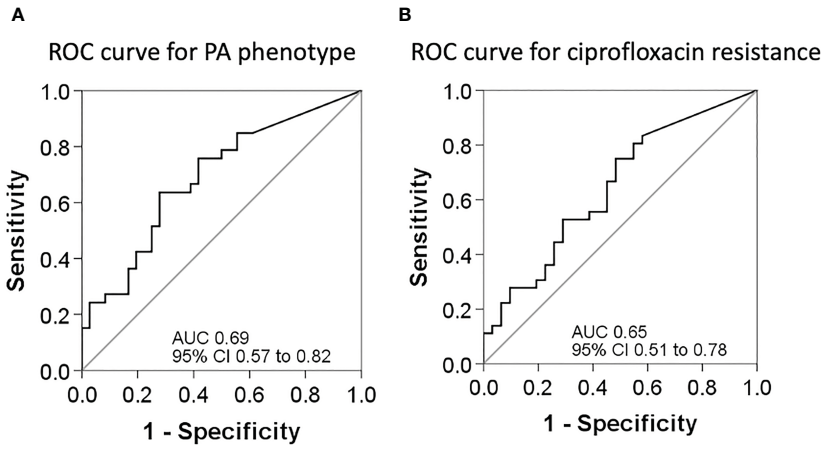

FIGURE 5
ROC curves for sensitivity and specificity. **(A)** ROC curve to assess the best cut-off point of the BPI for PA phenotype determination. **(B)** ROC curve to assess the best cut-off point of the BPI for PA resistance to ciprofloxacin.

Biofilm formation is a dynamic process that occurs in the first phase, when strains switch from the planktonic to a sessile mode of growth in which they increase their production of adhesins (Youden, 1950), grow in aggregates and are regulated by quorum-sensing signaling pathways (Berne et al., 2015). Biofilm maturation in human PA infections involves the overproduction of extracellular matrix, which is carried out by mucoid strains, and a sustained lethargic metabolism (Figure 6). We found that mucoid PA strains, associated with mature biofilms, presented a lower BPI compared to non-mucoid strains at 5 h. However, when the BRT was extended to 24 h, all the mucoid strains exhibited the highest BPI score, indicating that the performance of the mucoid PA strains in the BRT was influenced by the downregulated metabolism of the mucoid phenotype, which needed extra time to reveal their true BPI. Further analyses demonstrated that a BPI < 14.75 predicted the mucoid phenotype with 64% sensitivity and 72% specificity at 5 h. Such values could be, hopefully, improved with a greater sample size.

Interestingly, despite no differences were found for other antibiotics, ciprofloxacin resistant PA presented lower BPI than susceptible strains as it has already been seen in E. coli for extensive spectrum beta lactamase (Mukherjee and Bassler, 2019). This is

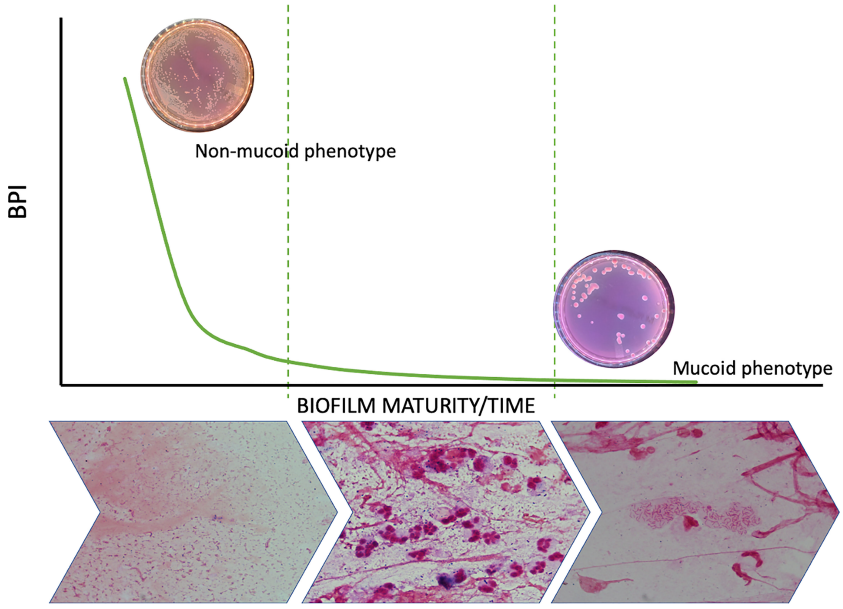

FIGURE 6
Biofilm dynamic during time and phenotype switch. The figure shows how the metabolic ratio of PA decreases whilst phenotype switches from a non-mucoid state to a mucoid phenotype and at the same time PA starts growing in biofilms instead of being found in planktonic state.

important since ciprofloxacin is the first recommended treatment for *Pseudomonas aeruginosa* eradication in bronchiectasis patients (Polverino et al., 2017). In spite of this, the mucoid PA has been previously linked to a more susceptible antimicrobial profile compared to the non-mucoid (Batoni et al., 2019). Here we found that PA isolates with more than 3 mutations on QRDR genes were those exhibiting the lowest BPI. Based on our data, the observed correlation between decreased BPI and ciprofloxacin resistance can be explained by an increase in the number of mutations in QRDR and the fitness-cost associated to these mutations. Strains exposed to high levels of environmental stress are more likely to undergo mutations in QRDR, particularly when their metabolism is downregulated. This downregulation could account for the observed link between quinolone resistance and decreased BPI at the 5-hour time point. Further investigation into the use of BRT to predict ciprofloxacin resistance is warranted, given that the traditional method requires a turnaround time of at least 48 hours, whereas BRT can provide results in as little as 5 hours. Recent research has shown that subinhibitory concentrations of β-lactams can induce the BioFilm index (Fernández-Barat et al., 2017), highlighting the potential of BRT as a promising diagnostic tool for Pseudomonas respiratory infections

Herein, we describe for the first time the association between mutations in mucA gene and BPI performance. Interestingly, our results are in accordance to what was observed for the mucoid phenotype. As mucoids, the 13 mutant PA presented a time dependent increase in BPI at 5 h to 24h. In contrast, wild type PA, as well as non-mucoid, presented a less time dependent BPI. In addition, we confirmed slow growth was associated with mucA mutations.

The lack of differences found in the BPI of patients with BE-COPD and BE is attributed to the fact that mucoid and non-mucoid were similarly distributed between BE-COPD and BE alone. Our findings are in line with previous reports indicating that the presence of BE does not influence mortality in long-term follow-up hospitalized COPD exacerbations (Olivares et al., 2020). Thus, the underlying respiratory disease may not have such a relevant role on PA phenotype and biofilm production which rather responds to the stage of chronic infection.

A limitation of this study was the variability in metabolic rates between PA strains, with some strains growing faster than others. To overcome this limitation, we assessed BRT at two different time points. It is also important to note that while we tested the BRT for PA, as it is the most common pathogen in our population, this test could also be applied to other biofilm producing microorganisms.

5 Conclusions

The BioFilm Ring Test® (BRT) is a promising technology that can be integrated into clinical practice due to its ability to rapidly assess the biofilm-forming capabilities of microorganisms within just 5 hours. While further validation is needed to assess its predictive value for the mucoid phenotype and the ciprofloxacin resistance, the BRT has the potential to shed light on biofilms that are currently underestimated in antimicrobial stewardship efforts.

Data availability statement

The original contributions presented in the study are included in the article/Supplementary Material. Further inquiries can be directed to the corresponding authors.

Ethics statement

The studies involving human participants were reviewed and approved by the Internal Review Board of the Hospital Clinic of Barcelona (registry number HCB/0236). Written informed consent was obtained from all patients.

Author contributions

LF-B and NV designed and performed the experimental work, analyzed the results and wrote the manuscript. AT, RA, AP, AC, VA, LB-F and PO contributed to the clinical follow-up and sample collection of BE patients. RL-A and RC did the genetic analysis on mucA. AM and AG assisted on the statistics and figure design. LM and JV assisted on the PA confirmation by MALDI and CP and TB assisted in the BPI technology and biofilm data collection. All authors reviewed the present manuscript before publication.

Funding

CB 06/06/0028/CIBER de enfermedades respiratorias- Ciberes, Intramural ciberes 2018 (ES18PI01X1-2021), ISCIII-FEDER (FIS18-PI18/00145 awarded to AT and LF-B; FI19/00090 awarded to RL-A), ICREA Academy/Institució Catalana de Recerca i Estudis Avançats, 2.603/IDIBAPS, SGR/Generalitat de Catalunya, SEPAR 2017, 2018 grants to LF-B. Funders did not play any role in paper design, data collection, data analysis, interpretation, writing of the paper.

Acknowledgments

We would like to thank the advanced microscopy service from the Scientific and Technological Centers of the University of Barcelona for the microscopy equipment.

Conflict of interest

AT has received grants from MedImmune, Cubist, Bayer, Theravance, and Polyphor and personal fees as Advisory Board member from Bayer, Roche, The Medicines CO, and Curetis. He has received bureau fees for keynote speaker presentations from GSK, Pfizer, Astra Zeneca, and Biotest Advisory Board, and are unconnected to the study submitted here. TB and CP were employed by BioFilm Pharma SAS and BioFilm Control SAS.

The remaining authors declare that the research was conducted in the absence of any commercial or financial relationships that could be construed as a potential conflict of interest.

Publisher's note

All claims expressed in this article are solely those of the authors and do not necessarily represent those of their affiliated organizations, or those of the publisher, the editors and the reviewers. Any product that may be evaluated in this article, or claim that may be made by its manufacturer, is not guaranteed or endorsed by the publisher.

Supplementary material

The Supplementary Material for this article can be found online at: https://www.frontiersin.org/articles/10.3389/fcimb.2023.1142274/full#supplementary-material

References

Alcaraz-Serrano, V., Fernández-Barat, L., Scioscia, G., Llorens-Llacuna, J., Gimeno-Santos, E., Herrero-Cortina, B., et al. (2019). Mucoid pseudomonas aeruginosa alters sputum viscoelasticity in patients with non-cystic fibrosis bronchiectasis. *Respir. Med.* 154, 40–46. doi: 10.1016/j.rmed.2019.06.012

Barker, A. F. (2002). Bronchiectasis. *N Engl. J. Med.* 346 (18), 1383–1393. doi: 10.1056/NEJMra012519

Berne, C., Ducret, A., Hardy, G. G., and Brun, Y. V. (2015). Adhesins Involved in Attachment to Abiotic Surfaces by Gram-Negative Bacteria. In *Microbial Biofilms* (eds Ghannoum, M.Parsek, M.Whiteley, M.Mukherjee, P. K.). doi: 10.1128/9781555817466.ch9

Cabrera, R., Fernández-Barat, L., Vázquez, N., Alcaraz-Serrano, V., Bueno-Freire, L., Amaro, R., et al. (2022). Resistance mechanisms and molecular epidemiology of pseudomonas aeruginosa strains from patients with bronchiectasis. *J. antimicrobial chemotherapy* 77 (6), 1600–1610. doi: 10.1093/jac/dkac084

Chandrasekaran, R., Mac Aogáin, M., Chalmers, J. D., Elborn, S. J., and Chotirmall, S. H. (2018). Geographic variation in the aetiology, epidemiology and microbiology of bronchiectasis. *BMC Pulmonary Med.* 18. doi: 10.1186/s12890-018-0638-0

Chavant, P., Gaillard-Martinie, B., Talon, R., Hébraud, M., and Bernardi, T. (2007). A new device for rapid evaluation of biofilm formation potential by bacteria. *J. Microbiol. Methods* 68 (3), 605–612. doi: 10.1016/j.mimet.2006.11.010

Ciofu, O., Mandsberg, L. F., Bjarnsholt, T., Wassermann, T., and Høiby, N. (2010). Genetic adaptation of pseudomonas aeruginosa during chronic lung infection of patients with cystic fibrosis: strong and weak mutators with heterogeneous genetic backgrounds emerge in mucA and/or lasR mutants. *Microbiology* 156 (4), 1108–1119. doi: 10.1099/mic.0.033993-0

Ciofu, O., Rojo-Molinero, E., Macià, M. D., and Oliver, A. (2017). Antibiotic treatment of biofilm infections. *Apmis* 125. doi: 10.1111/apm.12673

Cohen, M., and Sahn, S. A. (1999). Bronchiectasis in systemic diseases. *Chest.* 116 (4), 1063–1074. doi: 10.1378/chest.116.4.1063

Crisafulli, E., Guerrero, M., Ielpo, A., Ceccato, A., Huerta, A., Gabarrús, A., et al. (2018). Impact of bronchiectasis on outcomes of hospitalized patients with acute exacerbation of chronic obstructive pulmonary disease: a propensity matched analysis. *Sci. Rep.* 8 (1), 1–12. doi: 10.1038/s41598-018-27680-y

Dhand, R. (2018). The rationale and evidence for use of inhaled antibiotics to control pseudomonas aeruginosa infection in non-cystic fibrosis bronchiectasis. *J. Aerosol Med. Pulmonary Drug Delivery* 31. doi: 10.1089/jamp.2017.1415

Di Domenico, E. G., Toma, L., Provot, C., Ascenzioni, F., Sperduti, I., Prignano, G., et al. (2016). Development of an in vitro assay, based on the biofilm ring test®, for rapid profiling of biofilm-growing bacteria. *Front. Microbiol.* 7, 1429. doi: 10.3389/fmicb.2016.01429

Fernández-Barat, L., Alcaraz-Serrano, V., Amaro, R., and Torres, A. (2021). Pseudomonas aeruginosa in bronchiectasis. *Semin. Respir. Crit. Care Med.* 42 (4), 587–594. doi: 10.1055/s-0041-1730921

Fernández-Barat, L., Ben-Aicha, S., Motos, A., Vila, J., Marco, F., Rigol, M., et al. (2018). Assessment of in vivo versus *in vitro* biofilm formation of clinical methicillin-resistant staphylococcus aureus isolates from endotracheal tubes. *Sci. Rep.* 8 (1), 11906. doi: 10.1038/s41598-018-30494-7

Fernández-Barat, L., Ciofu, O., Kragh, K. N., Pressler, T., Johansen, U., Motos, A., et al. (2017). Phenotypic shift in pseudomonas aeruginosa populations from cystic fibrosis lungs after 2-week antipseudomonal treatment. *J. Cyst Fibros* 16 (2), 222–229. doi: 10.1016/j.jcf.2016.08.005

Finch, S., McDonnell, M. J., Abo-Leyah, H., Aliberti, S., and Chalmers, J. D. (2015). A comprehensive analysis of the impact of pseudomonas aeruginosa colonization on prognosis in adult bronchiectasis. *Ann. Am. Thorac. Soc.* 12 (11), 1602–1611. doi: 10.1513/AnnalsATS.201506-333OC

Flament-Simon, S. C., Duprilot, M., Mayer, N., García, V., Alonso, M. P., Blanco, J., et al. (2019). Association between kinetics of early biofilm formation and clonal lineage in escherichia coli. *Frontiers in microbiology* 10, 1183. doi: 10.3389/fmicb.2019.01183

Flume, P. A., Chalmers, J. D., and Olivier, K. N. (2018). Advances in bronchiectasis: endotyping, genetics, microbiome, and disease heterogeneity. *Lancet Lancet Publishing Group;* 392, 880–890. doi: 10.1016/S0140-6736(18)31767-7

Hill, A. T., Haworth, C. S., Aliberti, S., Barker, A., Blasi, F., Boersma, W., et al. (2017). Pulmonary exacerbation in adults with bronchiectasis: a consensus definition for clinical research. *Eur. Respir. J.* 49 (6). doi: 10.1183/13993003.00051-2017

King, P. T., Holdsworth, S. R., Freezer, N. J., Villanueva, E., and Holmes, P. W. (2006). Characterisation of the onset and presenting clinical features of adult bronchiectasis. *Respir. Med.* 100 (12), 2183–2189. doi: 10.1016/j.rmed.2006.03.012

Lewis, K. (2007). Persister cells, dormancy and infectious disease. *Nat. Rev. Microbiol.* 5 (1), 48–56. doi: 10.1038/nrmicro1557

Magiorakos, A. P., Srinivasan, A., Carey, R. B., Carmeli, Y., Falagas, M. E., Giske, C. G., et al. (2012). Multidrug-resistant, extensively drug-resistant and pandrug-resistant bacteria: an international expert proposal for interim standard definitions for acquired resistance. *Clin. Microbiol. Infect.* 18 (3), 268–281. doi: 10.1111/j.1469-0691.2011.03570.x

Malhotra, S., Limoli, D. H., English, A. E., Parsek, M. R., and Wozniak, D. J. (2018). Mixed communities of mucoid and nonmucoid pseudomonas aeruginosa exhibit enhanced resistance to host antimicrobials. *MBio* 9 (2). doi: 10.1128/mBio

Mukherjee, S., and Bassler, B. L. (2019). Bacterial quorum sensing in complex and dynamically changing environments. *Nat. Rev. Microbiol.* 17 (6), 371–382. doi: 10.1038/s41579-019-0186-5

Murray, P. R., and Washington, J. A. (1975). Microscopic and baceriologic analysis of expectorated sputum. *Mayo Clin. Proc.* 50 (6), 339–344.

Olivares, E., Badel-Berchoux, S., Provot, C., Jaulhac, B., Prévost, G., Bernardi, T., et al. (2016). The BioFilm ring test: a rapid method for routine analysis of pseudomonas aeruginosa biofilm formation kinetics. *J. Clin. Microbiol.* 54 (3), 657–661. doi: 10.1128/JCM.02938-15

Olivares, E., Tasse, J., Badel-Berchoux, S., Provot, C., Prévost, G., and Bernardi, T. (2020). Clinical biofilm ring test® reveals the potential role of β-lactams in the induction of biofilm formation by p. aeruginosa in cystic fibrosis patients. *Pathogens* 9 (12), 1065. doi: 10.3390/pathogens9121065

Pantanella, F., Valenti, P., Natalizi, T., Passeri, D., and Berlutti, F. (2013). Analytical techniques to study microbial biofilm on abiotic surfaces: pros and cons of the main techniques currently in use. *Ann. Ig* 25 (1), 31–42. doi: 10.7416/ai.2013.1904

Peeters, E., Nelis, H. J., and Coenye, T. (2008). Comparison of multiple methods for quantification of microbial biofilms grown in microtiter plates. *J. Microbiol. Methods* 72 (2), 157–165. doi: 10.1016/j.mimet.2007.11.010

Polverino, E., Goeminne, P. C., McDonnell, M. J., Aliberti, S., Marshall, S. E., Loebinger, M. R., et al. (2017). European Respiratory society guidelines for the management of adult bronchiectasis. *Eur. Respir. J.* 50 (3), 1700629. doi: 10.1183/13993003.00629-2017

Sulaeman, S., Le Bihan, G., Rossero, A., Federighi, M., Dé, E., and Tresse, O. (2010). Comparison between the biofilm initiation of campylobacter jejuni and campylobacter coli strains to an inert surface using BioFilm ring test®. *J. Appl. Microbiol.* 108 (4), 1303–1312. doi: 10.1111/j.1365-2672.2009.04534.x

Thieme, L., Hartung, A., Tramm, K., Klinger-Strobel, M., Jandt, K. D., Makarewicz, O., et al. (2019). MBEC versus MBIC: the lack of differentiation between biofilm reducing and inhibitory effects as a current problem in biofilm methodology. *Biol. Proced Online* 21 (1). doi: 10.1186/s12575-019-0106-0

Vogelmeier, C. F., Criner, G. J., Martinez, F. J., Anzueto, A., Barnes, P. J., Bourbeau, J., et al. (2017). Global strategy for the diagnosis, management, and prevention of chronic obstructive lung disease 2017 report. *Am. J. Respir. Crit. Care Med.* 195 (5), 557–582. doi: 10.1164/rccm.201701-0218PP

Hengzhuang, W., Wu, H., Ciofu, O., Song, Z., and Høiby, N. (2011). Pharmacokinetics/pharmacodynamics of colistin and imipenem on mucoid and

nonmucoid Pseudomonas aeruginosa biofilms. *Antimicrob. Agents Chemother.* 55 (9), 4469–4474. doi: 10.1128/AAC.00126-11

Yang, L., Haagensen, J. A. J., Jelsbak, L., Johansen, H. K., Sternberg, C., Høiby, N., et al. (2008). *In situ* Growth rates and biofilm development of pseudomonas aeruginosa populations in chronic lung infections. *J. Bacteriol* 190 (8), 2767–2776. doi: 10.1128/JB.01581-07

Youden, W. J. (1950). Index for rating diagnostic tests. *Cancer* 3 (1), 32–35. doi: 10.1002/1097-0142(1950)3:1<32::AID-CNCR2820030106>3.0.CO;2-3

frontiers | Frontiers in Cellular and Infection Microbiology

TYPE Original Research
PUBLISHED 13 July 2023
DOI 10.3389/fcimb.2023.1210195

OPEN ACCESS

EDITED BY
Rachna Singh,
Panjab University, India

REVIEWED BY
Ashraf Kariminik,
Islamic Azad University Kerman, Iran
Anjna Kumari,
Panjab University, India

*CORRESPONDENCE
Reham Wasfi
rwasfi@msa.edu.eg

RECEIVED 21 April 2023
ACCEPTED 20 June 2023
PUBLISHED 13 July 2023

CITATION
Amer MA, Wasfi R and Hamed SM (2023) Biosurfactant from Nile Papyrus endophyte with potential antibiofilm activity against global clones of *Acinetobacter baumannii*. *Front. Cell. Infect. Microbiol.* 13:1210195. doi: 10.3389/fcimb.2023.1210195

Biosurfactant from Nile Papyrus endophyte with potential antibiofilm activity against global clones of *Acinetobacter baumannii*

Mai A. Amer, Reham Wasfi* and Samira M. Hamed

Department of Microbiology and Immunology, Faculty of Pharmacy, October University for Modern Sciences and Arts (MSA), Giza, Egypt

Acinetobacter baumannii is a leading cause of biofilm-associated infections, particularly catheter-related bloodstream infections (CRBSIs) that are mostly recalcitrant to antimicrobial therapy. One approach to reducing the burden of CRBSIs is inhibiting biofilm formation on catheters. Owing to their prodigious microbial diversity, bacterial endophytes might be a valuable source of biosurfactants, which are known for their great capacity to disperse microbial biofilms. With this in mind, our study aimed to screen bacterial endophytes from plants growing on the banks of the River Nile for the production of powerful biosurfactants capable of reducing the ability of *A. baumannii* to form biofilms on central venous catheters (CVCs). This was tested on multidrug- and extensive drug-resistant (M/XDR) clinical isolates of *A. baumannii* that belong to high-risk global clones and on a standard strain of *A. baumannii* ATCC 19606. The drop collapse and oil dispersion assays were employed in screening the cell-free supernatants (CFS) of all endophytes for biosurfactant activity. Of the 44 bacterial endophytes recovered from 10 plants, the CFS of *Bacillus amyloliquefaciens* Cp24, isolated from *Cyperus papyrus*, showed the highest biosurfactant activity. The crude biosurfactant extract of Cp24 showed potent antibacterial activity with minimum inhibitory concentrations (MICs) ranging from 0.78 to 1.56 mg/ml. It also showed significant antibiofilm activity (p-value<0.01). Sub-MICs of the extract could reduce biofilm formation by up to 89.59%, while up to 87.3% of the preformed biofilms were eradicated by the MIC. A significant reduction in biofilm formation on CVCs impregnated with sub-MIC of the extract was demonstrated by CV assay and further confirmed by scanning electron microscopy. This was associated with three $\log_{10}$ reductions in adhered bacteria in the viable count assay. GC-MS analysis of the crude biosurfactant extract revealed the presence of several compounds, such as saturated, unsaturated, and epoxy fatty acids, cyclopeptides, and 3-Benzyl-hexahydro-pyrrolo [1, 2-a] pyrazine-1,4-dione, potentially implicated in the potent biosurfactant and antibiofilm activities. In the present study, we report the isolation of a *B. amyloliquefaciens* endophyte from the plant *C. papyrus* that produces a biosurfactant with potent antibiofilm activity against MDR/XDR global clones of *A. baumannii*. The impregnation of CVCs with the biosurfactant was demonstrated to reduce biofilms and, hence, proposed as a potential strategy for reducing CRBSIs.

KEYWORDS

***Acinetobacter baumannii*, global clones, endophytes, central venous catheter (CVC), biosurfactant, antibiofilm, *Bacillus amyloliquefaciens*, Papyrus**

1 Introduction

Acinetobacter baumannii (*A. baumannii*) has become a global threat in healthcare settings and a leading cause of healthcare-associated infections (Gedefie et al., 2021). This successful nosocomial pathogen is known for its adaptable genetic machinery that is capable to accumulate resistance genes and to acquire multidrug-, extensive drug-, and pan-drug-resistance phenotypes (Rolain et al., 2013; Wasfi et al., 2021; Zafer et al., 2021). In addition, it has remarkable environmental resilience partly due to its simple growth requirements and resistance to desiccation (Peleg et al., 2012).

One of the hallmark characteristics of *A. baumannii* is the propensity to form biofilms in which they live in surface-attached communities (Eze et al., 2018). Biofilm-embedded *A. baumannii* is properly shielded from antibiotics, immunity factors, and harsh environmental conditions. The close proximity within biofilms further enhances the acquisition of foreign genes through horizontal gene transfer. Hence, *A. baumannii* is a frequent cause of biofilm-related, particularly catheter-related bloodstream infections (CRBSI) and ventilator-associated pneumonia (VAP) (Gedefie et al., 2021). Such infections are mostly associated with devastating outcomes and are exceedingly resistant to a wide range of antimicrobial treatment modalities, posing a great challenge to infectious disease practitioners (Mansouri et al., 2013; Abd El-Rahman et al., 2023; Lafuente Cabrero et al., 2023).

Biofilm-related *A. baumannii* infections are mostly seen in intensive care units (ICU), where life support systems (e.g.; mechanical ventilation) and indwelling medical devices (e.g.; vascular and urinary catheters) are widely used (Lynch et al., 2017). A central venous catheter (CVC) insertion is the most common invasive procedure that leads to *A. baumannii* infections in ICUs (Castilho et al., 2017). Even using extreme aseptic techniques, the percutaneous insertion of catheters was found to permit the attachment of bacteria. This then progresses to biofilm formation and planktonic dispersion into the bloodstream, causing CRBSIs (Pathak et al., 2018). An estimated 250,000 bloodstream infections occur annually, and most are related to the presence of intravascular devices. In the United States, CRBSIs are still experienced by tens of thousands of patients annually, resulting in thousands of deaths and adding billions of dollars to the cost of the country's healthcare system (Guenezan et al., 2018). The likelihood of developing CRBSI was found to be increased by chemotherapy, immunosuppression, and long-term catheterization (Lafuente Cabrero et al., 2023). Previous studies have reported biofilm formation capacity in up to 76% of CVC devices reported to have *A. baumannii* (Nahar et al., 2013; Sanchez et al., 2013; Duarte et al., 2016; Castilho et al., 2017). Consequently, researchers have been long looking for innovative ways to maintain CVCs biofilm-free.

Catheter coating or impregnation with various compounds that prevent biofilm formation and bacterial colonization is one of the approaches proposed by many authors to reduce the incidence of CRBSIs. While antimicrobial agents have been commonly used for coating or impregnation of catheters (Wang et al., 2018; Neethu et al., 2020; Sivanandan, 2020; Corrêa Carvalho et al., 2022), only partial clinical efficacy was shown by some antimicrobial-coated catheters, particularly against MDR pathogens (Mansouri et al., 2013). In addition, the use of antimicrobial-treated catheters might contribute to the evolution of antimicrobial resistance (Donlan, 2011). Hence, antibiofilm compounds represent good alternatives to antimicrobial agents, as they inhibit biofilms without exerting selection pressure on bacterial growth and thus reduce the development of antibiotic resistance (Amer et al., 2022, Wang et al., 2018; Neethu et al., 2020). Examples include catheter pretreatment with bacteriophages, surfactants, or enzymes (Donlan, 2011).

Biosurfactants are among the promising candidates for application in inhibiting bacterial biofilms (Banat et al., 2014). Biosurfactants, also named green surfactants, are surface active agents of biological origin. They are amphiphilic in nature, having hydrophilic and hydrophobic parts. They are non-toxic and biodegradable and do not accumulate in the environment. Microbial biosurfactants have been gaining much attention, owing to their chemical properties and stability under several environmental conditions (Eras-Muñoz et al., 2022). These properties make them relevant molecules for applications in combating many diseases and as potential therapeutic agents.

Endophytes are a class of endosymbiotic microorganisms that colonize plants and serve as stores for unique bioactive secondary metabolites, such as alkaloids, phenolic acids, quinones, steroids, saponins, tannins, terpenoid, and biosurfactants (Gouda et al., 2016; Ashitha et al., 2020; Marchut-Mikołajczyk et al., 2021). Endophytes can stimulate plant growth, facilitate the *de novo* synthesis of biologically active compounds, such as antibiotics, biosurfactants, and phytohormones, increase the host's resistance to stressful environmental conditions, and increase the resistance of the host plant to pathogens and pests (Marchut-Mikołajczyk et al., 2021). Research into the biodiversity of endophytic strains for novel metabolites may lead to the discovery of new drugs, potentially contributing to the effective treatment of diseases in humans, plants, and animals (Ryan et al., 2008). Ongoing discoveries on the variety of metabolites produced by endophytes and their promising applications show that endophytes have inspired research in the development of biotechnological solutions. These solutions span from the exploration to the manufacture of industrially relevant metabolites that could help identify long-lasting sustainable solutions for the economic exploitation of biosurfactants that reduce biofilm formation, (Tidke et al., 2019).

Thus, the present study aimed to screen endophytes from Egypt for the ability to produce a powerful biosurfactant that can inhibit biofilms of MDR and XDR *A. baumannii* and to investigate the potential application of this biosurfactant in reducing biofilm formation on CVCs.

2 Materials and methods

2.1 Clinical strains and growth conditions

Five clinical isolates of multidrug- and extensive drug-resistant *A. baumannii* and a standard strain *A. baumannii* ATCC® 19606 were included in this study. The clinical isolates were recovered from different clinical specimens of patients admitted to Kasr Al-Ainy

Hospital, which were collected in a previous study conducted by Hamed et al. (2022). As part of the previous study, the multilocus sequence typing (MLST) revealed that these isolates belong to high-risk global clones (GCs), as shown in Table 1. Bacterial cultures were routinely grown in Luria-Bertani (LB) medium at 37°C for 24 hours.

2.2 Collection of plants and isolation of endophytes

From April to November 2019, samples from different plants growing along the banks of the River Nile were randomly collected and screened for biosurfactant-producing bacterial endophytes. For endophyte isolation, fresh and healthy samples of each plant were collected, stored in sealed plastic bags, and delivered to the laboratory on the same day of collection for further processing. All samples were surface sterilized in the method described by Katoch et al. (2017), with some modifications. Briefly, the samples were thoroughly washed under tap water and distilled water, then dried using tissue paper. All washed plant materials were cut into 5 cm segments that were surface sterilized by sequential immersion in 70% ethanol (v/v) for 3 min, 1% sodium hypochlorite (v/v) for 12 minutes, and then 70% ethanol (v/v) for additional 30 sec. Finally, the segments were rinsed three times in sterile distilled water to remove residual sterilant and then left to dry under an airflow cabinet until complete drying. The plant segments were aseptically cut using sterile surgical scalpels into 2 mm-thick segments that were placed on trypticase soy agar (TSA) plates, ensuring direct contact of the cut edges with the culture media. The plates were incubated at 30°C for 5 days. To confirm the effectiveness of the surface sterilization process, 50 µl samples of the last distilled water rinse were cultured on TSA, incubated at the same conditions, and checked daily for the growth of surface contaminants. Morphologically distinct bacterial colonies growing under the plant parts were isolated to obtain pure colonies. Endophyte isolates were preserved in trypticase soy broth (TSB) supplemented with 25% (v/v) glycerol at -20°C.

2.3 Screening the endophytes for biosurfactant production

Endophytes were screened for biosurfactant production after the preparation of cell-free supernatant (CFS) using the methods described by Amer et al. (2021). The turbidity of an overnight culture of endophytes grown in TSB was adjusted to be equivalent to an OD_{600} of 1. The diluted culture was then used to inoculate fresh TSB to achieve a final dilution of 1:100. Flasks were then incubated at 30°C with shaking at 120 rpm for 4 days. CFS was prepared by centrifugation at 10,000 rpm for 10 min at 4°C, followed by filtration using a 0.22 µm filter (Millipore, Bedford, MA, USA). These were then screened for their biosurfactant activity using the drop collapse, oil displacement, and emulsification assays described below.

2.3.1 Drop collapse assay

The drop collapse assay was carried out as described by Patel et al. (2021). First, a drop (35 µl) of the CFS was placed on the surface of a parafilm. Biosurfactant production was indicated by the spreading or collapse of the drop within 15 min (Patel et al., 2021).

2.3.2 Oil displacement test

Isolates that showed positive drop collapse assay were further subjected to the oil displacement assay that was carried out following the procedure described by Joe et al. (2019). Briefly, 50 ml of distilled water was added to a Petri dish. This was overlaid by a thin layer of castor oil (100 µl). Approximately 10 µl of the CFS was added to the center of the oil layer. After 30 seconds, the oil surface was observed for the emergence of a clear zone. Uninoculated TSB and Triton X-100 were used as negative and positive controls, respectively.

The isolate with CFS causing the greatest displacement of the oil layer was selected for further testing.

2.3.3 Emulsification assay

The emulsification assay confirmed the biosurfactant production potential of the endophyte that showed the highest oil displacement activity. Following the method described by Satpute et al. (2010), equal parts of the CFS and castor oil were combined by vortexing for 2 minutes before being left to stand for 24 hours. The emulsification activity was indicated by the emulsification index (% EI24), which was calculated according to the following formula:

$$\%\,EI24 = (\text{Height of the formed emulsion}/\text{Total height of the solution}) \times 100$$

2.4 Molecular identification of the bacterial endophyte-producing biosurfactant

The bacterial endophyte showing the highest emulsification activity was identified by its microscopic morphology, followed by molecular analysis based on the 16S *rRNA* gene sequence. DNA was extracted using the GeneJET Genomic DNA Purification Kit (Thermo

TABLE 1 MLSTs and GCs of the clinical isolates included in the current study (Hamed et al., 2022).

Isolate number	Specimen	Resistance Phenotype	ST^{Pas}	ST^{Oxf}	GC
M02	Wound swab	XDR	85	1089	9
M03	Blood	XDR	113	2246	7
M04	Sputum	XDR	2	1816/195	2
M15	Wound swab	MDR	1	1604/231	1

XDR, extensive drug resistance; MDR, multidrug resistance; ST^{Pas}, sequence type based on Pasteur scheme; ST^{Oxf}, sequence type according to Oxford scheme; GC, global clone.

Fisher Scientific Inc., USA) as per the manufacturer's instructions. The 16S *rRNA* gene was amplified by the universal pair of primers designed by Weisburg et al. (1991): 27F (5′AGAGTTTGATCCTGGCTCAG3′) and 1492R (5′CGGTTACCTTGTTACGACTT3′). The purified PCR product was then sequenced by Macrogen® (Seoul, South Korea) using ABI 3730xl DNA Analyzer. Gene sequences were compared to sequences in the National Center for Biotechnology Information (NCBI) database using the nucleotide Basic Local Alignment Search Tool (BLASTn). Gene sequences with high similarity to that determined in the study were retrieved and genetic diversity was analyzed using Molecular Evolutionary Genetics Analysis version 11.0 (MEGA 11). The phylogenetic tree was constructed by the maximum parsimony method (Tamura et al., 2013).

2.5 Preparation of the crude biosurfactant from the endophyte Cp24

For extraction of the crude biosurfactant, the CFS was prepared in the same way as in the preliminary screening for biosurfactant production. The CFS was acidified to pH 2.5 using HCl (5 N) and stored overnight at 4°C for precipitation of the biosurfactant compounds. The crude biosurfactant was then extracted twice from the acidified supernatant by shaking with double volumes of ethyl acetate (EtOAc) (Patel et al., 2021). The ethyl acetate extract was pooled and dried under a vacuum in a rotary flash evaporator (Heidolph, Germany) at 45°C. Based on the solubility, the dried extract was dissolved in 20% (v/v) Dimethylsulfoxide (DMSO) to obtain a stock solution of 50 mg/ml. The final concentrations of DMSO in all experiments were confirmed to not affect bacterial growth.

2.6 Assessment of the antibacterial activity of the crude biosurfactant against *A. baumannii*

The antibacterial activity of the crude biosurfactant extract against *A. baumannii* was evaluated using the broth microdilution assay. The minimum inhibitory concentrations (MICs) of the crude biosurfactant were determined according to the guidelines of the Clinical and Laboratory Standards Institute (CLSI) (CLSI, 2015). In 96-well microtiter plates, two-fold serial dilutions of the crude extract were prepared in Muller Hinton Broth (MHB; Oxoid, UK) to final concentrations ranging from 0.01 to 12.5 mg/ml. All wells were inoculated with approximately 5×10^5 CFU ml^{-1} of each test strain. After overnight incubation at 37°C, the MICs were visually recorded. Negative controls were prepared with MHB containing DMSO at the same concentrations as the extract.

2.7 Assessment of the antibiofilm activity of the crude biosurfactant against *A. baumannii*

2.7.1 Effect of the crude biosurfactant on bacterial adherence and biofilm formation

The ability of clinical strains to form biofilm was assayed using a crystal violet stain as described by Amer et al. (2021). Briefly, overnight cultures of *A. baumannii* strains adjusted to a count of 1.5 x 10^8 CFU/ml were diluted 1:50 in LB broth supplemented by 1% (w/v) glucose. Then 200 µl of the dilute cultures were inoculated into a 96-well flat-bottomed polystyrene microtiter plate (Greiner Bio One, Germany) The plates were incubated in static conditions for 24 h at 37°C. Following incubation, the planktonic microbial growth was then measured at a wavelength of 600 nm (OD_{growth}Planktonic) using an ELISA plate reader (Stat Fax®2100) Awareness Technology (Palm City, FA, USA). The wells were then washed three times with phosphate-buffered saline (PBS, pH=7.4) to remove unadhered or loosely adhered cells. After air drying, biofilms were stained with 0.1% (w/v) crystal violet (CV) solution for 15 min. The plates were then washed with water to rinse off the excess stain. The CV stain bound to the adherent cells was then solubilized by 33% glacial acetic acid and the biofilm biomass was quantified colorimetrically (OD_{CV} Biofilm) at 570 nm. To reduce background signals, a blank containing an uninoculated medium was included and measured (OD_{growth} Blank and OD_{CV} Blank). The biofilm index (BFI) of each clinical strain was calculated using the following equation:

$$\text{BFI} = (\text{OD}_{\text{CV}}\ \text{Biofilm} - \text{OD}_{\text{CV}}\ \text{Blank})/(\text{OD}_{\text{growth}}\ \text{Planktonic} - \text{OD}_{\text{growth}}\ \text{Blank})$$

Isolates were classified into non-adherent, weak, moderate, and strong biofilm-forming isolates according to the semiquantitative classification of biofilm production as described by Naves et al. (2008). The effect of the crude biosurfactant on biofilm formation by *A. baumannii* was tested as described by Amer et al. (2021). A volume of 100 µl of the diluted culture was inoculated into a 96-well flat-bottomed polystyrene microtiter plate (Greiner Bio-one®, Germany) containing equal volumes of the crude biosurfactant at concentrations equivalent to the MIC, reaching a final concentration of 0.5X MIC. Negative controls containing DMSO at the same final concentrations as in the crude biosurfactant (control) were also included. Biofilm was stained by crystal violet and BFI was determined. The antibiofilm activity of the crude biosurfactant was expressed as percentage biofilm inhibition (%BI) that was calculated according to the following formula:

$$\%\,\text{BI} = [(\text{BFI (control)} - \text{BFI (test)})/\text{BFI (control)}] \times 100$$

Where BFI (test) and BFI (control) are the BFIs of each strain in the presence and absence of the crude biosurfactant, respectively.

2.7.2 Effect of the crude biosurfactant on established biofilms

The efficacy of the crude biosurfactant in eradicating established biofilms was assessed using the method, with slight modifications, described by Lemos et al. (2018). First, 100 µl of overnight cultures of *A. baumannii* adjusted to 10^6 cells/ml in LBG were transferred to 96-well microtiter plates to form biofilms (Lemos et al., 2018). After overnight incubation in static conditions at 37°C, planktonic cells were delicately removed, and the wells were washed three times with PBS. The adherent cells remaining in the wells were then treated with 200 µl of the crude biosurfactant at concentrations equivalent to MIC. Wells treated with DMSO at the same final concentrations as in the crude biosurfactant served as control. The

plates were incubated at 37°C for an additional 24 h, after which the supernatants were removed, and wells were washed three times using PBS. The residual biofilms were quantified using two methods, namely, crystal violet staining as described in section 2.7.1 and viable count assays as described by Ziemyte et al. (2020). Using the crystal violet staining method, the biofilm eradication percentage was calculated using the following formula (Patel et al, 2021):

$$\text{Biofilm eradication percentage} = [(OD_{CV}\ \text{Control} - OD_{CV}\ \text{Test})/OD_{CV}\ \text{Control}] \times 100$$

Where OD_{CV} Control is the absorbance reading of control; OD_{CV} Test is the absorbance reading of biosurfactant treated biofilm.

To determine the number of viable biofilm-embedded bacteria after treatment with the crude biosurfactant, the wells were filled with 200 µl PBS and adherent cells were detached by sonication for 5 min. The viable count was determined using the drop plate method as described by Herigstad et al. (2001). Tenfold serial dilutions were prepared and 10 µl were plated onto MacConkey agar plates in triplicates, and incubated at 37°C for 24 h. The biofilm eradication percentage was expressed as a $\log_{10}$ reduction of the viable count in the biofilms treated by the crude biosurfactant compared to the negative control (Amer et al., 2022).

2.8 Evaluation of the antibiofilm effect of crude biosurfactant on central venous catheters (CVCs) *in vitro*

The catheter model was performed with a triple-lumen polyurethane CVC (Amecath® Ref. No. CTLC-0720-KGSN, Ameco Medical Industries, Egypt). In this model, the biosurfactant-impregnated CVC was challenged by the *A. baumannii* strain (M02) that showed the highest capacity for biofilm formation.

2.8.1 Preparation of the biosurfactant-impregnated CVC

The CVC was divided into 1-cm-long segments. Each was impregnated with the crude biosurfactant at a final concentration of 0.5X MIC (0.78 mg/ml) and kept at room temperature for 24 h (Amer et al., 2022). The catheters were then air-dried to restore their original size. Control segments were impregnated with DMSO at the same concentration used in the test.

2.8.2 Antibiofilm assay

The inhibitory effect of the crude biosurfactant on the ability of *A. baumannii* M02 (strong biofilm-forming isolate) to form biofilm on the CVC was evaluated according to the method, with slight modifications, described by Raad et al. (2012). First, the biosurfactant-impregnated and the control segments of the CVC were conditioned by plasma from a human volunteer (one of the authors). For this purpose, all CVC segments were placed in a sterile 12-well culture plate containing 2 ml of human plasma and incubated for 24 h at 37°C. The plasma was then replaced by LBG inoculated by ~$1X10^6$ CFU/ml of the test strain and the plate was incubated at 37°C for an additional 24 h. After incubation, the catheter sections were gently washed with sterile PBS to remove the non-adhered planktonic cells. The biofilms formed on the control and the biosurfactant-impregnated CVC segments were quantified by crystal violet staining and the viable count assay as described by Amer et al. (2022). For a detachment of the biofilm-embedded cells to determine the remaining viable bacteria on the catheter surface, CVC segments were sonicated in 1 ml PBS for 15 min, followed by 5 min vortexing. Aliquots of PBS were used for viable bacterial counting.

2.8.3 Scanning electron microscope analysis of biofilms on CVC

The efficacy of the CVC biosurfactant-impregnation against *A. baumannii* M02 biofilm was further confirmed through scanning electron microscope (SEM) analysis. Biofilms of *A. baumannii* M02 were allowed to develop on the biosurfactant-impregnated and the control CVC segments, as described in the antibiofilm assay. The segments were washed with PBS and then fixed using 2.5% glutaraldehyde. This was followed by gradual dehydration using increasing concentrations of 20, 40, 60, 80, and 100% ethanol. The dehydrated samples were plated by gold sputter for examination under SEM (Quanta™ 250 FEG, Thermo Fischer Scientific; New Hampshire, USA) (Yassin et al., 2019).

2.9 Cytotoxicity assay of the biosurfactant crude extract

The cytotoxicity assay of the crude biosurfactant extract was adapted from the ISO 10993-5 protocol. The assay was carried out using healthy human skin fibroblast cells obtained from Nawah Scientific Inc. (ATCC CCL-75) (Hou et al., 2020; Ivanova et al., 2021).

The biosurfactant crude extract was embedded in serum-free Dulbecco's Modified Eagle Medium (DMEM) overnight at 37°C. At the same time, the human fibroblast cell line was cultured in DMEM supplemented with 10% v/v fetal bovine serum (FBS) and 1% w/v penicillin–streptomycin for 24 h at 37°C, 5% v/v CO2.

After achieving the confluence, 100 µl of the cell suspension ($5X10^3$ cells/ml) was seeded in each well of the 96-well plate. Then, the cells were incubated overnight in a humidified atmosphere (>90% humidity) with 5% CO2 at 37°C. Cells were treated with another aliquot of 100 µl media containing biosurfactant extract at various concentrations. After 72 h of treatment, cells were fixed by replacing media with 150 µl of 10% trichloroacetic acid (TCA) and incubated at 4°C for 1 h. The TCA solution was removed, and the cells were washed 5 times with PBS. The viability of the cells was evaluated using sulforhodamine B (SRB) (0.4% w/v) assay as described by Allam et al. (2018), and color intensity was measured at wavelength 540 nm. The percentage of cell viability was calculated using the following formula: Viability (%) =

$$\text{Viability}(\%) = \frac{OD570\ \ of\ \ treated\ \ cells}{OD570\ \ of\ \ control\ \ cells} \times 100$$

2.10 Ex vivo hemolysis assay of the biosurfactant crude extract

The ex vivo hemolysis assay was conducted according to the method, with some modifications, described by Zhou et al. (2017). Briefly, freshly collected human red blood cells (RBCs) were centrifuged for 10 min at 2500 rpm, then washed three times and diluted to a final concentration of 5% v/v in sterile PBS (pH 7.4). Afterward, 500 µl of the diluted RBCs were added to 500 µl of crude biosurfactant extract at a final concentration of 0.5X MIC (0.78 mg/ml). Triton X-100 (0.1% in PBS), which can lyse RBCs completely, was used as the positive control while PBS buffer was used as the negative control. Shaking and incubation of samples at 37°C for 1 h was done and then samples were centrifuged again at 2500 rpm for 15 min. The supernatant was collected and transferred to wells of a microtiter plate, and its optical density was recorded by an ELISA plate reader at 545 nm. Sterile PBS (pH 7.4) was used as a blank. The same test was repeated with the addition of biosurfactant and DMSO-impregnated catheter to diluted RBCs. The hemolysis percentage was estimated using the following equation:

$$Hemolysis\ \ percentage\ \ (\%) = \frac{A_s - A_n}{A_p - A_n} \times 100$$

where A_s, A_n, and A_p are the absorbances of the sample, negative, and positive controls, respectively. The assay was calculated as the mean ± standard deviation of three replicates.

2.11 Gas chromatography-mass spectrophotometry analysis

Five milligrams of the extract dry weight was mixed with 120 µl silylating agent (N,O- Bis (tert-butyl dimethyl silyl) acetamide and incubated at 60°C for 30 minutes and analyzed by gas chromatography. The GC apparatus (Shimadzu®, Kyoto, Japan) coupled with a QP2010 Rtx-5MS was used to identify the structural analog of the crude biosurfactant. Helium was employed as a carrier gas, and a total of 10 µl of the sample was added to the apparatus. The runtime was 45 minutes with a flow rate of 1.24 ml/min. The oven was maintained at a temperature ranging from 60 to 260°C. The data were processed by matching the mass spectra and retention indices of peaks with references to retention index and mass spectra from the National Institute of Standards and Technology (NIST) library.

2.12 Statistical analysis

Statistical analysis was performed using GraphPad Prism 8.0.0 for Windows (GraphPad Software Inc., CA, USA). Independent samples t-test and two-way ANOVA (analysis of variance) were employed to analyze the statistical differences between crude biosurfactant and DMSO-treated cultures, where $p<0.05$ was considered to be statistically significant.

3 Results

3.1 Screening for biosurfactant-producing endophytic bacteria

In all, 10 plant samples were collected throughout the study period from different locations along the banks of the River Nile. A total of 44 bacterial endophytes were isolated from these plants. The plant species, their sites of collection, and the morphology of the isolates recovered from each plant are listed in Supplementary Table 1. CFSs of all endophytes were screened for their biosurfactant activity *via* different qualitative and quantitative assays. Of all endophytes that showed a positive drop collapse test, the CFS of an endophyte coded "Cp24" showed the highest biosurfactant activity. It produced a clear zone of 74 mm diameter in the oil dispersion assay and an %EI24 of 60 ± 2.5. Cp24 was isolated from the leaf of *Cyperus papyrus* collected from the Pharaonic Village in Cairo (29.9973° N, 31.2148° E). The growth of Cp24 from the leaf fragments of *C. papyrus* on TSA plates is shown in Figure 1.

3.2 Identification of endophytic isolate-producing biosurfactant

The endophytic isolate Cp24 grew on TSA plates as rough, opaque, fuzzy yellow to slightly orange colonies with jagged edges. Under a light microscope, it appeared as Gram-positive rods arranged in chains. The nucleotide sequence of the 16S *rRNA* gene carried by Cp24 showed the highest similarity to the corresponding gene of strain *B. amyloliquefaciens* HY-5 (GenBank accession: KY886133.1; percent similarity: 97.68%). A phylogenetic tree based on the 16S rRNA sequence of Cp24 and highly similar strains retrieved from the NCBI database showed that Cp24 was clustered with the same strain (Figure 2). Accordingly, Cp24 was tentatively identified as *B. amyloliquefaciens*.

3.3 Antibacterial activity of the crude biosurfactant against *A. baumannii* isolates

The crude biosurfactant extract of Cp24 (50 mg/ml) displayed considerable antibacterial activity against four MDR and XDR *A. baumannii* isolates in addition to the standard strain (ATCC® 19606). The MIC values of the crude biosurfactant in the tested strains ranged from 0.78 to 1.56 mg/ml, as shown in Table 2.

3.4 Sub-MIC concentration of crude biosurfactant extract significantly inhibits *A. baumannii* biofilm formation

All tested *A. baumannii* isolates and the standard strain displayed strong biofilm-forming capacity, with BFI ranging from

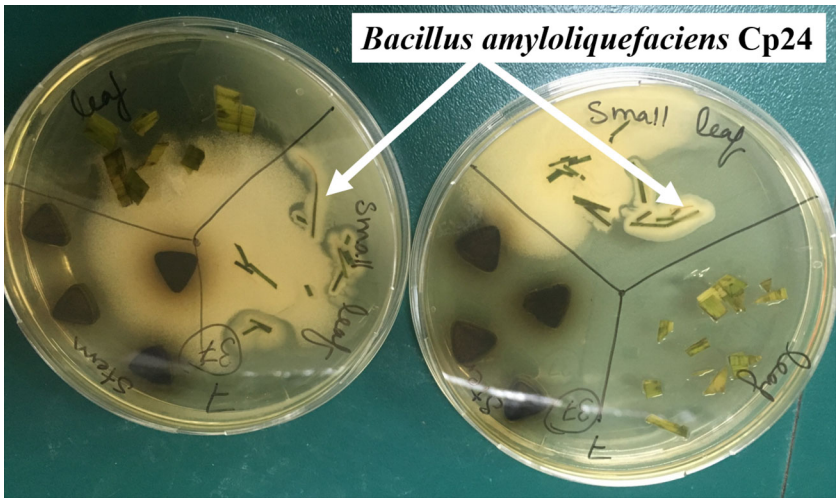

FIGURE 1
Growth of the endophytic isolates CP24 from the leaf fragments of *C. papyrus*.

1.25 to 2.2. The antibiofilm potential of *B. amyloliquefaciens* Cp24 crude biosurfactant was determined by its ability to impair the biofilm formation of the tested strains and inhibit their adhesion ability to the surface without any effect on their growth. Our results showed that the *B. amyloliquefaciens* Cp24 crude biosurfactant efficiently inhibited biofilm formation of all the tested strains at half of its MIC. At this concentration, the biofilm formation among all the treated *A. baumannii* isolates was significantly inhibited (p-value<0.0001), with the percentage of inhibition ranging from 71.6 to 89.59% (Figure 3).

3.5 Eradication effect of biosurfactant crude extract on established biofilm of *A. baumannii*

The antibiofilm potential of *B. amyloliquefaciens* Cp24 crude biosurfactant was further determined by its ability to impair the preformed biofilms of the tested strains. Our results showed that the *B. amyloliquefaciens* Cp24 crude biosurfactant efficiently disrupted the preformed biofilms. At the MIC concentrations, the eradication of the preformed biofilms by the *B. amyloliquefaciens* Cp24 crude biosurfactant ranged from 44.6% to 87.3% among all the tested strains (Figure 4).

3.6 *B. amyloliquefaciens* CVCs impregnated with crude biosurfactant have a significant *in vitro* antibiofilm activity against *A. baumannii*

Catheter impregnated with 0.5X MIC of the crude biosurfactant extract caused a significant reduction in the biofilm by three $\log_{10}$ cycles for the clinical isolate M02. The obtained results revealed that the viability of *A. baumannii* isolates M02 embedded in the biofilm were remarkably reduced upon coating by the Cp24 crude

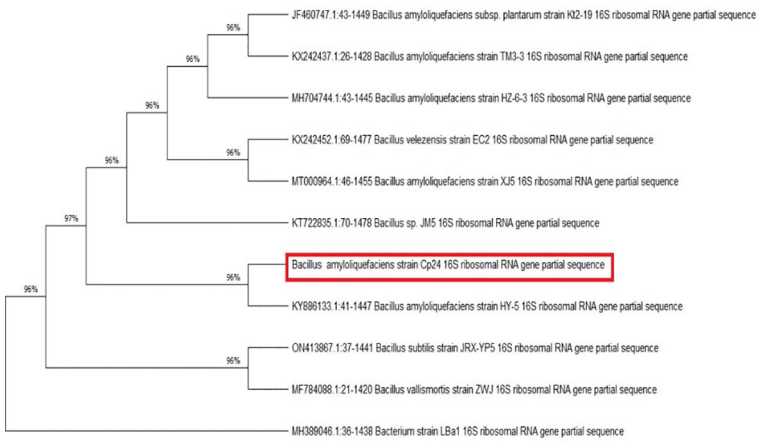

FIGURE 2
Evolutionary relationships between *B. amyloliquefaciens* Cp24 and highly similar strains. The phylogenetic tree was constructed by the maximum parsimony method (1000 replicates).

TABLE 2 MICs of the crude biosurfactant produced by Cp24 against *A. baumannii* strains.

Bacterial Strain	MIC of Cp24 crude biosurfactant extract (mg/ml)
A. baumannii isolate M02	1.56
A. baumannii isolate M03	1.56
A. baumannii isolate M04	1.56
A. baumannii isolate M15	0.78
A. baumannii standard strain (ATCC® 19606)	0.78

biosurfactant (Figure 5). The results obtained from the biofilm biomass quantification assay revealed that the impregnated CVCs caused a 43% reduction in biofilm formation.

3.7 SEM analysis revealed obvious antibiofilm activity of the impregnated CVC with the crude biosurfactant

The inhibition of biofilm formation on the impregnated CVC with the crude biosurfactant was confirmed by visualization using SEM analysis. *A. baumannii* growing on the control CVC surface showed higher bacterial cell density, while impregnated CVC showed scattered aggregation of fewer cells than the control (Figure 6).

3.8 Cytotoxicity assay for biosurfactant crude extract

No substantial change was observed in the viability of skin fibroblast cells at sub-MIC concentrations of the crude biosurfactant extract when compared to the untreated control cells. The viability of fibroblast cells at the concentration used in catheter impregnation (0.78 mg/ml) was more than 90% (Figure 7).

3.9 Ex vivo hemolysis assay of the biosurfactant crude extract

The potential hemolytic activity induced by the crude biosurfactant of *B. amyloliquefaciens* Cp24 was investigated as an indication of ex vivo blood biocompatibility. The Triton X 100 was used as a positive control and turned red color due to hemolysis, resulting in the release of hemoglobin (Hb) from the red blood cells (RBCs), whereas the negative control (PBS solutions) did not show visible hemolysis. Crude biosurfactant at a concentration of 0.78 mg/ml showed hemolysis of 6.6%. However, impregnated catheter with an equivalent concentration (0.78 mg/ml) caused a lower hemolytic effect, of 2.3%.

3.10 Gas Chromatography-Mass Spectrometry (GC–MS) Analysis

The analytical technique GC–MS consists of gas chromatography coupled with mass spectroscopy and it was used for the detection of various compounds present in the *B. amyloliquefaciens* Cp24 crude biosurfactant. The GC–MS chromatogram showed different peaks, indicating the presence of different compounds (Figure 8). Major peak compounds at the respective retention time were identified from the standard library compound, and are shown in Table 3.

4 Discussion

In the present study, we aimed to screen the antibiofilm activity of endophytes that produce biosurfactants against multidrug-

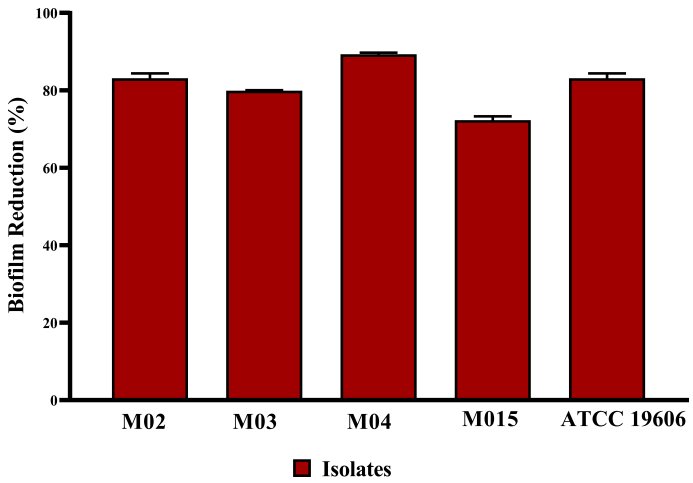

FIGURE 3
Quantification of the inhibitory effect of *B. amyloliquefaciens* crude biosurfactant on biofilms formation of *A. baumannii* isolates using crystal violet assay, showing the average reduction percentage of biofilm formation of *A. baumannii* isolates treated with 0.5X MIC of the crude biosurfactant Cp24 extract. Data represent the mean of at least three biological replicates, and error bars show the standard deviation.

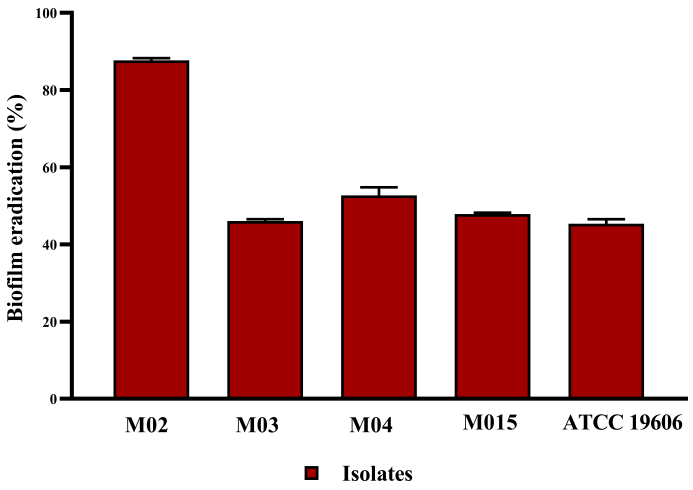

FIGURE 4
Quantification of the inhibitory effect of *B. amyloliquefaciens* crude biosurfactant on biofilms eradication of *A. baumannii* isolates using crystal violet assay, showing the average biofilm eradication percentage of established biofilms *A. baumannii* isolates. Data represent the mean of at least three biological replicates, and error bars show the standard deviation.

resistant *A. baumannii* isolates through the collection of plant samples along the banks of the River Nile. From 10 collected plant samples, a total of 44 bacterial cultures were isolated and screened for biosurfactant activity. Endophytic isolate Cp24, isolated from *Cyperus papyrus*, showed strong and instant biosurfactant activity and was selected for further study. *Cyperus papyrus*, commonly named papyrus and used by Ancient Egyptians as a writing surface, belongs to the Cyperaceae family and is one of the plants that are widespread in the African subtropical and tropical wetlands (Mburu et al., 2015). Little scientific studies are available on this plant and its associated endophytes.

Endophytic isolate Cp24 was further identified using 16s rRNA sequencing and found to be *Bacillus amyloliquefaciens*. Endophytic *B. amyloliquefaciens* is a well-known endophyte that has been used for biological control against crop diseases and insect pests. It is found to be a safe microorganism with proven excellence in plant colonization (Liu et al., 2017). Previous studies showed the antimicrobial activity of *B. amyloliquefaciens* through the production of secondary metabolites, such as low-molecular-weight lipopeptides, polyenes, phospholipids, amino acids, nucleic acids, and polyketides, as well as antimicrobial proteins (Koumoutsi et al., 2004; Luo et al., 2022).

We tested the effect of the produced biosurfactant against *A.baumanni*, which is the causative agent for many serious infections, including endocarditis, meningitis, necrotizing fasciitis, sepsis, urinary tract infections, skin and/or soft tissue infections, and pneumonia. Its ability to survive is significantly increased by the creation of biofilms, which also renders them resistant to desiccation and antimicrobial treatment. Microbial adherence to biotic and abiotic surfaces such as catheters, ventilators, or even gloves promotes the spread of the infection from one individual to another (Vijayashree Priyadharsini et al., 2018). In the current

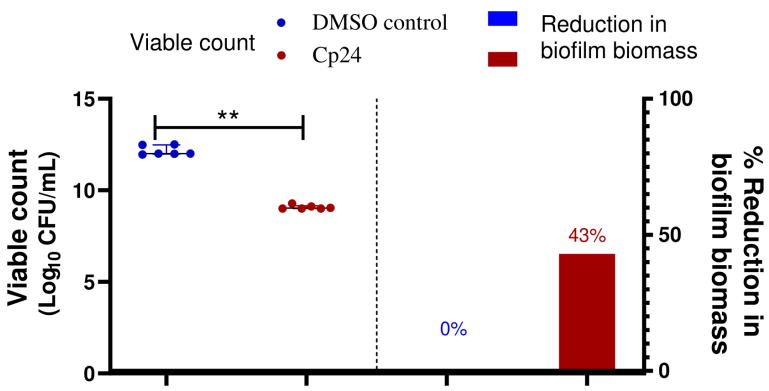

FIGURE 5
Quantification of the reduction in *A. baumannii* biofilm on crude biosurfactant extract (Cp24) impregnated CVCs compared to DMSO control. The percentage reduction in biofilm biomass was measured by crystal violet assay. The reduction in adhered viable bacterial counts of *A. baumannii* isolate M02 was measured by the drop plate method after 24 h of incubation. Data are represented as median with interquartile range and statistical difference was determined by student's t-test, where statistical significance is represented by $^{**}p < 0.01$.

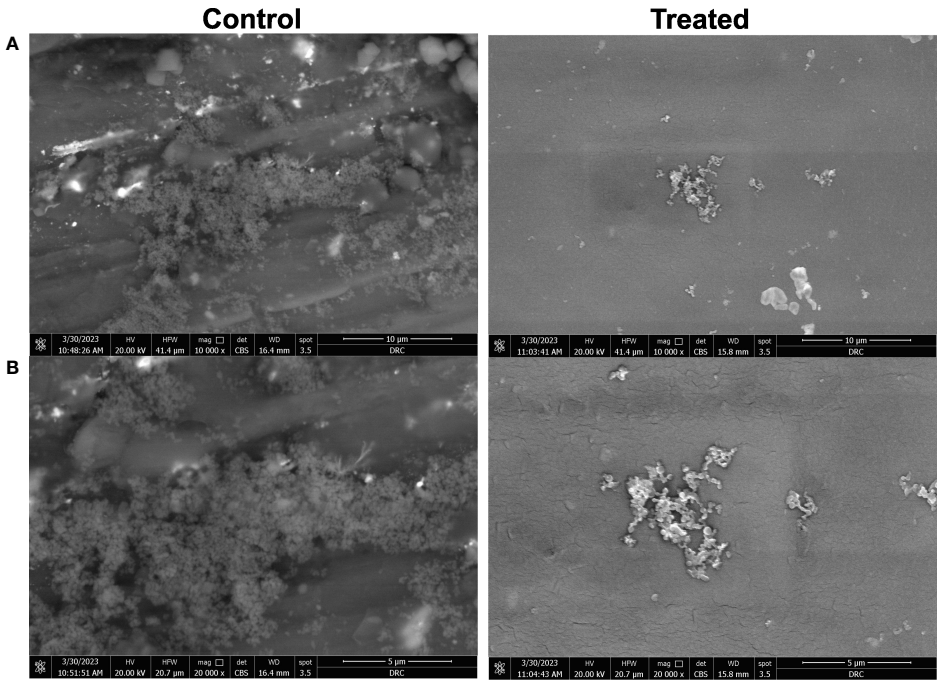

FIGURE 6
Microscopic visualization of biofilm formation by *A. baumannii* isolate M02 on CVC segments using scanning electron microscope (SEM). Biofilm formation on the catheter treated by impregnation with 0.5X MIC (0.78 mg/ml) of the crude biosurfactant extract (Cp24) was compared to the control DMSO-treated catheter. Visualization using SEM was done at magnifications of **(A)** 10,000 X and **(B)** 20,000 X.

study, the crude biosurfactant of *B. amyloliquefaciens* Cp24 showed considerable antibacterial effects against all the tested *A. baumannii* bacterial strains with MIC ranging from 0.78 to 1.56 mg/ml. Similarly, the antimicrobial activity of several biosurfactants has been previously reported (Gomaa, 2013; De Giani et al., 2021). Moreover, reports suggest that biosurfactants can prevent the growth of biofilms and microbial adherence without exhibiting antibacterial action (Tahmourespour et al., 2011; Hamza et al., 2017). The Cp24 crude biosurfactant was also tested for its antibiofilm activity against both biofilm formation and eradication of established biofilms. The antibiofilm activity against all *A. baumannii* isolates reached up to 71.6-89.59% at

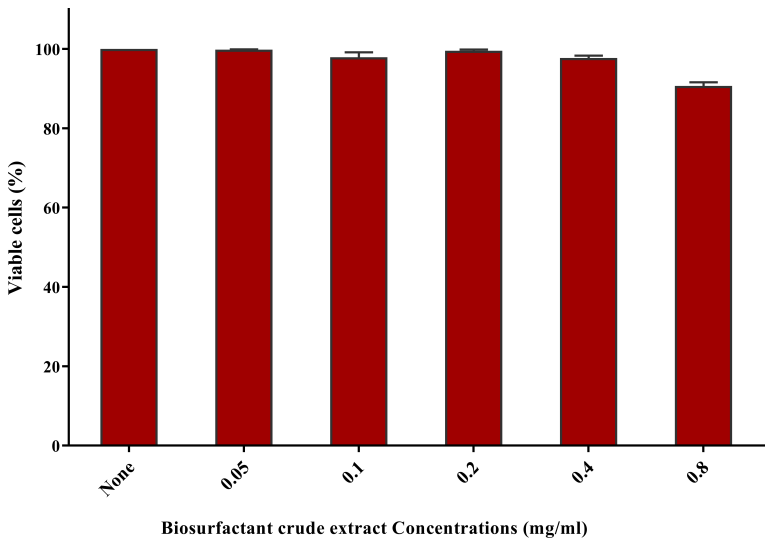

FIGURE 7
Cytotoxicity assay on human fibroblast cells after 24 h exposure to the nutrient medium interacting with serial dilutions of biosurfactant crude extract (0.05-0.8 mg/ml). Cytotoxicity was tested by sulforhodamine B (SRB) (0.4% w/v) and represented as the percentage of remaining viable cells after applying the treatment.

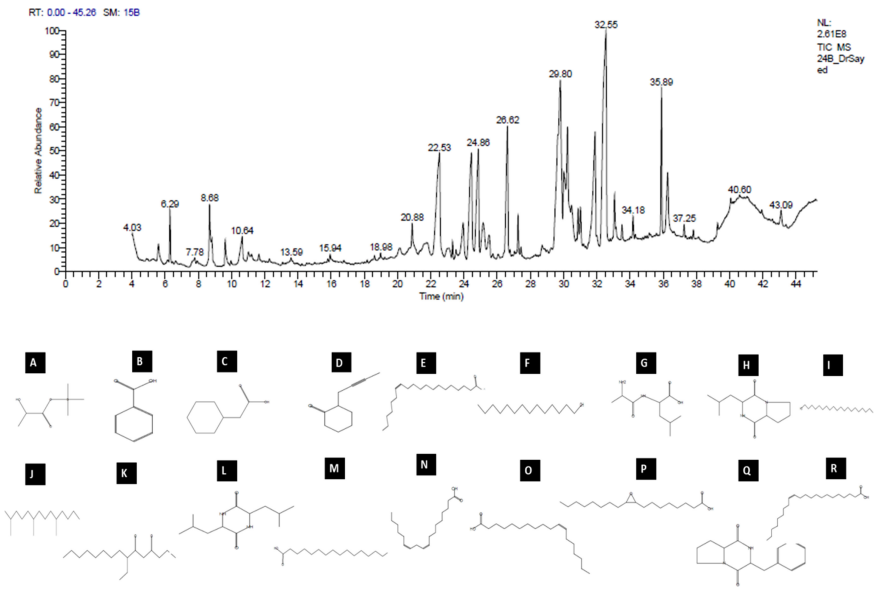

FIGURE 8
GC–MS analysis of the crude biosurfactants derived from *B. amyloliquefaciens* Cp24 endophyte. Identified compounds: **(A)** D-(-)-Lactic acid; **(B)** Benzoic acid **(C)** Benzeneacetic acid; **(D)** 2-(2-butynyl) Cyclohexanone; **(E)** cis-13-Eicosenoic acid; **(F)** 1-Tetradecanol; **(G)** dl-Alanyl-l-leucine; **(H)** [Cyclo (D-Leu-L-Pro)]; **(I)** 1-Eicosanol, **(J)** 2,6,10-Trimethyltetradecane (Farnesan); **(K)** 7-Ethyl-4,6-heptadecandione;**(L)** [Cyclo(Leu-Leu)]; **(M)** n-Hexadecanoic acid; **(N)** 9,12-Octadecadienoic acid; **(O)** cis-Vaccenic acid; **(P)** cis- (Epoxyoleic acid); **(Q)** 3-Benzyl-hexahydro-pyrrolo[1, 2-a] pyrazine-1,4-dione; **(R)** Erucic acid.

0.5X MIC (p-value<0.01). Additionally, it successfully eradicated the preformed *A. baumannii* biofilms with a range of 44.6% to 87.3% among all the tested strains. Although the particular mechanisms underlying the antibiofilm activity of biosurfactants are not yet fully known, biosurfactants may impact the interactions between microorganisms and surfaces in several ways, including (1) modifying the surface's physicochemical characteristics, such as surface energy, hydrophobicity, and surface charge, which lessens microbial adhesion (Giri et al., 2019); (2) downregulating the biofilm-related gene expression (Ohadi et al., 2020); (3) rendering the biofilms more soluble, which favors bacterial detachment (e Silva et al., 2017); and (4) decreasing biofilm formation through the interference with quorum sensing (Paraszkiewicz et al., 2021).

Numerous studies have shown that the previous coating of catheter surfaces with biosurfactants (surface conditioning) reduced microbial adhesion and colonization (Falagas and Makris, 2009; Janek et al., 2018). Therefore, our study also aimed to investigate the *in vitro* antibiofilm efficacy of CVC impregnated with a crude biosurfactant. Applying biosurfactants for catheter treatment reduced biofilm formation by 43%, whereas a previous study by Janek et al. (2018) showed a reduction in adherence by 70% for weak biofilm-forming *Escherichia coli*. The extracted biosurfactant reduced the number of viable cells adhering to CVCs by three $\log_{10}$ cycles, whereas previous studies on biosurfactant-coated catheters showed a reduction in the viable count by one $\log_{10}$ (Rodrigues et al., 2004). In addition to their ability to reduce biofilm formation, the crude biosurfactant exhibited, at its sub-MICs, no cytotoxic effect on human cell lines nor hemolytic activity against human blood, which makes it safe for use. The cytocompatibility and safety of biosurfactants have been reported in previous studies (Rodrigues, 2011; Gupta et al., 2017).

The GC-MS analysis of the Cp24 crude biosurfactant revealed the presence of 19 compounds. The nature of the majority of detected compounds was the fatty acids and peptides components of the lipopeptide biosurfactant, which conforms with the previously identified nature of *B. amyloliquefaciens* biosurfactants as a lipopeptide surfactant (Sarwar et al., 2018; Wu et al., 2022). The complex nature of biosurfactants and their mosaic distribution of polarity, as well as branched or circular structures, give them remarkable physical properties compared to synthetic surfactants. Therefore, biosurfactants, such as surfactin, with their cyclic nature and dynamic surface properties can combine densely at the interface, increasing their surface activity and providing them with properties that make them suitable for many potential applications (Otzen, 2017).

Cyclic peptides detected in the Cp24 extract have been detected as products by many *Bacillus* sp. and have been reported for many potential applications in the agricultural, pharmaceutical, and biotechnology industries due to their dynamic surface properties (Sarwar et al., 2018). Previous studies showed that the diketopiperazines (DKPs) cyclopeptides ((Cyclo(Leu-Pro) and Cyclo (Leu-Leu)), similar to those detected in our extract, inhibit quorum sensing mechanisms and biofilm formation by various microorganisms, such as soft rot-causing pathogen *Lelliottia amnigena* RCE and *P.aeruginosa* (Rashiya et al., 2021; Kachhadia et al., 2022). Additionally, the presence of nitrogen atoms in DKPs makes them physiologically more stable compared to their counterpart lactones (Almohaywi et al., 2019).

10.3389/fcimb.2023.1210195

TABLE 3 Major constituents of the crude biosurfactants of *B. amyloliquefaciens* Cp24 endophyte using GC–MS.

Compound no.	RT	% Area	Compound name	Molecular Formula	Class
1	6.29	1.43	D-(-)-Lactic acid	$C_6H_{14}O_3$	Short-chain fatty acid
2	8.83	0.69	Benzoic acid	$C_7H_6O_2$	Aromatic carboxylic acid
3	10.64	1.3	Benzeneacetic acid	$C_8H_8O_2$	Organic Acid
4	11.65	0.24	2-(2-butynyl) Cyclohexanone	$C_{10}H_{14}O$	Cyclic ketone
5	18.98	0.28	cis-13-Eicosenoic acid	$C_{20}H_{38}O_2$	Long-chain saturated fatty acid
6	20.88	0.76	1-Tetradecanol	$C_{14}H_{30}O$	Long-chain fatty alcohol
7	21.75	0.79	dl-Alanyl-l-leucine	$C_9H_{18}N_2O_3$	Dipeptide
8	22.53	5.51	Cyclo (D-Leu-L-Pro) 3-Isobutylhexahydropyrrolo [1,2-a]pyrazine-1,4-dione	$C_{11}H_{18}N_2O_2$	Cyclic dipeptide
9	23.31	0.46	1-Eicosanol	$C_{20}H_{42}O$	Long-chain fatty alcohol
10	23.52	0.31	2,6,10-Trimethyltetradecane (Farnesan)	$C_{17}H_{36}$	Acyclic farnesane sesquiterpenoids (Branched alkanes)
11	23.95	1.38	7-Ethyl-4,6-heptadecandione	$C_{19}H_{36}O_2$	Fatty Acyl
12	25.5	0.95	Cyclo(Leu-Leu) 2,5-Piperazinedione, 3,6-bis(2-methylpropyl)-	$C_{12}H_{22}N_2O_2$	Cyclic dipeptide
13	26.62	5.52	n-Hexadecanoic acid	$C_{16}H_{32}O_2$	Long-chain saturated fatty acids, surfactant
14	29.65	6.15	9,12-Octadecadienoic acid (alpha-Linoleic acid)	$C_{18}H_{32}O_2$	Long-chain unsaturated fatty acid
15	29.8	10.6	cis-Vaccenic acid	$C_{18}H_{34}O_2$	Long-chain monounsaturated fatty acid
16	30.01	1.79	Cyclo(Leu-Pro) Pyrrolo[1,2-a]pyrazine-1,4-dione,hexahydro-3-(2 methylpropyl)	$C_{11}H_{18}N_2O_2$	Cyclic dipeptide
17	31.02	1.44	Oxiraneoctanoic acid, 3-octyl-, cis- (Epoxyoleic acid)	$C_{18}H_{34}O_3$	Epoxy fatty acid
18	32.56	19.53	3-Benzyl-hexahydro-pyrrolo[1, 2-a] pyrazine-1,4-dione	$C_{14}H_{16}N_2O_2$	Organonitrogen compound
19	36.27	2.44	Erucic acid	$C_{22}H_{42}O_2$	Monounsaturated very long-chain fatty acid

There are three primary FA groups produced by *Bacillus* species: branched-chain FAs, straight-chain FAs, and complex FA types, such as cyclic, hydroxyl, or epoxy FAs. The fatty acid (FA) composition of bacterial cells differs depending on the species, and, as an adaptation to environmental changes is crucial for bacterial growth, the FA composition of the cell's membrane fluctuates according to the environment. The crude biosurfactant extract is composed of a mixture of fatty acids with a range of short-chain fatty acids (Lactic acid) to long-chain fatty acids, varying from C16 to C22 saturated (cis-13-eicosenoic acid and n-hexadecanoic acid) and unsaturated fatty acids (9,12-octadecadienoic acid, cis-vaccenic acid, and erucic acid). In addition, it also contained epoxy oleic acid. Previous studies showed that some *Bacillus* species are capable of producing epoxy FAs, which are FAs with one or two epoxy groups with antibacterial capabilities (Diomandé et al., 2015). Unsaturated fatty acids, such as cis-9-hexadecenoic acid and cis-9-tetradecenoic acid, were reported to inhibit the quorum sensing system and subsequently reduce the biofilm formation and suppress motility in *V. cholerae* and *A. baumannii* ATCC 17978 (Nicol et al., 2018). Previous studies revealed that fatty acids and their derivatives reduced the virulence characteristics of *Chromobacterium violaceum* (Santhakumari et al., 2017) and *Vibrio* Sp. (Pérez-López et al., 2018). Higher molecular-weight biosurfactants displayed higher emulsification activity, according to a study by Martins and Martins (2018).

The compound 3-Benzyl-hexahydro-pyrrolo[1, 2-a]pyrazine-1,4-dione represents 19% of the Cp24 extract component and it was previously identified in *Exiguobacterium indicum* SJ16 extract isolated from the rhizosphere of *Cyperus laevigatus*. It showed significant quorum sensing inhibition against the reference *Chromobacterium violaceum* CV026 strain and also inhibited the biofilm formation of *P. aeruginosa* (Singh et al., 2019).

5 Conclusion

In conclusion, this study demonstrates that impregnating catheters with crude biosurfactant of endophytic B. *amylolique faciens* strain Cp24 effectively reduces biofilm formation of *A. baumannii*, a multidrug-resistant bacterium that belongs to global clones and has a strong biofilm-forming capacity. An additional

advantage is the safety of this compound on human cell lines and its reduced hemolysis activity. GC-MS analysis confirmed the production of lipopeptides with cyclic peptide moiety providing them with dynamic surface properties that increased their surface activity. In addition, the presence of long-chain and epoxy-type fatty acids was observed, which reduced virulence factors and exhibited quorum sensing inhibition activity, therefore reducing biofilm formation. Further studies should evaluate this approach by *in vivo* analysis via long-term catheterization in animal models and study the possible synergistic activity of these fatty acids with other antivirulence compounds to increase their activity.

Data availability statement

The original contributions presented in the study are included in the article/Supplementary Material. Further inquiries can be directed to the corresponding author.

Ethics statement

The study was performed in accordance with relevant guidelines and regulations and has been approved by the Ethics Committee of October University for Modern Sciences and Arts with the reference number M1/EC1/2023PD.

Author contributions

All authors conceptualized the work, performed the experiments, analyzed the results, edited the manuscript, contributed to the article, and approved the submitted version.

Acknowledgments

The authors wish to thank Prof. Shahira M. Ezzat, Professor of Phytochemistry, Faculty of Pharmacy, Cairo University and October University for Modern Sciences and Arts for aiding in the identification of some plants. The authors extend their appreciation to Dr. Rana M. Merghany, Department of Pharmacognosy, National Research Centre for providing some of the plants included in the study.

Conflict of interest

The authors declare that the research was conducted in the absence of any commercial or financial relationships that could be construed as a potential conflict of interest

Publisher's note

Supplementary material

The Supplementary Material for this article can be found online at: https://www.frontiersin.org/articles/10.3389/fcimb.2023.1210195/full#supplementary-material

References

Abd El-Rahman, O. A., Rasslan, F., Hassan, S. S., Ashour, H. M., and Wasfi, R. (2023). The RND efflux pump gene expression in the biofilm formation of acinetobacter baumannii. *Antibiotics (Basel)* 12, 419. doi: 10.3390/antibiotics12020419

Allam, R. M., Al-Abd, A. M., Khedr, A., Sharaf, O. A., Nofal, S. M., Khalifa, A. E., et al. (2018). Fingolimod interrupts the cross talk between estrogen metabolism and sphingolipid metabolism within prostate cancer cells. *Toxicol. Lett.* 291, 77–85. doi: 10.1016/j.toxlet.2018.04.008

Almohaywi, B., Yu, T. T., Iskander, G., Chan, D. S. H., Ho, K. K. K., Rice, S., et al. (2019). Dihydropyrrolones as bacterial quorum sensing inhibitors. *Bioorg Med. Chem. Lett.* 29, 1054–1059. doi: 10.1016/j.bmcl.2019.03.004

Amer, M. A., Ramadan, M. A., Attia, A. S., and Wasfi, R. (2021). Indole derivatives obtained from Egyptian enterobacter sp. soil isolates exhibit antivirulence activities against uropathogenic Proteus mirabilis. *Antibiotics (Basel)* 10, 363. doi: 10.3390/antibiotics10040363

Amer, M. A., Wasfi, R., Attia, A. S., and and Ramadan, M. A. (2022). Silicone Foley catheters impregnated with microbial indole derivatives inhibit crystalline biofilm formation by Proteus mirabilis. *Front. Cell. Infection Microbiol.* 12. doi: 10.3389/fcimb.2022.1010625

Ashitha, A., Radhakrishnan, E. K., and Mathew, J. (2020). Characterization of biosurfactant produced by the endophyte burkholderia sp. WYAT7 and evaluation of its antibacterial and antibiofilm potentials. *J. Biotechnol.* 313, 1–10. doi: 10.1016/j.jbiotec.2020.03.005

Banat, I. M., De Rienzo, M. A., and Quinn, G. A. (2014). Microbial biofilms: biosurfactants as antibiofilm agents. *Appl. Microbiol. Biotechnol.* 98, 9915–9929. doi: 10.1007/s00253-014-6169-6

Castilho, S. R. A., Godoy, C. S. M., Guilarde, A. O., Cardoso, J. L., Andre, M. C. P., Junqueira-Kipnis, A.P., et al. (2017). Acinetobacter baumannii strains isolated from patients in intensive care units in goiânia, Brazil: molecular and drug susceptibility profiles. *PLoS One* 12, e0176790. doi: 10.1371/journal.pone.0176790

CLSI (2015). "Methods for dilution antimicrobial susceptibility tests for bacteria that grow aerobically; approved standard–tenth edition," in *CLSI document M07-A10* (Wayne: PA Clinical and Laboratory Standards Institute).

Corrêa Carvalho, G., Miguel Sábio, R., Spósito, L., De Jesus Andreoli Pinto, T., and Chorilli, M. (2022). An overview of the use of central venous catheters impregnated with drugs or with inorganic nanoparticles as a strategy in preventing infections. *Int. J. Pharmaceutics* 615, 121518. doi: 10.1016/j.ijpharm.2022.121518

De Giani, A., Zampolli, J., and Di Gennaro, P. (2021). Recent trends on biosurfactants with antimicrobial activity produced by bacteria associated with human health: different perspectives on their properties, challenges, and potential applications. *Front. Microbiol.* 12. doi: 10.3389/fmicb.2021.655150

Diomandé, S. E., Nguyen-The, C., Guinebretière, M. H., Broussolle, V., and Brillard, J. (2015). Role of fatty acids in bacillus environmental adaptation. *Front. Microbiol.* 6. doi: 10.3389/fmicb.2015.00813

Donlan, R. M. (2011). Biofilm elimination on intravascular catheters: important considerations for the infectious disease practitioner. *Clin. Infect. Dis.* 52, 1038–1045. doi: 10.1093/cid/cir077

Duarte, A., Ferreira, S., Almeida, S., and Domingues, F. C. (2016). Clinical isolates of acinetobacter baumannii from a Portuguese hospital: PFGE characterization, antibiotic

susceptibility and biofilm-forming ability. *Comp. Immunol. Microbiol. Infect. Dis.* 45, 29–33. doi: 10.1016/j.cimid.2016.02.002

Eras-Muñoz, E., Farré, A., Sánchez, A., Font, X., and Gea, T. (2022). Microbial biosurfactants: a review of recent environmental applications. *Bioengineered* 13, 12365–12391. doi: 10.1080/21655979.2022.2074621

Eze, E. C. , Chenia, H. Y., and El Zowalaty, M. E. (2018). Acinetobacter baumannii biofilms: effects of physicochemical factors, virulence, antibiotic resistance determinants, gene regulation, and future antimicrobial treatments. *Infect. Drug Resist.* 11, 2277–2299. doi: 10.2147/IDR.S169894

Falagas, M. E., and Makris, G. C. (2009). Probiotic bacteria and biosurfactants for nosocomial infection control: a hypothesis. *J. Hosp Infect.* 71, 301–306. doi: 10.1016/j.jhin.2008.12.008

Gedefie, A., Demsis, W., Ashagrie, M., Kassa, Y., Tesfaye, M., Tilahun, M., et al. (2021). Acinetobacter baumannii biofilm formation and its role in disease pathogenesis: a review. *Infect. Drug Resist.* 14, 3711–3719. doi: 10.2147/IDR.S332051

Giri, S. S., Ryu, E. C., Sukumaran, V., and Park, S. C. (2019). Antioxidant, antibacterial, and anti-adhesive activities of biosurfactants isolated from bacillus strains. *Microb. Pathog.* 132, 66–72. doi: 10.1016/j.micpath.2019.04.035

Gomaa, E. Z. (2013). Antimicrobial activity of a biosurfactant produced by bacillus licheniformis strain M104 grown on whey. *Braz. Arch. Biol. Technol.* 56. doi: 10.1590/S1516-89132013000200011

Gouda, S., Das, G., Sen, S. K., Shin, H. S., and Patra, J. K. (2016). Endophytes: a treasure house of bioactive compounds of medicinal importance. *Front. Microbiol.* 7. doi: 10.3389/fmicb.2016.01538

Guenezan, J., Drugeon, B., Marjanovic, N., and Mimoz, O. (2018). Treatment of central line-associated bloodstream infections. *Crit. Care* 22, 303. doi: 10.1186/s13054-018-2249-9

Gupta, S., Raghuwanshi, N., Varshney, R., Banat, I. M., Srivastava, A. K., Pruthi, P. A., et al. (2017). Accelerated *in vivo* wound healing evaluation of microbial glycolipid containing ointment as a transdermal substitute. *BioMed. Pharmacother.* 94, 1186–1196. doi: 10.1016/j.biopha.2017.08.010

Hamed, S. M., Hussein, A. F. A., Al-Agamy, M. H., Radwan, H. H., and Zafer, M. M. (2022). Genetic configuration of genomic resistance islands in acinetobacter baumannii clinical isolates from Egypt. *Front. Microbiol.* 13. doi: 10.3389/fmicb.2022.878912

Hamza, F., Satpute, S., Banpurkar, A., Kumar, A. R., and Zinjarde, S. (2017). Biosurfactant from a marine bacterium disrupts biofilms of pathogenic bacteria in a tropical aquaculture system. *FEMS Microbiol. Ecol.* 93. doi: 10.1093/femsec/fix140

Herigstad, B., Hamilton, M., and Heersink, J. (2001). How to optimize the drop plate method for enumerating bacteria. *J. Microbiol. Methods* 44, 121–129. doi: 10.1016/s0167-7012(00)00241-4

Hou, Z., Wu, Y., Xu, C., Reghu, S., Shang, Z., Chen, J., et al. (2020). Precisely structured nitric-Oxide-Releasing copolymer brush defeats broad-spectrum catheter-associated biofilm infections *In vivo*. *ACS Cent. Sci.* 6, 2031–2045. doi: 10.1021/acscentsci.0c00755

Ivanova, A., Ivanova, K., Perelshtein, I., Gedanken, A., Todorova, K., Milcheva, R., et al. (2021). Sonochemically engineered nano-enabled zinc oxide/amylase coatings prevent the occurrence of catheter-associated urinary tract infections. *Materials Sci. Engineering: C* 131, 112518. doi: 10.1016/j.msec.2021.112518

Janek, T., Krasowska, A., Czyznikowska, Z., and Lukaszewicz, M. (2018). Trehalose lipid biosurfactant reduces adhesion of microbial pathogens to polystyrene and silicone surfaces: an experimental and computational approach. *Front Microbiol* 9, 2441. doi: 10.3389/fmicb.2018.02441

Joe, M., Gomathi, R., Benson, A., Devaraj, S., Rengasamy, P., Henry, A., et al. (2019). Simultaneous application of biosurfactant and bioaugmentation with rhamnolipid-producing shewanella for enhanced bioremediation of oil-polluted soil. *Appl. Sci.* 9, 3773. doi: 10.3390/app9183773

Kachhadia, R., Kapadia, C., Singh, S., Gandhi, K., Jajda, H., Alfarraj, S., et al. (2022). Quorum sensing inhibitory and quenching activity of bacillus cereus RC1 extracts on soft rot-causing bacteria lelliottia amnigena. *ACS Omega* 7, 25291–25308. doi: 10.1021/acsomega.2c02202

Katoch, M., Phull, S., Vaid, S., and Singh, S. (2017). Diversity, phylogeny, anticancer and antimicrobial potential of fungal endophytes associated with monarda citriodora l. *BMC Microbiol.* 17, 44. doi: 10.1186/s12866-017-0961-2

Koumoutsi, A., Chen, X. H., Henne, A., Liesegang, H., Hitzeroth, G., Franke, P., et al. (2004). Structural and functional characterization of gene clusters directing nonribosomal synthesis of bioactive cyclic lipopeptides in bacillus amyloliquefaciens strain FZB42. *J. Bacteriol* 186, 1084–1096. doi: 10.1128/jb.186.4.1084-1096.2004

Lafuente Cabrero, E., Terradas Robledo, R., Civit Cunado, A., Garcia Sardelli, D., Hidalgo Lopez, C., Giro Formatger, D., et al. (2023). Risk factors of catheter- associated bloodstream infection: systematic review and meta-analysis. *PLoS One* 18, e0282290. doi: 10.1371/journal.pone.0282290

Lemos, A. S. O., Campos, L. M., Melo, L., Guedes, M., Oliveira, L. G., Silva, T. P, et al. (2018). Antibacterial and antibiofilm activities of psychorubrin, a pyranonaphthoquinone isolated from mitracarpus frigidus (Rubiaceae). *Front. Microbiol.* 9. doi: 10.3389/fmicb.2018.00724

Liu, H., Carvalhais, L. C., Crawford, M., Singh, E., Dennis, P. G., Pieterse, C. M. J, et al. (2017). Inner plant values: diversity, colonization and benefits from endophytic bacteria. *Front. Microbiol.* 8. doi: 10.3389/fmicb.2017.02552

Luo, X., Sun, J., and Lu, Y. (2022). Research progress in the biosynthesis, antimicrobial mechanism, and application of lipopeptides inBacillus amyloliquefaciens. *Sci. Technol. Food Industry* 43, 462–470. doi: 10.13386/j.issn1002-0306.2021100259

Lynch, J. P., Zhanel, G. G., and Clark, N. M. (2017). Infections due to acinetobacter baumannii in the ICU: treatment options. *Semin. Respir. Crit. Care Med.* 38, 311–325. doi: 10.1055/s-0037-1599225

Mansouri, M. D., Hull, R. A., Stager, C. E., Cadle, R.M., and Darouiche, R. O. (2013). *In vitro* activity and durability of a combination of an antibiofilm and an antibiotic against vascular catheter colonization. *Antimicrob. Agents Chemother.* 57, 621–625. doi: 10.1128/AAC.01646-12

Marchut-Mikołajczyk, O., Drożdżyński, P., Polewczyk, A., Smułek, W., and Antczak, T. (2021). Biosurfactant from endophytic bacillus pumilus 2A: physicochemical characterization, production and optimization and potential for plant growth promotion. *Microbial Cell Factories* 20, 40. doi: 10.1186/s12934-021-01533-2

Martins, P. C., and Martins, V. G. (2018). Biosurfactant production from industrial wastes with potential remove of insoluble paint. *Int. Biodeterioration Biodegradation* 127, 10–16. doi: 10.1016/j.ibiod.2017.11.005

Mburu, N., Rousseau, D. P. L., Van Bruggen, J. J. A., and Lens, P. N. L. (2015). Use of the macrophyte *Cyperus papyrus* in wastewater treatment. *In: ed. J. Vymazal The Role of Natural and Constructed Wetlands in Nutrient Cycling and Retention on the Landscape* (Cham: Springer International Publishing), 293–313. doi: 10.1007/978-3-319-08177-9_20

Nahar, A., Anwar, S., and Miah, M. (2013). Association of biofilm formation with antimicrobial resistance among the acinetobacter species in a tertiary care hospital in Bangladesh. *J. Med.* 14, 28-32. doi: 10.3329/jom.v14i1.14533

Naves, P., Del Prado, G., Huelves, L., Gracia, M., Ruiz, V., Blanco, J., et al. (2008). Measurement of biofilm formation by clinical isolates of escherichia coli is method-dependent. *J. Appl. Microbiol.* 105, 585–590. doi: 10.1111/j.1365-2672.2008.03791.x

Neethu, S., Midhun, S. J., Radhakrishnan, E. K., and Jyothis, M. (2020). Surface functionalization of central venous catheter with mycofabricated silver nanoparticles and its antibiofilm activity on multidrug resistant acinetobacter baumannii. *Microb. Pathog.* 138, 103832. doi: 10.1016/j.micpath.2019.103832

Nicol, M., Alexandre, S., Luizet, J. B., Skogman, M., Jouenne, T., Salcedo, S. P., et al. (2018). Unsaturated fatty acids affect quorum sensing communication system and inhibit motility and biofilm formation of acinetobacter baumannii. *Int. J. Mol. Sci.* 19, 214. doi: 10.3390/ijms19010214

Ohadi, M., Forootanfar, H., Dehghannoudeh, G., Eslaminejad, T., Ameri, A., Shakibaie, M., et al. (2020). Antimicrobial, anti-biofilm, and anti-proliferative activities of lipopeptide biosurfactant produced by acinetobacter junii B6. *Microb. Pathog.* 138, 103806. doi: 10.1016/j.micpath.2019.103806

Otzen, D. E. (2017). Biosurfactants and surfactants interacting with membranes and proteins: same but different? *Biochim. Biophys. Acta (BBA) - Biomembranes* 1859, 639–649. doi: 10.1016/j.bbamem.2016.09.024

Paraszkiewicz, K., Moryl, M., Płaza, G., Bhagat, D., , S, , K. S., Bernat, P., et al (2021). Surfactants of microbial origin as antibiofilm agents. *Int. J. Environ. Health Res.* 31, 401–420. doi: 10.1080/09603123.2019.1664729

Patel, M., Siddiqui, A. J., Hamadou, W. S., Surti, M., Awadelkareem, A. M., Ashraf, S. A., et al (2021). Inhibition of bacterial adhesion and antibiofilm activities of a glycolipid biosurfactant from lactobacillus rhamnosus with its physicochemical and functional properties. *Antibiotics (Basel)* 10, 1546. doi: 10.3390/antibiotics10121546

Pathak, R., Bierman, S. F., and D'arnaud, P. (2018). Inhibition of bacterial attachment and biofilm formation by a novel intravenous catheter material using an *in vitro* percutaneous catheter insertion model. *Med. Devices (Auckl)* 11, 427–432. doi: 10.2147/MDER.S183409

Peleg, A. Y., De Breij, A., Adams, M. D., Cerqueira, G. M., Mocali, S., Galardini, M., et al (2012). The success of acinetobacter species; genetic, metabolic and virulence attributes. *PloS One* 7, e46984. doi: 10.1371/journal.pone.0046984

Pérez-López, M., García-Contreras, R., Soto-Hernández, M., Rodríguez-Zavala, J. S., Martínez-Vázquez, M., Prado-Galbarro, F. J, et al. (2018). Antiquorum sensing activity of seed oils from oleaginous plants and protective effect during challenge with chromobacterium violaceum. *J. Med. Food* 21, 356–363. doi: 10.1089/jmf.2017.0080

Raad, I., Mohamed, J. A., Reitzel, R. A., Jiang, Y., Raad, S., Al Shuaibi, M., et al (2012). Improved antibiotic-impregnated catheters with extended-spectrum activity against resistant bacteria and fungi. *Antimicrob. Agents Chemother.* 56, 935–941. doi: 10.1128/aac.05836-11

Rashiya, N., Padmini, N., Ajilda, A. a. K., Prabakaran, P., Durgadevi, R., Veera Ravi, A., et al. (2021). Inhibition of biofilm formation and quorum sensing mediated virulence in pseudomonas aeruginosa by marine sponge symbiont brevibacterium casei strain alu 1. *Microb. Pathog.* 150, 104693. doi: 10.1016/j.micpath.2020.104693

Rodrigues, L. R. (2011). Inhibition of bacterial adhesion on medical devices. *Adv. Exp. Med. Biol.* 715, 351–367. doi: 10.1007/978-94-007-0940-9_22

Rodrigues, L., Van Der Mei, H. C., Teixeira, J., and Oliveira, R. (2004). Influence of biosurfactants from probiotic bacteria on formation of biofilms on voice prostheses. *Appl. Environ. Microbiol.* 70, 4408–4410. doi: 10.1128/aem.70.7.4408-4410.2004

Rolain, J. M., Diene, S. M., Kempf, M., Gimenez, G., Robert, C., and Raoult, D. (2013). Real-time sequencing to decipher the molecular mechanism of resistance of a clinical pan-drug-resistant acinetobacter baumannii isolate from marseille, France. *Antimicrob. Agents Chemother.* 57, 592–596. doi: 10.1128/AAC.01314-12

Ryan, R. P., Germaine, K., Franks, A., Ryan, D.J., and Dowling, D.N.. (2008). Bacterial endophytes: recent developments and applications. *FEMS Microbiol. Lett.* 278, 1–9. doi: 10.1111/j.1574-6968.2007.00918.x

Sanchez, C. J., Mende, K., Beckius, M. L., Akers, K. S., Romano, D. R., Wenke, J. C, et al. (2013). Biofilm formation by clinical isolates and the implications in chronic infections. *BMC Infect. Dis.* 13, 47. doi: 10.1186/1471-2334-13-47

Santhakumari, S., Nilofernisha, N. M., Ponraj, J. G., Pandian, S. K., and Ravi, A. V. (2017). *In vitro* and *in vivo* exploration of palmitic acid from synechococcus elongatus as an antibiofilm agent on the survival of artemia franciscana against virulent vibrios. *J. Invertebr Pathol.* 150, 21–31. doi: 10.1016/j.jip.2017.09.001

Sarwar, A., Brader, G., Corretto, E., Aleti, G., Ullah, M. A., Sessitsch, A, et al. (2018). Qualitative analysis of biosurfactants from bacillus species exhibiting antifungal activity. *PloS One* 13, e0198107. doi: 10.1371/journal.pone.0198107

Satpute, S. K., Banpurkar, A. G., Dhakephalkar, P. K., Banat, I. M., and Chopade, B. A. (2010). Methods for investigating biosurfactants and bioemulsifiers: a review. *Crit. Rev. Biotechnol.* 30, 127–144. doi: 10.3109/07388550903427280

Silva, E., Carvalho, J. W. P., Aires, C. P., and Nitschke, M. (2017). Disruption of staphylococcus aureus biofilms using rhamnolipid biosurfactants. *J. Dairy Sci.* 100, 7864–7873. doi: 10.3168/jds.2017-13012

Singh, V. K., Mishra, A., and Jha, B. (2019). 3-Benzyl-Hexahydro-Pyrrolo[1,2-a] Pyrazine-1,4-Dione extracted from exiguobacterium indicum showed anti-biofilm activity against pseudomonas aeruginosa by attenuating quorum sensing. *Front. Microbiol.* 10. doi: 10.3389/fmicb.2019.01269

Sivanandan, S. (2020). Do antimicrobial-impregnated central venous catheters prevent nosocomial bloodstream infection in neonates? *Acta Paediatrica* 109, 1907–1908. doi: 10.1111/apa.15268

Tahmourespour, A., Salehi, R., and Kasra Kermanshahi, R. (2011). Lactobacillus acidophilus-derived biosurfactant effect on GTFB and GTFC expression level in streptococcus mutans biofilm cells. *Braz. J. Microbiol.* 42, 330–339. doi: 10.1590/s1517-83822011000100042

Tamura, K., Stecher, G., Peterson, D., Filipski, A., and Kumar, S. (2013). MEGA6: molecular evolutionary genetics analysis version 6.0. *Mol. Biol. And Evol.* 30, 2725–2729. doi: 10.1093/molbev/mst197

Tidke, S. A., Kiran, S., Giridhar, P., and Gokare, R. A. (2019). "Current understanding and future perspectives of endophytic microbes vis-a-vis production of secondary metabolites," in *Endophytes and secondary metabolites*. Ed. S. Jha (Cham: Springer International Publishing), 459–474.

Vijayashree Priyadharsini, J., Smiline Girija, A. S., and Paramasivam, A. (2018). In silico analysis of virulence genes in an emerging dental pathogen a. baumannii and related species. *Arch. Oral. Biol.* 94, 93–98. doi: 10.1016/j.archoralbio.2018.07.001

Wang, H., Tong, H., Liu, H., Wang, Y., Wang, R., Gao, H, et al. (2018). Effectiveness of antimicrobial-coated central venous catheters for preventing catheter-related blood-stream infections with the implementation of bundles: a systematic review and network meta-analysis. *Ann. Intensive Care* 8, 71. doi: 10.1186/s13613-018-0416-4

Wasfi, R., Rasslan, F., Hassan, S. S., Ashour, H. M., and Abd El-Rahman, O. A. (2021). Co-Existence of carbapenemase-encoding genes in acinetobacter baumannii from cancer patients. *Infect. Dis. Ther.* 10, 291–305. doi: 10.1007/s40121-020-00369-4

Weisburg, W. G., Barns, S. M., Pelletier, D. A., and Lane, D. J. (1991). 16S ribosomal DNA amplification for phylogenetic study. *J. Bacteriol* 173, 697–703. doi: 10.1128/jb.173.2.697-703.1991

Wu, B., Xiu, J., Yu, L., Huang, L., Yi, L., and Ma, Y. (2022). Biosurfactant production by bacillus subtilis SL and its potential for enhanced oil recovery in low permeability reservoirs. *Sci. Rep.* 12, 7785. doi: 10.1038/s41598-022-12025-7

Yassin, M. A., Elkhooly, T. A., Elsherbiny, S. M., Reicha, F. M., and Shokeir, A. A. (2019). Facile coating of urinary catheter with bio-inspired antibacterial coating. *Heliyon* 5, e02986–e02986. doi: 10.1016/j.heliyon.2019.e02986

Zafer, M. M., Hussein, A. F. A., Al-Agamy, M. H., Radwan, H. H., and Hamed, S. M. (2021). Genomic characterization of extensively drug-resistant NDM-producing acinetobacter baumannii clinical isolates with the emergence of novel bla ADC-257. *Front. Microbiol.* 12. doi: 10.3389/fmicb.2021.736982

Zhou, C., Wu, Y., Thappeta, K. R. V., Subramanian, J. T. L., Pranantyo, D., Kang, E. -T, et al. (2017). *In vivo* anti-biofilm and anti-bacterial non-leachable coating thermally polymerized on cylindrical catheter. *ACS Appl. Materials Interfaces* 9, 36269–36280. doi: 10.1021/acsami.7b07053

Ziemyte, M., Rodriguez-Diaz, J. C., Ventero, M. P., Mira, A., and Ferrer, M. D. (2020). Effect of dalbavancin on staphylococcal biofilms when administered alone or in combination with biofilm-detaching compounds. *Front. Microbiol.* 11. doi: 10.3389/fmicb.2020.00553

Frontiers in
Cellular and Infection Microbiology

Investigates how microorganisms interact with their hosts

Explores bacteria, fungi, parasites, viruses, endosymbionts, prions and all microbial pathogens as well as the microbiota and its effect on health and disease in various hosts.

Discover the latest Research Topics

See more →

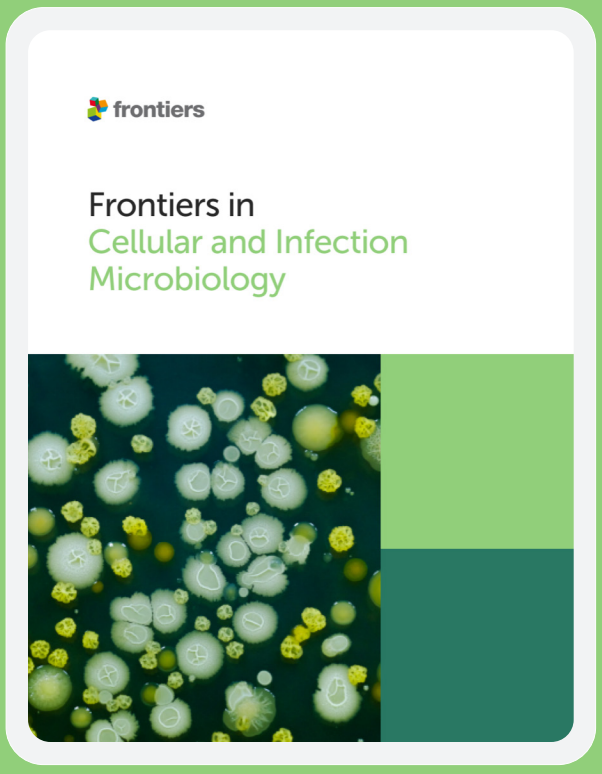

Frontiers

Avenue du Tribunal-Fédéral 34
1005 Lausanne, Switzerland
frontiersin.org

Contact us

+41 (0)21 510 17 00
frontiersin.org/about/contact